Biophysical and structural studies of bioactive peptides derived from the piscidin family in anionic membrane models

Kelton Rodrigues de Souza

UNIVERSITÉ DE STRASBOURG

ÉCOLE DOCTORALE DES SCIENCES CHIMIQUES

Institut de Chimie de Strasbourg, UMR 7177

THÈSE présentée par:

Kelton RODRIGUES DE SOUZA

soutenue le: **1 décembre 2023**

pour obtenir le grade de: **Docteur de l'université de Strasbourg**

Discipline/Spécialité: Chimie

Biophysical and Structural Studies of Bioactive Peptides Derived from the Piscidin Family in Anionic Membrane Models

THÈSE dirigée par :

M. BECHINGER Burkhard	Professeur, Université de Strasbourg
M. VERLY Rodrigo Moreira	Professeur, Universidade Federal dos Vales do Jequitinhonha e Mucuri

RAPPORTEURS :

M. KUHN Andreas	Professeur, Universität Hohenheim
Mme. LANDON Céline	DR, CBM-CNRS, Orléans

AUTRES MEMBRES DU JURY (INVITE):

Mme. MENARD-MOYON Cecilia	DR, IBMC-CNRS, Strasbourg

Études Biophysiques et Structurales de Peptides Bioactifs Dérivés de la Famille des Piscidines dans des Modèles de Membrane Anionique

Biophysical and Structural Studies of Bioactive Peptides Derived from the Piscidin Family in Anionic Membrane Models

Kelton Rodrigues de Souza

Université de Strasbourg,

Institut de Chimie de Strasbourg, UMR 7177

Laboratoire de RMN et biophysique des membranes

Thesis

December 2023

Contents

Acknowledgements

Agradeço ao Deus da Vida e de Todas as coisas por cada dia, por ter me concedido forças, sabedoria e alegria pra finalizar essa etapa. Obrigado por, entre tantos, ter me feito trilhar caminhos incríveis e que eu sonhava; pela oportunidade de estudar e por fazer acreditar que era possível. A curiosidade nos move e nos faz aprender sempre um pouco mais. E por poder aprender, obrigado por perceber que nada é por acaso... e que em Tudo há um toque especial que vem de Ti. À Mãe Maria, te agradeço mãezinha por estar sempre presente. Sentir o Teu carinho e cuidado sempre me faz descansar e estar pronto para um novo dia.

To my Professors, Masters, and Advisors Rodrigo Verly and Burkhard Bechinger, I thank you for guiding me, and for the encouragement throughout my doctoral studies. Having your support was very important to me; it made me believe in myself and overcome the difficulties I encountered along the way. To Professor Rodrigo, thank you very much for encouraging me since my undergraduate days, during my Master's degree, and for embarking with me on this journey to Strasbourg! Thank you for introducing me to science and for transmitting your enthusiasm for research; this has always driven me to study, improve and wish to learn more and more. To Professor Burkhard Bechinger, thank you very much for having me in your laboratory, even in the middle of COVID-19 pandemic, and for believing in my work throughout the thesis period. Thank you also for your support and the enlightening discussions that broadened my perspective with new ideas, questions, and insights. In addition, I thank you for opening the doors to the world of solid-state NMR.

I am also so grateful to Christopher Aisenbrey and Élise Glattard for welcoming me into the lab, for always pushing me to improve myself, and for allowing me to learn a lot about science and leadership. Both of you are a vital part of maintaining an excellent work environment.

I am very grateful to Evgeniy Salnikov and Ahmad Saad for the partnership, for helping me, and for engaging in discussions related to science, ssNMR, and other biophysical techniques during my stay in Strasbourg. Additionally, I thank you very much for the personal talks we have had since my first days in France. I have learned a lot from both of you.

I am also very grateful to Jesus Raya, Jarbas Resende, Philippe Bertani, and Victor Munhoz for supporting me with the experiments, interpretation, discussions, and simulations of solution and solid-state NMR assays. It has been a great time spent with all of you.

Furthermore, I am very honored to have been part of the teams of talented scientists who have passed through the Membrane Biophysics and NMR, and Laboratório de Síntese e Estruturas de Biomoléculas. The atmosphere was amazing, in which cooperation and support for each other were present among us. The list of mates I have lived within Diamantina and Strasbourg is long, but I cherish the moments shared with each of them. With some ones, we delved into intense discussions and experimental challenges. I thank Luís Pires, Lúcio Otávio, Kathakali, Adrien, Jian-Qiao, and Lucas Rocha for the time we spent together planning, learning, discussing, and sharing ideas related to experiments and results. Additionally, I am very pleased to have met and shared numerous moments and talks with Jasmin, Romu, Morane, Suresh Prabhu, Nele, and Lisa. My heartfelt thanks to you all for receiving me well, for the friendship, and also for helping me with many other matters! Your presence has made this journey lighter, enjoyable and has brightened my life here.

I am also very proud to have met amazing people along my academic journey as well as in my personal life. They are more than friends, they are a family that has accompanied and supported me and continues to do so to this day: Franciely, Rafael & Iza, meus Chames Deco & Jack, Marcell & Raissa, Adolfo & Amanda, Dan, Jhon & Zaíra, Leo & Fabi, Renanzin, Alander, Gabriel, Rafael, Ted, and the recent ones who have marked many moments together: Bruno, Yvilla, Carol, Thiago Pereira, Renato, David & Bea. Thank you so much! You are part of my journey and story up to here. May we continue like this, even if sometimes physically far apart, but always together.

Finally, I would like to express my sincere gratitude to the esteemed professors who served on my doctoral thesis jury committee. I am particularly thankful to Professor Dr. Céline Landon, the president of the Jury, whose extensive experience in chemical biology, peptide structure determination, and the identification of new therapeutic targets has greatly enriched my research. You have significantly pushed me to think about and discuss the subject of this thesis deeply, enhancing not only this manuscript but also my understanding of the biomolecules/peptides field. I am also deeply grateful to Professor Dr. Andreas Kuhn and Dr. Cecilia Menard-Moyon, whose expertise in biology, chemistry, and the self-assembly process of biomolecules provided valuable insights and perspectives. I deeply value the time dedicated

to reviewing my manuscript, along with their valuable comments and insights on my work. Their collective guidance and feedback have been invaluable throughout and after my defense.

I also thank the Funding Agencies and the financial support for the development of this work. This study was financed by the Coordenação de Aperfeiçoamento de Pessoal de Nível Superior – Brasil (CAPES) – Finance Code 001; L'Ambassade de France au Brésil, Campus France; and PRPPG-UFVJM. The financial contributions of the Agence Nationale de la Recherche and the LabEx Chemistry of Complex Systems, the University of Strasbourg, and the CNRS, are gratefully acknowledged.

Por fim, quero também agradecer a minha família, em especial aos meus pais José Dilson e Maria Rodrigues. Obrigado por acreditarem em mim, me incentivar, pelas orações e torcida! Obrigado também por sempre me apoiar e por priorizarem a minha educação, desde pequeno... lá do início rsrs. Tudo que sou e conquistei eu devo a vocês.

List of abbreviations

ACN	acetonitrile
AMPs	antimicrobial peptides
CD	circular dichroism
CHCA	alpha-cyano-4-hydroxycinnamic acid
HPLC	high performance liquid chromatography
CMC	critical micelle concentration
DCM	dichloromethane
DPC	dodecylphosphocholine
DIC	N,N′-diisopropylcarbodiimide
DMF	N,N-dimethylformamide
DMSO	dimethyl sulfoxide
DMPC	1,2-dimyristoyl-sn-glycero-3-phosphocholine
DMPG	1,2-dimyristoyl-sn-glycero-3-phosphoglycerol
Fmoc	fluorenylmethyloxycarbonyl
H	helical percentage, helicity
HOBt	1-hydroxybenzotriazole
IPA	isopropyl alcohol
LUVs	large unilamellar vesicles
MALDI	matrix-assisted laser desorption/ionization
MDR	multidrug resistant bacteria
MLV	multilamellar vesicle
MIC	minimal inhibitory concentration
MRSA	methicillin-resistant *Staphylococcus aureus*
MS	mass spectrometry
m/z	mass divided by charge number
POPC	1-Palmitoyl-2-oleoyl-*sn*-glycero-3-phosphocholine
POPG	1-palmitoyl-2-oleoyl-*sn*-glycero-3-phosphoglycerol
NMR	nuclear magnetic resonance
SA	simulated annealing
SDS	sodium dodecyl sulphate

θ	molar ellipticity
TFA	trifluoroacetic acid
TIS	triisopropylsilane
ToF	time of flight
Tris	tris(hydroxymethyl)aminomethane

Presentation

Biophysical and Structural Studies of Bioactive Peptides Derived from the Piscidin Family in Anionic Membrane Models

Antimicrobial peptides (AMPs) are important biomolecules that act in several functions in immune system against infections. Therefore, they are present in various organisms, both invertebrates and vertebrates, as well as in plants(1). Among the defense functions, antimicrobial peptides have been highlighted due to the emerging problem related to the multidrug-resistant pathogens(2).

Mechanism of action of AMPs have been widely studied focusing on the peptide-membrane interaction, mainly involving lipopolysaccharide or phospholipids as membrane models(1,3). It is well known that the phospholipid composition of the bacterial membranes differentiates it from human membranes due to its anionic character(4). While most AMPs is cationic, the electrostatic attraction contributes to the targeting and selectivity of these membranes(5), although hydrophobic residues are also important to the interaction with the membrane(6).

Despite many AMPs being unstructured in solution, most of them adopt a well-defined amphipathic α-helical conformation in the presence of an interaction interface(7). Thereby, the primary sequence, and the arrangement of the amino acid side chains in an ordered structure seems to be essential to the AMPs activity in bacterial membranes(8). Peptides which present these structural behaviors may act directly on the microbial membrane and some interaction models have been described for the AMPs(9–11).Therefore, it is of particular interest to analyze how AMPs interact with and modify the structure of the phospholipid bilayer, inducing membrane disruption and, consequently cell lysis.

Another point that is important to highlight is the presence of D-amino acids in antimicrobial peptide sequences. Although the presence of enantiomeric amino acid was usually addressed as an uncommon and rare occurrence in animal sources, recently natural antimicrobial peptides containing D-residues have been described. Interestingly, some peptides containing D-amino acids showed quantitative differences in antimicrobial activities when compared to the L-epimeric form. Besides that, their occurrence has been associated with a

higher resistance to peptidases than their counterparts(12). Some examples are the natural L-Phenylseptin and D-Phenylseptin peptides (FFFDTLKNLAGKVIGALT-NH_2) reported with D-epimer showing higher activity against *Staphylococcus aureus* and *Xanthomonas axonopodis* in comparison with the L-epimer(13). Other peptides presenting the same characteristic are antimicrobial Bombinin H(14), and the opioid peptide classes Dermorphins(15), and Deltorphins(16), both identified in amphibian skin.

In this context, the following chapters of this Thesis describes the mode of membrane interaction of two antimicrobial peptides originally isolated from *Epinephelus coioides* (orange-spotted grouper), named piscidin-4s (ecPis-4s), piscidin-2s (ecPis-2s), and an epimeric form of Piscidin-2s, called D-ecPis-2s. In order to understand how the structural features such as positively charged, aromatic amino acids, and secondary structure may influence on the membrane interaction, a set of structural and biophysical techniques has been employed.

Chapter 1: Introduction

Peptides are biomolecules with diverse biological activities and play an important role in the functional and physiological properties of living organisms(17,18). Similarly, peptides are formed by amino acid residues covalently linked through amide bonds, also known as peptide bonds(1,19).

The biological activity of peptides was firstly described by Mellander in 1950(20). This study showed phosphorylated peptides derived from casein increased bone calcification in children diagnosed with rickets, even in the absence of vitamin D(20). Since then, peptides have been the subject of many studies that continue to the present day(21).

Currently, there are several platforms or databases which classify bioactivity peptides based on their function/activity as antimicrobial, antithrombotic, antihypertensive, opioid, immunomodulator, antioxidant, wound healing, antidiabetic and antifilm, anticancer, among others(22–27). Thus, these molecules can act mainly on the immune, digestive, gastrointestinal, endocrine, cardiovascular, and nervous systems, as well as having preventive properties against infectious diseases(22,28).

Among the classes of bioactive peptides, antimicrobial peptides (AMPs) is one that has been highlighted in recent years. The relevance of studying AMPs arises from the increased resistance of microorganisms against conventional antibiotics, mainly due to their indiscriminate use to combat bacterial infections(29). As a result, bacterial resistance is now one of the most serious public health problems with worldwide economic impact(30–32). AMPs act by associating with cell membranes, predominantly those negatively charged(18) whose interaction results in the disorganization and/or disruption of the lipid bilayer, which can cause cell lysis(4,24,33). This mechanism differs from the mode of action of conventional drugs, which act on specific targets in the pathogens' cells. Therefore, when compared to conventional antibiotics the development of pathogen resistance is more difficult when treated with AMPs(34). In this context, AMPs have emerged as promising antibiotic agents and an alternative in the development of new drugs to combat infections caused by super-resistant bacteria.

Although many antimicrobial peptides have been studied and some mechanisms of action proposed, their mode of membrane interaction is difficult to analyze, and more

comprehensive studies are needed to answer some questions. The knowledge gained from structural techniques, biophysical interaction processes, and understanding of the structure-activity relationship of antimicrobial peptides helps in the design and development of more specific molecules with greater biological potential, resulting in more effective antibiotics with lower toxicity.

1.1 Antimicrobial resistance

Antibiotics have effectively extended life expectancy and they are the most widely distributed drugs by the pharmaceutical industries and the most prescribed in hospitals worldwide(35–37). These drugs are essential in healthcare treatments, especially in underdeveloped countries, where diseases caused by microbial infections are a common cause of death(38).

Bacterial resistance, also known as antibiotic resistance or antimicrobial resistance (AMR), is the ability of bacteria to resist the action or effects of medication previously used to treat them(30). In other words, antimicrobial resistance happens when a microorganism such as bacteria, fungi and parasites change when they are exposed to antimicrobial drugs, e.g., antibiotics and antifungals medicines(39). As a result, these drugs become ineffective and infections persist in the body, increasing the risk of spread to others(30). AMR is currently one of the most relevant public health problems at a global level, as it has worrying clinical and economic consequences, since many bacteria previously susceptible to the antibiotics usually used no longer respond to these same agents(31,38,40).

Although the development of bacterial resistance to antibiotics is a natural phenomenon, the overuse and misuse of antibiotics in healthcare and agriculture, together with inappropriate waste management and environmental transmission, have led to substantially increased antimicrobial resistance(30,35). The antimicrobial resistance process is resulted from the use of medicines, and the genetic mutation of bacteria(31), in addition the development of superbugs bacteria is also the result of the indiscriminate use of antibiotics such as in medicine, agriculture and livestock(41); poor infection control in hospitals and clinics; lack of hygiene and basic sanitation(31,40), etc. The major problem of bacterial resistance to antibiotics is not only related to the development of stronger strains and their rapid proliferation, but also to the

limitations of treatment options for these 'new' infections(30,39). In this way, antimicrobial resistance is an urgent global public health threat.

The World Health Organization (WHO) has reported that antimicrobial resistance (AMR) had killed at least 1.27 million people worldwide and associated with nearly 5 million deaths in 2019(30). In the U.S., the Centers for Disease Control and Prevention (CDC) reported over 2.8 million cases of antimicrobial-resistant infections annually, resulting in more than 35,000 fatalities, as outlined in the 2019 Antibiotic Resistance Threats Report(42). A recent report from the United Nations Environment emphasizes the need for increased attention to environmental factors fostering the development of drug-resistant bacteria, commonly known as "superbugs." The report predicts that by 2050, superbugs and associated forms of AMR could lead to up to 10 million deaths annually, matching the annual global death toll of cancer(43,44).

Besides that, a 2022 Lancet study indicates 860,000 deaths of occurred in Africa resulted directly from drug-resistant bacterial infections in 2019, while during the same year, Africa recorded 640,000 deaths from HIV(45). Addressing the economic impact, a collaborative CDC study reveals that the annual cost of treating infections caused by six frequently encountered multidrug-resistant microorganisms in healthcare settings in the United States exceeds $4.6 billion(32). In this way, antimicrobial resistance has been considered one of the top global public health challenges, posing imminent threats to animal and plant health, food security, and economic development. Therefore, with the emergence of pathogens that are super-resistant to commonly used drugs, many studies have been carried out to develop new drugs against infections caused by this new generation of bacteria(46–49).

There are mainly four mechanisms by which bacteria resist antibiotics(50), as shown in Figure 1. They are [1] bacterial enzyme-mediated drug inactivation, where the antibiotics are deactivated by the enzymes produced by the bacteria, such as the β-lactamase enzyme that inactivates Penicillin G from penicillin-resistant bacteria(51); [2] by reducing drug uptake through decreased cell permeability which, for instance, the bacteria modify their cell wall components, such as lipopolysaccharide lipid A or peptidoglycan precursors to avoid the interference of antibiotics with cell wall synthesis(52); [3] structural modification of the drug target due to gene mutation, which this process allows bacteria to change their target binding sites through genetic mutations. Examples of such modifications are the changes in penicillin-binding proteins, DNA gyrase and topoisomerase IV enzymes, and the methylation of the 30S and 50S ribosomal subunits(53,54); [4] drug efflux outside the bacterial cell membrane which is the expression of transmembrane efflux pumps. This process belongs to six major families

and enables bacteria to actively eject almost all classes of antibiotics from their cytoplasm(55). Plasmids, small mobile genetic elements composed of extrachromosomal DNA, can spread resistance genes between bacteria of the same or different species, with the plasmid-mediated quinolone resistance gene being one such example(50,53).

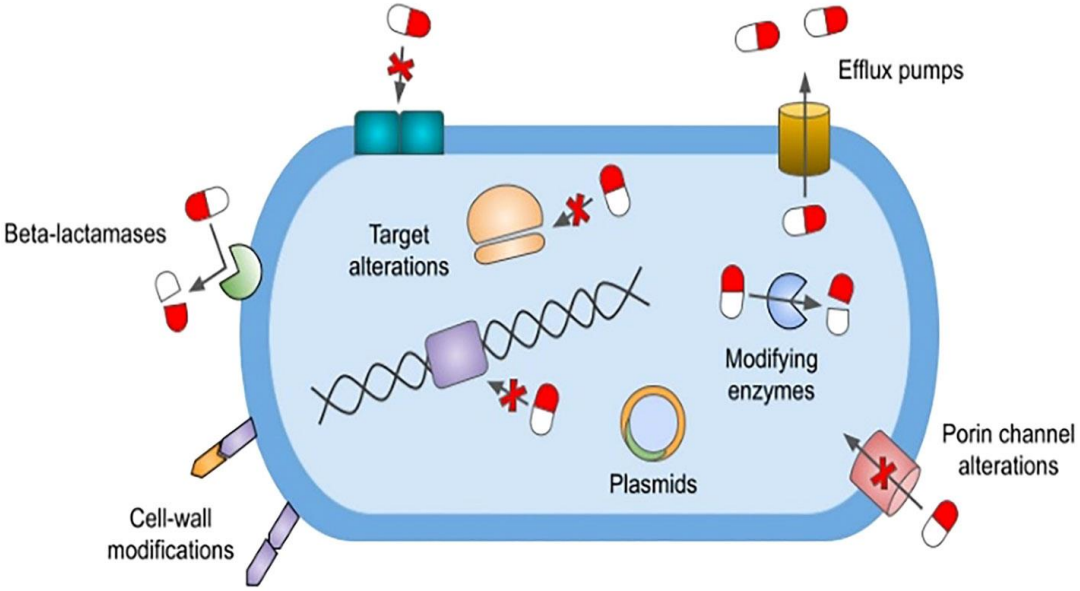

Figure 1. Mechanisms of antimicrobial resistance which are represented various antimicrobial resistance strategies utilized by ESKAPE pathogens(53).

The recent advancement in addressing antimicrobial resistance encompasses a range of strategies, including combinatorial drug methodologies, products based on antimicrobial polymeric biomaterials, bio-nanotechnology approaches, and others. The treatment currently applied against critical superbugs as methicillin-resistant *S. aureus* (MRSA), carbapenem-resistant *Enterobacteriaceae* (CRE), vancomycin-resistant *Enterococcus* (VRE), multidrug-resistant *P. aeruginosa* (MRPA), and multidrug-resistant *E. coli* (MREC) are applied respectively Vancomycin(56); Polymyxin, Tigecycline, and Aminoglycosides in a drug combination approach against CRE(57); Daptomycin(58); Ceftazidime–avibactam and Ceftolozane– tazobactam(59); and Mecillinam in which it inhibits penicillin-binding protein 2 in *E. coli* (MREC) strains(60).

Among the proposals discussed above and described in the literature, AMPs isolated from fish, called piscidins are another class of promising biomolecules with high antimicrobial activity potential and a broad spectrum against resistant pathogens(61). AMPs are a class of

small peptides that widely exist in nature and being an important player of the innate immune system of different organisms. They have been reported as presenting inhibitory effects against bacteria, fungi, parasites, and viruses(62). In contrast to conventional drugs, which target central cellular processes and cell wall metabolism, the main target of AMPs is the cell membrane(63,64). Although these biomolecules are highly diverse, they have several common properties such as [1] positive net charge, which helps them to reach the bacterial surface; [2] a have high hydrophobicity, and [3] amphipathicity, characteristics that together lead to a high partition coefficient in the lipid bilayer of the microbial membrane(65). AMPs studies are part of a still recent area of research that faces challenges that include searching for biomolecules in nature, investigating their roles in innate immunity and identifying their mechanisms of action(66,67).

1.2 Antimicrobial peptides

Antimicrobial peptides (AMPs) are biologically active molecules that can be found in a variety of living organisms such as bacteria, fungi, plants, amphibians, insects, mammals, etc(68). Generally, AMPs make part of the innate immunity system acting in the first line of defense against infections and elimination of invading molecules(25,69).

AMPs identified in nature from diverse sources vary in length, composition, charge and secondary structure, although they can share some similarities. On the other hand, different types of AMPs have the following commonalities as their number of amino acid residues is between 10 and 60, and almost all AMPS are cationic. Although, several anionic AMPs also exist, as they are formed by several acidic amino acids like aspartic acid and glutamic acid(62,70).

Pane and coworkers reported (71) that the inhibition potential of a peptide against pathogens is directly related to the presence of a positive charge and its amphipathic character. Commonly, AMPs present a net positive charge, i.e., they have a cationic character due to the presence of amino acid residues with basic and protonable side chains, such as arginine, lysine or histidine. The amphipathic character is associated with the conformation of the peptide in the cellular environment, for example, when interacting with the phospholipid bilayer(4). Thus,

they preferentially associate with the negatively charged cell membrane of bacteria due to electrostatic attraction(25,34,72).

Ongoing advancements in AMPs research have led to the accumulation of substantial datasets within AMPs databases. The classification of natural AMPs is challenging due to their natural diversity(73). AMPs are categorized according to [1] source, [2] activity, [3] structural characteristics, and [4] amino acid-rich species(74). Based on APD3 statistics, AMPs can originate from various sources, such as mammals (with a large fraction of human host defense peptides), amphibians, microorganisms, or insects(62,75–78). Figure 2 presents a classification of antimicrobial peptides.

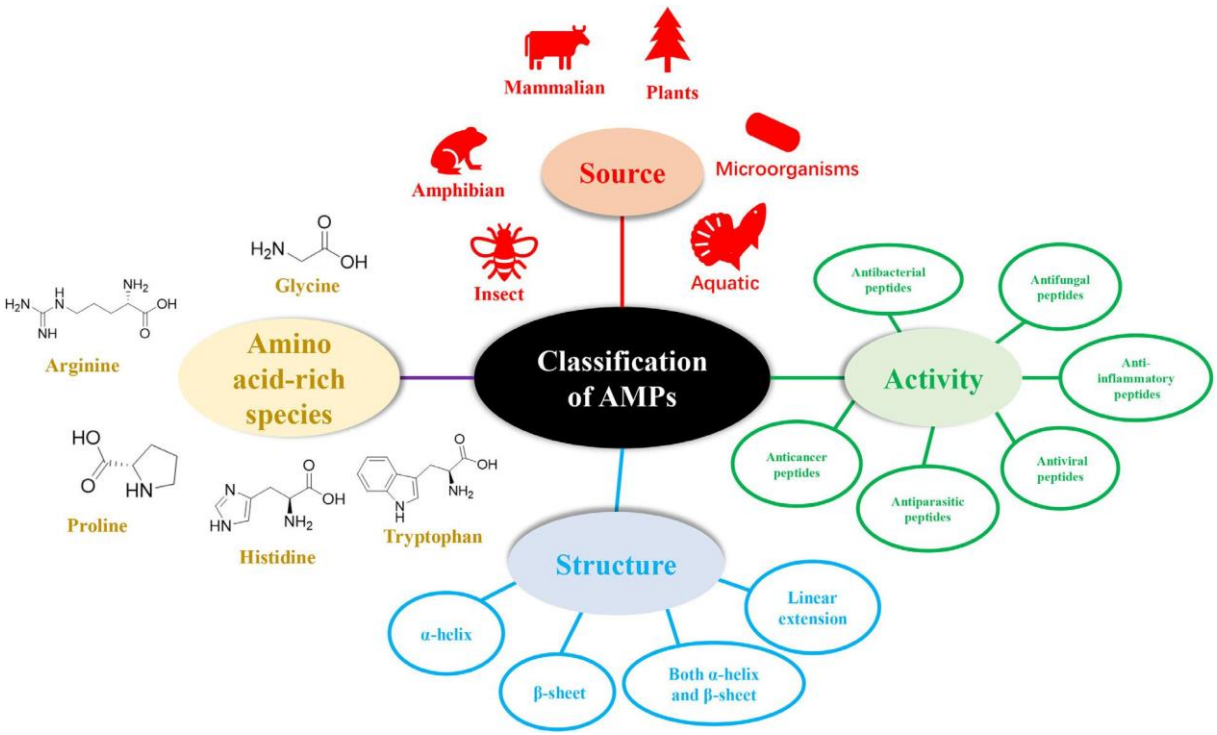

Figure 2. Classification of antimicrobial peptides according to statistical data in APD3(62,74).

As mentioned above, AMPs are host defense mechanisms that protect, for example, eukaryotes from pathogen invasion(79). They are well conserved because [1] as constituents of the innate immune system, the production of AMPs by host cells demands less time and energy compared to the synthesis of antibodies within the acquired immune system, and [2] they are small peptides that can reach the target faster than immunoglobulins (80); (3) they are essential for some eukaryotes that do not have a lymphocyte-based immune system, such as insects that

depend on the synthesis of a series of antibacterial compounds to eliminate invading microorganisms(81).

Since then, a large number of AMPs have been widely found in various organisms, shown in Figure 2; including microorganisms(82), plants(83), invertebrates(84), fish(61,77,85), amphibians(69,86), reptiles(87), and mammals(88); a brief description of the variety of AMPs is presented as follows. The first antimicrobial peptide identified in bacteria is named nisin, which is produced by the host strain, exhibits cytotoxicity towards other bacterial strains, and kills bacteria in order to compete for nutrients in the environment(89). AMPs have also been found in fungi(82). Furthermore, Copsin, derived from Coprinopsis cinerea (Mushroom), exhibits bactericidal effects on various Gram-positive bacteria by interfering with the biosynthesis of the cell wall in pathogens such as *Enterococcus faecalis* and *Listeria monocytogenes*(90).

Plants use AMPs to defend themselves from pathogenic microorganisms in the air and soil. There are multiple families of plants-derived AMPs, such as thionins, defensins and cyclotides(91). Thionins, a family of small proteins found solely in higher plants, are widely found in seeds, stems, roots and leaves(92), and they exert cytotoxic effects on a spectrum of microorganisms, including Gram-positive and Gram-negative bacteria(93), yeasts(94), and others. AMPs derived from plants typically exhibit a high cysteine residue content, that forms multiple disulfide bonds, which are crucial for structural stability(95). Invertebrates depend on the innate immune system as the primary host defense against pathogenic bacteria, due to the absence of a lymphocyte-based immune system(96). AMPs in invertebrates are widely distributed in hemolymph, skin mucosa, and other tissues. For example, cecropins, derived from the hemolymph of *Hyalophora cecropia*, exhibit high antibacterial effects against both Gram-positive and Gram-negative bacteria(76). The induced expression of drosocin, a 19-residue long antimicrobial peptide of flies first isolated in the fruit fly *Drosophila melanogaster*, in the intestinal tract of Drosophila serves to prevent infections caused by the pathogen *Pseudomonas entomophila*, thereby preserving intestinal homeostasis(97).

Concerning mammals, antibacterial proteins including lysozyme, azurocidin, cathepsin G, phospholipase A2, and lactoferrin, form the innate immune system of mammals(98). Currently, over 1770 species of antimicrobial peptides have been identified in vertebrates. The predominant classes of AMPs in most mammals are cathelicidins and defensins(99), while fish also have hepcidins and piscidins(100–102). Cathelicidins represent a class of Antimicrobial Peptides (AMPs) characterized by a highly conserved cathelin domain,

exhibiting distinct peptide lengths, amino acid sequences, and protein structures(103). Fish-derived cathelicidins demonstrate potent antibacterial activity against a wide range of Gram-positive and Gram-negative bacteria(104). In amphibians, the skin serves as a significant source of AMPs, for example, Cathelicidin-PV, an AMP identified in the skin of the frog *Paa yunnanensis*, exhibits strong antibacterial activity against Gram-positive and Gram-negative bacteria, fungi, as well as clinically isolated drug-resistant, while demonstrating low hemolytic activity(69,105). Additionally, cathelicidins and cathelicidin-related peptide have been identified in various species including for example birds(106), cattle(107), pigs(108) of South America which has presented antibacterial, anti-tumor and anti-fungal properties(109).

Defensins constitute another category of AMPs, further classified into three subtypes based on the arrangement of disulfide bonds: α-, β-, and θ-defensins(110). In humans, only α-defensins and β-defensins are present. Similar to cathelicidins, α-defensins are cleaved by elastase, metalloproteinase, or other proteolytic enzymes, ultimately producing a C-terminal peptide with potential antimicrobial activity(80). The first β-defensin was discovered in the epithelial cells of bovines(111). It was demonstrated that β-defensins derived from quail killed almost all of the 11 tested bacteria, including both Gram-positive and Gram-negative strains(112).

The therapeutic potential of AMPs has attracted considerable attention in the last decades, as evidenced by over 5,000 publications in this field since 2017(113). These publications encompass investigations into potential clinical applications of antimicrobial peptides, ranging from addressing infections involving multidrug-resistant bacteria(114–116) to managing chronic inflammatory diseases such as arthritis(117), asthma(118), and some types of cancer(119). Currently, peptide-based therapeutics undergoing clinical trials are predominantly oriented towards treating infections such as respiratory tract, oral, and catheter-related infections, as well as facilitating wound healing(113).

Although ongoing advancements in the study of Antimicrobial Peptides (AMPs) have yielded substantial datasets accessible across diverse environments and membrane media, the mechanism of action of AMPs remains incompletely understood, necessitating additional research efforts. Further investigations are required to elucidate the relationships between physicochemical properties, aiming to derive cost-effective and highly safe AMPs with pronounced antimicrobial efficacy and specificity. Moreover, the synergistic potential of AMPs should also be continually enhanced, investigated, and further developed.

As known and described in the literature, most AMPs when in contact with the membrane environment can adopt a defined secondary structure as a result of an efficient interaction(65,120). Mostly, when interacting with the membrane environment, AMPs acquire secondary structures such as α-helical and β-sheet, or even unusual well-defined conformations stabilized by loops, turns, among other structural folds(22,24,121,122). Figure 3 shows examples of the most commonly reported secondary structures in the literature for AMPs.

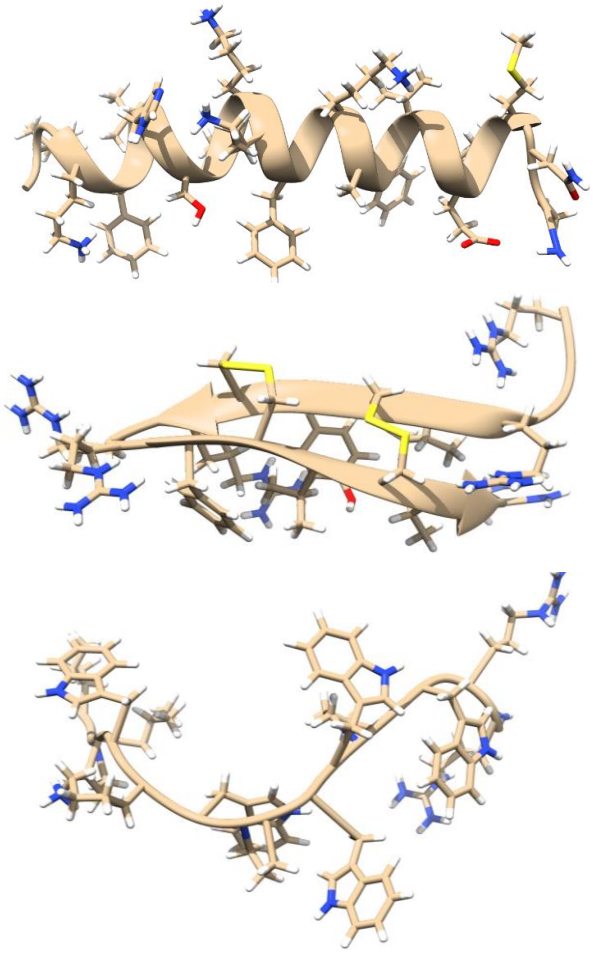

Figure 3. Secondary structures of antimicrobial peptides: α-helix structure of 23-residue magainin antibiotic peptide (PDB – 2MAG); β-sheet secondary structure of the Protegrin-1 peptide (PDB - 1PG1), and extended structure of the Indolicidin peptide (PDB - 1G89).

In addition to the secondary structures presented above, AMPs can present cyclic structures due to disulfide bonds(6), distorted arrangements of helices or β-sheet due to the presence of proline residues in the primary sequence(123). On the other hand, the secondary structure of extended peptides has also been described in the literature. Peptides such as Indolicidin (PDB - 1G89)(124) and Tritrpticin (PDB - 1D6X)(125) have had their three-

dimensional structures elucidated using solution NMR technique. The main characteristic of this structure is a short sequence involving one or two amino acid residues, as Trp, Arg, and Pro in the sequence(126,127). Although less common for antimicrobial peptides, complex structures such as supercoils or superhelices(128,129), stabilized by either disulfide bonds or interchain interactions have been reported such as the homodimeric peptide homotarsinin(6).

The secondary structure plays an important role for the mode of action of AMPs. Based on this characteristic, peptides act as a pore-forming resulting in the leakage of cytoplasmic content, followed by cell death(63,130). On the other hand, some antimicrobial peptides, act under a membrane permeation mechanism based on an amphipathic structure and target intracellular components, as LAH4 family peptides(131). Although the activity of AMPs has been widely discussed, the mechanism of action of these biomolecules is not yet fully understood. In addition, as AMPs can undergo conformational changes upon adsorption onto the bacterial membrane and evolve several mechanisms of action which further complicate the analysis of a structure-activity relationship (SAR), overcoming this gap in understanding may make antibiotic design closer to what is the common structure-based approach for drug design. Taking all these points into consideration, the mechanism of action is crucial to this goal(120).

1.3 Mechanisms of action of AMPs

AMPs have a mechanism of action that differs from the conventional antibiotics which are based on enzyme inhibition(132). Although AMPs can disrupt pathogenic cells in a variety of ways, including inhibiting cell wall, DNA, RNA, and protein synthesis, as well as enzymatic activity(79), the main mode of action of these molecules consists of the perturbation and disruption of cell membranes, leakage of cytoplasmic contents, and consequent cell lysis(72,133–135). Thus, AMPs can exert their antimicrobial activity by employing sophisticated modes of action, which involve interacting with the cell wall, cell membrane, and various intracellular components, as well as inhibiting biofilm formation and modulating the host immune system. The activity of antimicrobial peptides depends on various factors, such as their size, charge, hydrophobicity, secondary structure, or amphiphilic character. The conformation of AMPs may also play an important role in their antimicrobial efficacy.

Furthermore, peptides with amphipathic structures can interact more effectively with the pathogen's membrane.

The antibacterial effects of AMPs acting on the cell wall are primarily mediated by interfering with the synthesis of cell wall components and disrupting the cell wall integrity, for example AMPs that interfere with the biosynthesis of peptidoglycan (PGN)(136); AMPs which may play a damage cell wall integrity by inhibiting the biosynthesis of wall teichoic acid (WTA) or membrane teichoic acid(137), for example, in addition to inhibiting the biosynthesis of PGN precursors lipid I and lipid II, teixobactin - a natural undecapeptide from *Eleftheria terrae* that comprises several uncommon residues including d-amino-acids(138) - can simultaneously inhibit the biosynthesis of teichoic acid lipid III, the main precursor of WTA, thus exerting a bactericidal effect on methicillin-resistant *Staphylococcus aureus* (MRSA)(137). Moreover, some AMPs can induce the release of autolysins that degrade bacterial cell walls(139). Alternatively, AMPs can act on the cell membrane or on intracellular targets(122). A schematic representation of the antibacterial mechanism of AMPs is shown in Figure 4.

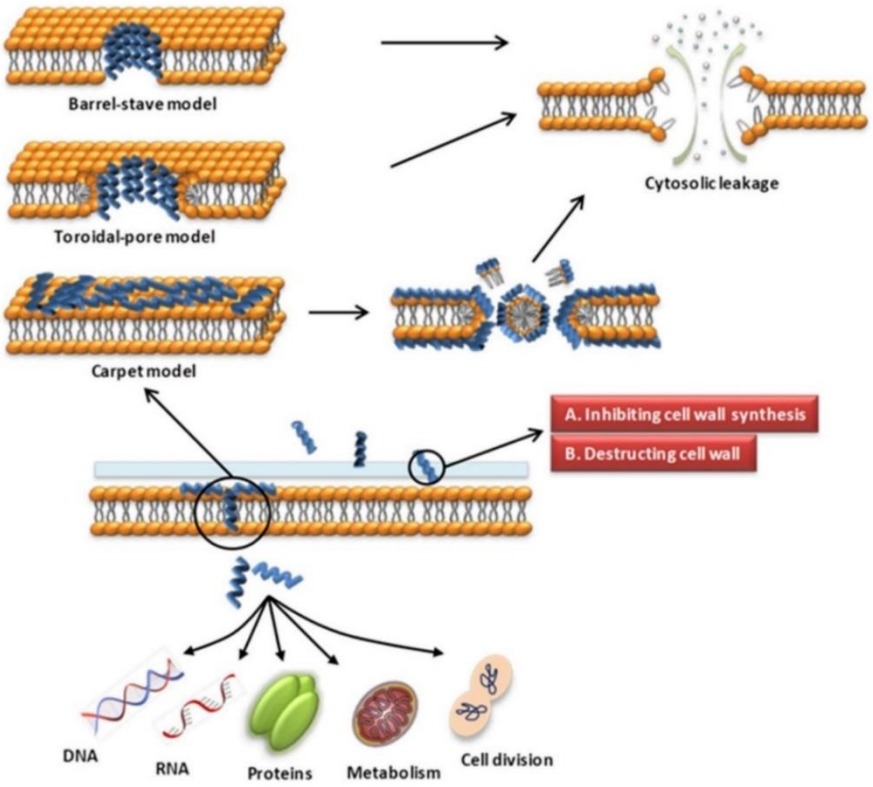

Figure 4. Different modes of action of antimicrobial peptides. AMPs may have direct neutralizing effects on bacteria e.g., by membrane disruption through pore forming or by targeting internal structures of bacteria(122).

The microbial cell membrane is an important target of most AMPs as they act by disrupting the integrity of the pathogen's membrane(63). Besides that, the difference from the mammalian cell membrane composition is a major factor in the selective killing of bacteria by AMPs(79). In the literature, various models have been proposed in the last 25 years that relate the activity of AMPs on the cell membrane to the eventual outcome of osmotic lysis(78). Figure 5 shows different events occurring at the bacterial membrane bilayer following initial AMPs adsorption. The mechanisms of action for AMPs known as the carpet model, barrel model, and toroidal pore model are the most discussed in the literature(140). These models describe the mode of peptide-membrane interaction which leading to pore-formation process based on a common mechanism that basically takes place on a combination of hydrophobic and electrostatic effects(141).

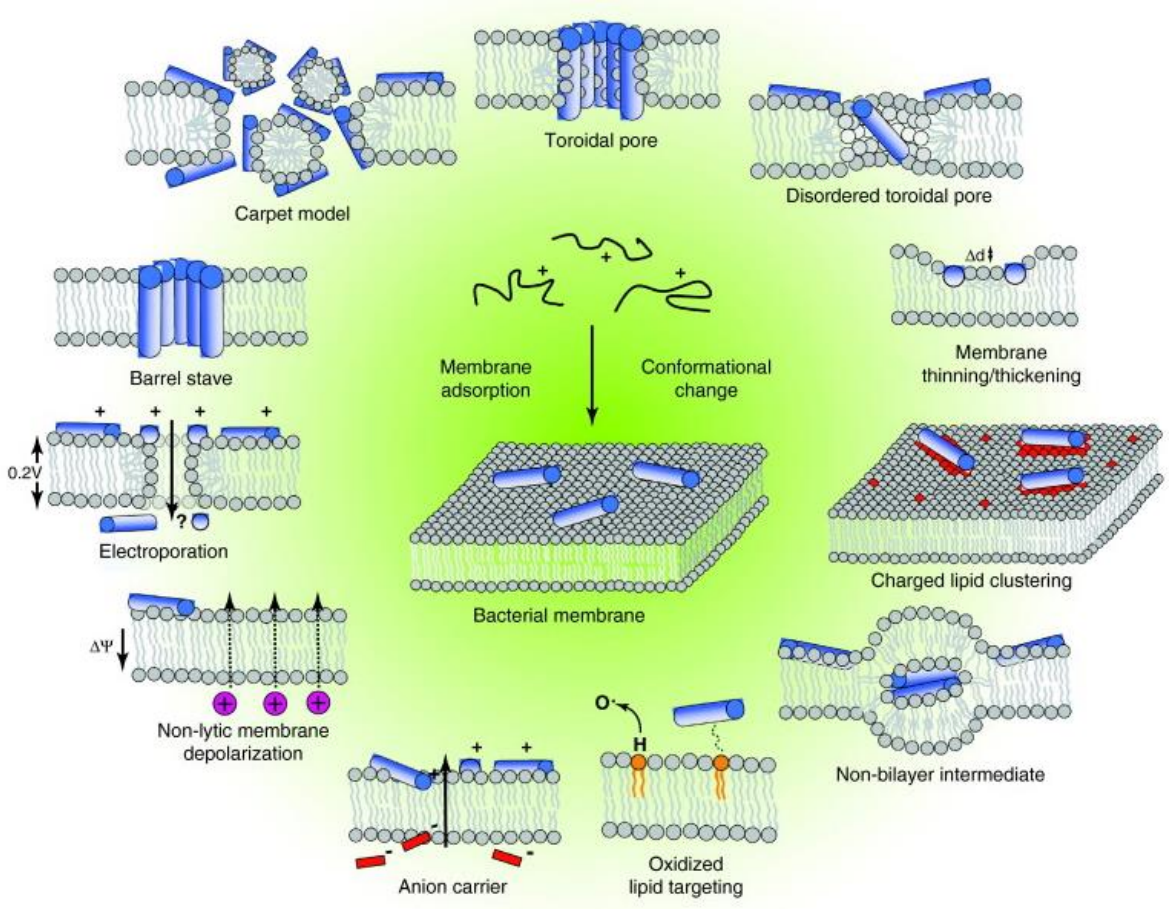

Figure 5. Schematic presentation of the modes of action of AMPs at the bacterial membrane following initial peptide (AMPs) adsorption. Some antimicrobial peptides act on cell membranes through different mechanisms, increasing membrane permeability, leading to leakage of cell contents and cell death as in the classical models of membrane disruption (barrel-stave, toroidal-pore, carpet models)(141).

In the classical models of membrane disruption, the peptides lying on the membrane reach a threshold concentration and insert themselves across the membrane to form either peptide-lined pores in the barrel-stave model(130,142,143). They can also solubilize the membrane into micellar structures in the carpet model, or still form peptide-and-lipid-lined pores in the toroidal pore model. Furthermore, in the revised disordered toroidal pore model, pore formation is more stochastic and involves fewer peptides located near the center of the water-permeable pore(144). The thickness of the membrane can be affected by the presence of the peptides, or the membrane itself can be remodeled surrounding the cationic peptides. In this way, the bilayer is influenced by the AMPs' lateral and orientational motions which affect membrane integrity and function, as observed for the human peptide LL-37, and antimicrobial

frog skin peptide PGLa(142). There are other specific cases, e.g., in which non-bilayer intermediates can be induced in the membrane(145); as well as when the peptide adsorption to anionic membranes can be achieved more strongly when they are targeted to oxidized phospholipids, as evidenced by peptide Temporin L, and Indolicidin peptides(146).

In addition, a set of biophysical approaches have been used to elucidate the mechanisms of action of antimicrobial peptides and their synergism due to interaction with more than one peptide(147). Figure 6 presents some models of peptide-membrane interaction through a set of biophysical approaches elucidating the mechanisms of action of antimicrobial peptides, and their synergism due to interaction with more than one peptide(33,147,148).

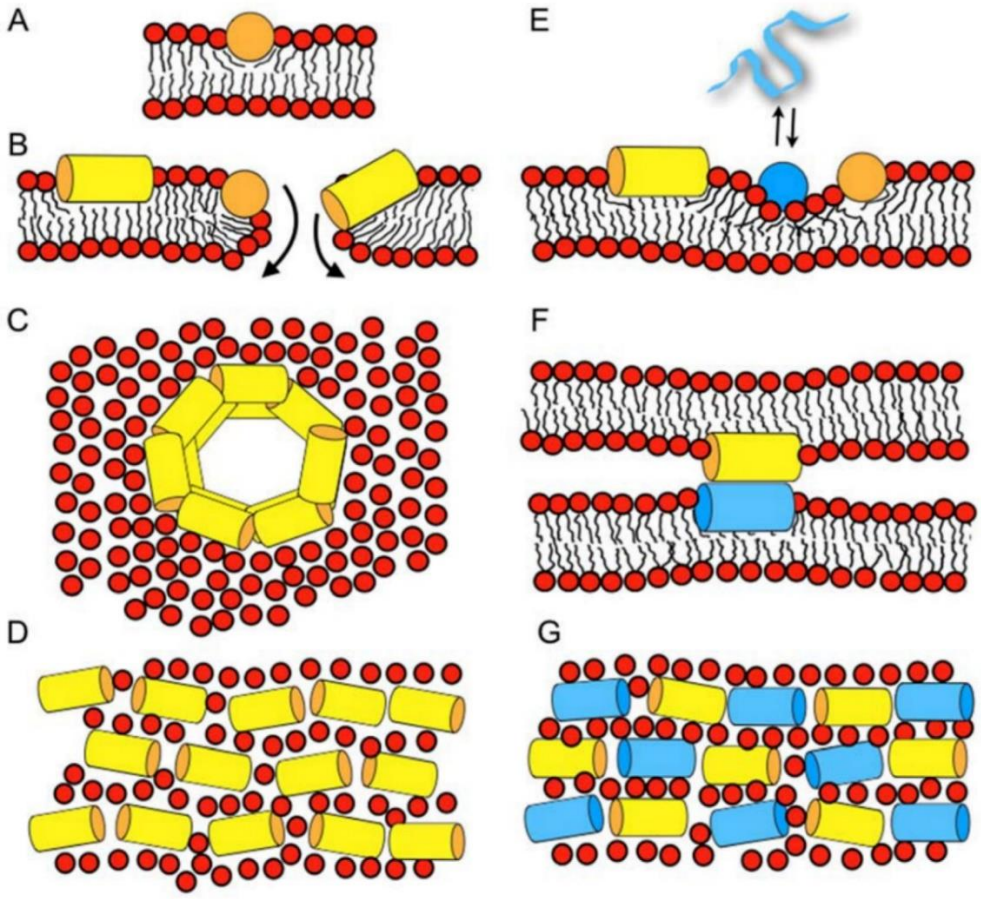

Figure 6. Schematic models illustrating how various biophysical methods have revealed the mechanisms of action of antimicrobial peptides (A-D). Panels A and B show side views, panels C and D top views of the lipid bilayer. Scheme of how two peptides can interact synergistically in a membrane environment (E–G)(147).

The scheme of the mechanism of action presented above is related to different processes of peptide when it reaches the membrane target e.g., Figure 6A illustrates the

interaction of a charged amphipathic peptide with a high hydrophobic moment such as the magainin peptide in which the partition into the membrane interface cause disordering of the lipid packing(148). When the peptide concentration is high enough at least locally, the membrane bilayer can rupture or the membrane disrupts at high peptide-to-lipid ratios(33) [Figure 6B]. Along the openings, peptides can insert and cross in in-planar or tilted alignments. Molecular dynamics of amphipathic helices have been simulated to form double belts(149), an arrangement that also agrees with the in-planar alignment of the peptide helices observed by solid-state NMR spectroscopy, representing another mode of action(150) [Figure 6C]. Figure 6D shows fluorescence quenching experiments that suggest mesophase structures formed by in-plane oriented helices(85). The schemes presented in Figure 6 E-G are related to the membrane disruptive properties in which one peptide (yellow) could help the insertion or approach of another one (blue), which by itself is less likely to partition into membranes(151). As can be seen, the mechanisms of action can be very diverse from peptide to peptide and it also depends on the lipid composition they are interacting.

Although common mechanisms of action have been described for AMPs, several studies have been widespread in recent years, and many new models have been used to describe their mode of interaction(150,151). As an example, the agglutination model has been reported for the antimicrobial peptide thanatin(77,152), in which a micellar complex is formed by the combination of cationic peptides and outer membrane lipopolysaccharides of gram-negative bacteria or cell wall peptidoglycans of gram-positive bacteria(152). In this model, the peptide molecules are not able to penetrate the cell membrane, instead, they induce bacterial membrane agglutination and they are subsequently phagocytized(153). As can be seen, the mechanisms of action can be very diverse from peptide to peptide and it also depends on the lipid composition they are interacting in(33).

Besides employing membrane-disruptive mechanisms, membrane-disruptive AMPs may also exert bactericidal effects through non-membrane disruptive pathways(72). Furthermore, they may function either autonomously or synergistically with non-membrane disruptive AMPs that can penetrate membranes and access their intracellular targets. Such AMPs may interfere with various cellular processes, such as protein-folding, protease activity, cell division, and the biosynthesis and metabolism of proteins, nucleic acids, and cell walls(136).

The results from pre-clinical studies employing AMPs demonstrated that AMPs could be used for the prevention and treatment of various clinical conditions. Nisin, gramicidin,

polymyxins, daptomycin and melittin are currently in clinical use as alternatives to antibiotics because of their antimicrobial potency(143). Nisin, also named nisin A, is a 34-amino acid peptide that comprises dehydrated, unsaturated and thioether amino acids, which form five lanthionine rings. It is naturally produced by lactic acid bacteria such as *Lactococcus lactis* and exhibits a wide-range of bactericidal activity(154,155). Nisins impede cell wall synthesis by interacting with lipid II, a precursor molecule that is essential for bacterial cell-wall bio-synthesis. Nisins also form membrane pores that induce cell lysis(156). The effect of nisin A has been examined in clinical trials using probiotics, which are the ingestion of live microorganisms (e.g., *L. lactis*) that produce nisin A. A systematic review of such trials revealed that these probiotics reduce infectious complications and may consequently lower intensive care unit mortality(157). Pruritus and flushing of the skin, as well as nausea and vomiting, are minor yet potential adverse effects of nisin A. The safety profile along with the broad-spectrum of bactericidal activity, suggested that the application of nisin could transcend food-related bacteria(158,159). Nisins are applied in humans for dental-care and pharmaceutical products such as for the therapy of stomach ulcer and colon infections(143,160).

Gramicidin or gramicidin D is a combination of gramicidin A, B and C peptides constituting 80%, 6%, and 14% of the mixture, respectively. These AMPs are hydrophobic linear polypeptides composed of 15 amino acids(161). They are naturally produced by Gram-positive *Brevibacillus brevis* frequently found in soil(162). Gramicidins form ion-channels within the bacterial membrane, facilitating the passive diffusion of Na+ and K+ along their concentration gradient(163). This leads to membrane depolarization, osmotic swelling, and lysis of bacterial cells. Gramicidin is efficacious against a range of Gram-positive bacteria and is clinically utilized for ophthalmic purposes as a component in Neosporin®. The results of the clinical trial which necessitated an average of 12.5 days for complete re-epithelialization of these ulcers, indicate that Neosporin® containing gramicidin could be employed as an alternative to conventional antibiotics for such ophthalmic purposes(163,164). Polymyxin B is another AMP in Neosporin®.

Polymyxins (A, B, C, D, and E) belong to a class of cyclic polypeptides that are naturally synthesized by the Gram-positive bacterium *Paenibacillus polymyxa*. These AMPs exhibit activity against MDR Gram-negative bacteria, such as Pseudomonas aeruginosa and *Escherichia coli*(164). By binding to the lipid A moiety of lipopolysaccharide (LPS) on the outer membrane of Gram-negative bacteria, polymyxins facilitate the insertion of the AMPs into the membrane(165). This results in increased cell-permeability through a detergent-like

mechanism, leading to cell death(166). Polymyxin B and E, which differ by a single amino acid residue, are the only polymyxins in clinical use(167,168). Polymyxin B is indicated for the treatment of ocular infections, while polymyxin E is employed for the management of wound infections. These AMPs are considered as essential but last-line therapeutic agents due to their potential to cause adverse effects. Although common mechanisms of action have been described for AMPs, several studies have been widespread in recent years, and many new models have been used to describe their mode of interaction(33,150,151,153).

1.4 Membrane models environments

Cell membranes are complex natural barriers that isolate the internal contents from the extracellular environment, and also control the flow of substances with the external environment(169). In general, they are made from phospholipid bilayers in which various other molecules are associated, such as membrane proteins, glycoproteins, steroids, etc(170). Membranes are approximately 7.5-10 nm thick in liquid phase(171), thus an ideal model should be morphologically similar. Due to the high complexity of cell membranes, membrane models have been used as mimetic systems to investigate the interactions with AMPs(172).

Membrane models can be divided into two classes: micelles (detergents) and bilayer (phospholipids), and they can be prepared by self-association of surfactants in aqueous solution(169). Micelles are spherical colloidal aggregates of amphipathic molecules containing a hydrophilic surface and a hydrophobic core. Sodium dodecylsulfate (SDS) and dodecylphosphocholine (DPC) consist of detergent molecules that aggregate above the critical micelle concentration (CMC) to form anionic and zwitterionic micelles, respectively(173). In a polar environment, these molecules spontaneously self-organize in supramolecular structures in which the hydrocarbon chains are oriented toward the interior of the micelles in order to isolate themselves from the aqueous phase(6). On the other hand, the hydrophilic portions are exposed to the aqueous interface and are solvated by water molecules. Cross and coworkers(174) reported that the selection of detergents and phospholipids must take into account both the physical characteristics of the membrane and the characteristics of the equipment used for biophysical and structural analysis(174). SDS and DPC micelles have been successfully used as mimetic membranes in tridimensional NMR solution determining of peptides, integral membrane proteins as well as protein domains(170,175–177). The micellar model is preferred as they are relatively small, which means that they rapidly rotate, on the time-scale required for NMR. Figure 7 presents the most common membrane models.

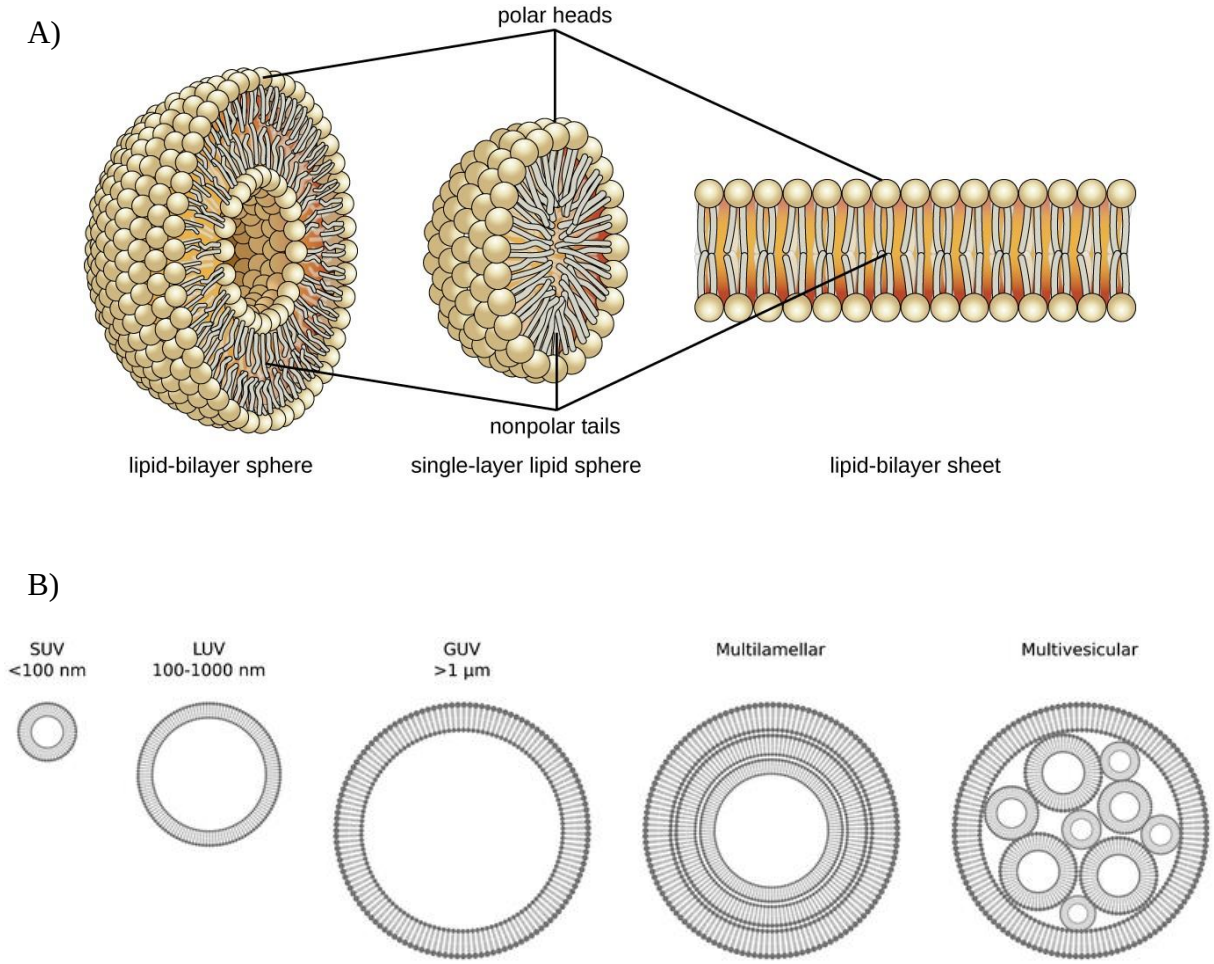

Figure 7. Mimetic membrane models. Structural representation of liposome (left), micelle (middle) and bilayer sheet (right). B) The classification of common vesicle size and lamellarity. In this figure, small unilamellar vesicles (SUV) are less than 100 nm in diameter; large unilamellar vesicles (LUVs) are between 100 and 1000 nm; and giant unilamellar vesicles (GUV) are larger than 1 µm. Multilamellar vesicles (MLV) have many membrane layers, and multivesicular vesicles (MVV) encapsulate smaller vesicles(178).

The lipids that form bilayers give rise to vesicles or flat bilayers. Vesicles are closed bilayer structures formed by phospholipids that organize spontaneously in the presence of water(169). This mimetic model is the most widely used to study the mode of peptide-membrane interaction, including membrane fusion, molecular recognition, pore-forming process, and peptide-membrane translocation(179). According to their preparation, vesicles can have different sizes and be classified as giant unilamellar vesicles (GUVs), large multilamellar vesicles (MLVs), large unilamellar vesicles (LUVs), or small unilamellar vesicles (SUVs)(172,173). LUVs are commonly used as mimetic models in peptide-membrane interaction studies, for example, by using isothermal titration calorimetry, differential scanning calorimetry, fluorescence, and circular dichroism spectroscopy(180–182).

In the model formed by a flat lipid bilayer, the mimetic membrane is supported on a solid surface of mica, glass, or silicon oxide(183). These models allow the investigation of interactions with lipid head groups using a variety of techniques, for example, in studies of peptide topology by solid-state NMR and analyses of interaction kinetics using the SPR technique, which provides detailed information regarding the orientation of the peptide in the bilayer, partition constant and kinetics of the peptide-membrane system under investigation(184). Figure 8 shows structures of some detergents most commonly used in the preparation of micelles as DPC and SDS, as well as lipids such as phosphatidylcholine - POPC (1-palmitoyl-2-oleoyl-*sn*-glycero-3-phosphocholine) and phosphatidylglycerol – POPG (1-palmitoyl-2-oleoyl-*sn*-glycero-3-phosphoglycerol).

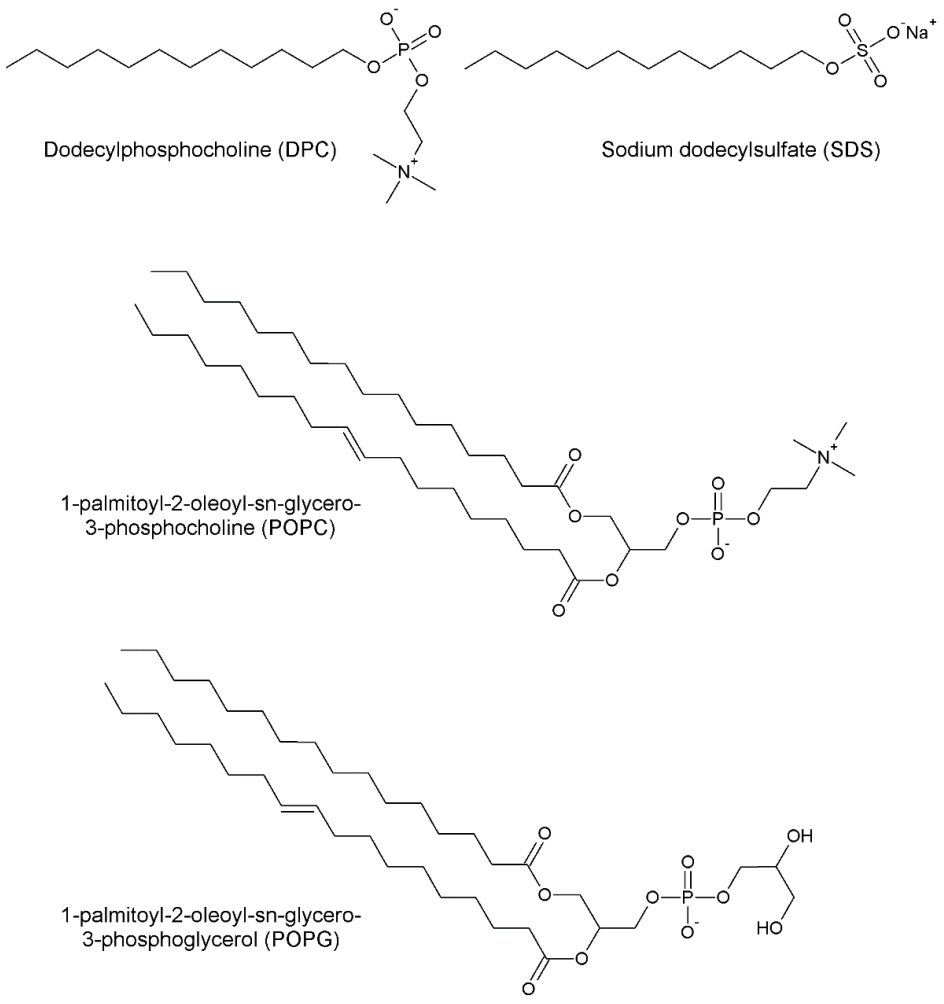

Figure 8. Molecular structures of phospholipids used for membrane models such as vesicles, lipid bilayers, and micelles.

1.5 Piscidin peptides

In recent years the marine environment has been increasingly explored and has become one of the richest sources of antimicrobial peptides(21,34,85). Among the classes of AMPs found in this environment, piscidins have emerged as one of the most important peptide families(185). Piscidin is a type of histidine-enriched AMPs that interacts with lipid bilayers commonly acquiring amphipathic α-helices(101,186). They are natural peptides commonly found in different fish species(187), being responsible for innate immune responses and display broad-spectrum activities against bacteria, fungi, and even viruses(79,188). In addition, piscidins are found in different parts, including mast cells, fish gill, and skin where the peptides exhibit immunomodulatory wound healing properties, and where other neuropeptides are expressed(189,190).

Although piscidin AMPs are still in the early stages of development and have not yet reached the advanced phases of clinical trials there are a few clinical trials involving piscidin AMPs or their derivatives. One of them is a preclinical study in China investigating the efficacy and mechanism of a modified piscidin peptide (Pis-2) against multidrug-resistant *Acinetobacter baumannii* infections(191). There are also some studies that report the synthesis and optimization of piscidin analogs, for instance, tilapia piscidin 3 (TP3) and tilapia piscidin 4 (TP4) for enhancing their stability, specificity, and bioavailability against *K. pneumonia* and multi-drug resistant *A. baumannii*(192). These trials suggest that piscidin-derived peptides have potential as novel antimicrobial agents against resistant bacteria. However, more studies are needed to confirm their safety and efficacy in humans.

Another example is the antimicrobial peptide Tilapia Piscidin 4 (TP4) which has shown broad-spectrum of antimicrobial activity, as well as anticancer, immunomodulatory, and wound-healing properties(190). The histidine-enriched nature of piscidins allows them to interact with lipid bilayers and exhibit pH-dependent permeabilization when their positive charge increases in acidic environments(133). Tilapia Piscidin 4 (TP4) is derived from fish Nile tilapia (*Oreochromis niloticus*) that presents antibacterial, antibiofilm, and wound healing properties(193). The antimicrobial peptide TP4 is not yet approved by the FDA, but it is in clinical trials for the treatment of *bacterial vaginosis* (BV), a common vaginal infection caused by an imbalance of bacteria. BV is prevalent among women of reproductive age and has a high rate of recurrence, which can be largely attributed to ineffective BV biofilm eradication by

current first-line antibiotics(194). In a previous study, tilapia piscidin 4 (TP4) exhibits broad-spectrum antimicrobial and antibiofilm activity against BV-associated bacteria, but not beneficial lactobacilli. The clinical trial aims to evaluate the safety, side effects, and maximum tolerable dose of TP4 in women with BV. Another piscidin peptide which is being tested in clinical trials are named chionodracine. This is a piscidin peptide isolated from the icefish *Chionodraco hamatus* which has presented strong activity against Gram-positive bacteria, including methicillin-resistant *Staphylococcus aureus* (MRSA)(102) as well as it also has shown anti-tumor activity against human melanoma cells. It is currently being evaluated for its safety, side effects, and maximum tolerable dose in a phase I clinical trial.

In this thesis, we focus on the mode of action and biological activity of natural piscidin peptides namely Piscidin-4s (ecPis-4s), Piscidin-2s (ecPis-2s), and an epimeric form of the ecPis-2s. The natural peptides were first isolated from *Epinephelus coioides* (orange-spotted grouper, also known as the estuary cod), a fish commonly found in Asian seas(195). These peptides presented high activity against gram-positive *(Staphylococcus aureus)* and gram-negative *(Escherichia coli, Vibrio Parahaemolyticus)* bacterial strains. Orange-spotted grouper (*E. coioides*) is also the source of other peptides such as epinecidin-1 (Epi-1)(196), which has shown effective activity against a wide range of bacterial and viral infections and exhibits immunomodulatory effects(196,197).

The peptides ecPis-4s (FFRHIKSFWKGAKAIFRGARQG-NH_2) and ecPis-2s (FFFHIIKGLFHAGRMIHGLV-NH_2) are 22 and 20 amino acid residues long, respectively, and are capable to arrange in amphipathic structures(195). As mentioned, in addition to the natural sequences, we proposed the synthesis of an ecPis-2s epimer by replacing the second L-Phe2 by a D-Phe2 residue, which was named D-ecPis-2s. As observed for other piscidin peptides, they are cationic (net charge equal +7 and +3, for ecPis-4s and ecPis-2s, respectively), linear, presenting amphipathic α-helical structures with a high proportion of aromatic residues(195). To further understand the mechanism of action of these peptides, this study has evaluated the mode of membrane interaction of both ecPis-4s and L-ecPis-2s as potential templates of therapeutic agents against pathogens, as well as the effect of epimerization of D-ecPis-2s in the antimicrobial activity and membrane interaction.

Outline of the chapters content

This thesis provides a further investigation of the piscidins peptides in different negative membrane models as well as in aqueous and buffered solutions. Despite some similarities, such as size of the polypeptide chain and conservation in the position of some amino acid residues, these peptides show different structural and interaction aspects. Thus, the results of the studies are presented in three different chapters.

In the first one, Chapter 3, the mode of membrane interaction of ecPis-4s was investigated in the presence of POPC:POPG (3:1, mol:mol) vesicles and bicelles; and SDS micelles. CD spectroscopy was used in order to evaluate the conformational preferences, while solution and solid-state NMR experiments were performed to obtain information related to the three-dimensional structure in high resolution, and the topology of ecPis-4s when interacting with the anionic membrane. Additionally, fluorescence, ITC, dynamic light scattering (DLS), and zeta potential were used to investigate the effect of ecPis-4s in the phospholipid membranes and to determine the partition constant in the presence of anionic models.

The second investigation of this work, Chapter 4, is also related to ecPis-4s piscidin peptide. Nevertheless, the investigation of the peptide-peptide interaction was performed only in the buffered or aqueous environment. In order to investigate the effect of concentration on the conformational preferences of ecPis-4s peptide, CD experiments were performed at the different concentration ranges in water and in the presence of 10 mM phosphate buffer at pH 6.0 and pH 8.0. The high-resolution structure was also obtained in aqueous media by solution NMR. Besides that, ecPis-4s peptide behavior as a function of its concentration was further characterized using diffusion-ordered spectroscopy (DOSY), and deuterium exchange by liquid state NMR. To access the hydrodynamic, self-association, aggregation, and stability of ecPis-4s peptide in buffered solution, sedimentation Velocity (SV) assays by Analytical ultracentrifugation (AUC) were performed. Moreover, proteolysis experiments were also performed in order to get information related to the peptide resistance to proteinase K and trypsin enzymes as a function of the peptide concentration. Finally, death time curves of the S. aureus bacteria strain with ecPis-4s peptide were carried out with or without proteinase K enzyme.

The last research chapter of this thesis, Chapter 5, concerns the studies of L-ecPis-2s and D -ecPis-2s epimers. The idea of this research is to better understand the mode of action of

D- and L-ecPis-2s, comparing the influence of the D-amino acid on the mechanism of action of the epimers when interacting with anionic membranes. Therefore, investigations on the structure and interaction in the presence of negative membranes for both epimers peptides have been carried out, including structural techniques such as CD, liquid, and solid-state NMR spectroscopies. In addition, biophysical assays such as isothermal titration calorimetry (ITC), differential scanning calorimetry (DSC), zeta potential (ζ), and carboxyfluorescein leakage (CF) were carried out to further investigate the interaction of L- and D-ecPis-2s peptides. Furthermore, antibacterial activity assays were also done against gram-positive and gram-negative strains to investigate the antimicrobial activity and the effect of structural distinction for ecPis-2s epimers.

Finally, we conclude this thesis by summarizing all the information to get an overview as well as define the next steps and perspectives for this work.

Chapter 2: Techniques

Investigations of the peptide structure and biophysical approaches to study peptide-membrane interactions

2.1 Circular dichroism spectroscopy

Circular dichroism (CD) spectroscopy is one of the most common methods to provide structural information on polypeptides as it is an excellent method to rapidly evaluate the secondary structure in aqueous solutions(198). CD is based on the differential absorption by chromophore groups of one of the circular components of plane-polarized light(199). The conformation adopted by peptides and proteins produces bands in defined regions of the spectrum as a result of electronic excitation in the chromophore groups. In peptides, the amide group (R-(C=O)-NH-R') corresponding to the peptide bond is the most important chromophore. This difference in light absorption is defined as ellipticity, which can take on positive or negative values. Thus, it is possible to monitor the secondary structure acquired by peptides in aqueous solutions and when interacting with model membranes(200).

The intensity of the absorptions depends on the values adopted for the φ and ψ dihedral angles [Figure 9], since these angles define the coplanarity conditions of the orbitals involved in the peptide bond. As the values of these angles depend on the intramolecular interactions, the state of aggregation, and the interactions with the solvent, the absorption is conformation dependent. Therefore, CD spectrum presents characteristic dichroic line shapes depending on the peptide structure.

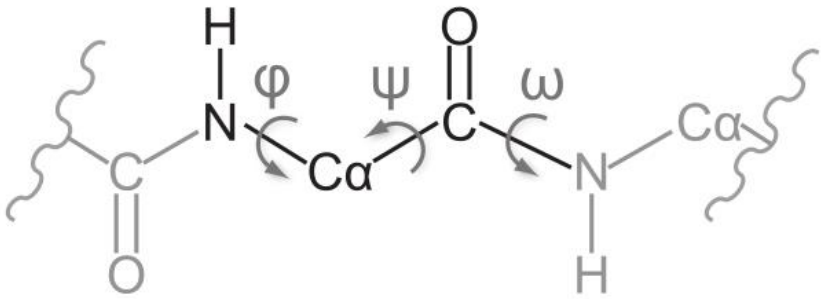

Figure 9. Backbone torsion angles of an amino acid in a peptide chain(201).

Through the CD study, it is possible to infer the predominance of α-helix, β-sheet, or random coil secondary structures. In general, *α*-helical structures present a double minimum at 208 and 222 nm, whereas a single minimum at 196 nm or 217 nm reflects random-coil or *β*-sheet structures, respectively(198). Figure 10 presents the standard CD spectra for peptides at these conformations.

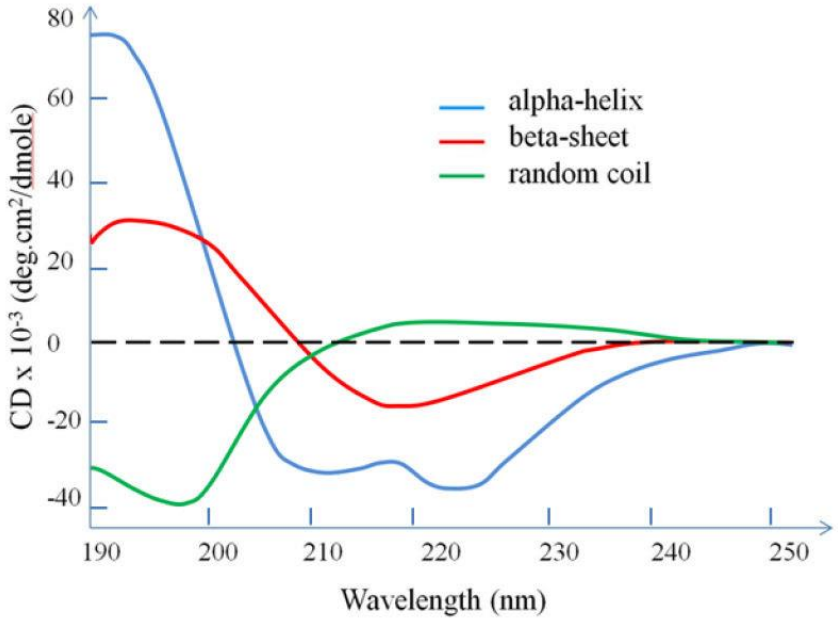

Figure 10. CD spectra reveal line shapes characteristic of the secondary structure. Helices exhibit negative peaks at 222 and 208 and a positive peak around 190 nm; β-sheet proteins have a negative peak around 218 and a positive peak around 195; and a random coil has a negative peak around 200 nm. Ellipticity values are displayed as a function of the wavelength of the applied UV light. The standard spectra shown are specific for different secondary protein structures(202).

2.2 Solution NMR spectroscopy

The characterization of three-dimensional structures of proteins and peptides is fundamental for understanding their structure-activity relationship(203). Solution NMR is an important tool for the structural determination of biomolecules(204,205). The use of two-dimensional solution NMR to obtain three-dimensional structures began to be intensively explored in the 80s, using theoretical methods and computer simulations(206).

Although membrane models are a simplified representation of the cell membrane environment, they make it possible to analyze important parameters for studying the mechanism of interaction between peptides, proteins, and membranes as well as structural aspects and conformational dynamics(6,169). Kawano and coworkers presented one of the first three-dimensional NMR structures of peptides isolated from marine animals, the peptide tachyplesin I (PDB - 1WO0), a 17-residue antimicrobial cationic peptide found in hemocyte cells of the horseshoe crab *(Tachypleus tridentatus)* (207). The structure was obtained in aqueous solution based on the nuclear Overhauser effect, the coupling constant, and the rate of exchange of amide hydrogens with deuterium. The result of the three-dimensional structure [Figure 11] showed that tachyplesin I, has a defined structure made up of two disulfide bonds (Cys3-Cys16 and Cys7-Cys12) which stabilize an antiparallel β-sheet fold. As can be seen in Figure 11, the bulky hydrophobic side chains are located on one side of the β ribbons, while the cationic side chains are distributed on the other side. It also presents a schematic structure of the three-dimensional of tachyplesin I peptide(207).

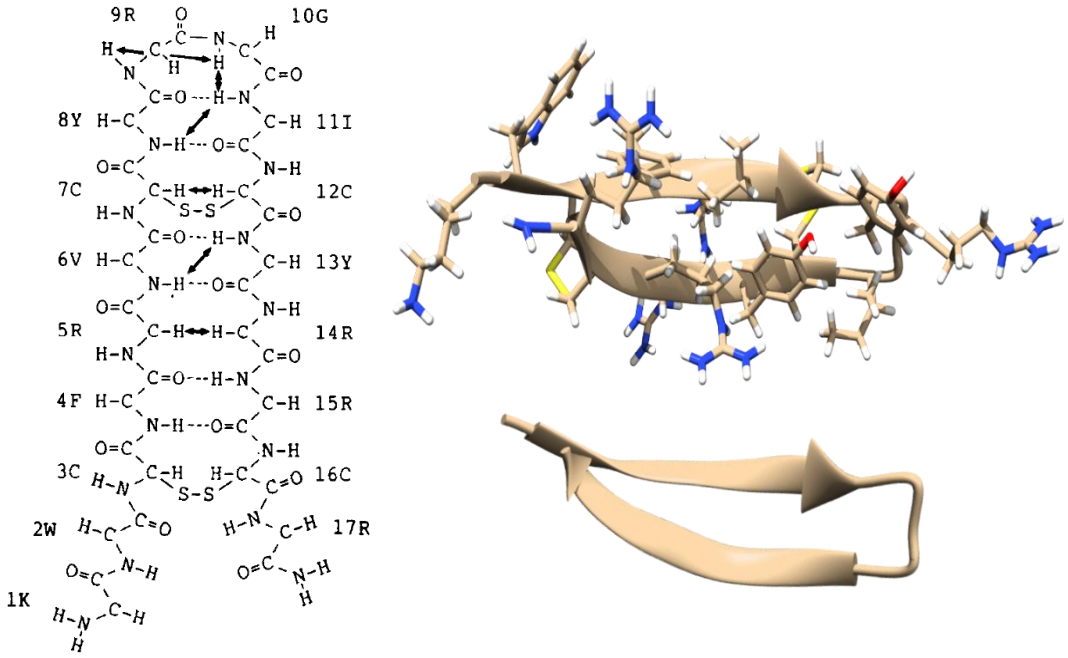

Figure 11. Cationic tachyplesin I peptide. A) Representation of the antiparallel β-sheet structure deduced from analysis of the NMR data; (B) Three-dimensional structure of the peptide tachyplesin I (PDB-1WO0) with its respective side chains and (C) without the side chains.

Solution NMR spectroscopy has played an important role in elucidating three-dimensional structures as well as understanding the interaction process of antimicrobial peptides. To elucidate protein and peptide structures using solution NMR four main factors are required: (a) development of multidimensional techniques; (b) methodologies for sequential assignment of resonances; (c) conversion of NOE (Nuclear Overhauser Effect) signals into conformational restrictions and (d) interpretation of conformational restrictions(203).

The sequential assignment methodology developed by Wüthrich(208) is based on the identification of unique spin systems in polypeptide and nucleic acid chains. Sequential assignment makes it possible to distinguish between signals from spin systems obtained from ^{1}H-^{1}H-TOCSY (Total Correlation Spectroscopy) spectra and spatial or distance couplings observed in ^{1}H-^{1}H-NOESY (Nuclear Overhauser Spectroscopy) spectra. Thus, by combining the intraresidual correlations obtained by bond couplings (J coupling) and distance restrictions, we can use molecular dynamics calculations to obtain the three-dimensional structure of the molecule under analysis. Besides that, HSQC (Heteronuclear Single-Quantum Correlation) and HMQC (Heteronuclear Multiple-Quantum Correlation) experiments can be used to determine or for the improvement of the three-dimensional structure of peptides and proteins. These

techniques are employed to assign heteroatoms and consist of magnetization transfer via ^{1}J scalar coupling, for example, between ^{1}H and ^{13}C, or ^{1}H and ^{15}N. In addition, chemical shift data obtained by these techniques can provide dihedral angle restrictions and also assist in the complete assignment of TOCSY and NOESY spectra, resolving ambiguities between nuclei with the same or similar chemical shifts(172).

Geometric restrictions obtained from the interpretation of spectra are important parameters for obtaining three-dimensional structures. The distance constraints (NOE) result from the transfer of magnetization that occurs through space between different nuclei at a distance less than 5.5 Å(209), even when they are distant in the primary structure of the peptide. Although it is possible to calculate the volume of NOE signals from the integral of the area in the spectrum, it is more common to classify them manually according to their intensity as strong (upper distance constraint of 2.8 Å), medium (3.4 Å), weak (5.0 Å)(210,211). To determine the ϕ and ψ dihedral angle restrictions, the ^{3}J type scalar coupling constant values are used. These values are obtained from the chemical shifts of the peptide's backbone from two-dimensional experiments(212). The conversion of chemical shift data into dihedral angle constraints is carried out by the TALOS+ program(213), making it possible to accurately determine the angular constraints of the target molecule.

The structures can be then obtained by a semi-quantitative analysis using the information from structural constraints with the application of simulated cooling (SA) calculations(214). SA is a procedure for minimizing energy to overcome local barriers by molecular dynamics. In short, the temperature in this simulation is raised to 1000 K, providing high kinetic energy to the system, followed by 6000 cooling steps until a temperature of 100 K is reached, and consequently low kinetic energy values(215,216). The structures obtained have ϕ and ψ dihedral angles which are restricted by molecular steric factors(215), and are used as indicators of structural quality based on the Ramachandran plot(206). This diagram shows regions whose combination values between the restriction angles ϕ and ψ are classified into favored, allowed, and "generously allowed" and prohibited regions. The favorable regions correspond to the best quality conformations of the structures. The allowed regions in turn indicate conformations at the limit of the Van der Waals radius. The less allowed or generously allowed regions suggest allowed conformations, but with greater conformational dynamics around the bond angles. Finally, the forbidden or non-allowed regions correspond to conformations in which the ϕ and ψ angles take on forbidden values due to the steric effect.

In addition to the Ramachandran diagram, the variability of the molecular coordinates can be calculated from the root mean square standard deviation (RMSD). This parameter can be used as a measure of the degree of convergence between the lowest energy structures obtained in the structural calculation. In general, low RMSD values indicate more accurate results and greater convergence or similarity between the overlapping structures. However, high RMSD values may reflect high conformational dynamics(217).

Therefore, solution NMR is an essential technique with great information power at the atomic level in studies of peptide and protein structures, since access to the three-dimensional structure with high sensitivity helps us to interpret and understand the mechanism of these molecules which is an important step in the development of new drugs and antimicrobial agents(218).

2.3 Solid-state NMR spectroscopy

Solid-state NMR (ssNMR) spectroscopy of oriented bilayers is used to identify the topology adopted by peptides in membrane models. This orientation refers to the tilt angle of the helical peptide in relation to lipid bilayer as well as the polar angle of internal rotation of the helix, the pitch angle. This technique provides valuable information regarding dynamics, the local environment, and molecular structure(219). Differently from solution NMR spectroscopy, in which fast molecular tumbling provides an isotropic average of the nuclear interaction, in ssNMR the chemical shifts, dipolar interactions, and quadrupolar splittings depend on the molecular alignment relative to the magnetic field(220).

The chemical shift in ssNMR spectroscopy is mathematically described as a tensor, represented by an ellipsoid, as shown in Figure 12. This tensor is defined in a Cartesian axis system so that it can be then represented by the three components (σ_{11}, σ_{22} and σ_{33}) for the ^{15}N nucleus relative to the main axis of the helical peptide structure [Figure 12]. The chemical shift recorded by the spectrometer is called σ_{zz} and it is defined as the projection of the tensor component σ_{33} onto the axis of the external magnetic field.

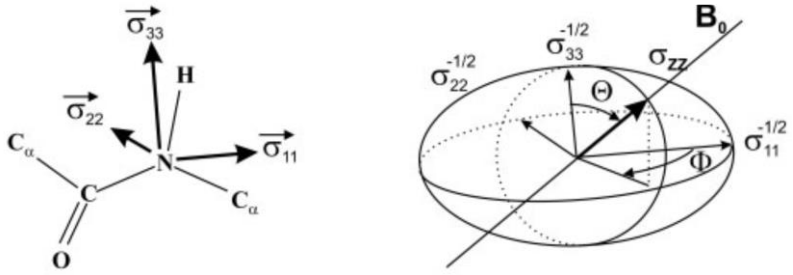

Figure 12. Representation of ^{15}N chemical shift tensor as an ellipsoid of a peptide bond. B) coordinate system by applying rotations with the three Euler angles (Φ, Θ). The ^{15}N chemical shift is a direct indicator of the approximate alignment of the helix with respect to the membrane surface(221).

Using the Euler angles (Φ, Θ, Ψ) to describe transformations of the chemical shift tensor in other coordinate system, it is possible to obtain the angular relation of σ_{zz} with Φ and Θ, as presented in Equation 1.

$$\sigma_{zz} = \sigma_{11}\sin^2\Theta\cos^2\Phi + \sigma_{22}\sin^2\Theta\sin^2\Phi + \sigma_{33}\cos^2\Theta \quad (1)$$

As the σ_{33} component of the ^{15}N chemical shift tensor exhibits an alignment approximately parallel to the main axis of α-helical polypeptides(222), it is then possible to define the angle Θ as the angle designed between the main axis of the helix and the external magnetic field, B_0. For samples in which the normal of the phospholipid bilayer is aligned parallel to B_0, Θ must be considered to refer to the angle between the main helix axis and the normal of the lipid bilayer. As a result of the dependence between the orientation of the peptide and the chemical shift of ^{15}N, this property is a sensitive indicator of the alignment of the helix with respect to the membrane surface or the lipid bilayer, making it possible to infer information on the topology of the peptide-membrane interaction(223). Therefore, ^{15}N chemical shift provides an approximate tilt angle of helical domains(221), in which a transmembrane α-helical peptide exhibits ^{15}N resonances with chemical shifts around 200 ppm, as observed in Figure 13. On the other hand, peptides oriented parallel to the membrane surface are characterized by chemical shifts < 100 ppm [Figure 13](222).

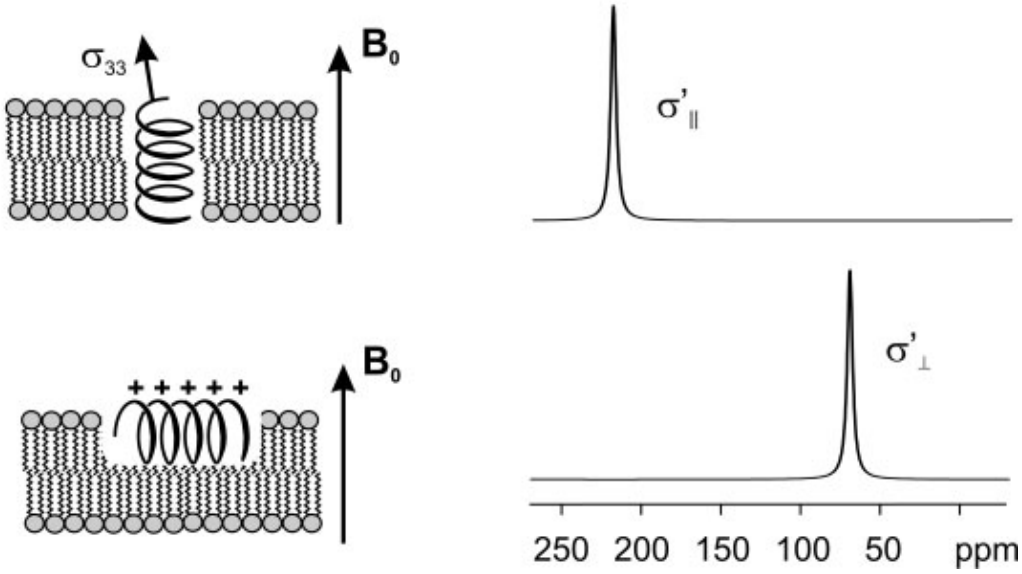

Figure 13. Simulated proton-decoupled ^{15}N solid-state NMR spectrum of a transmembrane peptide as well as for a peptide orientated parallel to the membrane surface(221).

Whereas the ^{15}N solid-state NMR signal of labeled peptide bonds are direct function of the α-helix alignment relative to the lipid bilayer normal/B_o-vector (tilt angle)(220), additional ^{2}H solid-state NMR spectra from methyl-deuterated alanines allow the determination of accurate tilt and pitch angles(224,225).

Because of fast rotation around the C_α-C_β bond the three methyl deuterons are equivalent(222) in which the resulting ^{2}H tensor is axially symmetric with respect to the C_α-C_β bond vector. Therefore, the measured splitting $\Delta\nu_Q$ is directly related to the angle Θ describing the orientation of the C_α-C_β bond relative to the magnetic field direction. Furthermore, in hydrated liquid crystalline membranes, the lipids and peptides freely diffuse about the membrane normal, therefore, the deuterium quadrupolar splitting also depends on the angle β between the membrane normal and the magnetic field direction. The averaged quadrupolar splitting is given by

$$\Delta\nu_Q = \frac{3}{2}\,\frac{e^2qQ}{h}\,\frac{(3\cos^2\theta-1)}{2}\,\frac{(3\cos^2\beta-1)}{2} \qquad (2)$$

where e^2qQ/h is the static quadrupolar coupling constant(226).

As the C_α carbons are an integral part of the polypeptide backbone, the orientation of the C_α-C_β bond also reflects the overall alignment of the peptide. The results provided by ^{15}N and ^{2}H NMR are complementary and are used to describe the orientation of the helical peptide in the presence of the phospholipid bilayer.

2.4 Isothermal titration calorimetry

In combination with the three-dimensional structures obtained from NMR experiments, the thermodynamics of peptide-membrane interaction is fundamental to understanding the mode of action of AMPs. Isothermal titration calorimetry (ITC) allows to study of the association of peptides with membrane mimetic vesicles and micelles, and it provides important data on the thermodynamic process of interaction such as enthalpy variation (ΔH^0), interaction constant (K), and Gibbs free energy variation (ΔG^0)(227).

ITC is one of the most widely used techniques in the thermodynamic analysis of biomolecular systems(228). The increasing use of the technique can be explained by the development of high-sensitivity microcalorimeters that allow the measurement of interactions at low concentrations (μM), followed by the diffusion of calorimetric methods in biophysics and molecular biology(229). Furthermore, ITC is based on the analysis of the binding interaction carried out at constant temperature in which only thermal effects are measured(230). Considering that the association of peptides with membrane models involves the disruption and formation of intermolecular interactions and that there is a heat flow associated with these phenomena, ITC becomes very useful in such investigations(6). Heat is a universal signal and practically all types of chemical and physical processes are accompanied by absorbed or released heat(231).

The microcalorimeter equipment consists of a thermal core with a titration and a reference cell, both identical [Figure 14]. The titrant is added to the injection syringe which automatically injects it into the reaction cell and also works as a stirrer to homogenize the solution in the reaction cell. The temperature between the sample and reference cells is kept constant. For this, the reference cell is kept under constant heating, while in the reaction cell, the heating is adjusted at each injection in order to correct the difference in the temperature between the cells after an exothermic (heat released) or endothermic (heat absorbed) process

that occurs during molecular binding events in the reaction cell. With each injection, the heat involved in the interaction is measured as a function of time.

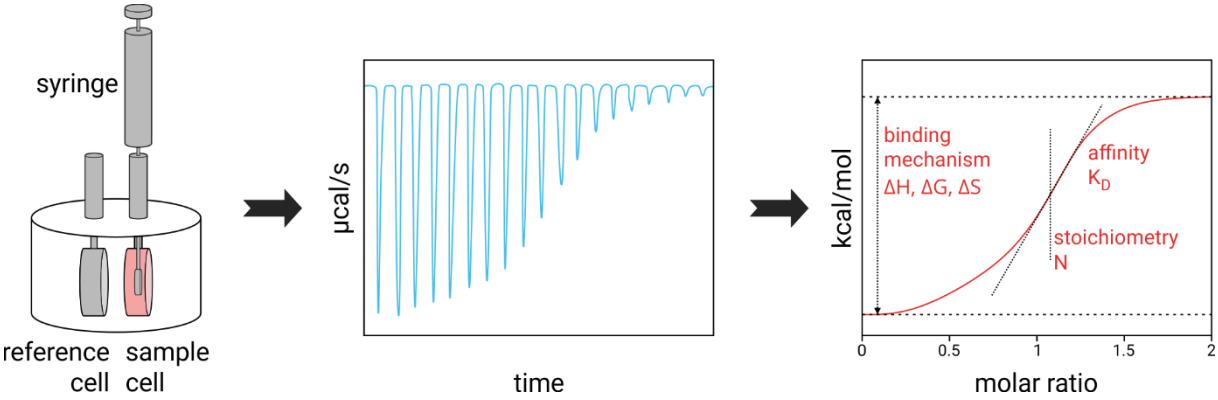

Figure 14. Basic principle of isothermal titration calorimetry. Schematic representation of the isothermal titration calorimeter (left) and a characteristic titration experiment (middle) with its evaluation (right). In the picture in the middle, the titration thermogram is represented as heat per unit of time-released after each injection of the ligand into the protein (blue line). In the plot on the right, the dependence of released heat in each injection versus the molar ratio between total ligand concentration and total protein concentration is represented.

In the model presented [Figure 14], each signal represents the heat change caused by a single injection of the titrant which, in this case, is exothermic represented by a negative deflection. Thus, an exothermic reaction causes an increase in temperature in the sample cell to the reference cell which results in a decrease in the heat flow supplied to the reaction cell to stabilize the calorimeter cell system(227). As the temperature of the two cells becomes equal, the signal returns to its initial position or initial heat values. Once the titrant becomes saturated with the titrant, smaller amounts of titrant will bind to the titrant as injections into the reaction cell continue, and therefore less heat will be generated. At the end of the experiment, the low heat values generated are due to the heat of dilution.

2.5 Dynamic light scattering (DLS) and zeta potential measurements

Dynamic light scattering measurements are based on studying the scattering of light caused by the Brownian movement of particles and measuring the amount of scattered light(232). In Brownian motion, larger particles move slowly, while smaller particles move faster. Thus, these cause greater light scattering, since they reach the detector more frequently than larger particles(232,233). The hydrodynamic diameter is obtained from the hydrodynamic radius, which in turn is related to the translational diffusion coefficient as shown in Stokes-Einstein equation.

$$D_t = \frac{k_B T}{6\pi\eta R_h} \quad (3)$$

where Dτ is the translational coefficient of diffusion, k_B the Boltzmann constant, T the temperature, η the viscosity of the medium and R_h the hydrodynamic radius(234). Thus, applying the equation it is then possible to determine the average hydrodynamic diameter of the particles in suspension.

In peptide-membrane interaction it is common to monitor the hydrodynamic diameter of phospholipid vesicles before and after adding antimicrobial peptides to the vesicle medium(235), thus, it is possible to measure the influence of the peptide in the hydrodynamic diameter of the target membrane. On the other hand, and under similar experimental conditions, ζ-potential can also be calculated by observing the electrophoretic mobility of phospholipid vesicles after the application of an electrical potential. This result, in addition to the effect of the peptide on ζ-potential of the vesicles can also be used to calculate the partition constant when titrating phospholipid vesicles with peptides, as has already been done for peptides as BP100(236,237).

To estimate the *K*p of peptides in membranes, peptides must be titrated into the vesicles and the results obtained are used in mathematical treatment. The values obtained in the method have been compared with those observed by fluorescence spectroscopy. The results have shown that ζ-potential is an effective technique for quantifying peptide-lipid interactions in a variety of charged molecules, overcoming the limitations of other techniques, such as the need for a fluorescent marker in fluorescence spectroscopy(236).

Chapter 3: Elucidating the mode of interaction and concentration-dependent membrane disruption of the antimicrobial peptide ecPis-4s

3.1 Introduction

Antimicrobial peptides (AMPs) play important roles in the innate immune system of several organisms. Most AMPs carry a positive net charge and electrostatic interactions result in their selectivity towards bacterial membranes(5,178). Although the vast majority of AMPs shows no conformational preferences in aqueous environments, most of them usually adopt a well-defined amphipathic α-helical structure in the presence membrane mimetic interfaces(7). Such structural behavior is indicative of direct actions on the microbial membrane, and so far, some theoretical models have been proposed to describe the membrane interactions of AMPs(9,10,238). Thereby, the arrangement of the peptide sequence and the organization of the amino acid side chain into an ordered structure has been described as fundamental to the biological activity of several peptides towards bacterial membranes(8).

Piscidins are host-defense peptides mainly found in fish. Originally isolated from hybrid striped bass (white bass, *Morone chrysops*, female and striped bass, *Morone saxatilis*, male), these molecules were recognized as important effectors of innate immune responses(239). Piscidins are present in different types of cells and tissues, including at mucosal surfaces of the skin, gills and the alimentary canal(240,241), and it is known that infection by pathogens may boost gene expression of these compounds(79,242,243). These peptides constitute a large family of highly active AMPs with broad-spectra antimicrobial activities(34,79).

Some structural properties of the piscidins are closely related, such as cationic charges, conserved amino terminus, and a high number of histidine residues within the peptide primary structure(239). The main focus of this work is on ecpiscidin-4s (or ecPis-4s) (FFRHIKSFWKGAKAIFRGARQG-NH_2). This piscidin was originally isolated from *Epinephelus coioides* (orange-spotted grouper), a fish commonly found in Asian seas, this

peptide showed biological activity against gram-positive and gram-negative bacteria as well as fungi(195).

Solution and solid-state NMR (ssNMR) spectroscopy have been widely used to investigate the structure and topology of AMPs in membrane models(220,221,244–246). Considering the relatively small number of structural data available for piscidins as well as aspects regarding the interactions of these peptides with membranes multidimensional solution NMR and solid-state NMR spectroscopies were used to determine the high-resolution structure of ecPis-4s in presence of anionic SDS micelles as well as the peptide topology in the presence of negatively charged 1-palmitoyl-2-oleoyl-*sn*-glycero-3-phospholcholine (POPC): 1-palmitoyl-2-oleoyl-*sn*-glycero-3-phospho-(1'-rac-glycerol) (POPG) (3:1, mol:mol) lipid bilayers to model the composition of bacterial membranes.

Thus, in this chapter the structure and membrane topology of ecPis-4s is presented. In addition, the biophysical features of the peptide-membrane interaction have been assessed by fluorescence spectroscopy, dynamic light scattering (DLS), zeta potential, and leakage measurements. Furthermore, the thermodynamics of the binding process was also investigated by isothermal titration calorimetry (ITC). Taken together, the results reveal molecular features of the peptide that may affect the lipid assembly/structure, the location of the peptide in the bilayer, its membrane-destabilizing capability, and the antimicrobial potency of ecPiscidin-4 and ultimately its mechanism of action.

Finally, we propose the mode of action of ecPis-4s in presence of anionic membrane. For that, a huge biophysical and structural characterization was done in order to obtain enough data to elucidate the interaction process of ecPis-4s peptide. All the experiments were homemade, except the simulations of ssNMR data. Both geometry alignments and simulations of the membrane topology were analyzed in collaboration with the Department of Chemistry of the Federal University of Minas Gerais, using a homemade program developed in one of our teamwork laboratories.

3.2 Materials and Methods

3.2.1 Peptide synthesis, purification and characterization

ecPis-4s peptide as well as two selectively labeled analogues [Table 1] were manually synthetized through solid-phase synthesis via the 9-fluorenylmethyloxycarbonyl (Fmoc) strategy(247), on a Fmoc-Rink Amide® polystyrene resin (0.68 $mmol.g^{-1}$) from NovaBiochem® (Darmstadt, Germany). For the solid-state NMR experiments, selectively labeled ecPis-4s* (3,3,3-$^{2}H_3$-Ala-12, ^{15}N-Leu-14) and ecPis-4s** (^{15}N-Ala-12, 3,3,3-$^{2}H_3$-Leu-14) peptides were prepared by the incorporation of Fmoc-3,3,3-$^{2}H_3$-Ala-OH and Fmoc-^{15}N-Ala-OH derivatives during the respective coupling reactions.

Table 1. The primary sequence and the isotopic labeling of synthetized ecPis-4s peptide

Peptide	Sequence labeling
ecPis-4s	FFRHIKSFWKGAKAIFRGARQG-NH_2
ecPis-4s*	FFRHIKSFWKG<u>A</u>K**A**IFRGARQG-NH_2
ecPis-4s**	FFRHIKSFWKG**A**K<u>A</u>IFRGARQG-NH_2

^{15}N-Ala-labeled residues are shown in bold, and the 3,3,3-$^{2}H_3$-Ala-labeled residues are underlined.

The unlabeled amino acid derivatives were purchased from Iris Biotech GmbH, whereas the isotopically enriched derivatives were from Cambridge Isotopes Laboratories, Inc (Andover, MA, USA). The coupling steps were performed using the *N,N'*-diisopropylcarbodiimide (DIC, 4 eq.), 1-hydroxybenzotriazole (HOBt, 4 eq.) from Sigma Aldrich (St Louis, USA), and the respective Fmoc amino acid derivative solubilized in 2 mL of DMF:DCM (1:1) under stirring (240 rpm) for 120 minutes. After each coupling step, the Fmoc group was removed through stirring (240 rpm) for 15 minutes in presence of 2.5 mL of 4-methylpiperidine at 25% in DMF (v/v). Cleavage and side-chain deprotections were achieved by treatment with a TFA:triisopropylsilane:water (95.0:2.5:2.5, v:v:v) solution. The crude peptides were precipitated with cold diisopropyl ether (-4 °C), extracted with deionized water and freeze-dried. Purifications were performed on a RP-HPLC Pro Star 335 system from Varian® (Santa Clara, USA) using a semipreparative C18 Waters Bondapack® (7,8 x 300 mm) (Mississauga, Ontario) column at a flow rate of 1.5 $mL.min^{-1}$. Elution was performed by using

a gradient of water containing 0.1% TFA and acetonitrile containing TFA 0.08%. HPLC experiments were performed at room temperature, and the peptides were monitored at 215 nm and 280 nm. The identities of the purified peptides were confirmed by MALDI-ToF/ToF mass spectrometry on an Autoflex® III SmartBeam spectrometer (Bruker Daltonics, Germany). The peptide samples were placed in *MTP AnchorChip® 400/384* (Bruker Daltonics®) plates for the analysis. The monoisotopic mass of the peptides was recorded using a mass range between 400 and 4000 Da, in positive reflective mode.

3.2.2 Preparation of phospholipid large unilamellar vesicles (LUVs)

Lipid vesicles were prepared as described elsewhere [Junior et al., 2017]. 1-palmitoyl-2-oleoyl-*sn*-glycero-3-phosphocholine (POPC), and 1-palmitoyl-2-oleoyl-phosphatidylglycerol (POPG) lipids were purchased from Avanti Polar Lipids (Birmingham, AL). The appropriated amounts of POPC:POPG (3:1, mol:mol) were added to a glass tube and then solubilized in 1.0 mL of chloroform. The solvent was evaporated until the formation of a thin phospholipid film, which was hydrated with 10 mM Tris-HCl (pH 8.0, and 100 mM NaCl), or 10 mM potassium phosphate (pH 5.0, pH 6.0, pH 8.0, and 100 mM KF) buffer solution to obtain multilamellar vesicles (MLVs). LUVs were obtained from MLVs, after eight sequential freezing in liquid nitrogen, and heating in a water bath under sonication during two minutes. Then the vesicles were extruded (8 times) through polycarbonate membranes with defined pores of 100 nm (Whatman Nuclepore, Sigma-Aldrich) in an Avanti Polar Lipids Inc® mini extruder (Alabaster, AL, USA) to obtain LUVs for DLS, Zeta Potential.

For CD experiments, an equivalent methodology was used, however the lipid film was hydrated with aqueous 10 mM potassium phosphate buffer (pH 6.0, and 8.0) containing 100 mM KF. An equivalent methodology was used to obtain carboxyfluorescein-loaded (Sigma-Aldrich, St Louis, USA) vesicles for dye leakage experiments. POPC:POPG (3:1, mol:mol) film was hydrated with a 20 mM carboxyfluorescein solution at pH 8.0 (10 mM Tris-HCl buffer) containing NaCl at 100 mM before undergoing five freeze-thaw cycles and then extrusion (8 times) through membranes with pores of 100 nm diameter. The dye outside the carboxyfluorescein-loaded vesicles was removed by gel filtration through a Sephadex G-25 (Sigma-Aldrich, St Louis, USA) column equilibrated with the same buffer solution.

For the determination of the order parameters *(S_{CD})* using ^{2}H solid-state NMR spectroscopy, lipids were prepared by dissolving deuterated POPC-d_{31} or POPG- d_{31} in 10 mM phosphate buffer (pH 7.0), vortexing and bath sonication as well as three heat cycles at 40 ˚C to produce multilamellar vesicles.

3.2.3 Circular dichroism spectroscopy

The conformational preferences of ecPis-4s were investigated by circular dichroism (CD) spectroscopy on a JASCO® J-810 spectropolarimeter (Tokyo, Japan), equipped with a Jasco Peltier temperature control system - PFD-425S (Tokyo, Japan). Samples of the peptide at 50 μM were prepared in 10 mM phosphate buffer (pH 6.0, and pH 8.0) containing 100 mM KF in the absence and in the presence of POPC:POPG (3:1, mol:mol) LUVs (lipid concentration ranging from 0.05 mM to 2.40 mM) or SDS micelles (100, 200, and 400 mM). All analyses were performed at 25 °C using a quartz cuvette of 1.0 mm path length. The spectra were recorded from 190 to 260 nm, with 4 accumulations, a bandwidth of 0.1 nm, step resolution of 0.2 nm, 50 nm.min^{-1} scan speed and 1 s response time. Similar experiments in the absence of peptide were recorded with the respective blank solutions to allow background subtraction. The molar ellipticity of ecPis-4s peptide at fixed 222 nm was plotted against phospholipid:peptide molar ratio.

3.2.4 Intrinsic tryptophan fluorescence

Tryptophan-emission fluorescence measurements of ecPis-4s peptide were recorded from 290 to 450 nm with excitation at 280 nm, averaging 3 scans, using a quartz cuvette (1 mL), and processed with FluorEssence software version 3.9.0.1 (Horiba Scientific, OriginLab Corporation version 8.6001). Membrane incorporation studies were performed by adding small volumes of concentrated vesicle stock solution to the peptide sample to obtain samples containing 10 μmol ecPis-4s in the presence of different POPC:POPG (3:1 mol:mol) concentrations (from 7.50 to 2128 μM) suspended in 10 mmol phosphate buffer with 100 mmol KF at pH 6.0 and pH 8.0. Spectra were corrected for light scattering, baseline, and dilution after adding lipid vesicles for each titration step. Blue shifts were calculated from the emission

maxima of peptide and peptide–lipid mixtures at room temperature. The standard deviation of the blue shift was 1 nm.

The partition coefficient (*Kp*) of the peptide in the system was defined by the equation:

$$Kp = \frac{{}^{n_L}/_{V_L}}{{}^{n_W}/_{V_W}} \quad (4)$$

where *n* is the moles of peptide, *V* is the volume of the phase, and the subscripts *L* and *W* refer to the lipid and water phases, respectively. The K_p of the ecPis-4s peptide in the lipid membrane was obtained from fluorescence intensity data(248), *I*, using the equation 5:

$$I - I_W = \frac{(I_L - I_W) K_p \gamma_L [L]}{1 + K_p \gamma_L [L]} \quad (5)$$

where I_W and I_L are the limit fluorescence intensities with all the peptide in water and in the lipid phase, respectively; γ L is the molar volume of the phospholipid, considering $\gamma_{POPC/POPG}$ = 0.762 M^{-1} and [L] is the lipid concentration. *Kp* and I_L were obtained by a nonlinear regression(249,250) in the graphical of I - I_W plotted vs lipid concentrations [L].

3.2.5 Two-dimensional solution NMR spectroscopy

Two-dimensional solution NMR experiments were carried out to determine the three-dimensional structure of ecPis-4s in the presence of SDS-d_{25} micelles at 25 °C on a Bruker® Avance III spectrometer (Bruker, Germany) operating at 500.13 MHz (for ^{1}H). The sample consisted of an aqueous solution of 2.0 mM ecPis-4s and 300 mM SDS-d_{25} containing 10% (v/v) D_2O/H_2O and 1% (v/v) of 2,2-dimethyl-2-silapentane-5-sulfonate-d_6 (DSS-d_6) as the internal reference.

Two-dimensional homonuclear Total Correlation Spectroscopy (^{1}H-^{1}H-TOCSY) spectra were acquired using a pulse sequence with a mixing time of 60 ms, 512 t_1 increments, 60 transients of 4096 points for a spectral width of 6009.6 Hz. Nuclear Overhauser Spectroscopy (^{1}H-^{1}H-NOESY) spectra were obtained using mixing times of 60, 120, and 160 ms to check for spin diffusion, 512 t_1 increments with 60 transients of 4096 points for a spectral width of 6009.1 Hz.

Heteronuclear Single Quantum Coherence ($^{1}H,^{13}C$-HSQC) experiment was acquired using edited mode in which CH_2 correlations show negative phase and CH and CH_3 correlations show positive phase(251). The data were recorded with F1 and F2 spectral widths of 20831.9 Hz and 6009.6 Hz, respectively. 256 t_1 increments were accumulated with 64 transients of 4096 points. Heteronuclear Multiple Quantum Coherence ($^{1}H,^{15}N$-HMQC) experiment was performed with F1 and F2 spectral widths of 2000 and 6009.6 Hz, respectively. 80 t_1 increments were accumulated with 4000 transients of 1024 points(252).

3.2.6 NMR analyses and structure calculations

Proton resonances were assigned by simultaneous analyses of homonuclear $^{1}H,^{1}H$-TOCSY and $^{1}H,^{1}H$-NOESY spectra using the Wüthrich method(208). Heteronuclear spectra were used as an extra control. The NMR assignments were performed manually using NMRViewJ (version 9.2.0-b20) program(253). The NOE intensities were converted into a of semi-quantitative distance restraints with limits of 2.8, 3.4, and 5.0 Å(254). The dihedral angle restraints were obtained based on the H_N, H_α, H_β, C_α, C_β, and N chemical shifts using the TALOS+ program(213) of the NMRPipe® computational package(255). The $^{13}C\alpha$ chemical shift index was calculated in accordance with Wishart method(212). The geometric restraints were validated (according to their consistency and contribution) from data of uniqueness information from the QUEEN program (Quantitative Evaluation of Experimental NMR Restraints)(256).

The XPLOR-NIH software (version 2.27) was used for the calculation and refinement of the three-dimensional structures(257,258). A total of 100 structures, starting with an extended conformation, were generated using simulated annealing protocol in torsional angle dynamics, followed by 20,000 steps of simulated annealing at 1,000 K and a subsequent decrease in temperature in 15,000 steps in the first slow-cool annealing stage. The structures were obtained and then refined in a subsequent calculation, using more stringent topology parameters as *ref_sa_new.php*(259). The ten lowest-energy structures were visualized and analyzed with MolMol(260), and Chimera(261), and the quality of the structures were verified by the Ramachandran diagram and the RMSD (Root Mean Square Deviation), both obtained from the online platform PSVS(262).

3.2.7 Solid-state NMR spectroscopy applied for oriented samples

A homogeneous mixture of ecPis-4s and POPC:POPG (3:1, mol:mol) phospholipid was obtained by dissolving the appropriate amount of peptide in a stepwise manner to a solution of 20-40 mg of lipids in chloroform with a final peptide-to-lipid (P/L) molar ratio of 4%. Thereafter the sample was vortexed and the solvent partially evaporated following a previously elaborated protocol (263). The resulting viscous solution was spread onto 21 ultrathin cover glasses (8 x 22 mm, thickness 00; Marienfeld, Germany), and dried first in air at room temperature, followed by high vacuum overnight. The solvent-free lipid films were transferred to a hydration chamber equilibrated at 93% relative humidity with ^{2}H-depleted water. The plates were then stacked on top of each other and properly sealed with Teflon® tape and plastic wrapping.

Proton-decoupled ^{31}P solid-state NMR spectra were acquired at 121.577 MHz on a Bruker® Avance wide-bore 300 NMR spectrometer (Bruker, Billerica, MA) equipped with a solid-state double resonance flat-coil static probe (Rheinstetten, Germany). A Hahn-echo pulse sequencewas used with a $\pi/2$ pulse width of 8 μs, a spectral width of 100 kHz, an echo delay of 100 μs, and a recycle delay of 3 s and dwell time of 5 μs(264). The spectra were referenced externally to 85% H_3PO_4 at 0 ppm. The temperature was set to 25 ^{o}C for all samples.

Deuterium solid-state NMR spectra were recorded on a Bruker® Avance wide-bore 300 NMR spectrometer employing a commercial triple resonance flat-coil probe for solid-state NMR (Bruker, Rheinstetten, Germany). A quadrupolar echo pulse sequence with $\pi/2$ pulse of 5 μs, dwell time of 0.5 μs, echo delay of 100 μs, acquisition time of 8.2 ms, and recycle delay of 0.5 s. The spectra were referenced relative to D_2O (0 Hz)(265). Exponential apodization function corresponding to a line broadening of 100 Hz was applied before Fourier transformation.

Proton-decoupled ^{15}N cross-polarization (CP) spectra were acquired at 30.43 MHz on a Bruker Avance wide bore 300-MHz NMR spectrometer equipped with a double-resonance flat-coil probe(266). An adiabatic CP pulse sequence was used with 25 kHz spectral width, dwell time of 20 μs, 0.4 ms CP contact time, and 3 s recycle delay time(267). The spectra were recorded at 25 °C for both labeled peptide samples using an Oxford temperature control unit. An exponential line broadening of 100 Hz was applied before Fourier transformation and an external reference of $^{15}NH_4Cl$ was used for calibration of the ^{15}N chemical shift scale (40

ppm)(268). All spectra were recorded with the sample normal positioned parallel to the external magnetic field direction.

3.2.8 Simulations of the membrane topology

The solution NMR structure of ecPis-4s was used for the simulation of ^{15}N chemical shifts (σ_{zz}) and deuterium quadrupolar splittings ($\Delta\nu_Q$) to determine the orientation of the peptide reconstituted in the POPC:POPG (3:1, mol:mol) lipid bilayers. Both geometry alignments and simulations of the membrane topology were carried out using a homemade program developed in one of our laboratories as described elsewhere(269).

3.2.9 Deuterium order parameters of labeled phospholipids

ecPis-4s samples were prepared by mixing POPC, deuterated POPC (POPC-d_{31}), and POPG for LUVs made of POPC: POPC-d_{31}-POPG, 2:1:1 molar ratio. Non-oriented samples were also prepared using deuterated POPG lipid by dissolving 4.27 mg of POPC and 1.5 mg of deuterated POPG lipid (POPG-d_{31}), (POPC:POPG-d_{31}, 3:1, mol:mol). The appropriate amount of peptide (~ 0.82 of ecPis-4s peptide to give 4 mol%; pH adjusted to 7) and lipids were dissolved in $CHCl_3$. The solvent was evaporated under a stream of nitrogen and high vacuum overnight; thus, a film forms on the walls of the small glass tube (6 mm outer diameter). The sample was then resuspended in 26 μL of 10 mM phosphate buffer (pH 7) by vortexing and sonication in a water bath, as well as five chill/heat cycles at 0 and 40 ˚C to produce multilamellar vesicles. For NMR spectral acquisition, the glass tube with the sample was directly inserted into the solenoidal coil of a static solid-state NMR probe.

^2H solid-state NMR spectra of deuterated POPC-d_{31} or POPG-d_{31} were recorded by applying a quadrupolar pulse-echo sequence[167]. The recycle delay was 0.3 s, echo time 100 μs, dwell time 0.5 μs and π/2 pulse 5 μs. An exponential apodization with line broadening of 300 Hz was applied before Fourier transformation. The temperature was set to 25 °C for both samples. The deuterium order parameters (S_{CD}) of the CD_2 and CD_3 groups were calculated by de-Pake-ing(270), according to the equation 6:

$$S_{CD}^{i} = \frac{4}{3}\frac{\mathrm{h}}{e^2 qQ}\Delta_{\upsilon}^{i} \quad (6)$$

where, $\Delta^{i}\upsilon$ is the quadrupolar splitting of segment *i* and (e^2qQ/h) is the static quadrupole coupling constant (167 kHz) for C–D deuterons(271).

The quality of the spectra allows to determine the quadrupolar splitting with an accuracy of ~1 kHz. This corresponds to an error of 0.01 for the order parameters and 0.014 for the relative order parameters. Here we compare order parameter profiles encompassing up to *n* = 13 data points rather than individual order parameters. In this case Student's t can be calculated from the sample average (*D*) and the standard deviation (S_d) of the pair-wise differences between corresponding points of two data sets according to $t = D/S_d * \sqrt{n}$, where *n* is the number of data points/differences(272). From reference *t*-values, it can be estimated that relative order parameters profiles that are at least 0.02 units apart are different with high probability.

3.2.10 Isothermal titration calorimetry

Isothermal titration calorimetry (ITC) experiments were carried out at 25 °C and 35 °C on a VP-ITC microcalorimeter (Malvern, UK) for ecPis-4s peptide in the presence of POPC:POPG (3:1, mol:mol) LUVs suspended in 10 mM Tris-HCl buffer solution (pH 8.0) containing 100 mM NaCl. The peptide and LUVs samples were previously degassed in a Microcal Thermovac® (Grovewood Rd, Malvern, UK). The data obtained were recorded and processed using Origin software for ITC (Microcal Origin® 7.0; OriginLab Corporation, Northampton, USA). The peptide solution (25 μM) was titrated with 30 successive injections of 20 mM POPC:POPG (3:1, mol:mol) LUVs. The first 1.0 μL injection was discarded in order to eliminate diffusion effects of the material from syringe to calorimeter cell, followed by 29 injections of 5.0 μL. Injection times of 2 s with intervals of 300 s were used in the experiments.

Similar experiments were performed titrating 10 mM Tris-HCl buffer solution (pH 8.0) containing 100 mM NaCl on LUVs suspensions to determine the corresponding heats of dilution, which were subtracted from the heats determined in the corresponding peptide:lipid binding experiments. Non-linear fitting was carried out using the equation 7 to obtain the partial molar enthalpy of complexation ($\Delta_{comp}H = dQ/d[X]$) at a constant pressure(273):

$$\Delta_{comp}H = \left(\frac{dQ}{d[X]_{tot}}\right)_P = \Delta_{\text{int}}H°V_o\left[\frac{1}{2} + \frac{1-X_R-r}{2\sqrt{(1+X_R-r)^2-4X_R}}\right] \quad (7)$$

where X is the molar ratio of titrant and M ($X_R = [X]_t/[M]_t$) molar ratio of titrated at any point during the titration in the experiment. The parameter r is the composition variable ($r = 1/[M]_t.K_{app}$), and the parameters $\Delta_{int}H°$, V_0 and K_{app} are respectively the standard complexation enthalpy, effective volume of the solution in the titration cell and apparent equilibrium constant.

3.2.11 Dynamic light scattering and zeta potential (ζ)

The hydrodynamic diameter (D_h), and the zeta (ζ) potential measurements of the POPC:POPG (3:1, mol:mol) LUVs solution (10 mM pH 8.0 Tris-HCl buffer, containing 100 mM NaCl) upon addition of ecPis-4s were carried out at 25 ºC on a Malvern Zetasizer® Nano ZS equipment (Worcestershire, UK). All measurements were performed at room temperature using a 700 µL Malvern® cuvette (Malvern, Model DTS1060). The D_h measurements were performed using monochromatic light (Ne 4 mW laser, λ 633 nm) and ζ at potentials greater than 500 mV. Each experiment was collected in triplicate consisting of successive titrations of 10 µL aliquots of 336 µM ecPis-4s solution into the cuvette containing 550 µL of 500 µM LUVs solution. The D_h and ζ were measured 60 minutes after each addition of 10 µL of peptide solution for the system stabilization.

The formalism for the determination of the partition constant (K_p) by ζ-potential can be described by equation 9. Using the equations 8 and 9, the fraction of membrane-bound (X_L) peptide and ζ-potential in presence of peptide can be related to the K_p(236,237), as followed:

$$X_L = \frac{K_p\gamma_L[L]}{1+ K_p\gamma_L[L]} \quad (8)$$

$$\frac{\zeta_{\text{final}}}{\zeta_0} = 1 + \frac{X_L Z_{Peptide}}{f_{PL}Z_{Lipid}[L]} \cdot [P] \quad (9)$$

where X_L represents the fraction of peptide that is bound to the lipid, [L] is the phospholipid concentration; and γ_L is the molar volume of the lipid; $Z_{peptide}$ is the global charge of the peptide, Z_{lipid} is the absolute charge of the lipid; f_{PL} is the fraction of anionic phospholipids in the lipid

mixture. ζ_{final} and ζ_0 are the ζ-potential value for each titration with peptide and ζ-potential value in the absence of peptide, respectively. To further investigate and to determine K_p value, it is also necessary to know the net charge of the peptide and the proportion and effective charge of the ionic phospholipids in the vesicles. In this way, plotting ζ_{final}/ζ_0 versus [P], a linear variation is performed, and it is possible to find out the value of K_p from the slope using the equations above.

3.2.12 Carboxyfluorescein leakage measurements

Measurements of calcein release from POPC:POPG (3:1, mol:mol) LUVs (20 μM in 10 mM Tris-HCl buffer, at pH 8.0) induced by ecPis-4s peptide was carried out at room temperature. The increase of carboxyfluorescein fluorescence as a function of time was continuously recorded on a Varian Cary Eclipse detection platform (Santa Clara, CA, USA) using λ_{ex} = 490 nm and λ_{em} = 515 nm. Aliquots of LUVs were added to cuvette (1.0 cm optical path) for measurement of fluorescence emission in media containing different peptide concentrations (ranging from 1.01 μM to 16.18 μM) diluted in the respective LUVs suspension. The total calcein fluorescence (maximum leakage) was determined by adding 10 μL of 10% Triton X-100 (v/v) solution after 45 min. The percentage of CF leakage (% CF) was determined(274) using equation 10

$$\text{Leakage (\%)} = \left[\frac{I_{(t)}-I_0}{I_T-I_0}\right] \text{x } 100 \qquad (10)$$

where, $I_{(t)}$ is the fluorescence intensity as a function of time (t), I_0 is the fluorescence intensity before the addition of the peptide, and I_T is the fluorescence intensity after the addition of the Triton X-100 solution.

3.3 Results

3.3.1 Effect of pH in the peptide-membrane interaction

Conformational preferences: In order to access the conformational preferences of ecPis-4s in aqueous solution and when interacting with mimetic membranes, circular dichroism (CD) experiments were carried out in phosphate-buffered peptide solutions in the absence and in the presence of POPC:POPG (3:1, mol:mol) phospholipid vesicles at pH 8.0 and 6.0.

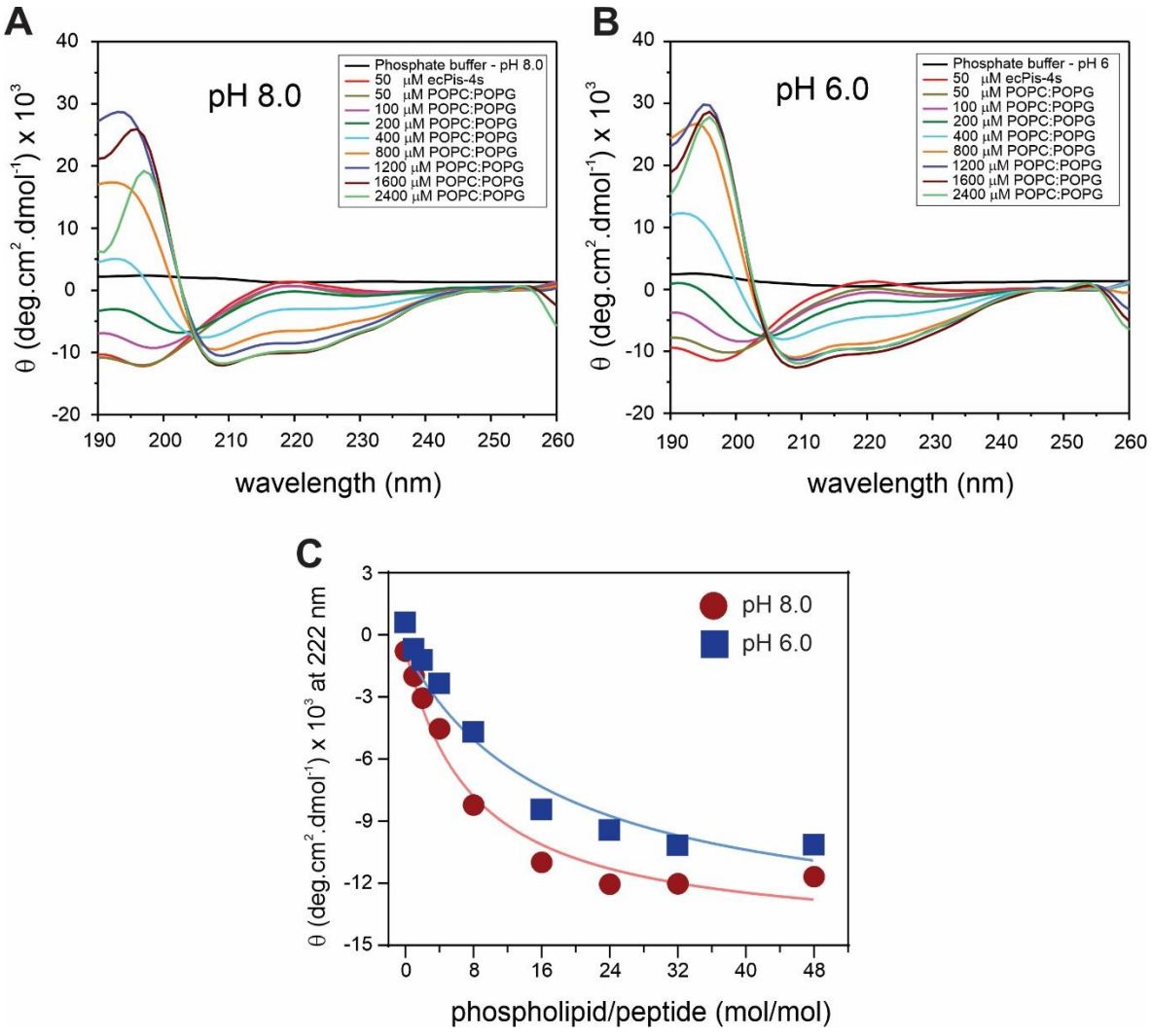

Figure 15. CD spectra of 50 μM ecPis-4s peptide as a function of increasing amounts of POPC:POPG (3:1, mol:mol) LUVs at (A) pH 8.0, and (B) pH 6.0. (C) Molar ellipticity of ecPis-4s at 222 nm as a function of the lipid:peptide ratio.

CD spectra of ecPis-4s in aqueous buffer and in the presence of LUVs at low phospholipid:peptide ratios (≤4) indicate predominantly random coil conformations. Helical profiles appear at higher phospholipid:peptide molar ratios (≥8), characterized by the pronounced maximum near 195 nm as well as two minima around 208 and 222 nm(275). Although significant helicity is noticed for ecPis-4s under in both pH conditions investigated, the helical content is higher at pH 8.0. The molar ellipticity at 222 nm as a function of lipid:peptide ratio at different pH values is presented in Figure 15C.

Circular dichroism experiments were also acquired for the ecPis-4s peptide in the presence of SDS micelles to evaluate the peptide helical propensity in a mimetic medium suitable for high-resolution solution NMR spectroscopy(218). The spectra are consistent with α-helical profiles at all SDS concentrations [Figure SM2], as noticed for the peptide in the presence of POPC:POPG (3:1, mol:mol) vesicles for lipid concentrations ≥ 400 μM [Figure 15].

Intrinsic Tryptophan Fluorescence: The tryptophan (Trp) fluorescence spectra of ecPis-4s were recorded in phosphate buffered solutions at pH 6.0 and 8.0, respectively, and at different concentrations of POPC:POPG (3:1, mol:mol) LUVs [Figure 16]. For both pH conditions, the Trp intrinsic fluorescence of ecPis-4s shows a maximum emission at 350 nm in the absence of LUVs. The small shoulder visible at low wavelengths (310 nm, black line) is due to Raman scattering of the buffer(276). When POPC:POPG (3:1, mol:mol) vesicles are titrated to the ecPis-4s solution, a blue shift from 348 to 323 nm is noticed at both pH 8.0 and pH 6.0. In both cases, the increase of the lipid concentration is accompanied within an increase in the Trp maximum fluorescence intensity (λ_{max}) until a plateau is reached.

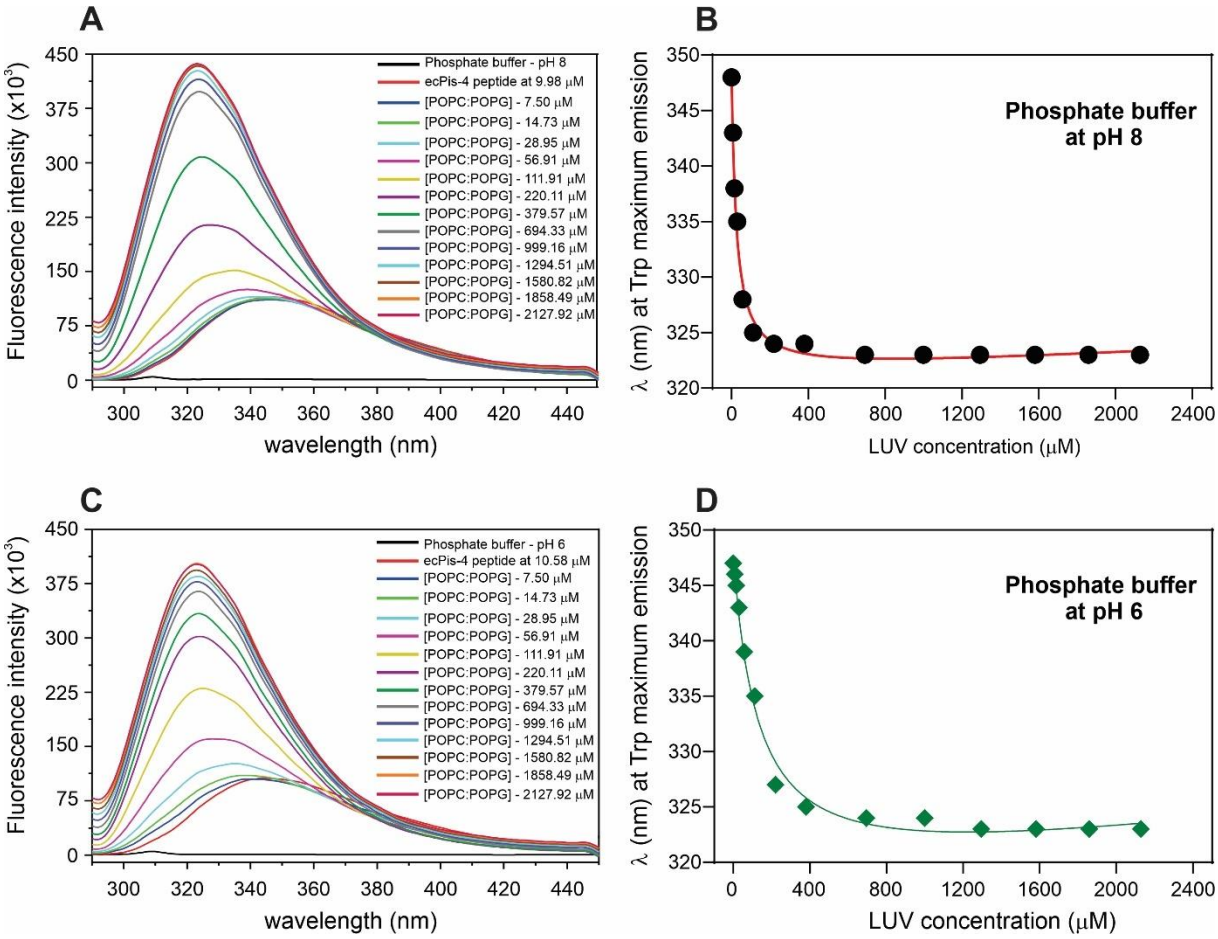

Figure 16. Effect of LUVs on the intrinsic Trp fluorescence emission spectra of the ecPiscidin-4s peptide. λex = 280 nm. Tryptophan fluorescence from ecPis-4s solutions as a function of LUVs concentration (A and C). Effect of the variation of lipid concentration on the wavelength of maximum Trp emission by increasing POPC:POPG (3:1, mol:mol) LUVs concentration at pH 8.0 and pH 6.0 (B and D, respectively). LUVs of 100 nm were prepared in 10 mmol phosphate buffer, pH 8.0 or pH 6.0, repectively, containing 50 mmol NaF. Assays were carried out at 25 °C.

Such Trp fluorescence shifts are related to the changes in the environment polarity, which depends on the location of the respective amino acid residue(277). Figure 17 shows an increase in the tryptophan fluorescence intensity in a phospholipid concentration- dependent manner. The fluorescence increases as a consequence of high number of molecules in contact with the nonpolar membrane environment. *Kp* determination was achieved by a non-linear fitting of the obtained results using equation 4. Values of $Kp = (6.8 \pm 0.8) \times 10^3$ M^{-1} and I_L = 432.7×10^3 at pH 8.0; and $Kp = (2.9 \pm 0.1) \times 10^3$ M^{-1} and $I_L = 522.4 \times 10^3$ at pH 6, were obtained, considering γ_{POPC} and $\gamma_{POPG} = 0.762$ M^{-1}.

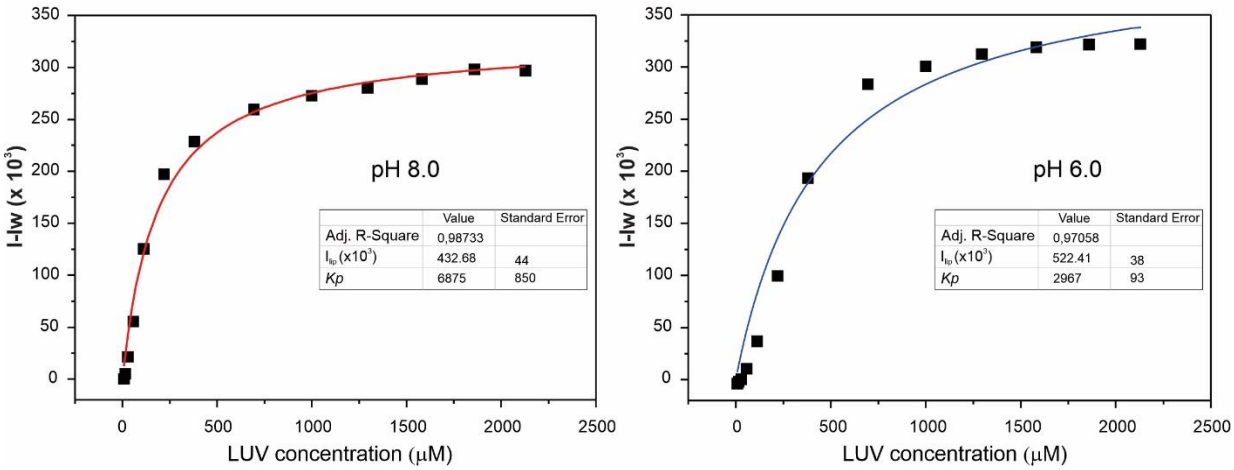

Figure 17. Determination of the partition constant by fluorescence spectroscopy. Solutions of 10 and 10.5 μM ecPis-4s peptide solution at pH 8.0 and pH 6.0, respectively, were titrated with increasing POPC:POPG (3:1, mol:mol) lipid concentrations. The partition constant was obtained by the non-linear fitting of equation 4.

3.3.2 Peptide Structure and membrane topology

Solution NMR Spectroscopy: To perform multidimensional solution NMR experiments, 2 mM ecPis-4s was solubilized in a 300 mM SDS-d_{25} micellar solution(278). The dispersion of chemical shifts of alpha and amide hydrogens suggests a folded peptide conformation [Figure SM3]. Therefore, the spin systems of all amino acid residues and their respective ^{1}H and ^{13}C, ^{15}N chemical shifts were identified by analyzing intra-residual correlation in the ^{1}H,^{1}H-TOCSY; ^{1}H,^{13}C-HSQC and ^{1}H,^{15}N-HMQC two-dimensional spectra. The high number of inter-residual cross-peaks detected in the NOESY contour map [Figure 18] allowed to resolve all ambiguities. The sequential $d_{\alpha N}$ (*i, i*+1) and medium range $d_{\alpha N}$ (*i, i*+n) (n = 2, 3 and 4) as well as the $d_{\alpha\beta}$ (*i, i*+3) connectivities are summarized in Figure SM4. Medium range NOE cross-peaks are observed from R3 up to G22 (*C*-terminus), confirming that ecPis-4s presents a well-defined helical arrangement covering much of its sequence. The calculated H_α and C_α chemical shift indices (CSI) are presented in Figure SM5, in which the positive values of ^{13}C CSI throughout the entire peptide backbone also suggest that the peptide adopts a helical structure from the *N*- to the *C*-terminus(279).

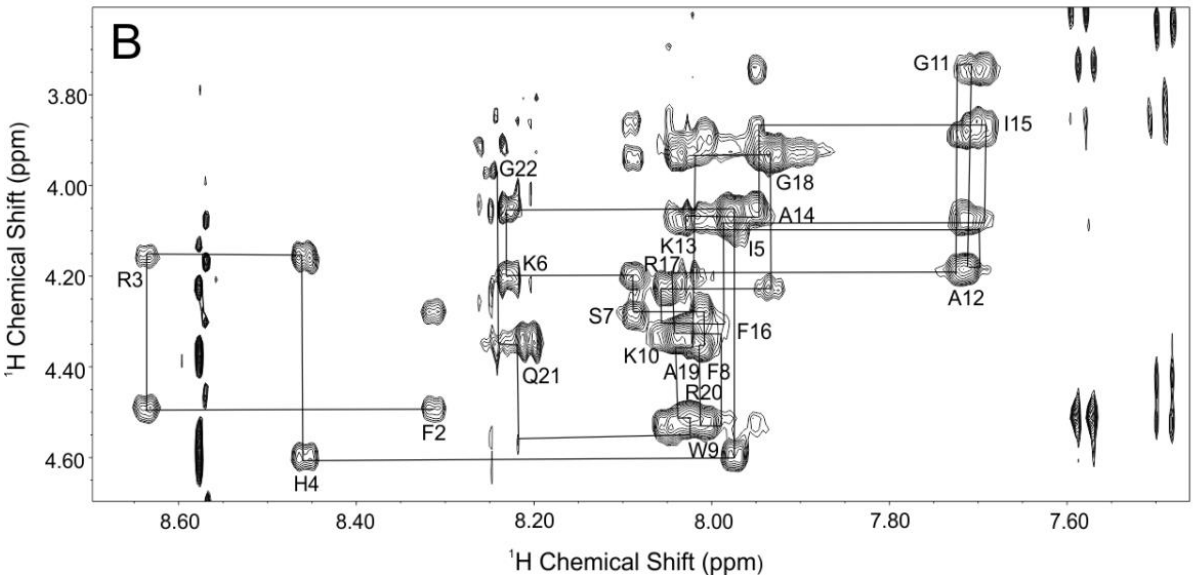

Figure 18. H_N-H_α region of the NOESY spectrum of 2 mM of ecPis-4s in presence of 300 mM SDS-d_{25} at 25 ºC, 500 MHz. The HN-Hα *(i, i +1)* sequential correlations connected through lines to the respective HN-Hα intraresidue correlations.

The ensemble of three-dimensional structures of ecPis-4s was calculated based on distance restraints obtained from NOE data as well as from ϕ and ψ angular restraints derived from chemical shifts. Table SM1 presents a summary of all input data used in the calculations as well as the respective quality parameters. All ϕ and ψ dihedral angular pairs are found in the most favored regions of the Ramachandran plot [Figure SM6], indicating the high stereochemical quality of the calculated structures. The superposition of the ten lowest-energy structures of ecPis-4s over the backbone and side-chain, as well as the lowest-energy structure are shown in Figure 19.

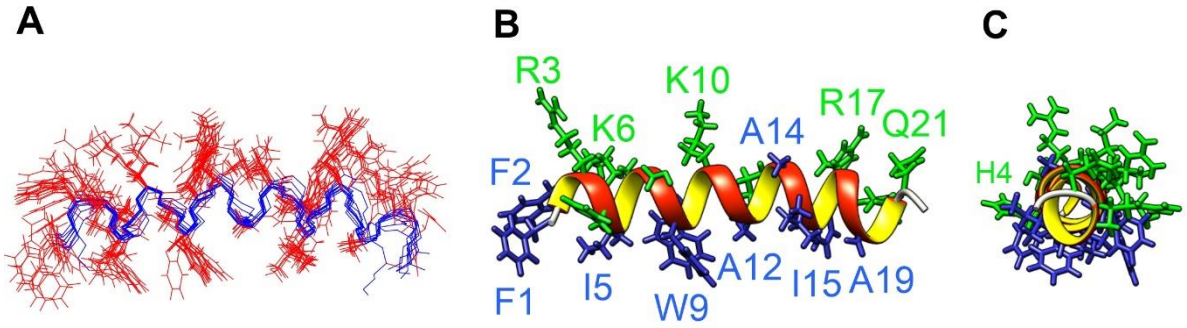

Figure 19. Three-dimensional structures of ecPis-4s (2 mM) in the presence of SDS-d_{25} micelles (300 mM) at 25 °C obtained from NMR at 500 MHz (A) The overlap of the ten lowest-energy structures for ecPis-4s in micelles (from F1 to G22). (B) Horizontal perspective and (C) front-view of the lowest-energy structure (the *N*-terminus is in the back). The hydrophobic residues are shown in green and the hydrophilic residues in blue.

A RMSD of 0.8 Å (± 0.1) was obtained for the backbone atoms considering all residues, whereas a RMSD of 1.4 Å was obtained when all heavy atoms are taken into account, which is in line with a well-ordered structure(260). Figure 19B shows a horizontal perspective of the lowest-energy structure, in which the partitioning of hydrophilic and hydrophobic side chains within two distinct faces becomes evident. The six positively charged lysine (K7, K11, and K15) and arginine residues (R3, R17, and R20) are clearly located within the hydrophilic face. Interestingly, as can be noted from the helical front-view [Figure 19C], H4 lies at the interface of the hydrophilic and hydrophobic faces, which is a characteristic already observed for other histidines within antimicrobial peptide sequences(280).

Oriented Solid-state NMR spectroscopy: To investigate the topology of ecPis-4s in membranes, selectively labeled analogs of the peptide containing 3,3,3-$^{2}H_3$-Ala and ^{15}N-Ala residues at positions 12 or 14 [Table 1] were reconstituted into uniaxially oriented POPC:POPG (3:1, mol:mol) bilayers. The samples containing 4% (mol:mol) of ecPis-4s* or ecPis-4s** in these negatively charged bilayers were inserted into the NMR spectrometer with the glass plate normal parallel to the magnetic field direction.

The proton-decoupled ^{31}P NMR spectra [Figure 20A, B] of both samples present an intense signal near 30 ppm, which is characteristic of lipid molecules with their main axis aligned parallel to B_o(220,281). Smaller intensity ^{31}P resonances reaching up to -15 ppm are related to phosphorus headgroups which deviate their relative orientations to B_o and/or with different conformations(281,282). Nevertheless, the ensemble of solid-state NMR spectra

[Figure 20] indicate a good degree of membrane alignment in the presence of the ecPis-4s, where the line shapes suggest that membrane disturbances were not caused during sample preparation, but rather are intrinsic to the interactions of the peptides with the membranes(281).

Proton-decoupled ^{15}N NMR spectra of (^{15}N-Ala-14)-ecPis-4s* and (^{15}N-Ala-12)-ecPis-4s** [Figure 20C, D] exhibit narrow line shapes with chemical shifts at 85 ppm and 68 ppm, respectively. These values are consistent with helix alignments parallel to the bilayer surface(221). The narrower line shapes observed in the ^{15}N NMR spectrum of (^{15}N-Ala-12)-ecPis-4s** indicates that the N–H bond vector of Ala-12 residues are more homogeneously aligned when compared to the Ala-14 residues.

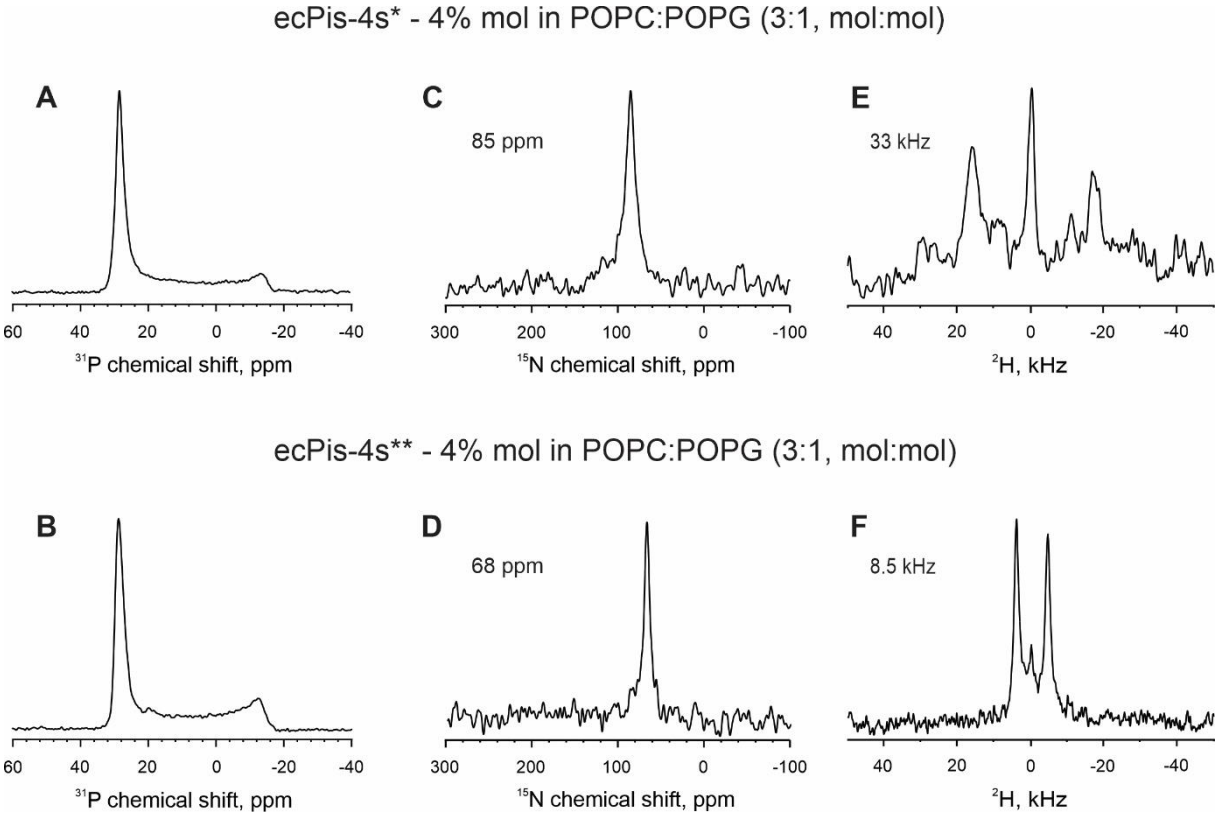

Figure 20. (A and B) Proton-decoupled 31P, (C and D) proton-decoupled 15N and (E and F) 2H solid-state NMR spectra of the labeled (A, C, and E) (3,3,3-2H3-Ala-12; 15N-Ala-14)-ecPis-4s* and (B, D, and F) (15N-Ala-12; 3,3,3-2H3-Ala-14)-ecPis-4s** at 4.0 mol % in uniaxially oriented POPC:POPG (3:1, mol:mol) bilayers.

The ^{2}H solid-state NMR spectra of both samples are presented in Figures 20E and 20F and provide additional constraints for determining the accurate orientation in relation to the

membrane normal. For the (3,3,3-$^{2}H_3$-Ala-12)-ecPis-4s* a deuterium quadrupolar splitting of 33 kHz is observed while 8.5 kHz is found for (3,3,3-$^{2}H_3$-Ala-14)-ecPis-4s**. This data provides highly complementary information about the alignment of the C_α-C_β bond vector relative to the magnetic field / membrane normal which allows one to narrow down further the tilt angle and to also determine the helix rotational pitch angle(222). The deuterium spectra show a central resonance related to the residual HDO of deuterium depleted water, whereas the other two signals correspond to the quadrupolar doublet of the labeled peptide site(225).

To determine the topology of ecPis-4s in the negatively charged lipid bilayers, the lowest-energy structure obtained from solution NMR was used for the simulations of σ_{zz} and $\Delta\nu_Q$(269). As described, these two parameters provide highly complementary topological restraints, which have been used in combination to obtain an accurate definition of orientations of peptide reconstituted in lipid bilayer(281). Figure 21 represents the peptide alignments in relation to the phospholipid bilayer as a function of the rotational pitch and tilt angles. For the (3,3,3-$^{2}H_3$-Ala-12; ^{15}N-Ala-14)-ecPis-4s* peptide, the traces in black represent orientations in which the simulated ^{15}N chemical shift agrees with the experimental data within ± 2 ppm, whereas the red lines trace the angular pairs where the ^{2}H quadrupolar splitting agrees with experimental values within ±1 kHz. For (^{15}N-Ala-12; 3,3,3-$^{2}H_3$-Ala-14)-ecPis-4s**, the traces presented in turquoise correspond to agreements between simulated and experimental ^{15}N chemical shift, while angular pairs in brown indicate agreements between simulated and experimental ^{2}H quadrupolar splitting within the limits just above described. When only the topological restraints of (3,3,3-$^{2}H_3$-Ala-12; ^{15}N-Ala-14)-ecPis-4s* are considered, five orientations agree with the respective experimental parameters simultaneously (intersections in blue). The corresponding molecular alignments are shown beneath the contour plot [Figure 21B I:V), where the hydrophilic sidechains are presented in green and the hydrophobic ones in blue. When the topological restraints of (^{15}N-Ala-12; 3,3,3-$^{2}H_3$-Ala-14)-ecPis-4s** are also considered, only the orientation II (86/49^{o}) simultaneously affords agreement will all four experimental NMR measurements. Two lateral perspectives of topology II in which the positions of histidine-4 and arginine-20 are indicated are shown in Figure 21C.

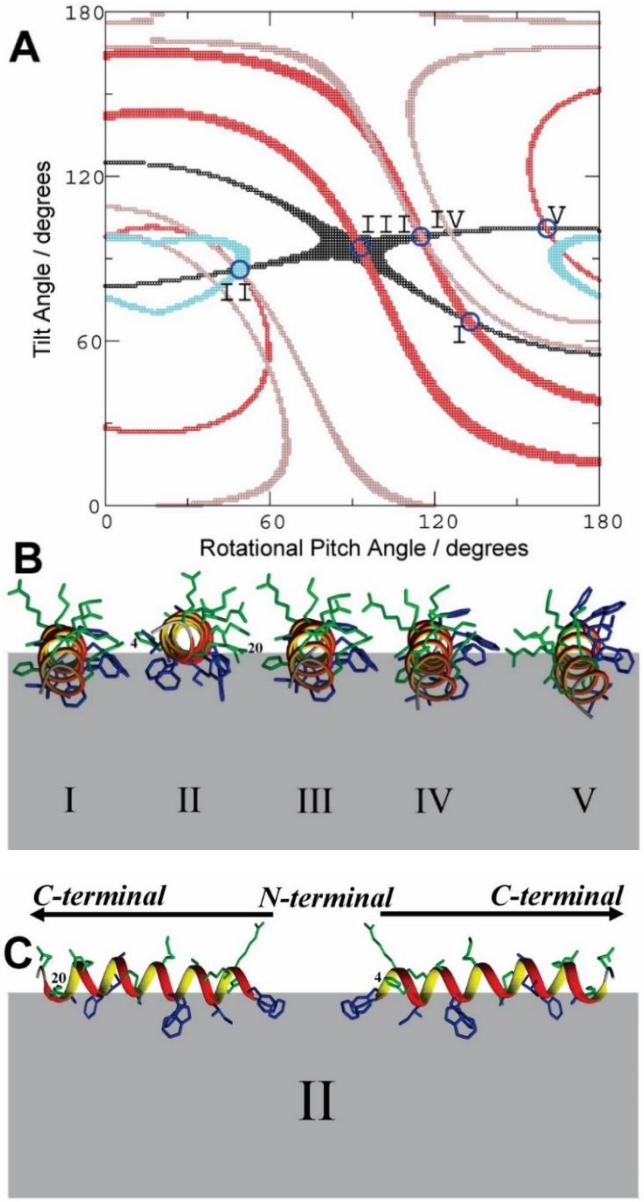

Figure 21. (A) Alignments analysis (tilt and rotational pitch angles) from solid-state NMR data of ecPis-4s reconstituted in POPC:POPG (3:1) lipid bilayers. Angular pairs that represent agreement between the simulated ^{15}N chemical shift of ^{15}N-Ala-12 and ^{15}N-Ala-14 are shown in black and turquoise, respectively. Alignments in which the simulated deuterium quadrupolar splitting of 3,3,3-$^{2}H_3$-Ala-14 and 3,3,3-$^{2}H_3$-Ala-12 agree with the respective experimental values are shown in red and brown, respectively. The intersections shown by blue circles indicate orientations that simultaneously agree with both ^{15}N chemical shift and deuterium quadrupolar splitting measured from a single peptide (3,3,3-$^{2}H_3$-Ala-12; ^{15}N-Ala-14)-ecPis-4s*. (B) The frontal view of such topologies with the *N*-terminus located in the back. (D) Horizontal views of the only topology, which agrees with all four experimental restraints obtained from two complementary peptide preparations. Hydrophilic residues are shown in green and hydrophobic residues in blue. The gray areas represent the hydrophobic region of a monolayer. The positions of histidine-4 and arginine-20 residues are indicated for topology II in panels (B and C).

3.3.3 Effect of peptide-membrane interactions on phospholipid vesicles

Order parameters of POPC-d_{31} and POPG-d_{31}: ^{2}H solid-state NMR spectroscopy of deuterated fatty acyl chains were used to monitor how ecPis-4s affects the order parameters, hydrophobic thickness, packing, and dynamics of POPC:POPG lipid bilayers(283). To investigate the lipid fatty acyl chain packing and dynamics in the presence of ecPis-4s peptide, POPC:POPG vesicles were prepared with POPC or POPG lipids deuterated throughout their palmitoyl chain. The ^{2}H solid-state NMR spectra of POPC:POPC-d_{31}:POPG (2:1:1) and POPC:POPG-d_{31} (3:1, mol:mol) vesicles in the absence of peptides are shown in Figure 22. Deuterium solid-state NMR spectra from such samples in the absence and presence ecPis-4s peptide encompass several overlapping characteristic quadrupolar splittings, each providing information about the order parameter of the deuterated CD_2 and CD_3 sites(220).

For the POPC:POPC-d_{31}:POPG (2:1:1) membranes [Figure 22A], the largest quadrupolar splitting (assigned to the relatively rigid CD_2 groups closest to the glycerol backbone) is similar either in the absence or in the presence of ecPis-4s at 4 mol % (24.6 and 25.0 kHz, respectively) somewhat larger changes are observed for chain segments further into the hydrophobic core [Figure 22C]. Only a small difference is observed for the smallest quadrupolar splitting (assigned to the methyl group at the end of the chains within the bilayer core) which decreases from 2.5 kHz to 2.3 kHz when ecPis-4s is at 4 mol % is reconstituted into the bilayers. The deuterium order parameters (S_{CD}) of each C−D bond extracted directly from these spectra are plotted in a position-dependent manner [Figure 22C]. Notably, ecPis-4s at 4% mol the exerts a moderate effect on the POPC-d_{31} acyl chains, as can be observed in the relative order parameter plot [Figure 22E], which reflects the ratio of POPC:POPC-d_{31}:POPG order parameters in the presence and absence of the peptide.

When ecPis-4s at 4% mol is added to the deuterated POPC:POPG-d_{31} membrane, higher disturbances of the ^{2}H quadrupolar splittings are observed in the respective spectrum [Figure 22B], when compared to the effect noticed for the spectrum when the POPC-d_{31} lipid carries the labels [Figure 22A]. The largest and smallest quadrupolar splitting in the presence of ecPis-4s decrease from 24.2 to 21.5 kHz, and from 2.3 kHz to 1.9 kHz, respectively. These changes correspond to relative order parameters of 0.89 for the largest and 0.78 for the smallest quadrupolar splittings, when compared to the order parameters of POPG-d_{31}, in absence of peptide [Figure 22D, and F].

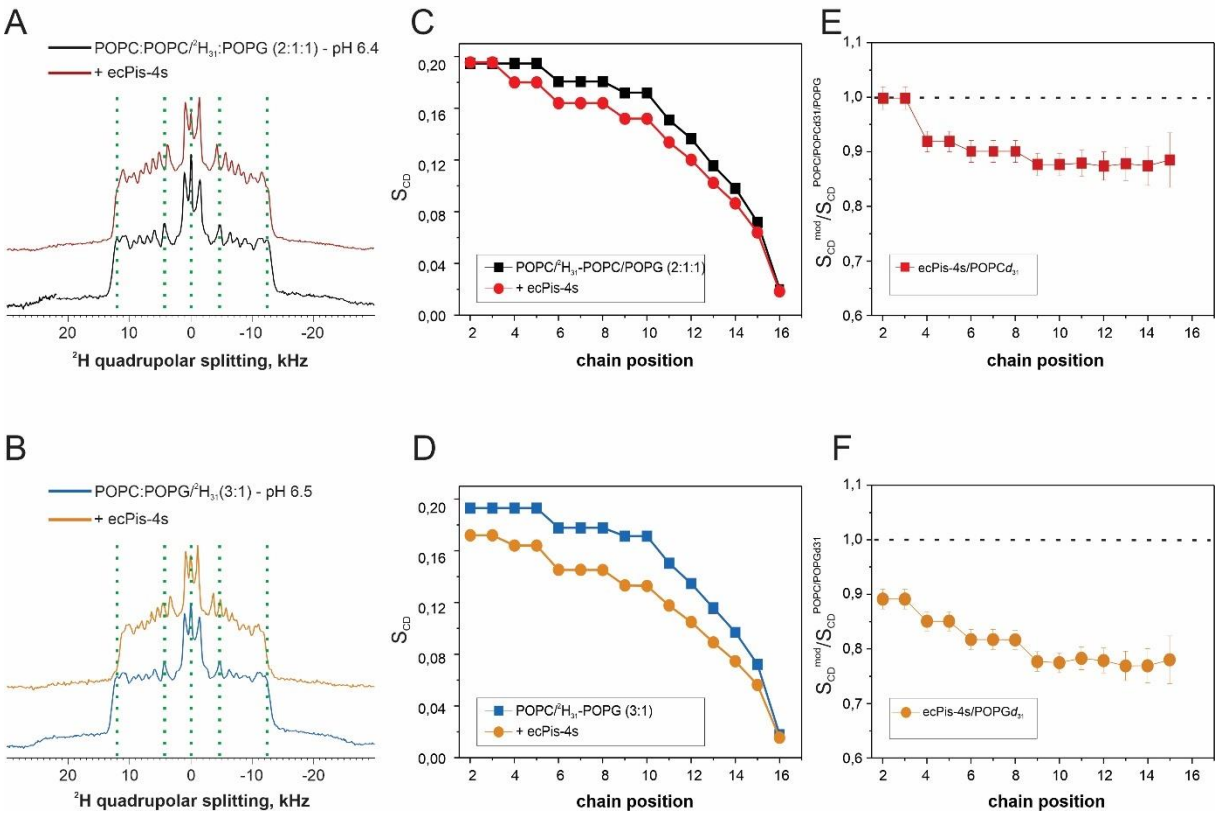

Figure 22. (A, B) ^{2}H solid-state NMR spectra of lipids deuterated throughout the palmitoyl chain, (C, D) order parameter, and (E, F) relative order parameter profiles for (A, C, E) POPC:POPC-d_{31}:POPG (2:1:1) and (B, D, F) POPC:POPG-d_{31} (3:1) in the absence and in the presence of 4 mol% ecPis-4s at pH 6.4 and 6.5. Experiments were performed at 300 K. Dashed lines in panels (A) and (D) are shown to guide the eye. From (C to F), squares represent data related to the pure lipid bilayer, whereas circles represent data obtained for samples containing the peptide.

Thermodynamics of peptide-membrane interactions: The interaction of ecPis-4s with POPC:POPG (3:1, mol:mol) LUVs was evaluated in a quantitative manner by ITC. Figure 23 presents the titration of 20 mM POPC:POPG (3:1, mol:mol) LUVs at 298 K and 308 K, into a 25 μM peptide solution, both solubilized in 10 mM Tris-HCl buffer at pH 8.0. The heat flow presents a predominant exothermic behavior at both temperatures [upper panel, Figure 23].

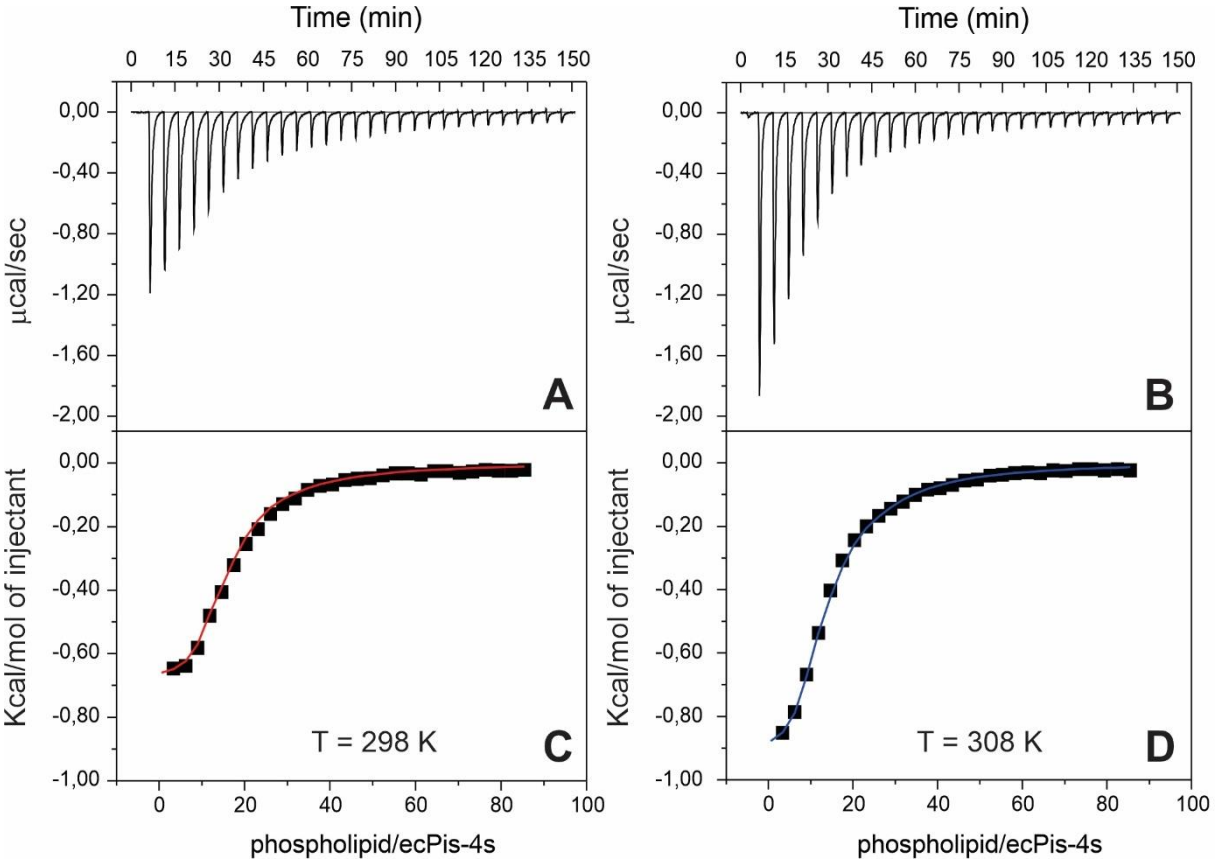

Figure 23. Isothermal titration calorimetry of 25 µM ecPis-4s with 20 mM POPC:POPG (3:1, mol:mol) LUVs suspended in 10 mM Tris–HCl (pH 8.0) containing 100 mM NaCl at (A and C) 298 K and (C and D) 308 K. (A and B) The heat flow for each ecPis-4s injection as a function of time. (B and D) The enthalpy as a function of the peptide:phopholipid molar ratio. The heat of dilution was subtracted from each experimental point.

The corresponding heats of injection as a function of the total lipid:peptide ratio is presented at the bottom panels of Figure 23. The titration heat flows are higher at 35 °C than at 25 °C, nevertheless, at both temperatures, the heat flow decreases with LUVs addition until values close to the respective dilution heats are reached, indicating a high partition coefficient of the peptides with the anionic vesicles(153). The binding isotherms were determined by non-linear curve fitting using the model of equivalent binding sites, and the calculated interaction parameters ($\Delta G°$, $\Delta H°$, $\Delta S°$, apparent binding constant - K_{app}, and the stoichiometric coefficients - n) are presented in the Table SM3. Exergonic processes were observed for the interaction of ecPis-4s with the anionic LUVs. The interaction constants (K_{app}) are characterized by similar magnitude values (10^3 M^{-1}). The apparent binding constant at 35 ºC and at 25 ºC were 7.7 ± 0.4 x 10^3 $L.mol^{-1}$ and 7.1 ± 0.3 x 10^3 $L.mol^{-1}$, respectively. ITC results also indicate

that ecPis-4s interacts with more phospholipid molecules at the higher temperature ($n_{25}^{o} \sim 15$, $n_{35}^{o} \sim 10$).

Vesicle size, surface charge, and membrane-disruptive properties: Some properties of phospholipid vesicles such as size and charge are subject to changes as a result of the peptide-membrane interaction(284). In this sense, measurements of the hydrodynamic diameter (D_h) and the zeta potential (ζ) of POPC:POPG (3:1, mol:mol) LUVs were carried out upon addition of ecPis-4s. Figure 24 shows the changes in D_h and ζ as a function of the peptide:phospholipid molar ratio. Aliquots of ecPis-4s solution were added to the LUVs dispersions and no significant changes are noted in the D_h until a peptide:phospholipid ratio of ~0.05 [Figure 24A]. However, an abrupt change (D_h 20 nm) in the mean D_h associated with a high standard deviation is observed for ratios $\geq$ 0.06. These findings are consequences of the broadening in size distribution which may be related to the vesicle aggregation [Figure SM9]. The addition of ecPis-4s leads to an linear increase of the ζ values from approximately − 30 mV (pure anionic POPC:POPG) to a ζ value near to netralization (~5 mV) at a peptide:phospholipid ratio of 0.06 [Figure 24B]. Therefore, ζ-potential measurements were also used to estimate the partition constant of the peptide in the presence of anionic membranes.

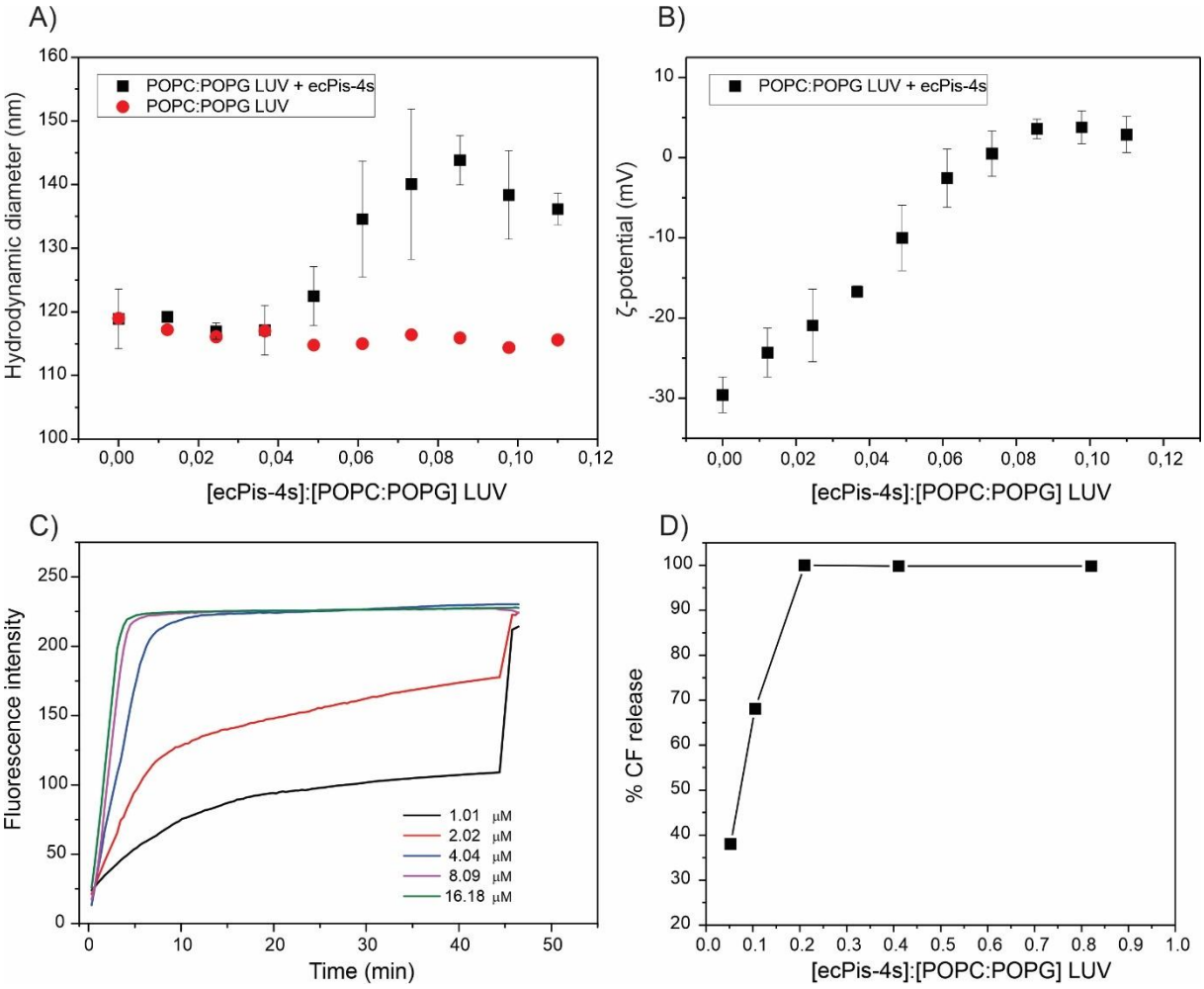

Figure 24. Effect of the addiction of ecPis-4s (336 μM) on (A) the hydrodynamic diameter, (B) the zeta potential of 500 μM POPC:POPG (3:1, mol:mol), and (C) the kinetics of dye release from calcein-encapsulated POPC:POPG (3:1, mol:mol) vesicles (20 μM). (D) Percentage of calcein released from LUVs 30 min after the addition of the peptide. Experiments were performed at 25 °C.

As the ζ-potential is known to be dependent on the binding of a peptide to lipid vesicles when the net charge is affected(285), the partition constant (K_p) of ecPis-4s to POPC:POPG (3:1, mol:mol) LUVs was determined by using equation 8 and 9. The values of -1, and +6 were used as the net charges for the anionic phospholipids and ecPis-4s peptide, respectively. A $Kp = 7.1 \pm 1.6 \times 10^3$ M^{-1} of the ecPis-4s peptide to LUVs was obtained from ζ-potential measurements, assuming a stoichiometry of 1:1 (peptide-charge:lipid-charge) in which each positive charge of the peptide can be neutralized by one negative charge of the anionic lipid in the model(236).

The membrane-disruptive properties of ecPis-4s were investigated by the release of calcein encapsulated in POPC:POPG (3:1, mol:mol) unilamellar vesicles suspended in 10 mM Tris-HCl buffer solution at pH 8.0. Figure 24C presents the results obtained for calcein fluorescence after addition of peptide solution. Dye release is observed even at the lowest concentration tested (~ 1.0 μM) and the lytic activity increases with the peptide concentration, reaching a maximum at 4.0 μM. Figure 24D shows the percentage of calcein released 30 min after the addition of the peptide solution as a function of peptide:phospholipid molar ratio. Dye release above 50% is observed only at molar ratios greater than 0.05, reaching approximately 100% at the 0.2 molar ratio.

3.4 Discussion

In this study, different spectroscopic and biophysical approaches have been used to assess the mode of action and the concentration-dependent membrane disruptive effects of ecPis-4s, a peptide from the piscidin family of great biological interest due to its broad antimicrobial activity(147). As commonly observed in piscidins, ecPis-4s presents a high positive net charge (+7 at neutral medium) due to the presence of three lysine and three arginine residues, as well as an N-terminal amine in combination with a C-terminal carboxamide. Whereas most piscidins are histidine-rich, this peptide carries only a single histidine residue, but a high number of other aromatic residues, most of them located in the first half of the primary structure. Histidines are usually pH-responsive under physiological conditions and therefore may carry another positive charge in medium-acidic environments. In this context, we investigate the mode of interaction of ecPis-4s peptide at acidic and basic pH in the presence of mimetic membranes. Whereas at pH 6 the amino terminus is likely completely and the histidine only partially charged, both have lost all or most of their charge at pH 8.

The association of linear AMPs with the bacterial membranes is usually accompanied by a conformational rearrangement(286). In this context, ecPis-4s is characterized by a random coil-alpha-helix transition in the presence of anionic LUVs under acid and basic conditions [Figure 15A, 15B]. The structure of ecPis-4s in the presence of anionic micelles was obtained at the atomic level using multidimensional solution NMR spectroscopy [Figure 19], which revealed a canonical highly amphipathic helical segment extending from F2 to Q21. A closer look at the three-dimensional structure reveals that His-4 is located at the interface of the hydrophilic and hydrophobic faces.

Oriented solid-state NMR spectroscopy shows an almost perfect in-plane alignment of selectively labelled ecPis-4s within the POPC:POPG (3:1, mol:mol) bilayer surface (orientation II, $86^{o}/49^{o}$ tilt/rotational pitch angular pair [Figure 21] where the hydrophilic residues are either exposed to the aqueous environment or located at the membrane interface. This peptide orientation allows for the complete insertion of the non-charged residues into the hydrophobic core of the bilayer [Figure 21C]. As noticed from distinct perspectives of the topology II [Figure 21B, C], His-4 and Arg-20 residues are located at the interface of negatively charged membranes and Phe-16 and the N-terminal Phe-1 and -2 side chains into the hydrophobic core of the bilayer. The intrinsic fluorescence of Trp-9 reveals the complete membrane insertion of

this site, in excellent agreement with the peptide topology II derived from solid-state NMR spectroscopy. The slightly tilted membrane-alignment of ecPis-4s [Figure 21C] reconstituted into oriented bilayers is likely due to a deeper insertion of the hydrophobic residues especially near the peptide N-terminus.

An amphipathic helical peptide residing at the membrane interface takes more space at the lipid head group region when compared to the hydrophobic inner region(220,287). As a consequence, the order parameters obtained from ^{2}H solid-state NMR data of ecPis-4s in the presence of deuterated POPC-d_{31} and POPG-d_{31} in mixed POPC:POPG (3:1, mol:mol) membranes exhibit a decrease in the presence of the cationic ecPis-4s peptide. While vesicles containing chain deuterated zwitterionic POPC-d_{31} as a reporter caused a moderate reduction of order within the lipid acyl chain region [Figure 22E], the disordering of the fatty acyl chain of POPG-d_{31} lipids increases significantly in the presence of the same proportion of peptide including methylenes in the hydrophobic core of the membrane [Figure 22F]. Thereby, the data also reveal a preferential accumulation of anionic POPG in the vicinity of the cationic peptide when compared to the zwitterionic POPC, as observed previously for other cationic amphipathic sequences(288).

The partition coefficients from fluorescence spectroscopy showed a membrane incorporation of ecPis-4s approximately 2.5 times larger (K_p = 6.8 ± 0.8 × 10^3 M^{-1}) when the peptide was solubilized in the presence of negative LUVs at pH 8, when compared the peptide interaction in the same membrane at pH 6.0 (K_p = 2.9 ± 0.1 × 10^3 M^{-1}) [Figure 17]. These findings are in accordance with CD data which shows higher ellipticities at 222 nm at higher pH, suggesting a greater interaction and deeper bilayer insertion under basic conditions. Such a moderately higher association constant at higher pH and deeper membrane insertion are probably linked to changes in the protonation of the His-4 side chain and/or the N-terminus. However, it should also be noted that with six cationic Lys and Arg within the peptide sequence the pH-dependent changes in the protonation state of the histidine and/or the N-terminus probably do not make much of a difference.

Notably, predicting the charge state of these titratable sites is quite difficult. While the histidine pKa is usually thought to be around 6, it can shift to lower values when exposed to an interfacial or hydrophobic environment(289,290). In a related manner, a range of pKa values (6.8 to 9.1) have been published for the amino-terminal amines(291). The situation is further complicated by the negatively charged membrane surface which can results in very different local H^+ concentrations when compared to the bulk solvent, an effect that not only depends on

the salt concentration but also changes with the membrane-association of the strongly cationic peptide(227,292). Interestingly, the K_{app} value (7.1 ± 0.3 x 10^3 M^{-1}) obtained from ITC is in excellent agreement with the partition constants obtained by Trp-fluorescence (6.8 ± 0.8 × 10^3 M^{-1}) and ζ-potential (7.1 ± 1.6 × 10^3 M^{-1}) measurements in a similar environment. The partition coefficient is widely used to characterize the interactions of AMPs with membrane models in order to predict antimicrobial or cytotoxic activities(130). When compared to other antimicrobial peptides such as Melittin(293,294), Indolicidin(295), Dermaseptin(296), the *K*p values on the interaction of these peptides with membranes are in order of 10^4, ten times higher than ecPis-4s peptide. On the other hand, the piscidin-4 peptide presents the Kp value in the order of 10^3 (as shown), the same one presented for the Magainin-2-amide antimicrobial peptide(297–299). When compared to other piscidin peptides, for instance, Trematocine, a peptide from a red-blooded Antarctic fish, *Trematomus bernacchii*, piscidin-4 peptide also presented a similar partition interaction value. The Kp obtained for Trematocine was also in order of 10^4, as demonstrated by Dalla Pelle and coworkers (2020)(300).

Finally, the effect of the peptide concentration on membrane stability was also investigated by hydrodynamic diameter and zeta potential measurements of POPC:POPG (3:1, mol:mol) LUVs. Membrane destabilization is observed in the peptide:phospholipid molar ratio around 0.06, in which the peptide-membrane interaction results in the vesicle neutralization [Figure 24B] when at the same time agglutination of the LUVs is noted [Figure SM9]. Interestingly, the stoichiometric coefficient indicates that one ecPis4s molecule is associated with fifteen phospholipid molecules ($n \cong 15$ from ITC at 298K), which is in accordance with a peptide:phospholipid molar ratio of 0.06 [Figure 24B].

3.5 Conclusion

In conclusion, different biophysical and structural approaches have been used to investigate the interaction of the antimicrobial peptide ecPis-4s with anionic membranes which allowed to gain insight on how structural and topological aspects of the peptide are important to ensure effective binding to the bilayer. The amphipathic α-helical structure of the highly cationic ecPis-4s peptide ensures high affinity towards anionic membranes driven by strong electrostatic contributions and an insertion of the hydrophobic side chains just below the membrane interface. The resulting partitioning of the amphipathic helix into the membrane interface at a helix orientation parallel to the surface has pronounced effects on the lipid bilayer. Indeed, dye release and DLS experiments indicate pore-formation and membrane-lytic activity which depends on the local peptide concentration. Interestingly a critical peptide:phospholipid ratio of ~0.06 is required to neutralize the membrane surface charge.

When the deuterium order parameters of POPC-d_{31} were investigated, the presence of ecPis-4s had an influence on the zwitterionic acyl chain mainly deep inside the membrane core. Notably, the disordering is more pronounced for POPG-d_{31}, which suggests that this anionic lipid accumulates in the vicinity of the cationic peptide. This is in-line with the importance of electrostatic interactions for membrane association. Titration experiments using Trp fluorescence, ζ-potential, and ITC techniques all provide similar affinity constants for ecPis-4s to POPC:POPG (3:1, mol:mol) membranes that saturate at a concentration corresponding to nominal charge neutrality. Overall, these findings indicate that ecPis-4s follows a well-defined mode of interaction with the anionic membrane, where electrostatic interactions assure selectivity for bacterial membranes. Openings occur involving in-plane oriented amphipathic peptides and lipids as has been previously been shown for other cationic amphipathic peptides of similar size(220).

All these findings indicate that ecPis-4s cover the membrane surface in a mechanism of interaction suggesting a membrane-lytic action via pore-forming activity once the local concentration or peptide reaches a threshold, in which ecPis-4s peptide interacts with a well-defined amphipathic structure with its hydrophilic side chains face the aqueous solution, and the hydrophobic to the phospholipid bilayer, enhancing membrane order destabilization as well as its lytic activity.

Chapter 4: The structural stability of bioactive ecPis-4s peptide in aqueous solution is a determinant of its proteolytic resistance

4.1 Introduction

Multidrug-resistant (MDR) bacterial infection has become a serious threat in human therapeutics make raising the development of new antibiotics(2). Therefore, many research and new approaches have been investigated in order to identify new drug candidates(147,301). Antimicrobial peptides (AMPs) have been proposed as a promising alternative to the treatment of infections due to multidrug-resistant bacteria and to avoid bacterial resistance development(1).

Different from conventional antibiotics, which act on specific cell targets, AMPs interacts with the phospholipid membrane leading to cell lysis(2,302). Studies of AMPs activity against bacteria focus on some of its important membrane components, such as lipopolysaccharide and phospholipids whose compositions are predominantly anionic(1,3,178,303). Therefore, most AMPs are cationic and the electrostatic attraction seems to contribute to the targeting and selectivity of these membranes(5).

Although a great number of antimicrobial peptides acquire secondary structure when they interact with the phospholipid membrane, some peptides display ordered conformation even in aqueous media, before achieving the target membrane(304). This structural behavior is observed for dimeric peptides(6,305), and aggregate forms of some peptides.

NMR studies in an aqueous solution of the heterodimeric peptide Distinctin revealed a three-dimensional structure of a dimer of dimers, in which the closely packed four helical chains assures that the hydrophobic residues are screened from the solvent. The molecular dynamics studies of Bombinin H2 demonstrated that the peptide self-aggregates adopting a single-helix structure in an aqueous solution(306). Other peptides such as Magainin 2 (MG2), and Tachyplesin 1 (TP1) act in a synergistic way on an aggregation process, which potentiates the biological activity against different bacteria strains(307). Besides excerpt direct effect in the

antimicrobial activity, the oligomerization and aggregation process could prevent the peptides from degradation by peptidases(305,308). It is well known that proteolytic cleavage can be avoided by the cyclization of the peptide or the introduction of a D-amino acid in the peptide sequence(309). However, the naturally occurring aggregation process can be a feature that also protects antimicrobial peptides against peptidases and is fully associated with the resistance to enzymatic degradation of these biomolecules(310).

Taking all these into consideration, in this work we chose two enzymes which break down proteins or peptides. Trypsin and proteinase K are two common proteases that are used in proteolysis assays(311). The first enzyme, trypsin is a serine protease that cleaves peptide bonds on the C-terminal side of arginine and lysine residues, except when they are followed by proline(312,313). Trypsin is useful for digesting proteins into smaller peptides that can be analyzed by mass spectrometry or other techniques(314,315). On the other hand, proteinase K is a broad-spectrum protease that cleaves peptide bonds on the N-terminal side of aliphatic, aromatic, or hydrophobic amino acids(316). This enzyme can digest a wide variety of proteins, including those that are resistant to other proteases. Besides that, proteinase K is also used to remove surface proteins from membrane vesicles, and to study the structure and function of prion proteins(315).

In this chapter, we performed different physico-chemical investigations of the concentration dependence of structure and resistance to the enzymatic degradation of ecPis-4s piscidin peptide. We have highlighted structural features of ecPis-4s in aqueous solution which provides insights about the interaction of ecPis-4s as well as the enzymatic resistance of the peptide. Additionally, we have determined in a quantitative manner the critical concentration to the aqueous folding and the enthalpy associated to the unfolding process. Furthermore, the three-dimensional structure of ecPis-4s peptide was obtained in an aqueous solution. Thereby, to our knowledge, this is the first structural and physico-chemical characterization of a piscidin peptide in aqueous environments.

For this chapter, some results were obtained in collaboration. Thus, AUC assays and data analysis were carried out in collaboration with the Institut de Biologie Structurale, Grenoble, France. Besides that, the biological activity and bacterial death kinetics experiments were performed by the Institute of Biological Sciences of the Federal University of Minas Gerais, Brazil.

4.2 Materials and Methods

4.2.1 Peptide synthesis, purification and characterization

The carboxamide ecPis-4s peptide was synthesized, purified, and characterized as indicated in item 2.1 (pg. 11). The purified fractions of interest were pooled, evaporated, and lyophilized. The peptide was dissolved in 4% (by volume) acid acetic at a concentration of 1 mg/ml with subsequent lyophilization, repeated three times, to ensure the exchange of the TFA anions with acetates, and stored at - 20 °C.

4.2.2 Circular dichroism spectroscopy

The secondary structure preferences of the ecPis-4s peptide in aqueous environment were investigated by circular dichroism (CD) spectroscopy on a JASCO® J-810 spectropolarimeter (Tokyo, Japan), equipped with Peltier Jasco temperature control system - PFD-425S (Tokyo, Japan). The samples were prepared containing 50 μM of ecPis-4s peptide, then they were solubilized in aqueous solution or in 10 mM phosphate buffer containing 100 mM KF at pH 6.0 and pH 8.0(275). The analyzes were performed at 25 °C in a cuvette of 1.0 mm path length. The spectra were recorded from 190 to 260 nm, with the accumulation of three scans, bandwidth of 0.1 nm, step resolution of 0.2 nm, 50 $nm.min^{-1}$ scan speed and 1 s response time. Similar experiments in absence of peptide were recorded as the respective blank solution to allow the subtraction of the background.

4.2.3 Solution nuclear magnetic resonance spectroscopy

Two-dimensional solution NMR experiments were carried out to determine the three-dimensional structure of ecPis-4s peptide at 4 mM in presence of aqueous environment. The experiments in water were performed at 25 °C on a Bruker® *AVANCE NEO* OneBay spectrometer operating at 600.15 Hz (for ^{1}H). The samples consisted of 4 mM of ecPis-4s diluted in 10% (v/v) D_2O/H_2O containing 1% (v/v) of 2,2-dimethyl-2-silapentane-5-sulfonate (DSS) as the internal reference.

Two-dimensional homonuclear Total Correlation Spectroscopy (^{1}H-^{1}H TOCSY) spectra were obtained using the *dipsi2esgpph*(317) pulse sequence with 32 t_1 increments, 4096 transients of 4096 points for a spectral width of 6849.315 Hz. Two dimensional Nuclear Overhauser Spectroscopy (^{1}H-^{1}H NOESY) spectra were obtained using the *noesysgpphwzs*(317) pulse sequence collecting 32 t_1 increments with 512 transients of 2048 points for a spectral width of 6849.315 Hz.

4.2.4 NMR analyses and structure calculations

The proton resonances were assigned by simultaneous analyses of homonuclear ^{1}H,^{1}H-TOCSY and ^{1}H,^{1}H-NOESY contour maps using Wuthrich method(208). The NMR assignments for this peptide were performed manually by using NMRViewJ (version 9.2.0-b20) program(253). The NOE intensities were converted into semi-quantitative distance restrictions with limits of 2.8, 3.4, and 5.0 Å(254). The dihedral angles φ (phi) and ψ (psi) restrained list was obtained based on the chemical shifts of H_N, H_α, H_β, C_α, C_β and N using the TALOS+ program(213) of the NMRPIPE® computational package(255). The ^{13}Cα chemical shift index obtained from natural abundance were calculated for ecPis-4s peptide in the presence of aqueous solution in accordance with Wishart method(212). The geometric restraints were validated (according to their consistency and contribution) from data of uniqueness information from the QUEEN program (Quantitative Evaluation of Experimental NMR Restraints)(256).

The XPLOR-NIH software was used for the calculation and refinement of the three-dimensional structures employing simulated annealing protocol in torsional angle dynamics(257,258). First, the system was rapidly heated to 5000 K and then slowly cooled to the temperature of 1000 K, for 1000 cycles. Next, another slow cooling from 1000 K to 300 K was carried out in 1000 steps. A total of 100 structures were obtained and refined in a subsequent calculation, using more stringent topology parameters(259). The 10 lower energy structures were visualized and analyzed with Chimera(261), and the quality of the structures verified by the Ramachandran diagram and the RMSD (Root Mean Square Deviation), both obtained from the online platform PSVS(262).

4.2.5 Analytical ultracentrifugation – Sedimentation velocity

Sedimentation velocity (SV) experiments were performed at 20 °C using a Beckman Optima XL-I (Beckman Coulter, Brea, USA) analytical ultracentrifuge equipped with a four hole An-60-Ti rotor, an UV-vis absorbance spectrometer and a Rayleigh-interferometer for optical detection, and the ProteomelabTM software for data acquisition. Samples of lyophilized ecPiscidin-4 peptide at concentrations 2400, 1200, 600, 100 and 25 µM were solubilized in 10 mM monobasic dihydrogen phosphate and dibasic monohydrogen phosphate in 100 mM Potassium fluoride (KF), pH 8.5. Peptide samples were loaded to epon double-sector centerpieces cells of 1.5 and 12 mm pathlength equipped with sapphire windows (Nanolytics, Potsdam, DE). The samples were centrifuged at 60000 rpm and the scans were collected at 280 nm (absorbance) and 655 nm (interference)(318–322). *Data analysis*: the time errors of the collected scans were corrected using REDATE software (version 1.0.1) (*biophysics.swmed.edu/MBR/software.html*)(209), and the data were fitted using Continuous c(s) Distribution model in SEDFIT software (version 16.36)(319,321) to obtain sedimentation coefficient distribution values (s-values). Graphical of representative SV data were made using GUSSI software (version 1.4.2)(323).

4.2.6 Diffusion ordered spectroscopy (DOSY) experiments

1D ^{1}H and 2D DOSY (Diffusion Ordered Spectroscopy) NMR experiments of ecPis-4s were acquired on a Bruker Avance III-500 spectrometer operating at a ^{1}H frequency 500.13 MHz, with a 5 mm z-gradient inverse probe at the temperature 298.15 K. The ecPis-4s samples were prepared at different concentrations (4.0 mM, 2.0 mM, 1.2 mM and 0.6 mM), in aqua solution (H_2O:D_2O/ 90:10% v/v), using DSS-d_6 as an internal reference standard.

Diffusion parameters time (d20) and the diffusion gradient length (p30) was optimized using the pulse sequence from the Bruker library in order to obtain at least 95% signal attenuation due to diffusion. After optimizing the parameters obtained was 0.1 s for d20 and 2000 µs for p30. The 2D DOSY experiments was acquired using the pulse sequence *stebpgp1s19* varying the gradient strength from 2 to 95%, at 25 linear steps in 64 transients with 4096 points, and spectral width of 7500 Hz in F2 and 5000 for F1. Data processing was

performed using the Bruker Topspin 3.5 software, and the diffusion coefficient (D) was estimated using Bruker software Dynamics Center version 2.8.0.1.

4.2.7 Isothermal titration calorimetry

Isothermal titration calorimetry (ITC) assays were carried out on a VP-ITC microcalorimeter (Malvern, UK). Two strategies were used for obtaining information to determine the corresponding heat of dilution with ecPis-4s peptide used as a titrant in the experiments. For the first assay, the syringe was fulfilled with ecPis-4s solution (1200 μM) in 50 mM phosphate buffer at pH 6.0 containing 100 mM NaCl, and the calorimeter cell was filled up with the same buffer solution. In the second one, ecPis-4s peptide (1200 μM) suspended in 50 mM phosphate buffer at pH 8.0 containing 100 mM NaCl was transferred to the syringe, while the reaction cell was filled up with the same phosphate buffer. The reference cell was filled with the equivalent solvent for each experiment and the instrument was pre-equilibrated at 25 °C. Afterwards, aliquots of ecPis-4s solution (5 μL) were added with 30 successive injections into the sample cell with 2 s injection times, and intervals of 300 s. ecPis-4s peptide samples were previously degassed in a Microcal Thermovac® (Malvern, UK). The data obtained were recorded and processed using Origin software for ITC (Microcal Origin® 6.0). Furthermore, the enthalpy of unfolding (ΔH_{unfold}) in both assays was calculated by a data treatment previously described(284,324), in which linear fits of the dataset in the lower and upper concentration ranges were performed, and then, the y-intercepts of the two straight lines were determined. The enthalpy of unfolding was calculated as the difference between the two intercepts.

4.2.8 Degradation assays

ecPis-4s peptide samples at different concetrations (100 and 1200 μM) were digested with trypsin in 10 mM potassium phosphate buffer pH 8.0 at 37 ℃ using an enzyme:substrate ratio of 1:50 (w/w) in a total volume of 300 μL. Equivalent samples (20 μL) were prepared for each concentration and submitted to different times of digestion (0h – 8h). Enzyme inactivation was achieved by adding 5 μL of a HCl (1 mM) solution. Aliquots from the enzymatic reaction (1 μL) were withdrawn on a time course basis and directly analyzed with a matrix-assisted laser

desorption ionization technique (MALDI-TOF Autoflex mass spectrometry, Bruker Daltonics, Bremen, Germany). A mixture of 1 μL of analyte solution (ecPis-4s peptide digested sample), and 1 μL of matrix solution (α-cyano-4-hydroxy-cinnamic acid (10 mg/mL in 30% acetonitrile) were applied to the target plate, mixed and dried at room temperature. Peptide and protein molecular mass standards were eventually added.

At the second step, ecPis-4s at different concentrations (50 and 150 μM) were also digested in the presence of proteinase K enzyme in 10 mM potassium phosphate buffer pH 8.0 at 37 °C using an enzyme:substrate ratio of 1:25 (w/w) in a total volume of 200 μL. Equivalent samples were prepared for each concentration and submitted to different times of digestion (0h – 8h). Enzyme inactivation was achieved by adding 5 μL of a HCl (1 mM) solution. Samples were also analyzed by LC-ESI-MS technique using LC MS-2020 single-quadrupole mass spectrometer (Shimadzu). Peptide mixtures were separated with a Vydac C18 column (250 mm × 1 mm, 5μm), using a linear gradient from 10 to 90% acetonitrile containing 0.1% TFA, over a period of 60 min, at a flow rate of 0.8 mL/min. Spectra were acquired in the range of m/z 10-1500.

4.2.9 Kinetics of bacterial death

The bacterial death kinetics experiments were designed based on Ling and coworkers(325), and performed in triplicate. The bacterium *S. aureus* was grown in MH broth (10^5 CFU.mL^{-1}), bacteria were exposed to ecpis-4s peptide at different concentrations (½, 1, 2 and 4 times the MIC value), at 37 °C, for different incubation time (0, ½, 1, 2, 4, 6, 8, 10, and 12h). Then, the viability of the cell suspensions was determined by the microdrop technique(326). Therefore, the suspensions were subjected to serial dilutions (10^{-1}, 10^{-2}, and 10^{-3}), and drops of 5 μL were transferred to plates containing BHI agar. The plates were incubated at 37 °C for up to 12 hours, when the colonies were counted per drop. The number of colonies counted was multiplied by the reciprocal of the dilution and the result was expressed as colony forming units (CFU).

4.3 Results

4.3.1 Structural analyses of ecPis-4s peptide in aqueous solution

Circular Dichroism (CD) spectroscopy: In order to investigate the effect of concentration on the conformational preferences of ecPis-4s peptide, CD experiments were performed at the 0.3 – 2.4 mM range in water environment, pH 5.0, and in the presence of 10 mM potassium phosphate buffer at pH 8.0 [Figure 25].

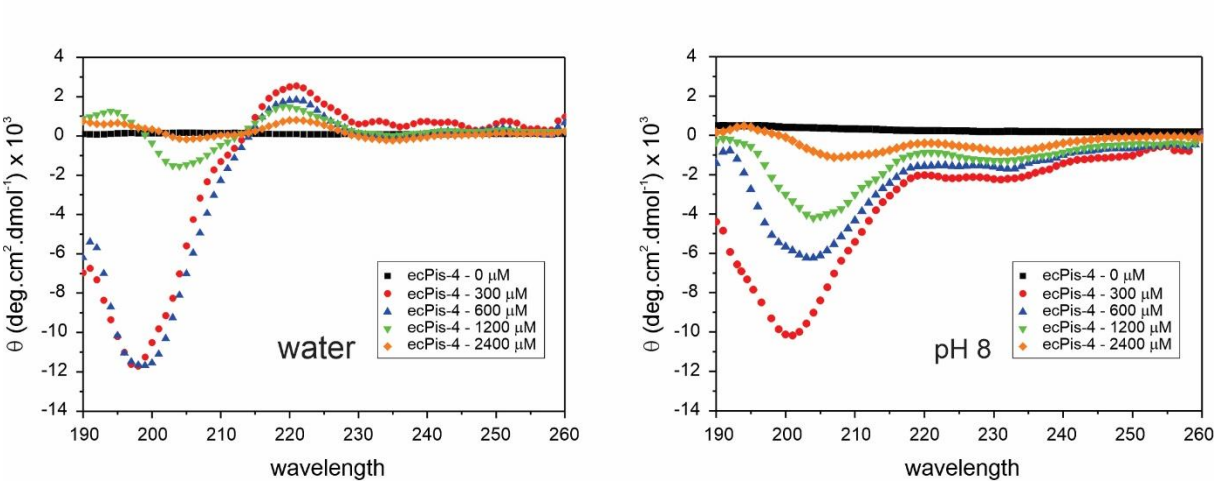

Figure 25. CD spectra of ecPis-4s in water environment (A), and in the presence of 10 mM phosphate buffer at pH 6.0 (B) and pH 8.0 (C). Peptide concentration ranging from 0.3 – 2.4 mM.

As we can observe, in water environment a minimum at ~198 nm is noted for 0.3- and 0.6-mM peptide concentration while in pH 8 buffered solution a signal around 200 nm is observed only for the peptide concentration of 0.3 mM, which is typical of predominantly random coil conformations(327). On the other hand, considerable wavelength shifts are noticed for peptide concentrations ≥ 1.2 mM. In both environments, the spectra at 1.2 and 2.4 mM are characterized by a minimum near 208 nm showing a degree of ordered alpha helical conformations. Spectral profiles change substantially at 2.4 mM, despite it presents a low ellipticity. These conformational changes seem to indicate a beginning of an ordering of the peptide which takes place at a critical peptide concentration, mainly at higher pH [Figure 25].

Two-dimensional solution NMR spectroscopy: As CD spectroscopy indicated that ecPis-4s presents some structural arrangement in aqueous environments [Figure 26], it was proposed to investigate in further details the structure of the peptide in similar condition by NMR spectroscopy. Therefore, NMR spectra of ecPis-4s at 4.0 mM in water containing 5% of D_2O were recorded.

Most of the amino acid spin systems were identified in the TOCSY spectrum [Figure SM10] since there was no observed superposition in the H_N-H_α region. Unequivocal assignments were obtained from sequential and some medium range NOE correlations, as showed in the H_N-H_α region of NOESY spectra [Figure 26].

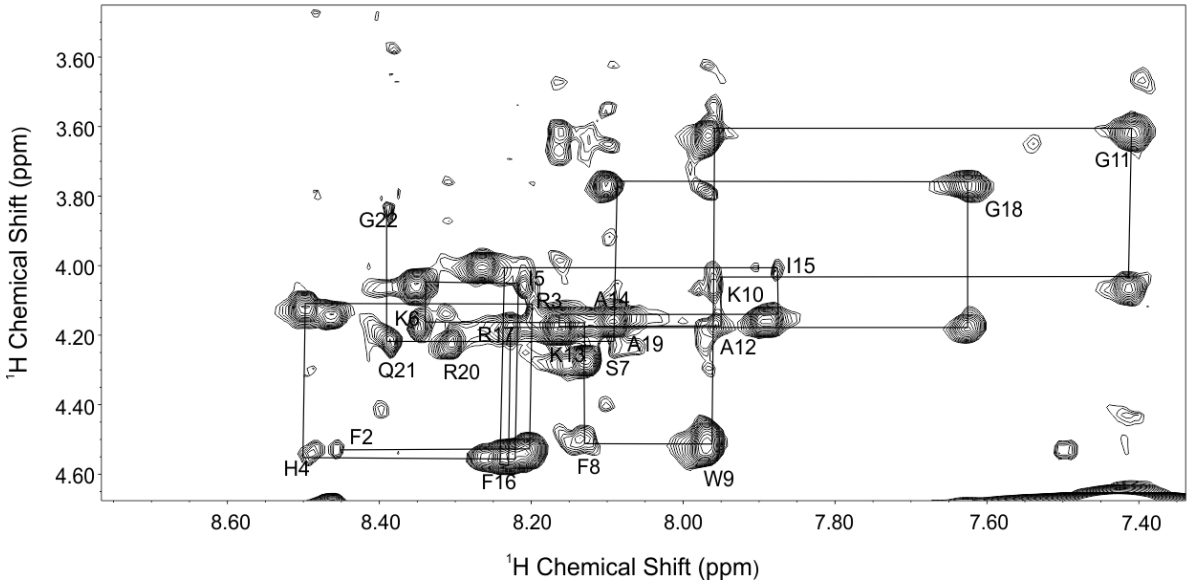

Figure 26: H_N-H_α region of NOESY spectrum of ecPis-4s at 4.0 mM in water containing 5% of D2O. Spectrum recorded at 25 ºC, 600 MHz. Only the inter-residual HN-Hα (i, i +1) cross peaks are labeled.

Although no d_{NN} (i, i+1) correlation has been observed, sequential and medium-range $d_{\alpha N}$ NOE correlations ranging from F2 up to R17 are identified in the NOESY spectrum of ecPis-4s which suggests the existence of helical segment encompassing these amino acid residues. The NOE connectivities characteristics of helical secondary structure are graphically summarized in Figure SM11.

The three-dimensional structures of ecPis-4s were obtained based on NOE distance and dihedral angle restraints derived from NOE and chemical shift data, respectively. The superposition of the 10 lowest energy structures presented in Figure 27A is characterized by a RMSD of 2.12 for the backbone atoms from K10 to R20 which suggests a significant degree of

conformational flexibility for the ecPis-4s in water, and as observed a high conformational dynamic for this peptide at the N-terminus region. Table SM4 presents a summary of all the input data used in the calculation as well as the quality parameters. The majority of the ϕ and ψ dihedral angular pairs are found in the most favored regions of the Ramachandran plot, indicating the high stereochemical quality of the obtained structures. However, approximately 40% of the residues are found in disallowed regions which comprise the N-terminus region of the peptide chain.

ecPis-4s structure is characterized by a relatively small helical segment extending from K10 to R20 [Figure 27B] which reveals a significant amphipathic character as the positively charged K10, K13, R17, and R20 residues lye within the hydrophilic face [Figure 27D]. The more flexible region of the peptide encompasses four aromatic residues, namely W9 along with F1, F2, and F8 at the peptide N-terminus.

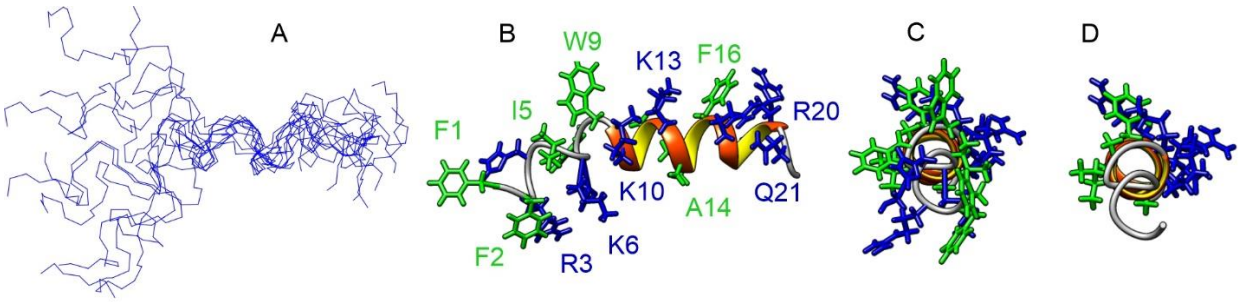

Figure 27: Three-dimensional structures of ecPis-4s (4.0 mM) in water at 25 °C. (A) Overlap of the ten lowest-energy structures (from F10 to R20). The lowest-energy structure is presented from different perspectives, *i.e.*, (B) with the hydrophilic face of the helix, and (C and D) with the peptide N-terminus facing forward. Whereas in (B and C) all side chains are explicitly presented, in (D) only side chains of residues from the helical segment are shown. The hydrophobic residues are presented in green and the hydrophilic residues in blue.

Diffusion-ordered spectroscopy (DOSY) NMR Studies: The diffusion of a molecular species depends on its effective molecular size which should change with any intermolecular interaction; therefore, mixtures in which chemical entities are part of a network of interactions in equilibrium can be analyzed(328). In this way, DOSY NMR can be very helpful to understand the rate of protein aggregation and oligomer formation. To further characterize ecPis-4s peptide behavior as a function of its concentration, the coefficient diffusion of ecPis-

4s peptide was determined by using DOSY NMR. The experiments were recorded in the concentration range from 0.6 to 4.0 mM [Figure 28].

The eight selected signals from the ecPis-4s peptide observed in all DOSY plots are related only to one diffusion coefficient for each concentration tested which suggest that only one molecular structure is presented in each solution. The diffusion coefficients for ecPis-4s in all concentrations were determined to be between 1.37 and 1.46 x 10^{-10} m2 /s [Table 2] which is lower than the internal reference, 5.98 x 10^{-10} m2 /s due to the smaller hydrodynamic volume of the reference standard.

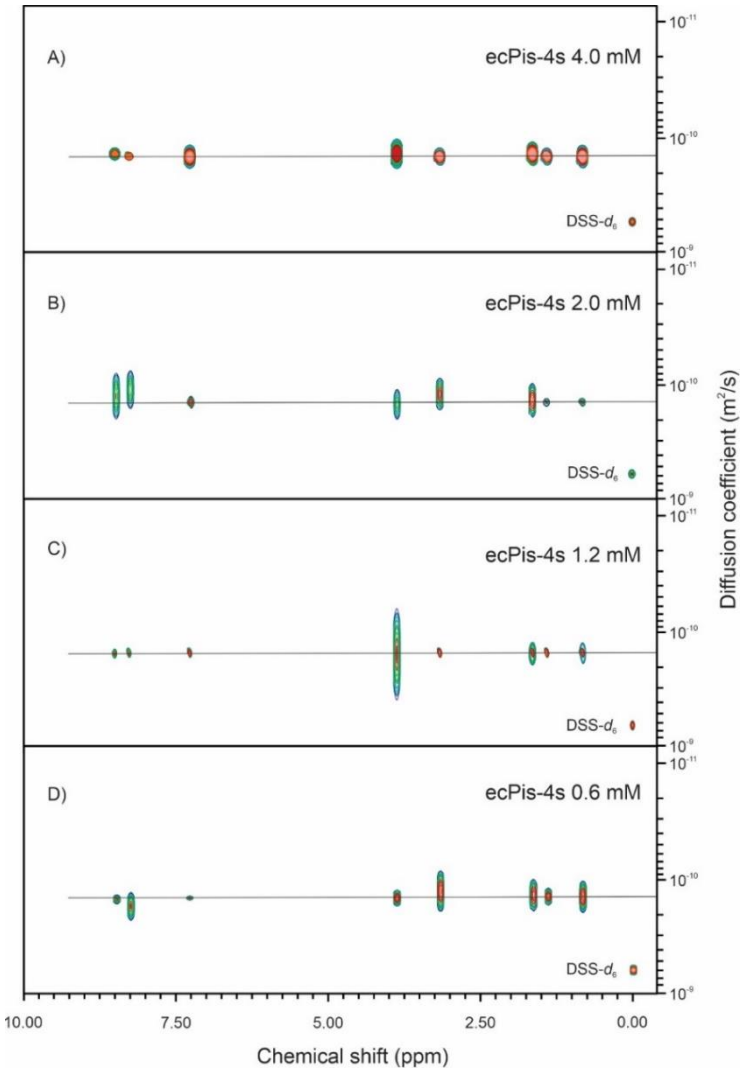

Figure 28: DOSY plot from ecPis-4s peptide at 4.0 mM (A), 2.0 mM (B), 1.2 mM (C), and 0.6 mM (D) in water environment (H_2O:D_2O 90:10% v/v). DSS-d_6 is presented at 0 ppm. Data were collected on a Bruker Avance III 500 spectrometer operating at a ^1H frequency 500.13 MHz and processed in Bruker software Dynamics Center version 2.8.0.1.

Table 2. Diffusion coefficients determined by DOSY NMR in H_2O/ D_2O solution at 298.15 K

Peptide concentration	**D_{obs} (x 10^{-10} m^2/s)**	**Standard error (10^{-10})**
ecPis-4s 4 mM	1.40	0.02
ecPis-4s 2 mM	1.37	0.08
ecPis-4s 1.2 mM	1.43	0.10
ecPis-4s 0.6 mM	1.46	0.13

Sedimentation Velocity (SV) analysis of ecPis-4s by Analytical ultracentrifugation (AUC):
AUC is a versatile and powerful method for the quantitative analysis of aggregates in solution(329). AUC-SV experiments were performed to assess the hydrodynamic, self-association, aggregation and stability of ecPiscidin-4 peptide in buffer, i.e., in the absence of lipid mimic membrane [Figure 29]. The sedimentation coefficient distribution- $s_{w,20}$ = (0.43 ± 0.03) S and estimate MW = (2877 ± 231) Da is compatible to monomeric species in the range of peptide concentrations studied (25 – 2400 μM). The frictional ratio value ($*f/f_o$ = 1.47 ± 0.07) correspond to a globular conformation for the peptide. The monomer peak represents ≥ 95% of the total intensity, indicating the absence of significant self-association.

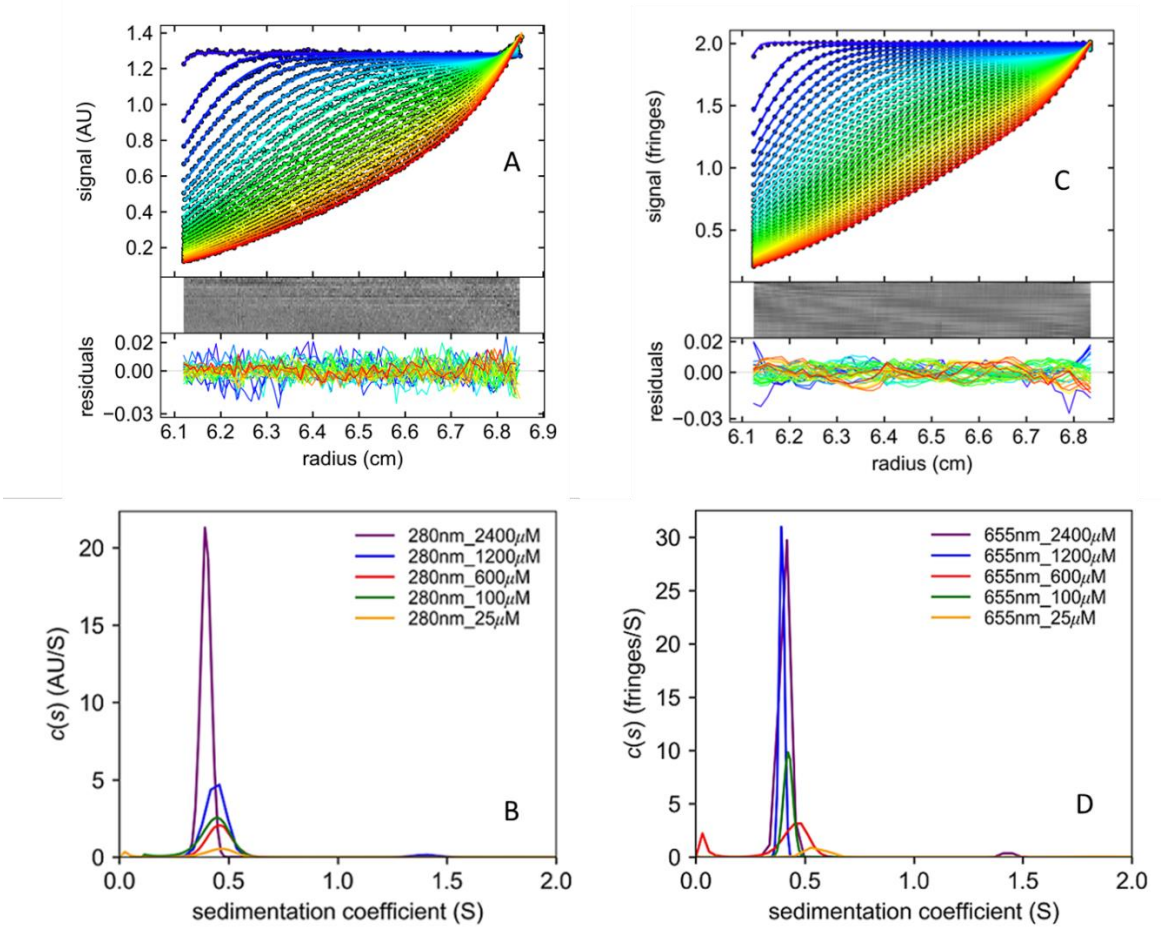

Figure 29: Top: Sedimentation velocity profile of the scans collected to sample of ecPiscidin-4 peptide at 2400 μM using absorbance (panel A) and interference (panel C) optics. Circles: experimental sedimentation boundaries; Solid line: best-fit model calculated using *Continuous c(s) Distribution model* on SEDFIT; Midlle (panels A and C): grey scale for residual bipmap(330). Bottom (panels A and C): residuals of the fit with a root-mean-square deviation (rmsd) of 0.006252 OD to absorbance and 0.004472 fringes to interference. Panels B and D: Sedimentation coefficient c(s) distribution calculated on SEDFIT to the tested concentration range of ecPiscidin-4 peptide from absorbance at 280 nm (B) and interference at 655 nm (D) data.

4.3.2 Biophysical studies of ecPis-4s peptide in absence of membrane media

Isothermal titration calorimetry (ITC): The critical concentration and the enthalpy of the unfolding process (ΔH^{o}_{unfold}) of the ecPis-4s peptide in aqueous solution were evaluated by using the isothermal titration calorimetry (ITC) technique(284). The experiment consisted of the dilution of a concentrated peptide solution into phosphate buffer at pH 6.0, or pH 8.0. The

experiments were carried out at 25 °C with sequential additions of 5 μL of the peptide solution at 1200 μM into the calorimetric cell filled containing the respective phosphate buffer.

Figure 30 presents the heat flow and the integrated heats in function of ecPis-4s peptide concentrations which shows a typical sigmoidal profile. The heat flow of each peptide addition is endothermic and the enthalpogram displays a decreasing trend before reaching an inflection point. As shown, on increasing the peptide concentration in the reaction cell, the heat flow decreases and reaches constant values (peptide dilution heats) at the end of the experiment.

The ΔH^{o}_{unfold} values were obtained by a linear fitting of the data between the upper and lower concentration ranges according to the method applied by Tiné and coworkers(284). According to this approach, the ΔH^{o}_{unfold} is defined as the difference between the two intersection points from each straight lines with the y axis. In both investigated media, the unfold process characterized by endothermic events with enthalpy values of ΔH^{o}_{unfold} equal to 4.4 kcal.mol^{-1} at pH 6.0, and 6.9 kcal.mol^{-1} at pH 8.0 phosphate buffer [Figure 30B, and 30D]. These results also indicate that the aggregation process of ecPis-4s in aqueous solution is enthalpically driven. Moreover, we can observe the inflection point in the enthalpograms results [Figure 30B, and 30D] which present the concentration of disassembly or unfolding process, around 40 μM.

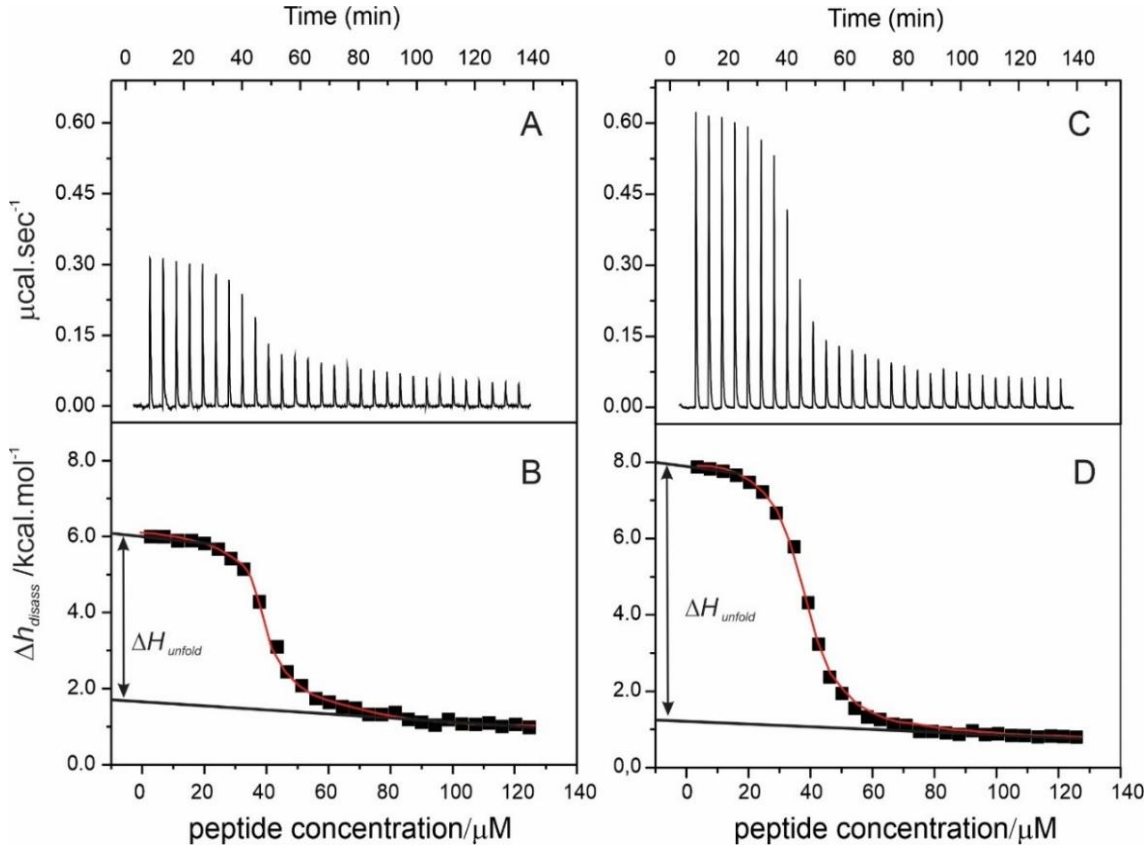

Figure 30: Isothermal titration calorimetry of ecPis-4s peptide at 1200 µM at 25 °C in phosphate buffer at pH 6.0 (A), and pH 8.0 (C). (A; C) Heat flow for piscidin-peptide injection as a function of time (raw data). (B) Enthalpy as a function of the dilution of ecPis-4s in water, which reveals a typical dilution enthalpogram of unfold process.

Degradation assays by peptidases: Proteolysis experiments have been carried out to investigate the degradation of polypeptides by peptidases as well as to identify folded and/or resistant structural regions of these bioactive compounds(331). Time course proteolysis experiments were performed by digesting ecPis-4s peptide at 100 µM and 1200 µM [Figure 31A, and 31B, respectively] with 1:50 (w/w) trypsin to substrate ratio, or ecPis-4s peptide at 50 µM and 150 µM with 1:25 (w/w) proteinase K to substrate ratio [Figure 31C, and 31D, respectively].

The enzyme kinetics of trypsin is similar at both tested concentrations and the peptide is almost completely degraded after 1h of digestion [Figure 31A, and 31B]. The peak at m/z 847.4 corresponds to the segment encompassing the six first amino acids residues of the peptide sequence (FFRHIK) which reveals that the N-terminal region seems to be at least partially resistant to trypsin cleavage. On the other hand, differences are noticed in the degradation kinetics by proteinase K [Figure 31C, and 31D]. The complete degradation of 50 µM ecPis-4s

occurs after 2 h of exposure of the peptide to this enzyme [Figure 31C]. However, at the high peptide concentration (150 μM) the kinetics of degradation is clearly slower and the almost complete degradation is achieved only after 8h of incubation [Figure 31D].

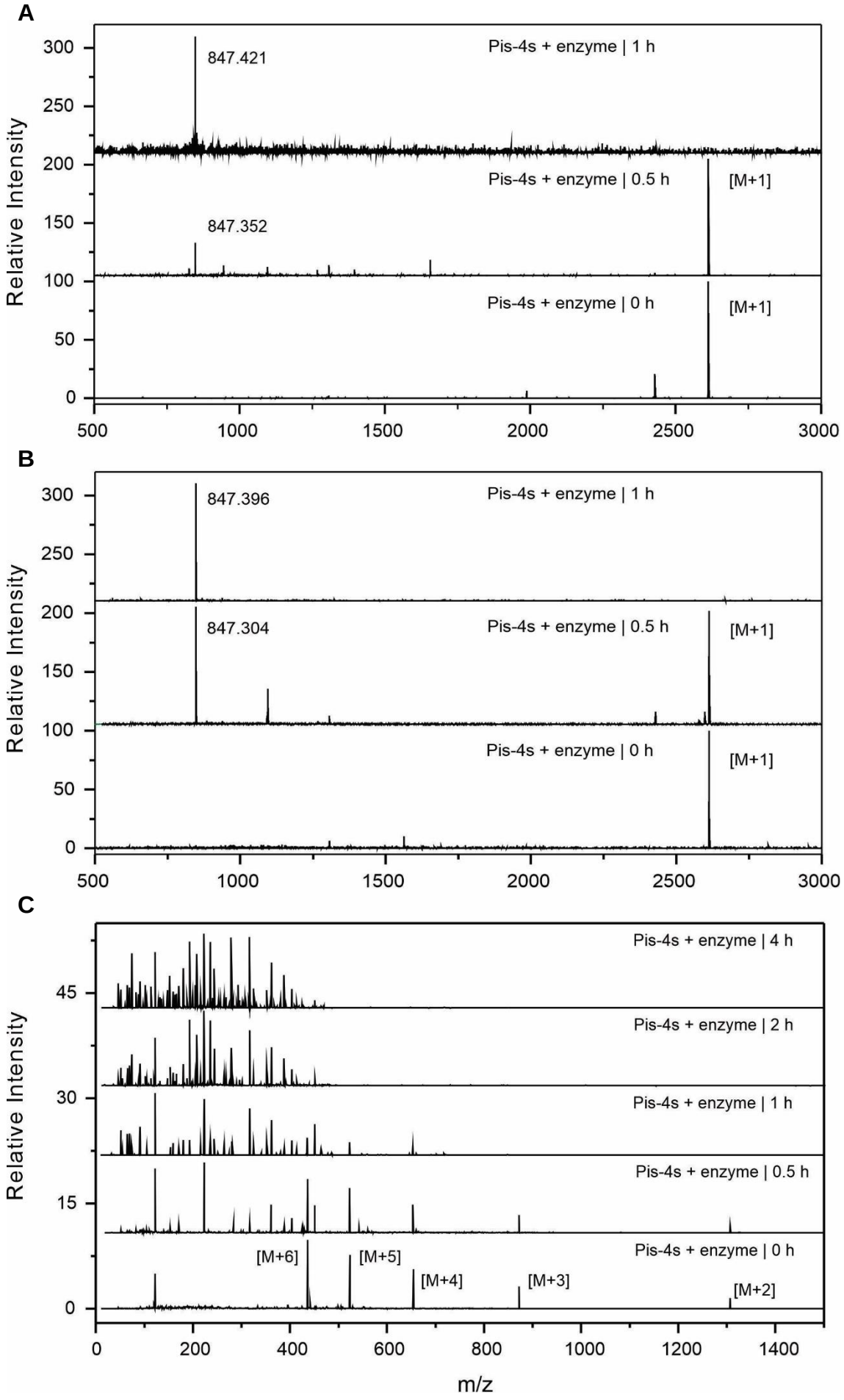
A
Relative Intensity
847.421
Pis-4s + enzyme | 1 h
Pis-4s + enzyme | 0.5 h
[M+1]
847.352
Pis-4s + enzyme | 0 h
[M+1]
B
Relative Intensity
847.396
Pis-4s + enzyme | 1 h
847.304
Pis-4s + enzyme | 0.5 h
[M+1]
Pis-4s + enzyme | 0 h
[M+1]
C
Relative Intensity
Pis-4s + enzyme | 4 h
Pis-4s + enzyme | 2 h
Pis-4s + enzyme | 1 h
Pis-4s + enzyme | 0.5 h
Pis-4s + enzyme | 0 h
[M+6]
[M+5]
[M+4]
[M+3]
[M+2]
m/z

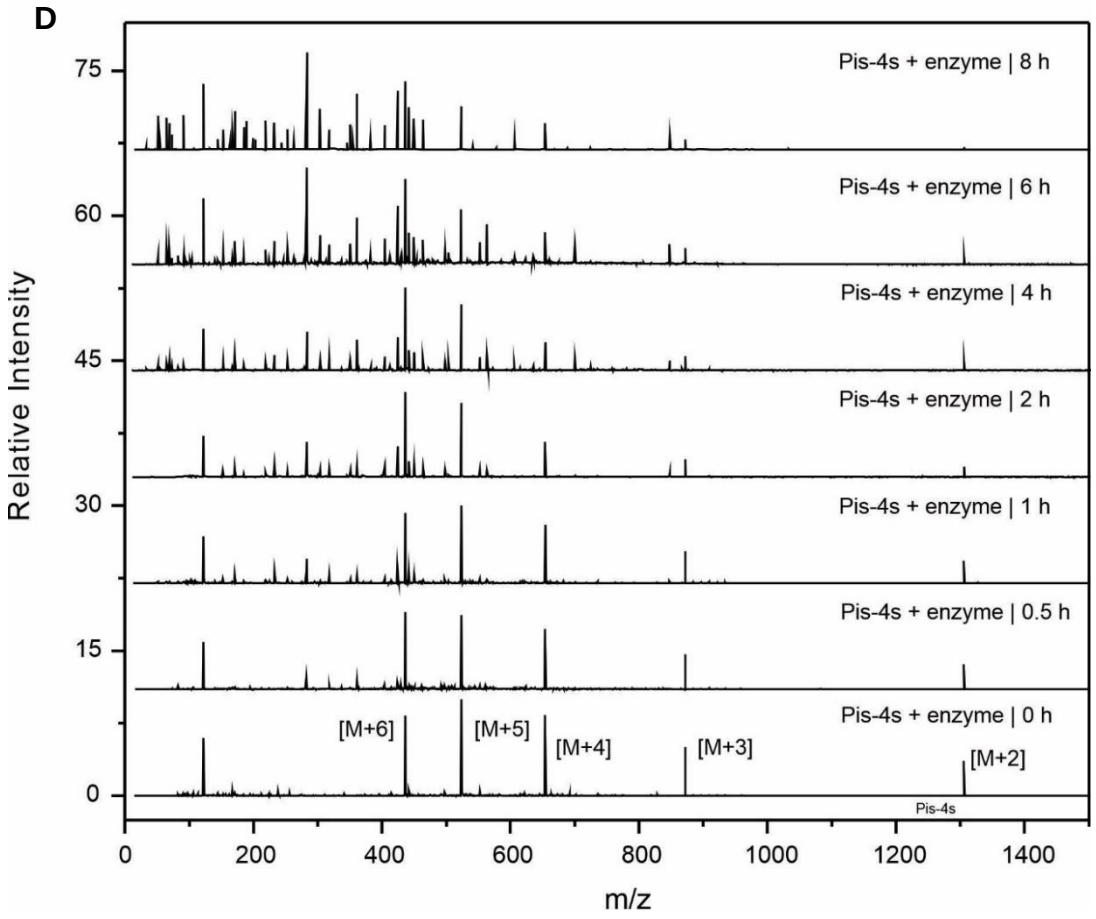

Figure 31: Comparative proteolytic degradation of ecPis-4s. ecPis-4s at different concentrations was incubated with a weight ratio of 1:50 (enzyme to substrate) of trypsin and 1:25 (enzyme to substrate) of proteinase K both in 10 mM potassium phosphate, pH 8.0 at 37 °C. (A) After 0, 0.5, and 1.0 h of digestion, aliquots (5 μL) of ecPis-4s peptide at (A) 100 μM, and (B) at 1200 μM were withdrawn on a time course basis, and directly analyzed by MALDI-TOF MS. (C and D) HPLC-ESI-MS analysis of the degradation of ecPis-4s by proteinase K. (C) Peptide at 50 μM after 0, 0.5, 1, 2, and 4 h of incubation and (D) at 150 μM after 0, 0.5, 1, 2, 4, 6, and 8 hours of incubation. The absorbance profile of the control (peptide in absence of enzyme, not shown) is pretty similar to the result obtained for the peptide + enzyme at T = 0 h.

4.3.3 Biological assays for ecPis-4s peptide

Antibacterial activity: The antibacterial activity of ecPis-4s was investigated against gram-positive (*S. aureus, S. agalactae,* and *L. monocytogenes*) and gram-negative (*S. typhimurium, E. coli, P. miravilis, K. oxytoca* and *P. aeruginosa*) strains, and the results observed were compared with the chloramphenicol at 30 $mg.ml^{-1}$. The peptide was highly active against the tested bacteria and the respective minimum inhibitory concentrations (MIC) values are

presented in Table 3. Whereas ecPis-4s was able to eradicate the growth of *P. miravilis,* and *S. agalactae* strains at 50 μM, similar activity for *S. typhimurium, E. coli, K. oxytoca* and *S. aureus)* was achieved at 25 μM of peptide. An even higher antibacterial potential was observed in the assays against *L. monocytogenes,* and *P. aeruginosa* which revealed an MIC of 12.5 μM.

Table 3. Minimum inhibitory concentrations (μM) of ecPis-4s in the presence of bacteria strains

L. monocytogenes	12.5
S. typhimurium	25.0
E. coli	25.0
P. miravilis	50.0
K. oxytoca	25.0
S. aureus	25.0
P. aeruginosa	12.5
S. agalactae	50.0

Kinetics of bacterial growth and time-dependent killing: The time-dependent killing induced by ecPis-4s was evaluated through experiments of kinetics of bacterial death of *Staphylococcus aureus*. Since the peptide presents significant resistance to proteinase K, similar experiments were carried out in the presence of the enzyme (0.05 w/w, enzyme:peptide). Figure 32 shows the pattern of growth and kill of *S. aureus* in the presence and absence of proteinase K treated with ecPis-4s at different concentrations. The growth curves in absence of the enzyme [Figure 32A] reveal a sort of dose-dependent response. At the smallest tested peptide concentration, which corresponds to ½ x MIC [Figure 32A, open square], a sharp drop in viable bacteria in the first two hours is observed. However, after this time of exposure, the bacteria recover their exponential growth. An accentuated death in the first six hours is noticed at the MIC concentration [Figure 32A, filled circle], and a plateau is reached after this time. When assayed at 2 or 4 x MIC concentrations (open circle and filled triangle, respectively), a similar sharp drop in the number of viable bacteria is noticed, although the bactericidal activity occurred only

between 4, and 6 h of exposure. Finally, at 8 x MIC the bactericidal effect is reached within the first two hours of exposure of the bacteria to the ecPis-4s.

Significant differences in the killing characteristics of ecPis-4s were observed in the presence of proteinase K [Figure 32B]. When compared with the growth control, no significant bactericidal activity is noted at ½ x MIC (open square). Contrarily, a clear population decrease is observed at either MIC or 2 x MIC concentrations, and the lowest CFU counts is reached at 4 hours. After that, the bacterial growth is recovered. A more substantial decrease in CFU is observed only at 4 × MIC or 8 x MIC concentrations in which assays reveal a maximum decrease only after 14 h, and 8 h of experiment, respectively.

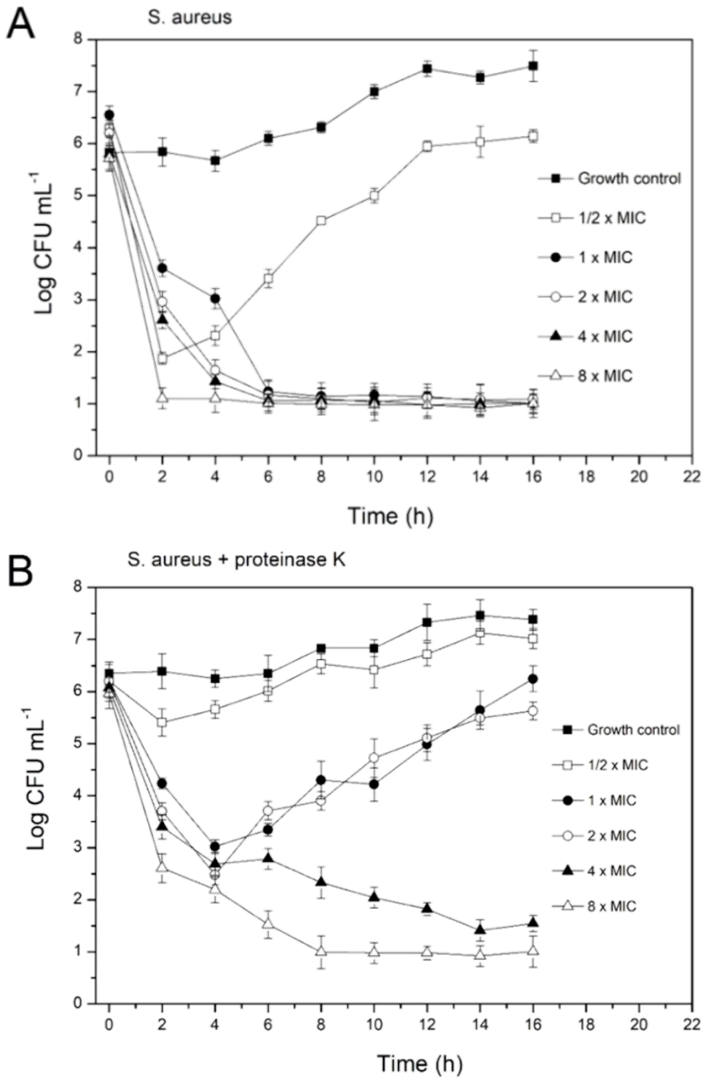

Figure 32: Bacterial Death Curve of *Staphylococcus aureus* incubated with ecPis-4s peptide at different concentrations in the absence (A), and in the presence (B) of proteinase K enzyme. The assays were performed for 16 hours, at 37ºC. The density of viable cells was estimated as $CFU.mL^{-1}$ using the microdrop technique.

4.4 Discussion

Some antimicrobial peptides may acquire ordered structures even before reaching the target membrane. This characteristic may impart important effects on their antimicrobial activity and selectivity towards microbial cells(332,333). Ordered structures are observed for some hetero, and homodimeric peptides(6) in aqueous solutions in which the linear polypeptide chains are linked by a single disulfide bond by cys residues. Some good examples are distinctin(334), dicynthaurin(335), halocidin(336), cathelicidins(337,338), and homotarsinin(6) for which the structure in aqueous environment is favored by interchain interactions. For instance, this last one, homotarsinin a homodimeric antimicrobial peptide, which was found in *Phyllomedusa tarsius* anurans, consists of two identical cystine-linked polypeptide chains each composed by 24 amino acid residues(6). In this study, we present the three-dimensional structure of ecPis-4s in absence of a membrane medium and investigate the potential effect of this arrangement on the resistance to peptidases and on antimicrobial activity.

Conformational analyzes indicate that ecPis-4s acquires some ordered structure in aqueous solution in either neutral or basic buffered media. Under basic conditions, the H4 side chain is uncharged suggesting that the overall charge neutralization of ecPis-4s exerts a stabilization effect on the peptide conformation. Further structural investigations using solution NMR spectroscopy were performed to obtain the three-dimensional structure of the ecPis-4s in atomic details [Figure 27]. The RMSD of 2.12 Å for the superposition of the 10 lowest energy structures indicates that piscidin-4 presents a significant conformational dynamic in aqueous environment. Nevertheless, even in absence of a membrane model, several sequential connectivities observed from K10 to R20 [Figure SM11] indicate the existence of a well-defined helical segment [Figure 27B]. In addition, the helical segment is marked by a well-established partition between hydrophobic and hydrophilic residues [Figure 27D]. This amphipathic structure indicates that ecPis-4s can reach further stability by hydrophobic effect due to efficient inter-chain interactions, and therefore, the structural arrangement maintains the hydrophobic residues of different chains face-to-face, while leaving a solvent exposed surface composed of hydrophilic residues. That peptide structure in an aqueous environment plays an important role in the biological activity and the resistance to enzymatic degradation.

In order to evaluate the possibly of oligomerization, DOSY NMR assays were also performed in an aqueous media. The diffusion coefficient of a molecular species depends on its

effective molecular size which is dependent on the forces that mediates interaction between molecules in equilibrium. The diffusion coefficients ranged between 1.37 - 1.46 x 10^{-10} m^2/s for ecPis-4s and this difference could be related by the small difference of the integrated area in the software adjustment [Table 2]. Therefore, DOSY experiments show the presence of a monomeric structure of ecPis-4s peptide in aqueous media. In addition, these values are in accordance with other peptides describing in the literature(339,340).

Analytical ultracentrifugation experiments were also carried out to better understand the behavior of ecPis-4s in water media, and which phenomena could influence its conformation or structural stability, for example, a self-assembly process. A key feature of sedimentation experiments for studying protein interactions using AUC technique is that the faster sedimenting complexes migrate through a solution of the slower sedimenting components(341). As a consequence, reversibly formed complexes that dissociate can re-associate during the experiment, thus permitting the characterization of even weak interactions(342). Interestingly, sedimentation velocity results obtained from AUC assays indicated that in all concentrations ecPis-4s peptide presents only one main peak with a sedimentation coefficient distribution at 0.43 ± 0.03 and an estimated molar weight of 2877 ± 231 Da [Figure 29]. Thus, AUC assays confirm that ecPis-4s is able to fold in a helical conformation even in a monomeric form, independent of the formation of a well-stabilized oligomeric arrangement. Therefore, the formation of amphipathic helix suggests a critical concentration to form a transient interchain interaction induced by the hydrophobic effect [Figure 27D], responsible to move away from the apolar helical faces from the aqueous environment.

In order to access the critical concentration associated to the fold/unfold process, the thermodynamic of dilution for ecPis-4s was evaluated by ITC technique [Figure 30]. The titration of 1200 μM peptide solution into a phosphate buffer solution shows an endothermic profile of addition of ecPis-4s into buffered solution at pH 6.0 or at pH 8.0. In both conditions, the enthalpograms [Figure 30] are characterized by a great decrease of the dilution heat up to around 60 μM of peptide concentration. This finding is attributed to the unfolding process since the peptide does not acquire an oligomeric arrangement in all concentrations employed in ITC experiments. The titration above 60 μM of peptide concentration achieves a plateau around 0.85 $kcal.mol^{-1}$, consistent with peptide dilution heats which were estimated as an average of the heat spikes from the last 10 injections(343). As expected, the enthalpy of unfolding is higher in basic conditions (ΔH^{o}_{unfold} = 6.9 kcal mol^{-1}), since higher helicity was noted by CD in this media

when compared to acid condition whose ΔH^{o}_{unfold} was 4.4 kcal mol^{-1}. Interestingly, the inflection point of each sigmoid is virtually equal in both media (~ 40 μM), which is related to the minimum peptide concentration needed to reach the equilibrium between folded and unfolded conformations or process.

The concentration-dependent in proteolytic resistance of ecPis-4s was evaluated either in the presence of trypsin or proteinase K. Clearly, the peptide is degraded by trypsin after 1h of digestion in all investigated concentrations tested [Figure 31]. Interestingly, a single peak at m/z 847.3 in the spectra of all samples is consistent with the expected mass for the first six amino acid residues (FFRHIK) of the peptide at the N-terminus. These results indicate that the helical portion of the structure is completely degraded since the hydrophilic residues are exposed to the aqueous media, whereas the unstructured N-terminus is stable to the trypsin. This is an important finding since the N-terminal regions composed of Phe residues are known to anchor peptides into the membrane surface(11). On the other hand, the degradation of ecPis-4s in the presence of proteinase K is marked by significant differences in the proteolysis kinetics depending on the peptide concentration. Notably, the stability of ecPis-4s peptide to proteinase K for longer periods of time is observed only at 150 μM of peptide concentration, suggesting that the helical structure leads to partial protection of the hydrophobic residues which are the target of proteinase K.

The process of resistance by peptides or not completely degradation by enzymes is important for several reasons. For instance, it can help us understand the mechanisms and factors that influence the resistance, such as the type and source of the enzyme, the structure and properties of the AMP, and the environmental conditions(79,344); it can help us evaluate the potential and limitations of AMPs as alternative or complementary therapies to conventional antibiotics, especially against multidrug-resistant bacteria(345,346); besides that, it can help us design better strategies to prevent or overcome the enzyme activity, such as modifying the AMPs to increase their stability and specificity, combining them with other antimicrobial agents, or inhibiting the enzyme activity(347,348).

This hypothesis of a resistant peptide to protease activity was also investigated by in vitro assays performing time-dependent killing of selected bacteria in the presence of proteinase K. Firstly, further antibacterial assays were carried out by considering the previous data presented by Zhuang and co-authors(195). The peptide was highly able to eradicate the growth of *P. miravilis*, *S. agalactae* strains, *S. typhimurium*, *E. coli*, *K. oxytoca*, *S. aureus*, *L.*

monocytogenes and *P. aeruginosa*. Considering the importance of the *S. aureus*, this strain was used to monitor the time-dependent killing experiments and the length of action of ecPis-4s in absence and presence of proteinase K enzyme. The time of action is one of the main steps for the characterization of a new drug. Since ecPis-4s peptide presents significant resistance to proteinase K, similar patterns of dose-dependent activity for the peptide at higher concentrations were expected. Indeed, at 4 x MIC, and 8 x MIC ecPis-4s exerts its bactericidal activity even in presence of protease enzyme [Figure 32]. It is worth mentioning that faster kinetics of death is observed at the assays with 8 x MIC.

In addition, these findings are in accordance with Joshi and coworkers(349), who observed that cationic peptides which cause damage to the cell membranes showed bactericidal action in the range of 1 to 4 hours of incubation, whereas Ling and collaborators(325) demonstrated that an unusual depsipeptide named teixobactin which acts by blocking lipid II, a precursor of peptidoglycan - has bactericidal action after 16 hours of incubation. Our results showed relatively low values of bacterial cell death time and suggest a pore-forming activity of ecPis-4s(350,351).

4.5 Conclusion

In conclusion, several techniques have been used to investigate the behavior of the antimicrobial peptide ecPis-4s in an aqueous and buffered solution. The secondary structure profiles of ecPis-4s peptide in water and phosphate buffer at pH 8.0 showed a gradual dependence on the peptide concentration. The three-dimensional structure by solution NMR is characterized by an amphipathic and well-defined helical segment from K10 to R20. Interestingly, the unstructured N-terminus formed by four aromatic amino acids (phenylalanine, histidine) is not degraded by the trypsin proteolytic enzyme which suggests that this region is naturally resistant to the action of this enzyme. In addition, DOSY NMR and AUC results indicated a diffusion coefficient that is in accordance with other peptides of same length, described in literature, and, the presence of only a monomeric form for ecPis-4s in aqueous solution. The unfolding process was observed by ITC and the folded/unfolded equilibrium concentration determined to be around 40 μM of ecPis-4s. Moreover, ecPis-4s is partially stable and active against *S. aureus* even in the presence of proteinase K enzyme as shown by the kinetics of growth and time of death assays. Therefore, the results indicate that the folded structure of ecPis-4s in aqueous media plays an essential role to protect the peptide against completely peptidase degradation while retaining its bacterial activity. Finally, our results provide new structural features of the piscidin peptide, and besides that, the combined data obtained by CD spectroscopy, solution NMR, AUC, DOSY NMR assays and ITC presented in this work allows us to conclude that ecPis-4s, unlike most AMPs peptides, presents a defined or ordered structure even before reaching the target membrane.

In perspective, although we have applied a set of biophysical and structural techniques to understand the mode of action of ecPis-4s peptide in anionic membrane models, the studies of this peptide in aqueous solution need to be extended. The structure of ecPis-4s has been proposed, however, to be sure about this feature other assays will be performed. As vicinal $^{3}J(H,H')$ couplings are a function of HCCH' dihedral angles(352), as shown by Karplus(353), we will use ^{3}J coupling constants to determine the ecPis-4s structure in aqueous environment(246,353).

In this way, HMBC (Heteronuclear Multiple Bond Correlation) experiments will be carried out in order to get the J couplings and also investigate the chemical shift index (CSI) using backbone NMR chemical shifts (C_{α}, CO, C_{β}, N, H_{α}, NH)(354) from NMR data to support

our proposal structure for ecPis-4s. Furthermore, the rotational correlation time experiments (*T*1 and *T*2 values) will be also performed for ecPis-4s in different peptide concentrations. As *T*1 and *T*2 values are affected, for example, by the increased molecular weight and viscosity of crowded samples(355), thus, the heteronuclear 15N *T*1/*T*2 method(356) will be performed in order to guarantee with support from other techniques, the absence of any aggregate formation for ecPis-4s peptide.

Chapter 5: A comparative study of D- and L-ecPis-2s epimers peptides: the effect of the D-amino acid on the bacteria mimetic models

5.1 Introduction

Antimicrobial peptides (AMPs) have awakened attention in recent years due to their potential activities being considered alternative to conventional antibiotics(357,358). These peptides, naturally produced by various organisms, are effective against a wide spectrum of pathogens as gram-positive and gram-negative bacteria, including multidrug-resistant strains, viruses, and fungi(357). Although rare, natural antimicrobial peptides containing D-residues have been described, showing quantitative differences in antimicrobial activities when compared to the epimeric form. The natural occurrence of L- and D-Phenylseptin peptides (FFFDTLKNLAGKVIGALT-NH_2) was first reported(13) in which D-epimer showed higher activity against *Staphylococcus aureus* and *Xanthomonas axonopodis* in comparison with the L-epimer. Similarly, Bombinin H peptides which present antimicrobial activity(14), the opioid peptide Dermorphinsmon(15), and Deltorphins(16), both identified in amphibian skin have shown an even higher affinity and biological activity than their analogs.

Antimicrobial epimers peptides hold particular interest in the field of antimicrobial research. Their distinctive structure arises from the replacement of L- by D-amino acids, which provide enhanced resistance to enzymatic degradation(358,359), making them chemically stable and increasing their antimicrobial properties(11,357,358). In the case of antimicrobial epimers peptides, the strategic replacement of a single D-amino acid introduces a chirality mismatch that disrupts the symmetry and rigidity of the peptide, resulting in unexpected and often enhanced antimicrobial activity. In this way, antimicrobial peptides containing D-amino acids have been explored as a potential approach to enhance the antimicrobial activity. Studies have shown that AMPs with D-residues exhibit improved stability towards proteases, enhancing their resistance to degradation and potentially prolonging their therapeutic effects. Additionally, the presence of D-amino acids in AMPs can alter their conformational

structure, potentially leading to enhanced antimicrobial activity and novel structural characteristics not observed in natural peptides.

Taking all these into consideration, the D- antimicrobial peptides have shown higher spectrum of activity against bacteria, fungi, and viruses, when compared to their L- natural epimers. For instance, here are presented some AMPs containing D-residues discussed in the literature: Bactenecin, a family of AMPs found in bovine neutrophils. They contain D-amino acids and exhibit antimicrobial activity against both Gram-positive and Gram-negative bacteria, including some drug-resistant bacteria(360). Another family are Dermaseptins, isolated from the skin of frogs, they contain both L- and D-amino acids(361). These peptides have potent antifungal and antibacterial properties. Besides, Temporins are found in the skin secretions of European red frogs, they contain D-amino acids and exhibit activity against Gram-positive and Gram-negative bacteria(362) with a lower hemolytic activity. In addition, Protegrins antimicrobial peptides are a class of AMPs found in porcine leukocytes in which a unique structure with a β-sheet and α-helix is stabilized by disulfide bonds. Protegrins are active against both Gram-positive and Gram-negative bacteria(363).

Although several studies have been described for epimer peptides, there is insufficient information on the mode of interaction to describe its structure-activity relationship. In this context, a new D-ecPis-2s peptide derivative from the Piscidin-2s (L-ecPis-2s) a natural 20 amino acid residues peptide (FFFHIIKGLFHAGRMIHGLV-NH_2) was proposed. D-ecPis-2s consist of an epimer of L-ecPis-2s by replacing the second L-Phe with a D-Phe amino acid.

In this way, this chapter provides a further investigation of the L-ecPis-2s and its D-peptide in order to evaluate the effect of epimerization on the activity and mode of action of both piscidin-2s peptides. Despite their high similarities, such as the size of the polypeptide chain, charge, and the conservation in the position of the amino acid residues with the only epimerization difference, these peptides show different structural aspects and biological power/activity. Thus, the antibacterial effect of epimerization has been evaluated against gram-positive and gram-negative strains. The biological assays were performed in collaboration with the Department of Pharmacy of the Federal University of Jequitinhonha and Mucuri Valleys, as well as the kinetics of growth and time-dependent killing were carried out in the Institute of Biological Sciences of the Federal University of Minas Gerais, Brazil.

The structure-activity relationship has been investigated by determining three-dimensional structure and topology in membrane models using CD, solution, and solid-state

NMR spectroscopies. The structure of L*-ecPis-2s peptide by solution NMR was elucidated by Nunes*(364) *[not published]; other assays as the pore-forming activity of the epimers peptides and the thermodynamics of the peptide-membrane interaction were characterized by fluorescence spectroscopy and isothermal titration calorimetry in presence of anionic vesicles. In addition, the effect of both peptides on the stability of the negative membrane has been acquired using DSC and deuterium order parameters by ssNMR technique. DSC studies were carried out in collaboration with the Chemistry Institute of the Federal University of Espírito Santo, Brazil.*

5.2 Materials and Methods

5.2.1 Peptide synthesis, purification and characterization

L-ecPis-2s (F-LF-FHIIKGLFHAGRMIHGLV-NH_2), and D-ecPis-2s (F-DF-FHIIKGLFHAGRMIHGLV-NH_2) peptides were obtained through the Fmoc (9-fluorenylmethyloxycarbonyl) solid phase synthesis strategy(247) on a Fmoc-Rink Amide® polystyrene resin (0.22 meq.g^{-1}), using a Millipore 9050 automatic peptide synthesizer with amino acids from Merck-Novabiochem (Hohenbrunn, Germany). For the solid-state NMR experiments, both L- and D-ecPis-2s were produced with selective labeling on the same amino acid sites: ^{15}N-G13 and $^{2}H_3$-A12, while for the other experiments, both peptides were prepared without any isotopic labeling. The cleavage step for the L- and D-ecPis-2s were carried out with TFA:ethanedithiol:water:triisopropylsilane (94:2.5:2.5:1, v:v:v:v) solution, and the crude peptide was precipitated with cold diisopropyl ether (-4 °C), extracted with deionized water and freeze-dried. The peptides were then purified by reverse phase HPLC (Gilson, Villiers-le-Bel, France) using a preparative C18 column (Luna, C18-100 Å-5 µm, Phenomenex, Le Pecq, France), and an acetonitrile/water gradient with 0.1% TFA was used as the mobile phase: solvent A contains 10% acetonitrile, 90 % water, and 0.1% TFA; and solvent B was made of acetonitrile at 100%, 0.1% TFA. The experiments recorded at room temperature was monitored at 214 nm, and the main peak was collected and its identity and purity were checked by mass spectrometry (MALDI-ToF Autoflex, Bruker, Bremen, Germany). The purified peptides were dissolved three times in 4% (v/v) acid acetic at a concentration of 1 mg/ml with subsequent lyophilization to ensure the exchange of the TFA anions with acetates, and stored at - 20 °C. Table 4 presents the sequence with selective labeling for L- and D-ecPis-2s peptides.

Table 4. Isotopic labeling peptide synthesis for solid-state NMR experiments.

Peptide	Sequence labeling
(^{15}N-G13,$^{2}H_3$, A12)-L-ecPis-2s	F-LF-FHIIKGLFH***A*****G**RMIHGLV-NH_2
(^{15}N-G13,$^{2}H_3$-A12)-D-ecPis-2s	F-DF-FHIIKGLFH***A*****G**RMIHGLV-NH_2

Where, *A* residue is labelled with 3,3,3-$^{2}H_3$-Ala.**G** residue is ^{15}N-Gly labelled for both L-ecPis-2s and D-ecPis-2s.

5.2.2 Preparation of phospholipid large unilamellar vesicles (LUVs)

LUVs were prepared using POPC:POPG (3:1, mol:mol) lipids as previous described above (see item 3.2.2) and used for CD, ITC, DLS and ζ-potential measurements experiments, and a mix of 1,2-dimyristoyl-sn-glycero-3-phosphocholine (DMPC) and 1,2-dimyristoyl-sn-glycero-3-phosphoglycerol (DMPG) for DSC experiments. An equivalent methodology was used to obtain carboxyfluorescein-loaded vesicles for dye leakage experiments. For this assay, POPC:POPG (3:1, mol:mol) film was hydrated with a 20 mM carboxyfluorescein solution at pH 8.0 (10 mM Tris-HCl buffer) containing NaCl at 100 mM before undergoing five freeze-thaw cycles and then extrusion (8 times) through membranes with pores of 100 nm diameter. The dye outside the carboxyfluorescein-loaded vesicles was removed by gel filtration through a Sephadex G-25 column equilibrated with the same buffer solution. For the determination of the order parameters *(S_{CD})* using ^{2}H solid-state NMR, lipids were prepared by dissolving deuterated POPC-d_{31} or POPG- d_{31} in 10 mM acetate buffer (pH 5.0), vortexing and bath sonication as well as three heat cycles at 40 °C to produce multilamellar vesicles.

5.2.3 Circular Dichroism Spectroscopy

The secondary structure preferences of both L-ecPis-2s or D-ecPis-2s peptides were investigated by circular dichroism (CD) spectroscopy on a JASCO® J-810 spectropolarimeter (Tokyo, Japan), equipped with Peltier Jasco temperature control system - PFD-425S (Tokyo, Japan). The samples were prepared containing 50 μM of peptide which were solubilized in 10 mM phosphate buffer containing 100 mM KF at pH 5.0, and the experiments were carried out in absence and presence of biomimetic media composed of POPC:POPG (3:1, mol:mol) LUVs or SDS micelles(275). LUVs were employed at lipid concentrations at 0.05 mM – 1.60 mM range, and micelles were tested at 100, 200, and 400 mM SDS, both suspended in water solution. The analyzes were performed at 25 °C in a cuvette of 1.0 mm path length. The spectra were recorded from 190 to 260 nm, with the accumulation of four scans, bandwidth of 0.1 nm, step resolution of 0.2 nm, 50 nm.min^{-1} scan speed and 1 s response time. Similar experiments in absence of peptide were recorded as the respective blank solution to allow the subtraction of the background.

5.2.4 Solution NMR spectroscopy

Two-dimensional solution NMR experiments were carried out to determine the three-dimensional structure of D-ecPis-2s peptide in presence of SDS-d_{25} micelles at 25 °C. Two-dimensional homonuclear TOCSY and NOESY, edited ^{1}H-^{13}C-HSQC and ^{1}H-^{15}N-HMQC heteronuclear experiments were performed. All spectra were acquired at the Multi-user Magnetic Resonance Laboratory at the Federal University of Minas Gerais on a Bruker® Avance Neo OneBay spectrometer operating at 600.15 Hz (for ^{1}H). The sample consisted of an aqueous solution containing 2.0 mM of D-ecPis-2s peptides, at 300 mM SDS-d_{25} diluted in 10% (v/v) D_2O/H_2O containing 1% (v/v) of 2,2-dimethyl-2-silapentane-5-sulfonate (DSS) as the internal reference. TOCSY experiments were carried out using pulse sequence(317) with a mixing time of 80 ms. 512 t_1 increments, 60 transients of 4096 points for a spectral width of 6009.6 Hz. Nuclear Overhauser Spectroscopy (^{1}H-^{1}H-NOESY) spectra were obtained using the *noesygpphw5*(317) pulse sequence, and using mixing times of 120, and 150 ms collecting 512 t_1 increments with 60 transients of 4096 points for a spectral width of 6009.1 Hz. Heteronuclear Single Quantum Coherence (^{1}H,^{13}C-HSQC) experiment was also performed using edited mode in which CH_2 correlations show negative phase and CH and CH_3 correlations show positive phase(251). The data were recorded with F1 and F2 spectral widths of 20831.9 Hz and 6009.6 Hz, respectively. 256 t_1 increments were accumulated with 64 transients of 4096 points. Heteronuclear Multiple Quantum Coherence (^{1}H,^{15}N-HMQC) experiment was performed with F1 and F2 spectral widths of 2000 and 6009.6 Hz, respectively. 80 t_1 increments were accumulated with 4000 transients of 1024 points(252).

5.2.5 NMR analyses and structure calculations

Proton resonances were assigned by simultaneous analyses of homonuclear ^{1}H,^{1}H-TOCSY and ^{1}H,^{1}H-NOESY spectra using Wuthrich method(208). The NMR assignments for epimers peptides were performed manually by using NMRViewJ (version 9.2.0-b20) program(253). The NOE intensities were converted into semi-quantitative distance restrictions with limits of 2.8, 3.4, and 5.0 Å(254). The geometric restraints were validated (according to their consistency and contribution) from data of uniqueness information from the QUEEN program (Quantitative Evaluation of Experimental NMR Restraints)(256).

The XPLOR-NIH software (version 2.27) was used for the calculation and refinement of the three-dimensional structures employing simulated annealing protocol in torsional angle dynamics(257,258). First, the system was rapidly heated to 5000 K and then slowly cooled to the temperature of 1000 K, for 1000 cycles. Then, another slow cooling from 1000 K to 300 K was carried out in 1000 steps. A total of 100 structures were obtained and refined in a subsequent calculation, using more stringent topology parameters(259). The ten lowest-energy structures were visualized and analyzed with MOL-MOL and Chimera softwares(261), and the quality of the structures verified by the Ramachandran diagram and the RMSD (Root Mean Square Deviation), both obtained from the online platform PSVS(262).

5.2.6 Solid-state NMR spectroscopy

L-ecPis-2s and D-ecPis-2s peptides were reconstituted in POPC:POPG (3:1, mol:mol) membrane bilayer at 4 mol% (mol:mol), and prepared as described previously (see item 3.2.7). Proton-decoupled ^{31}P solid-state, proton-decoupled ^{15}N cross-polarization (CP), and ^{2}H spectra of static aligned samples were recorded on a Bruker® Avance wide-bore 300 NMR spectrometer employing a commercial triple resonance flat-coil probe for solid-state NMR (Bruker®, Rheinstetten, Germany) (see item 3.2.7).

5.2.7 Differential scanning calorimetry (DSC)

Phase transition profile of 3 mM DMPC:DMPG (3:1, mol:mol) lipids in the absence and in the presence of D-ecPis-2s or L-ecPis-2s at 10, 25, 50 and 100 μM were investigated on a VP-DSC® microcalorimeter (Malvern® Instruments, UK). All LUVs and peptide-LUVs mixtures were prepared immediately before the experiments. LUVs and peptide-LUVs samples were run against 10 mM pH 7.0 Tris-HCl buffer solution containing 50 mM NaCl in the reference cell. Experiments with buffer in both cells were also performed for subsequent blank correction. Three successive heating scans were performed for each sample, over the temperature range from 8-9°C till 35 °C at a heating rate of 1.0 °C/min. Microcal Origin® DSC (GE HealthCare-Microcal®, USA) software was used for blank subtraction, transition temperature (T_m - gel to liquid crystalline) and the phase transition enthalpy ($\Delta_{trans}H$) calculations using a linear baseline to integrate the areas under the DSC curves.

5.2.8 Zeta potential (ζ)

The determination of the zeta potential (ζ) of the POPC:POPG (3:1, mol:mol) LUVs diluted in 10 mM sodium acetate buffer (containing 100 mM NaCl, pH 5.0) in presence of L-ecPis-2s and D-ecPis-2s peptides were carried out at 25 °C on a Malvern Zetasizer® Nano ZS equipment (Malvern, UK). All measurements were performed at room temperature using a 700 μL Malvern® cuvette, model DTS1060 (Malvern). The experiment was performed in triplicate in different peptide concentration with 200 μM POPC:POPG (3:1, mol:mol) LUVs solution. ζ-potential was measured 30 minutes after each sample preparation for the system stabilization. Partition constant (K_p) of epimers peptides was also calculated in presence of anionic vesicles and the formalism for this determination using ζ-potential is described in the item 3.2.11.

5.2.8 Calcein leakage measurements

Calcein release experiments were carried in polystyrene microplates (128 × 86 × 14.5 mm) for fluorescence emission measurement in LUVs suspension of POPC:POPG (3:1, mol:mol) at different volumes of peptide (250 μM) and buffer (10 mM Tris-HCl, 100 mM NaCl, pH 7.0) solutions to a final volume of 300 μL as detailed in Table 5.

Table 5. Samples composition used for calcein release measurements

Sample	V_{pep} (μL)	V_{LUVs} (μL)	V_{buffer} (μL)	[Peptide] (μM)
1	0	150	150	0
2	5	150	145	4,2
3	10	150	140	8,3
4	20	150	130	16,7
5	40	150	110	33,3
6	80	150	70	66,7

V_{pep} = volume of 2 mM peptide stock solution; V_{LUVs} = volume of 200 μM POPC:POPG LUVs stock solution and V_{buffer} = volume of 10 mM Tri-HCl buffer solution (pH 7.4).

The increase of calcein fluorescence as a function of time at 25°C was recorded every 1 minute in the Spectra Max®Paradigm detection platform (Molecular Devices, LLC,

Sunnyvale, US) at excitation and emission wavelengths of 480 and 520 nm, respectively. The stability of the LUVs was monitored for 5 min before the peptide was added. The calcein release after the addition of the peptide was recorded for 15 min. The total calcein released from the LUVs (100%) was determined in a similar experiment using 0.1% Triton-X 100 in the absence of the peptide. Calcein leakage was calculated using equation 11:

$$\text{Dye leakage (\%)} = \frac{(F-F_0)}{(F_T-F_0)} \text{ x } 100\% \quad (11)$$

where, F_0, F, F_T denotes the basal fluorescence intensity, florescence intensity after addition of peptides and maximum florescence intensity obtained after addition of 0.1 % Triton X-100, respectively. Tris-HCl buffer was used as negative control. The experiments were performed in triplicate on independent samples of calcein-loaded LUVs. The results are presented as the average with their standard deviations.

5.2.9 Antimicrobial activity

Pseudonomas aeruginosa (ATCC 27853), *Staphylococcus aureus* (ATCC 29313) *Salmonella typhimurium* (ATCC 14028), *Staphylococcus aureus* (ATC 29313), and *Proteus mirabilis* (ATCC 25931) obtained from the American Type Culture Collection (Manassas, VA, USA) were cultured at 37 °C on agar plate containing BHI medium (Brain Heart Infusion) from HiMedia Laboratories (Mumbai, India) for 12 h. The highest peptide concentration used was 200 µM in an initial inoculum of 2 × 108 CFU.mL^{-1} (colony forming units mL^{-1}). The samples were dissolved in a Mueller Hinton liquid broth by serial dilution in a range of 3.12 –200 µM of both ecPis-2s peptides. All assays were performed in triplicate. The final volume was 100 µL per well, 50 µL of the peptide and 50 µL of the inoculum. Chloramphenicol (MM: 323.1 g.mol^{-1}) was used as positive control at 92.8 µM. The experiments were carried out in stationary culture at 35 °C and 10 µL of 4% MTT aqueous solution was added after 20 h of incubation in each well of the plate. The spectrophotometer readings were performed after a total of 24 h of incubation. The minimal inhibitory concentrations (MIC) were determined based on three independent measurements, using the optical density parameter (A595 nm) recorded in a SpectraMax® Paradigm detection platform (Molecular Devices, LLC, Sunnyvale, CA, USA).

5.2.10 Kinetics of growth and time dependent killing

Staphylococcus aureus strains (ATC 29313) were grown in MH broth at a concentration of 10^5 cells per milliliter. Both L-ecPis-2s and D-ecPis-2s peptides were added at concentrations ranging from half the MIC value (MIC = 12.5 μmol L^{-1}) to four times the MIC value, at 37°C. At time intervals (0, ½, 1, 2, 4, 6, 8, 10, 12 h), aliquots of 10 μL were collected for cell viability determination by the microdrop technique(365). Then, the suspensions were subjected to serial dilutions (10^{-1}, 10^{-2} and 10^{-3}) and aliquots of 5 μL were plated on BHI agar. The plates were incubated for up to 12 h, and the number of colonies per drop was counted and multiplied by the reciprocal of the dilution. The result was expressed as colony forming units (CFU). Kinetics of bacteria growth assays were performed in triplicate.

5.3 Results

5.3.1 Biological activity of D- and L-ecPis-2s peptides

Antibacterial activity: The antimicrobial activity of the D- and L-epimers was assayed against gram-positive (*L. monocytogenes,* and *S. aureus*), and gram-negative bacteria (*S. typhimurium, P. mirabilis,* and *P. aeruginosa*). A positive control was established using chloramphenicol antibiotic at a concentration of 30 mg. mL^{-1}. D-ecPis-2s epimer shows similar or higher antimicrobial activities when compared to L-ecPis-2s [Table 6]. When compared with L-ecPis-2s, D-ecPis-2s peptide show MIC values that are 2-, 3-, and 4-times lower against *L. monocytogenes, P. aeruginosa*, and *S. typhimurium*, respectively. For the *P. mirabilis* both epimers show the same MIC values of 50 μmol L^{-1}.

Table 6. Minimum inhibitory concentrations (μmol.L^{-1}) of ecPis-2s epimers in presence of bacteria

Bacteria	**L-ecPis-2s**	**D-ecPis-2s**
S. typhimurium	>100	12.5
P. mirabilis	50	50
P. aeruginosa	50	12.5
L. monocytogenes	50	25
S. aureus	12.5	12.5

Bacterial death kinetic studies: The time-dependent killing induced by ecPis-2s epimers was evaluated through kinetic experiments on the bacterial death of *Staphylococcus aureus* strain. Figure 33 shows the pattern of growth and kill of S. aureus treated with D- and L-ecPis-2s at different concentrations.

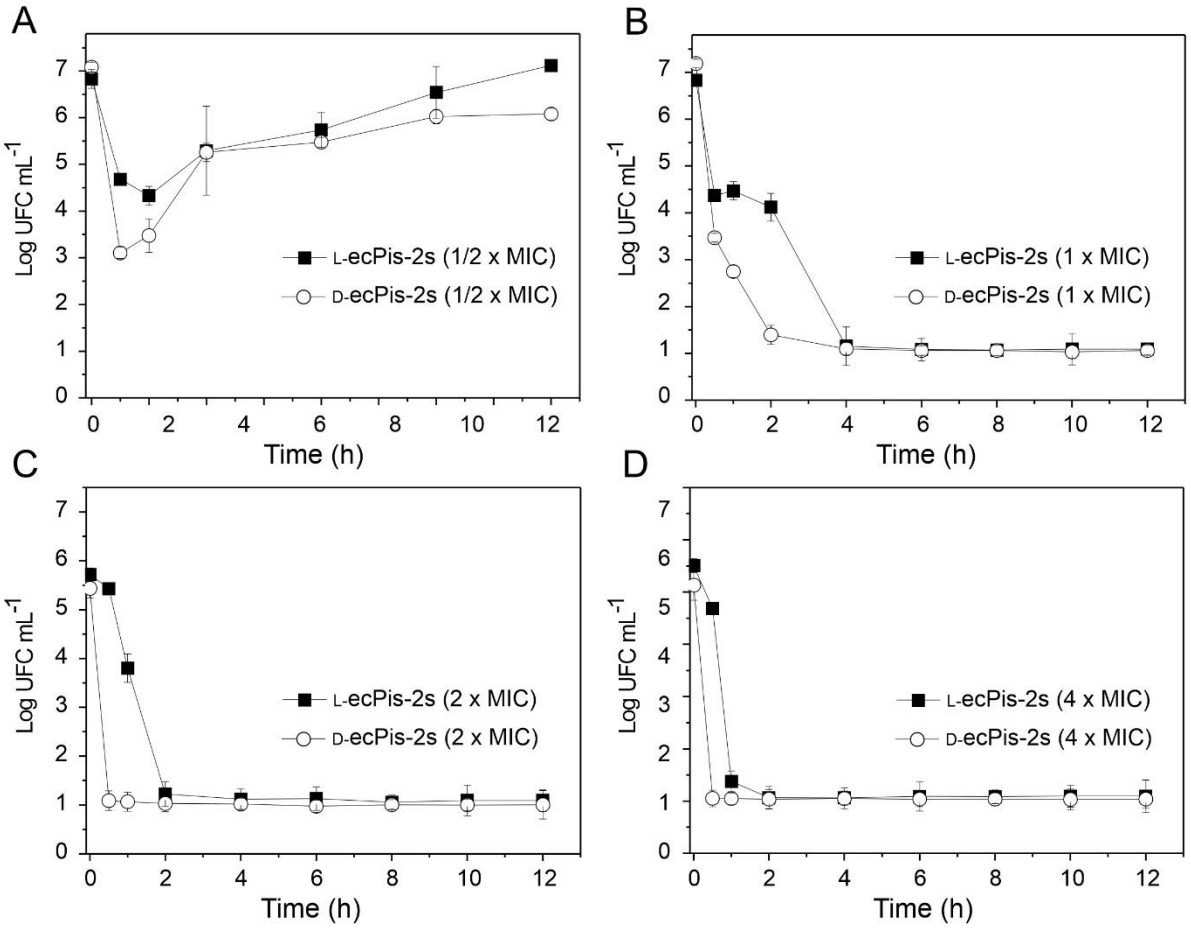

Figure 33: Bacterial death kinetic assay of D- and L-ecPis-2s epimers at ½ x MIC, 1 x MIC, 2x MIC, and 4 x MIC against *Staphylococcus aureus*.

In a 0.5 x MIC (6 µM) [Figure 33A] a decrease in viable bacteria is observed in the first half hour. However, a significant bacterial growth is noted after one hour of exposure to the. At the concentration corresponding to the MIC (12 µM) [Figure 33B], a pronounced bacterial killing effect is observed for both epimers, without bacterial recovery. Interestingly, whereas complete bacterial death for L-epimer occurs after four hours of bacterial incubation, the D-epimer promotes an equivalent effect after two hours. At peptide concentrations of 25 µM and 50 µM [Figures 33C, and 33D], the D-epimer shows faster activity, killing the bacterial strains in thirty minutes, while the L-epimer achieves this effect only after one (50 µM) and two (25 µM) hours of incubation.

5.3.2 Effect of epimerization on the membrane stability

Dye leakage experiments: The membrane-disruptive properties of D-ecPis-2s and L-ecPis-2s peptides were investigated by monitoring the release of calcein from POPC:POPG (3:1, mol:mol) vesicles. Figure 34 presents the results obtained of calcein leakage after the addition of epimers. As we can observe, dye released increases in a peptide concentration-dependence manner for both piscidins [Figure 34A, and 34B].

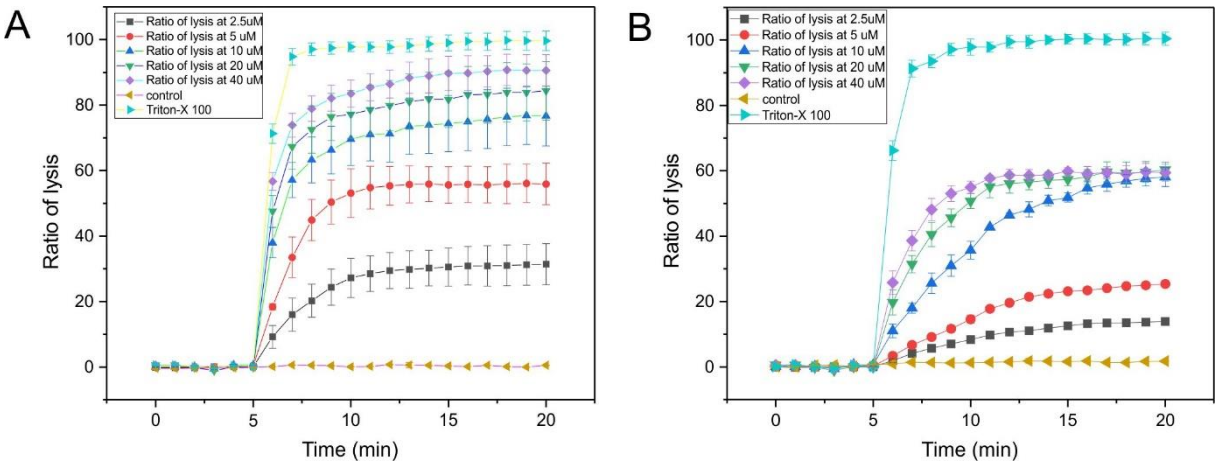

Figure 34: Calcein released as a function of time for crescent concentrations of D-ecPis-2s (A) and L-ecPis-2s (B) in the presence of POPC:POPG (3:1, mol:mol) LUVs.

At all peptide concentrations tested, the calcein release increases with time until reaches a plateau around 15 minutes. Notably, higher calcein leakage is promoted by D-ecPis-2s peptide in comparison with the L-ecPis-2s, in which around 90% of dye released is achieved at 40 $mmol^{-1}$ for D-epimer, while only 60% is released in the presence of the L-epimer.

Differential scanning calorimetry: DSC data were acquired in order to measure the influence of ecPis-2s epimers on the thermotropic phase transition of liposomes. In this study, a system made of DMPC:DMPG (3:1, mol:mol) lipids was employed and the DSC profiles in the absence and presence of different peptide concentrations are presented in Figure 35.

DSC data show that D-ecPis-2s causes a perturbation on the thermodynamic parameters of the DMPC:DMPG (3:1, mol:mol) transition at all concentrations [Figure 35A], whereas for L-ecPis-2s a pronounceable effect is only observed at concentrations ≥ 25 μM of peptide [Figure

35B]. Significative changes in the shape of the DSC curves are noted as a result of the membrane interaction of D-ecPis-2s, mainly at concentrations higher than 25 μM.

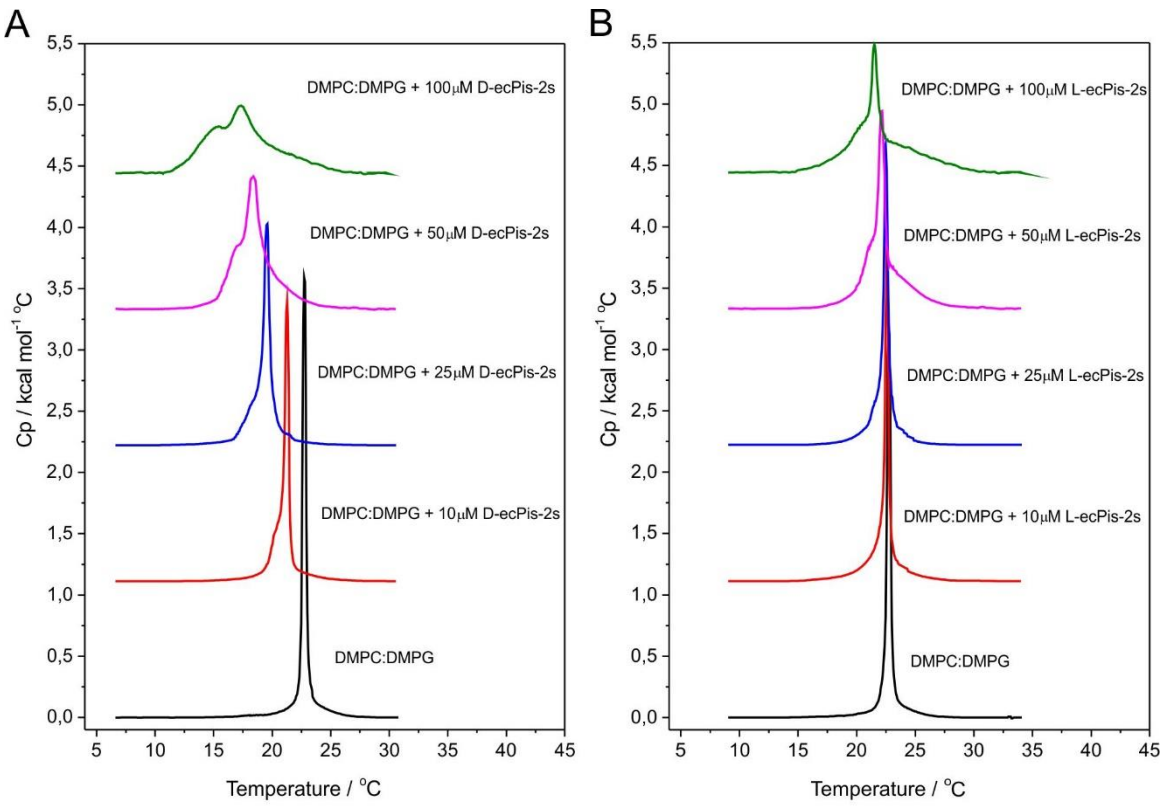

Figure 35: DSC profile of DMPC:DMPG (3:1, mol:mol) in absence and presence of crescent concentrations of (A) D-ecPis-2s and (B) L-ecPis-2s.

Investigation of the POPC-d_{31} and POPG-d_{31} order parameters in the presence of epimers peptides: In order to investigate the lipid fatty acyl chain packing and dynamics in the presence of D- and L-ecPis-2s epimers, POPC:POPG vesicles were prepared with POPC-d_{31}, and then POPG-d_{31} lipids deuterated throughout their palmitoyl chain. The ^{2}H solid-state NMR spectra of POPC:POPC-d_{31}:POPG (2:1:1, mol:mol:mol) and POPC:POPG-d_{31} (3:1, mol:mol) vesicles in the absence of peptides are shown in Figure 36A and 36B. Deuterium solid-state NMR spectra were acquired from samples in the absence and in the presence of ecPis-2s epimers, encompassing several overlapping characteristic quadrupolar splittings in order to provide information about the order parameter of the deuterated CD_2 and CD_3 sites. ^{2}H order parameters (S_{CD}) of each C−D bond extracted directly from NMR spectra of POPC:POPC-d_{31}:POPG (2:1:1) are plotted in a position-dependent manner [Figure 36C]. Both epimers exert a slight

effect on the POPC-d_{31} acyl chains, as can be observed in the relative order parameter plot [Figure 36E], which considers the order parameters ratio of POPC:POPC-d_{31}:POPG (2:1:1, mol:mol:mol) membranes in the absence or in the presence of peptide.

When D-ecPis-2s is added to the deuterated POPC:POPG-d_{31} (3:1, mol:mol) membrane, changes in the ^{2}H quadrupolar splittings are observed in the respective spectrum [Figure 36B]. Figure 36D presents the deuterium order parameters (S_{CD}) for each C−D bond plotted in a position-dependent manner. Notably, D-ecPis-2s exerts a higher effect on the POPG-d_{31} acyl chains, in which a greater variation in the relative order parameter plot for this peptide is shown [Figure 36F].

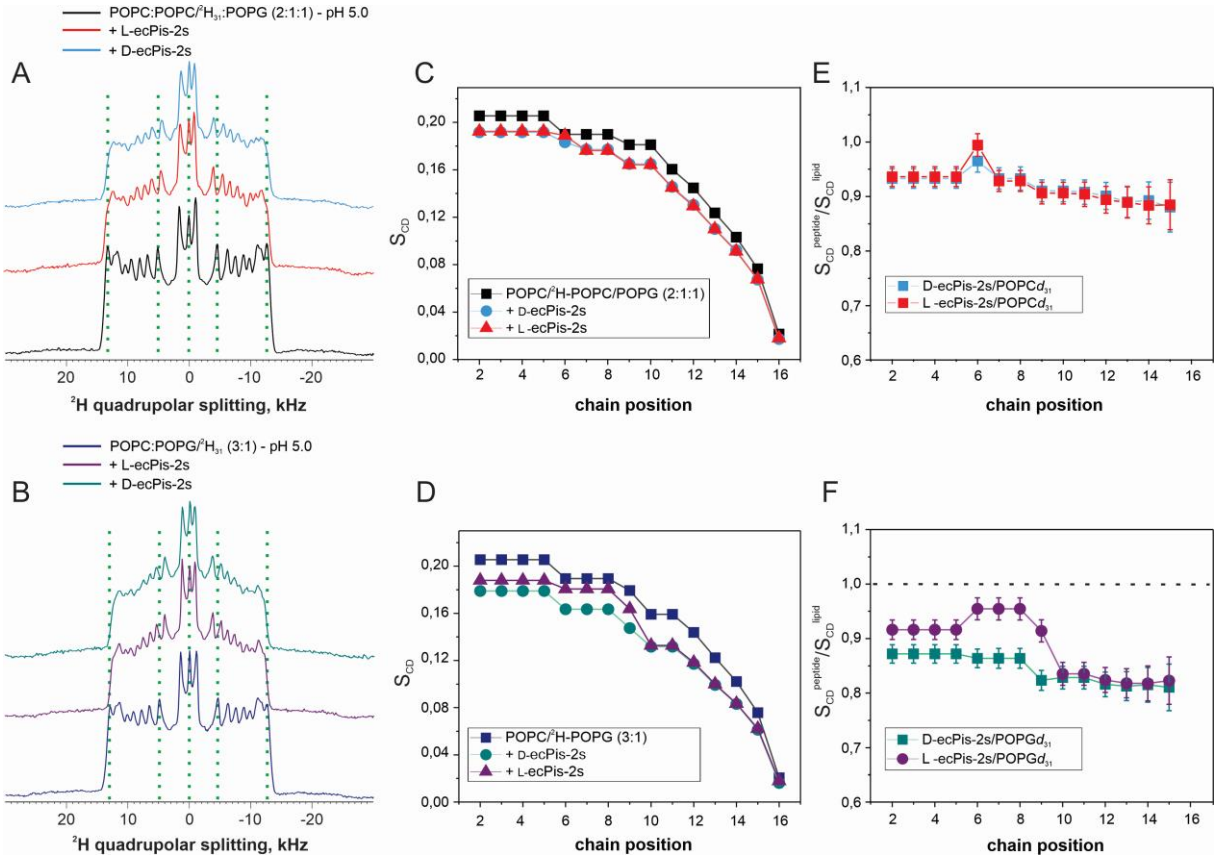

Figure 36: (A, B) ^{2}H solid-state NMR spectra, (C, D) order parameter, and (E, F) relative order parameter profiles for (A, C, E) POPC:POPC-d_{31}:POPG (2:1:1) and (B, D, F) POPC:POPG-d_{31} (3:1) without and with D-ecPis-2s and L- ecPis-2s epimers. Experiments were performed at 300 K.

5.3.3 Effect of epimerization in the peptide-membrane affinity

Isothermal titration calorimetry: The thermodynamic behavior of membrane interaction between D- and L-ecPis-2s peptides with anionic phospholipidic vesicles was investigated by isothermal titration calorimetry (ITC). The heat flow curve upon injection of 5 μL aliquots of POPC:POPG (3:1, mol:mol) LUVs into D- and L-ecPis-2s epimers solution as well as the integrated heat flow peaks as a function of the lipid-to-peptide ratio for the epimers are displayed in Figure 37. The control experiment consisted of the LUVs injection into a buffer solution. The heat of vesicles dilution is relatively small, around 0.15 μcal/inj. The raw data of the peptide–membrane binding indicate isothermal titration curves typical of exothermic-driven reactions with moderate affinity [Figure 37A, 37B]. The value per injection derived from the integration of the titration peaks was approximately −0.65 μcal and 0.52 μcal for D-ecPis-2s and L-ecPis-2s peptides, respectively. ITC curves saturating around phospholipid-peptide molar ratio approximately 40 μM.

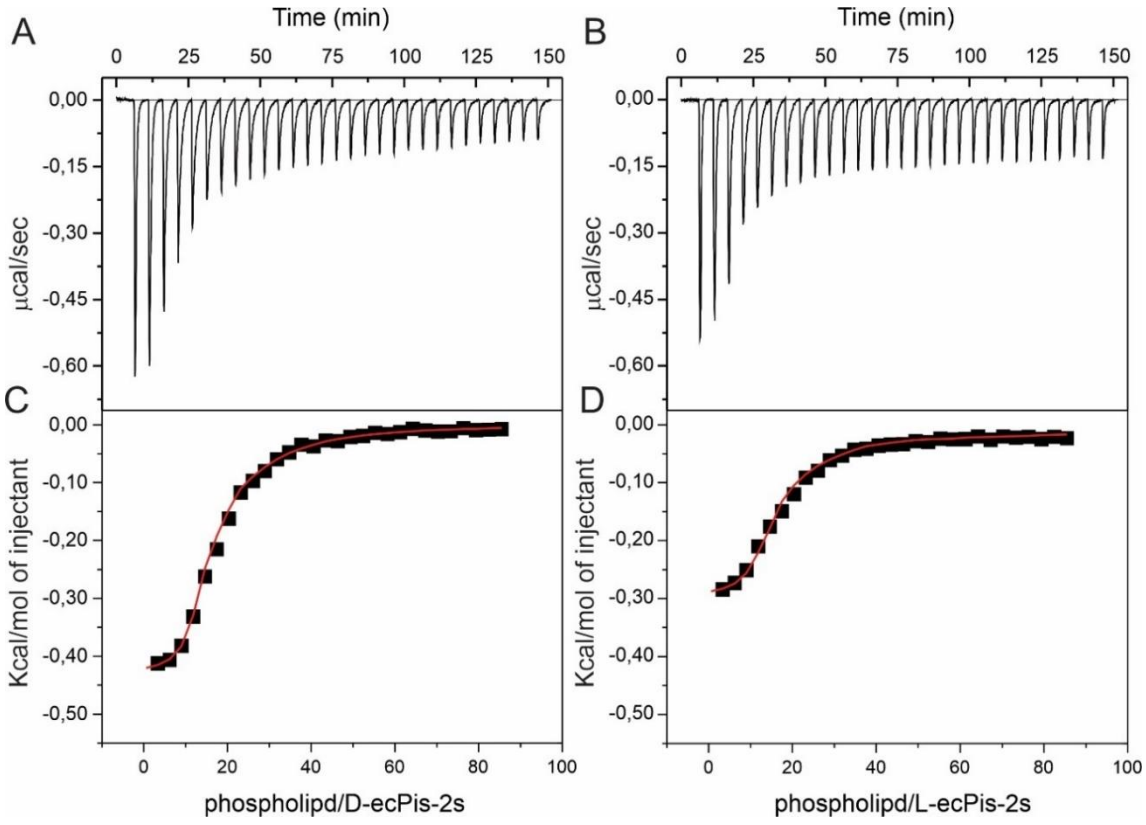

Figure 37: Isothermal titration calorimetry of D-ecPis-2s (A) and L-ecPis-2s (B) with POPC:POPG (3:1, mol:mol) LUVs in acetate buffer solution, pH 5 at 308 K.

The heats of binding for each injection between ecPis-2s epimers and POPC:POPG (3:1, mol:mol) LUVs are presented in Figure 37C and 37D. The molar enthalpies of binding (ΔH^o) were calculated from the cumulative heat of binding after each injection divided by the total amount of injected peptide. The enthalpic contribution of D-ecPis-2s interacting with anionic LUVs (ΔH°= - 392 cal.mol^{-1}) was about one and a half times lower than the value obtained for the binding of L-ecPis-2s (ΔH°= - 528 cal.mol^{-1}) to anionic vesicles. On the other hand, the entropy contribution is higher for the interaction of D-peptide ($T\Delta S$ = 5236 cal.mol^{-1}) when compared to L-ecPis-2s ($T\Delta S$ = 4620 cal.mol^{-1}). Moreover, in the presence of the negative LUVs, D-ecPis-2s presents a binding constant (K_{app} = 10.2 x 10^3 M^{-1}) larger than the natural peptide (K_{app} = 6.8 x10^3 M^{-1}). All the thermodynamics parameters obtained from titration calorimetry assays are presented in Table SM6 where we can observe a higher ΔG° of peptide-membrane interaction for D-ecPis-2s peptide when compared to the L-epimer.

Zeta potential of negative LUVs: Some vesicle properties, such as zeta potential (ζ), are susceptible to changes as a result of peptide-membrane interaction (Manzini *et al.*, 2014). Therefore, changes in the ζ of 200 μM POPC:POPG (3:1, mol:mol) LUVs suspension were observed upon titration of D-ecPis-2s and L-ecPis-2s peptides at 220 μM. Figure 38 shows the changes in the ζ-potential as a function of the ratio peptide/phospholipid for the titration into the anionic LUVs.

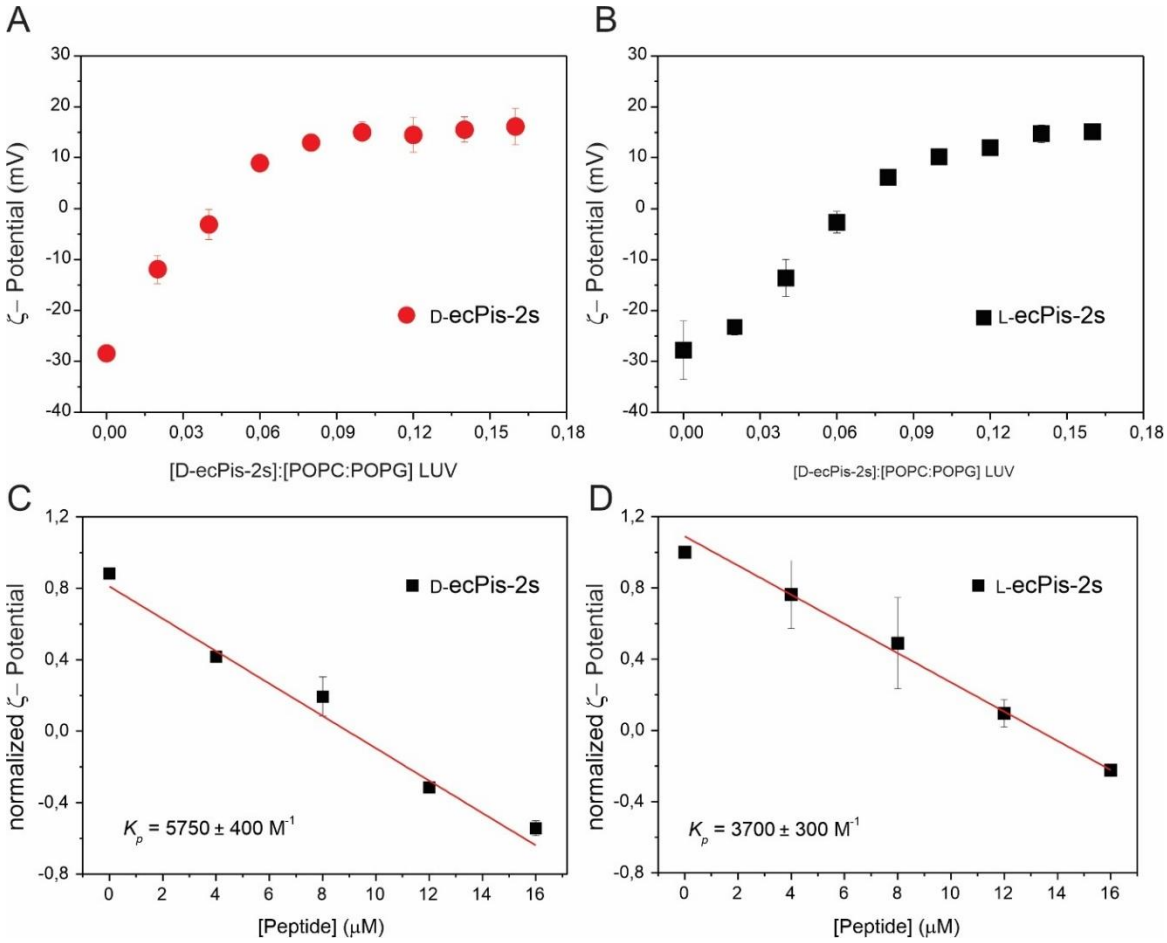

Figure 38: Changes of the zeta potential as a function of the molar ratio of peptide/phospholipid in the titration of 200 μM of POPC:POPG (3:1, mol:mol) vesicles with 220 μM of D-ecPis-2s (A) and L-ecPis-2s (B). ζ-potential normalized for epimer D-ecPis-2s (C), and L-ecPis-2s (D) both in the presence of anionic LUVs suspension in acetate buffer at pH 5, 25 °C.

Figure 38 displays a ζ-potential close to −30 mV for POPC:POPG (3:1: mol:mol) LUVs in the absence of the peptides. The addition of each epimer results in increases in the ζ-potential up to reach positive values. Whereas a maximum of ζ-potential (~15 mV) is reached at a D-peptide:phospholipid ratio of around 0.08, while a similar value can be observed at a peptide:phospholipid ratio of 0.14, with the addition of the L-epimer. Similarly, the zeta potential of anionic LUVs approaches neutrality at a lower peptide:phospholipid ratio in the presence of D-epimer (0.04) when compared to the L-epimer (0.06).

Besides that, the partition constants (K_p) of D- and L-ecPis-2s to POPC:POPG (3:1, mol:mol) LUVs were determined using equation 8 and 9 (see item 3.2.11). Figure 38C and 38D show the normalized ζ-potential dependence on the concentration of D-ecPis-2s and L-ecPis-2s, respectively. The values of -1 was used as the net charge for the anionic phospholipid, and +3

as the charge of ecPis-2s peptides. A *Kp* values of 5750 (± 400) M^{-1} and 3700 (± 300) M^{-1} were obtained for D-ecPis-2s and L-ecPis-2s from ζ-potential measurements, respectively.

Circular Dichroism (CD) spectroscopy: To investigate the conformational preferences of D-ecPis-2s and L-ecPis-2s peptides, CD spectra were recorded in the absence and presence of POPC:POPG (3:1, mol:mol) LUVs. The peptides remain unfolded in the absence of membranes and the molar ellipticity values increase with the increasing LUVs concentration. The spectra show two minima near 208 and 222 nm and a maximum at 193 nm for both peptides in the presence of POPC:POPG (3:1, mol:mol) negative LUVs [Figure 39] which are characteristics of α-helix conformation(275).

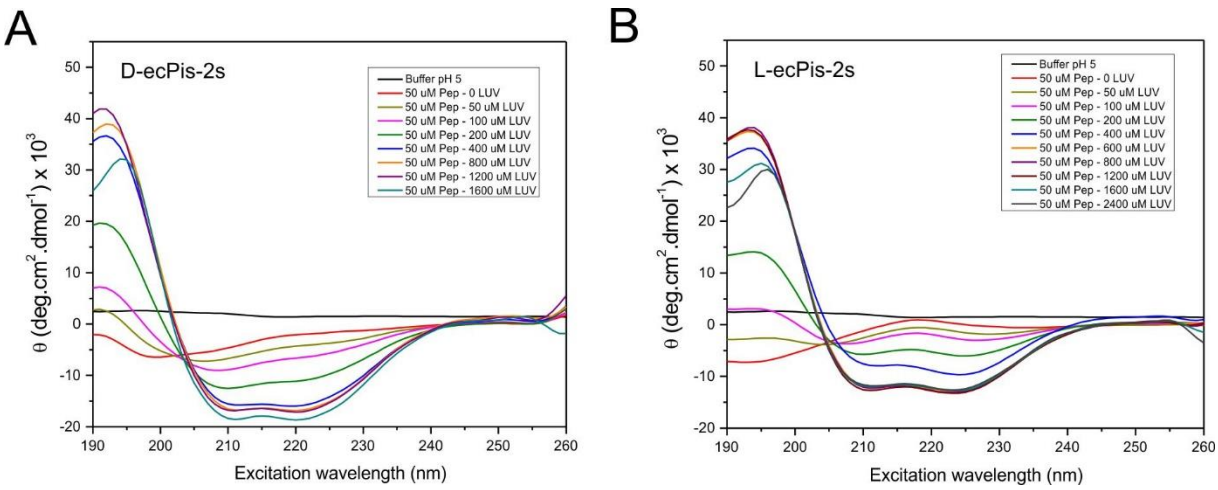

Figure 39: Circular dichroism spectra obtained for 50 μM of D- and L-ecPis-2s epimers in the presence of different concentrations of POPC:POPG (3:1, mol:mol) LUVs.

Although both peptides present helical structures in the presence of negative vesicles, L-ecPis-2s presents lower molar ellipticity values in all LUVs concentrations tested when compared to its epimer.

5.3.4 Effect of epimerization in the peptide-membrane structure

Solution NMR structures of D-ecPis-2s and L-ecPis-2s: The high-resolution three-dimensional structures of D-ecPis-2s and L-ecPis-2s were determined in the presence of 300 mM SDS-d_{25} micelles. SDS-d_{25} micelles mimic the bacterial membrane due to the negative charge observed

in the membrane of these microorganisms. Although micelles do not mimic perfectly the membrane interface, this detergent provides a suitable medium for solution NMR(218). Previous CD spectra of the epimer peptides were acquired in the presence of SDS micelles [Figure SM12] to evaluate the peptide helical propensity as it is appropriate for high-resolution solution NMR spectroscopy.

The sequence assignment of the D-ecPis-2s peptide was performed by analyzing the intra- and inter-residue correlation identified in the ^{1}H-^{1}H-NOESY spectrum [Figure 40], as the ^{1}H-^{1}H-TOCSY spectrum did not show sufficient dispersion of the alpha and amide hydrogen signals.

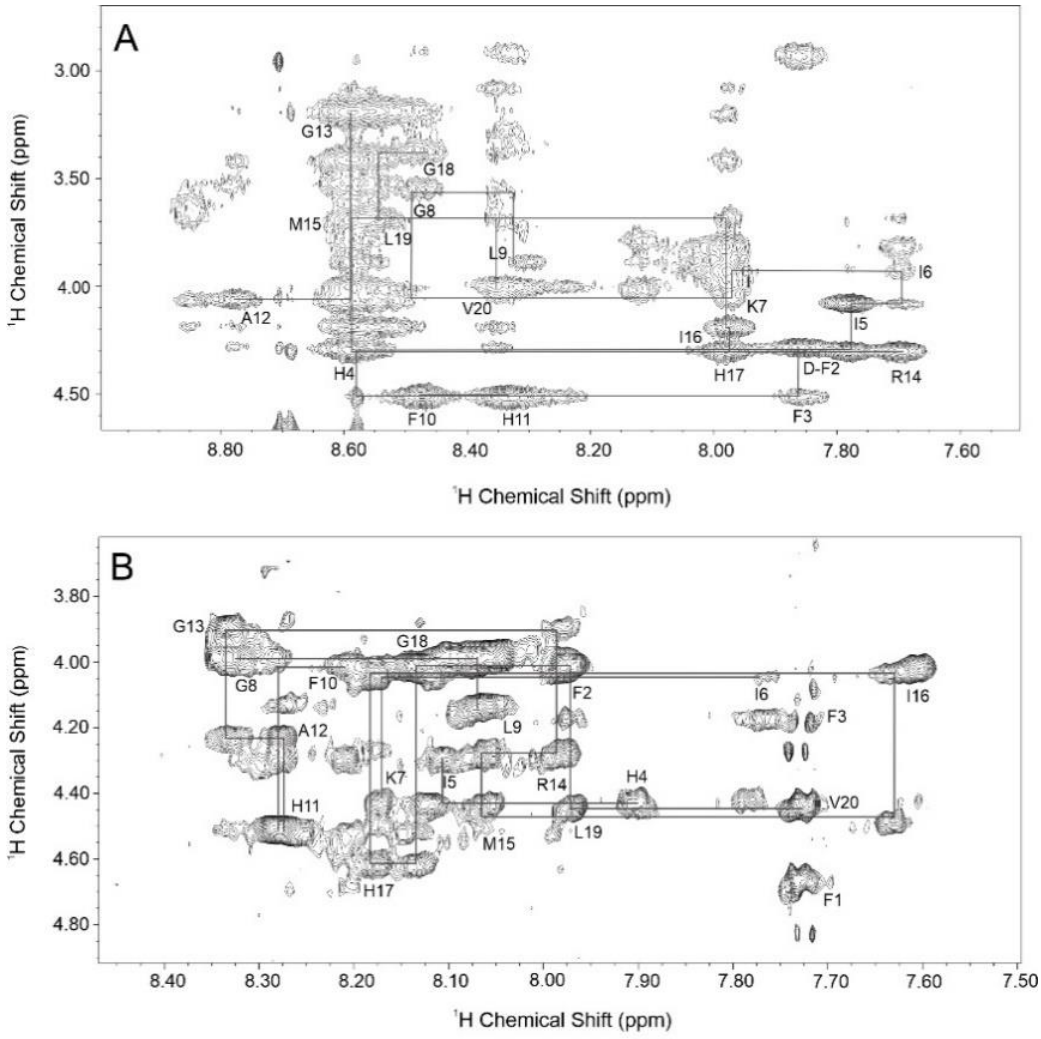

Figure 40: N_H-H_α region of NOESY spectra of 2 mM of (A) D-ecPis-2s, (B) L-ecPis-2s in the presence of 300 mM SDS-d_{25} at 25 ºC, 500 MHz. (C) Overlapping of D-ecPis-2s and L-ecPis-2s NOESY spectra. Only the intraresidual NH-Hα cross peaks are labeled.

Since amidic hydrogens are dispersed in the ^{1}H-^{1}H-NOESY spectrum, H_N-H_α cross-peaks were identified throughout the primary sequence. Several medium range $d_{\alpha N}$ (*i, i + 3*), $d_{\alpha N}$ (*i, i + 4*), and $d_{\alpha\beta}$ (*i, i + 3*) NOE correlations characteristic of a helical conformation was observed for both epimers. Continuous $d_{\alpha N}$ *(i, i + 3)* connectivities were noted for L-ecPis-2s peptide backbone, ranging from F3 up to L19 residues(364) [Figure SM13]. On the other hand, D-ecPis-2s showed interrupted $d_{\alpha N}$ (*i, i + 3*), $d_{\alpha N}$ (*i, i + 4*), and $d_{\alpha\beta}$ (*i, i + 3*) correlations in the NOESY spectrum [Figure SM13]. ^{1}H-^{13}C-HSQC heteronuclear spectrum showed that most residues of L-ecPis-2s present a positive $^{13}C_\alpha$ chemical shift index (CSI)(364). In contrast, heteronuclear experiments by HSQC and HMQC for D-ecPis-2s were performed, but further investigation will be needed to obtain ^{13}C and ^{15}N chemical shift information. In this way, the structure of D-peptide was obtained using only the homonuclear chemical shift information.

Three-dimensional structural calculation of the D- epimers: Intra-residual, sequential (*i, i + 1*), and medium range (*i, i* + 2; *i, i* + 3; and *i, i* + 4) connectivities were converted in a semi-quantitative manner into distance restraints for calculation of D-ecPis-2s structure. The RMSD calculated of 2.4 Å for the backbone, and 4.0 Å for heavy atoms were obtained for the superposition of the entire chain of 10 lowest energy structure of D-ecPis-2s. Table SM5 presents a summary of all the input data used in the calculation as well as the quality parameters. D-ecPis-2s presents 1.3 % residues in the disallowed region of the Ramachandran plot [Figure SM14], while 18% are found in generously allowed regions, followed by 38.7 % and 42 % found in additional allowed and most favored regions, respectively. Figure 41 presents the superposition of the 10 lowest energy structures for D-ecPis-2s, and L-ecPis-2s elucidated by Nunes(364), as well as the lowest energy structures of epimers peptides.

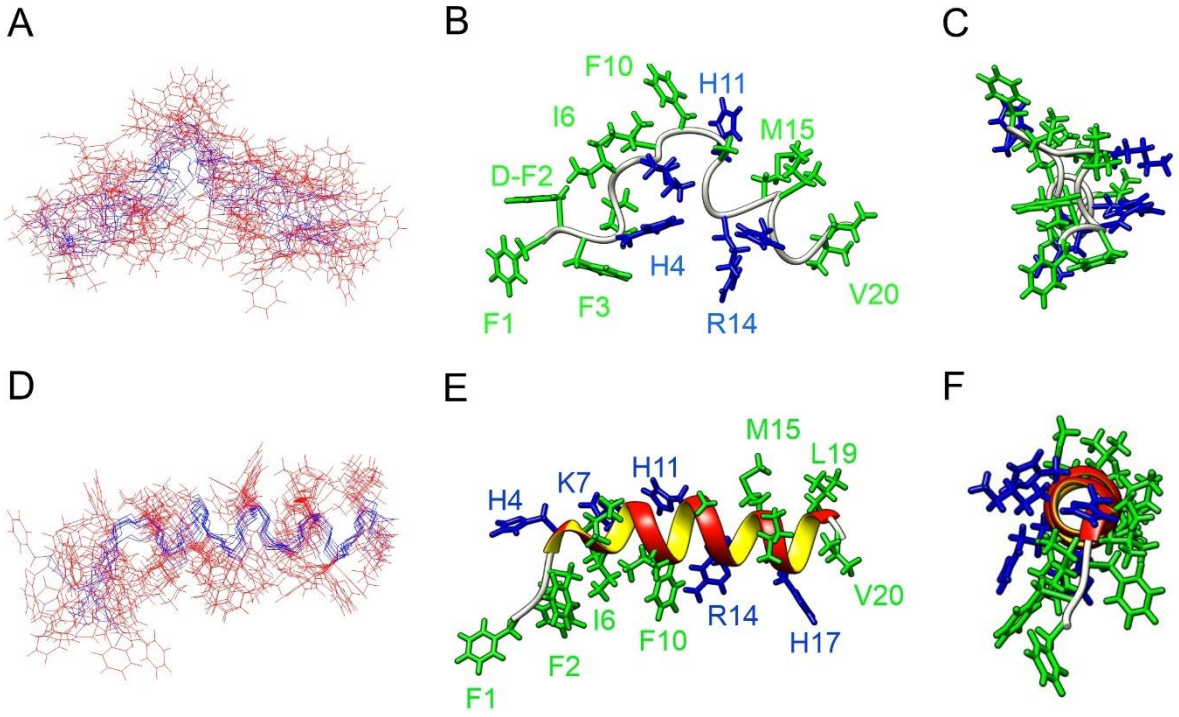

Figure 41: Three-dimensional structures of D-ecPis-2s, and L-ecPis-2s[240] both in the presence of SDS-d_{25} micelles (300 mM) 25 °C, 500 MHz. The low-energy structures are presented for D-ecPis-2s (B and C), and for L-ecPis-2s (E and F). The overlap of the ten lowest-energy structures is presented in panel A (D-ecPis-2s), and in panel D (L-ecPis-2s). The hydrophobic residues are highlighted in green and the hydrophilic residues in blue.

As we can observe, in the presence of SDS-d_{25} micelles, L-ecPis-2s peptide presents a well-defined helical segment from residue H4 to L19(364), while for D-epimer the helical conformation presents a random-coil structure that requires further refinement and validation. Besides that, unusual signals and correlations were observed in the NOESY spectrum for D-ecPis-2s peptide which must be related to diffusion spin process. On the other hand, the helical structure of L-ecPis-2s does not show a perfectly defined partition of hydrophobic and hydrophilic side chains.

Solid-state NMR of D-ecPis-2s and L-ecPis-2s reconstituted in phospholipid bilayers: Solid-state NMR experiments were performed to assess the effects of the peptides on oriented membranes and their alignments relative to the lipid bilayer. The proton-decoupled ^{31}P NMR spectra for labeled (3,3,3-$^{2}H_3$-A12, and ^{15}N-G13) L-ecPis-2s and D-ecPis-2s incorporated in oriented POPC:POPG (3:1, mol:mol) bilayers [Figure 42A and 42B] show a high intensity peak near 32.0 ppm (width at half maximum of 273 Hz for both peptides), indicating a good

alignment of the phospholipids(222). Figure 42C, and 42D show the ^{1}H-decoupled ^{15}N spectra for labeled L- and D-ecPis-2s, in which a single peak related to amidic ^{15}N-G-13 nucleus is observed at 65 (± 6) ppm, and 65 (± 4) ppm, respectively. These results indicate a homogenous alignment of the peptides and a helix orientation practically parallel to the membrane surface. Although ^{15}N spectra reveal equivalent chemical shifts for the epimers, a slightly broader signal is observed for L-ecPis-2s (12 ppm) when compared to D-ecPis-2s (8 ppm), suggesting a slightly higher ordered population for D-ecPis-2s.

^{2}H spectra [Figure 42E, 42F] reveal a slightly different behavior for both epimers. While a defined quadrupolar splitting of 52 ± 3 kHz is presented for D-ecPis-2s epimer, which corresponds to the 3,3,3-2H3-Ala-12 labeled amino acid, the ^{2}H quadrupolar signal for L-ecPis-2s is broader (48 ± 6 kHz). Second splittings are also observed for D- and L-ecPis-2s peptides in the ^{2}H spectrum of approximately 28 kHz, and 24 kHz due to membrane-associated water molecules in the sample. The main deuterium quadrupolar splittings are related to the peptide's orientation relative to the helix rotational pitch angle [Figure 42C, and 42F].

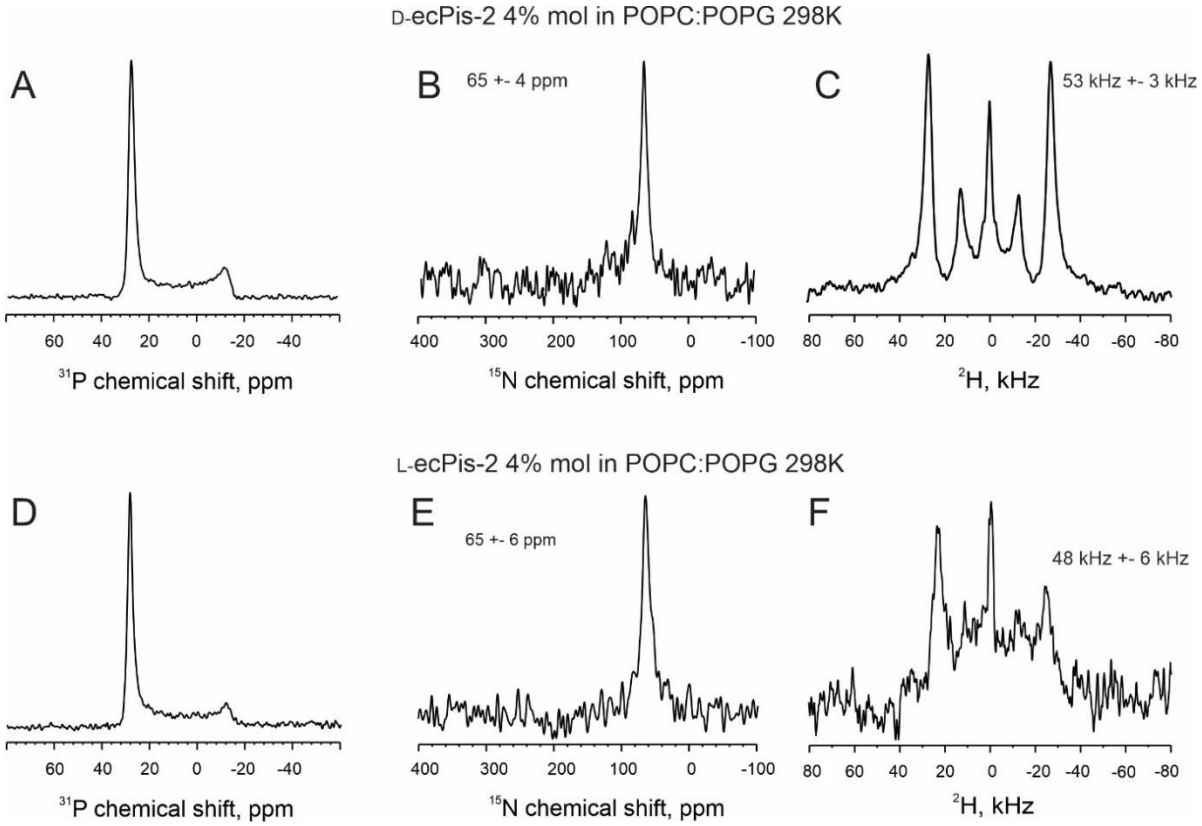

Figure 42: Solid-state NMR spectra for the labeled (3,3,3-$^{2}H_3$-Ala12; ^{15}N-Gly13)-D-ecPis-2s peptide, and (3,3,3-$^{2}H_3$-Ala12; ^{15}N-Gly13)-L-ecPis-2s samples incorporated in oriented POPC:POPG (3:1, mol:mol) bilayers. The proton-decoupled ^{31}P NMR spectra of (A) D-ecPis-2s, and (D) L-ecPis-2s. ^{15}N solid-state NMR spectra of (B) D-ecPis-2s, and (E) L-ecPis-2s. ^{2}H solid-state NMR spectra of (C) D-ecPis-2s, and (F) L-ecPis-2s.

5.4 Discussion

Previously, our research group explored the effect of epimerization on antimicrobial activities and the mode of membrane interaction concerning the phenylseptin (Phes) epimers(11,13). Both D- and L-phenylseptin are naturally occurring peptides, the epimerization of the second phenylalanine residue (Phe-2) led to a 90° conformational change at the *N*-terminus of the D-peptide structure(11), being the reason for the differences in the antimicrobial activities of the two epimers(13). Similarly, to the phenylseptin (Phes), ecPis-2s presents an FFF sequence in the *N*-terminal region. However, there is no reported epimer occurrence regarding this peptide. Therefore, this present work reports antimicrobial and membrane interaction investigations of ecPis-2s epimers (L- and D-ecPis-2s), which differ from each other by the second phenylalanine residue. In this context, we present biological, structural, and biophysical assays to establish correlations between conformational features and aspects of peptide-membrane interactions, aiming to understand the impact of epimerization on antimicrobial activity.

Both D- and L-epimers have a high proportion of hydrophobic and neutral residues, resulting in a low cationic net charge (+2). As observed from the biological experiments, the substitution of the L-Phe2 by D-Phe2 in the primary sequence of the peptide improved the activity in the D-ecPis-2s against *S. typhimurium, P. aeruginosa, and L. monocytogenes*, while maintaining equivalent activity to the L- epimer against *P. mirabilis* [Table 6]. Additionally, the study of bacterial death kinetics shows that the D-epimer also presents a higher activity at all concentrations tested, reducing the number of viable bacteria [Figure 33]. In this way, the biological results reveal that the D-epimer of ecPis-2s peptide presents a pronounced antimicrobial activity property as previously described in the case of the phenylseptins. Therefore, the mode of membrane interaction of both ecPis-2s was further investigated.

D- and L-ecPis-2s pore-forming properties were measured using the dye calcein release approach. The data shows that the D-peptide causes a higher leakage when compared to L-ecPis-2s, at the concentrations tested [Figure 34]. The D-epimer peptide also reaches release values close to the maximum while the maximum value of release for L- epimer is ≤ 60% [Figure 34B]. These findings are in agreement with the biological results, as we have discussed above, in

which D-epimer has presented more activity against most of the bacteria tested as well as a higher performance in the bacterial death kinetics assays.

Calorimetry titration assays were performed in order to check the thermodynamic parameters of the interaction of epimers peptides with negative vesicles. The raw of the peptide–membrane binding data [Figure 37] shows isothermal titration curves typical of exothermic-driven reactions with moderate affinity(6). The value per injection obtained from the integration of the titration peaks was approximately −0.60 μcal/s and 0.53 μcal/s for D and L-ecPis-2s peptide, respectively, in the presence of anionic LUVs [Figure 37 A, 37C]. The results indicated a binding constant of K_{app} = 1.02 x 10^4 M^{-1} for D-ecPis-2s in the presence of the negative LUVs and K_{app} = 6.77 x 10^3 M^{-1}, a higher interaction for D-epimers, as shown in Table SM5. When calculated, the ΔG^o of peptide-membrane interaction is also higher for D-ecPis-2s when compared to the L-epimer.

CD and ζ-potential results of ecPis-2s peptides show similar results. Although the CD spectra present a slightly higher molar ellipticity for D-ecPis-2s, both spectra indicate the same structure preference when the LUVs concentration is increased. In turn, ζ-potential data seem to present a higher interaction for the D-ecPis-2s peptide, showing a faster increase of the ζ-potential on negative LUVs were titrated with both peptides. This finding indicates also a higher partition constant (*Kp*) for D-ecPis-2s [Figure 38 C]. At the final of the experiment, both epimers peptides reach the same potential values which can be related to the same net charge of peptides.

On the other hand, the intrinsic interaction of the peptides with the membrane appears to be quite different. DSC studies reveal significant changes in the liquid-crystalline phase transition of the membrane when interacting with the D-epimer compared to the L-epimer [Figure 35] suggesting a direct consequence of the presence of D-Phe2. As observed, the Tm of pure DMPC:DMPG (3:1, mol:mol) is around 23 ◦C [Figure 435] and very similar for all system compositions, anionic vesicles and both epimer peptides(366). Whereas D-ecPis-2s causes a shift of around 3 ◦C in Tm (19.5 ◦C), at 25 μM, the Tm result of DMPC:DMPG (3:1, mol:mol) in the presence of L-ecPis-2s, at the same concentration can be considered unaltered (Tm ~ 22.7 ◦C). At the highest concentration (100 μM) of peptides, the Tm decreases for both of them and the main phase transition peak gets broader and loses symmetry. This result is mainly observed for D-ecPis-2s indicating a high insertion of the peptide into the fluid DMPC:DMPG membrane. Once again, these data show and confirm a stronger effect of D-epimer by a lower Tm around

17.3 ◦C and 15.2 ◦C (second peak) [Figure 35A] on the mimetic bacterial membrane when compared to the measured results for L-ecPis-2s (Tm = 21.5 ◦C), both at the same concentration.

Interestingly, this result is also supported by solid-state NMR studies using labeled phospholipids. The effect of D- and L-ecPis-2s peptides on the membrane stability shows a significant difference in the deuterium order parameter of each C-D bond in which D-ecPis-2s causes a higher perturbation on the acyl chain of POPG-d_{31} lipids [Figure 36F]. These findings confirm a higher interaction of D-ecPis-2s peptide with the membrane, as suggested by ITC experiments [Figure 37], and are in accordance with the previous biological and calcein release results already discussed here. The evidence of the higher membrane insertion of D-ecPis-2s also indicates the higher ability of the epimer to interact with the hydrophobic portion of the bilayer, probably due to the hydrophobic moment or portion at the peptide N-terminus.

In addition, as AMPs are also susceptible to proteolytic degradation by enzymes from the host or the pathogens which can reduce their antimicrobial activity and stability(367), the proteolytic cleavage can also be different for D- and L-epimers and alter their structures, leading to changes in their mechanism of action(121). As we have discussed, D- amino acid which composed the antimicrobial peptides seems to be more resistant to proteolytic activity. However, the relationship between the proteolytic effect and the activity of AMPs is complex and depends on the type, location, and extent of the proteolytic cleavage(63), as well as the original structure and function of the AMPs. To overcome the proteolytic degradation of AMPs, various strategies have been developed, such as backbone cyclization, dimerization, PEGylation, and conjugation with cell-penetrating peptides(63), as well as the addition of D-amino acid in the primary sequence of a peptide(368). These methods can even improve the stability, activity, and specificity of AMPs, and make them more suitable for clinical applications.

Finally, as a consequence of interactions with the bilayer, D- and L-epimers seem to present similar three-dimensional NMR structures in solution. The higher molar ellipticity values, showed in the CD for the D- peptide, indicates a secondary structure that is not observed by solution NMR. On the other hand, solid-state NMR data reveal a well-defined topology of the D-epimer in an oriented bilayer. These findings together show that the intrinsic interaction of the peptide with the bilayer is different for peptides with D- and L-residues and may also help to explain the difference in biological activity of the epimers.

5.5 Conclusion

The interaction and biophysical features of the epimers piscidin peptides with anionic membranes have been reported in this study. Though both peptides present the same primary sequence, except an enantiomer D-phenylalanine amino acid, the effect of this replacement seems to improve the biological activity of D-peptide when compared to the L-epimer. Even with similar conformation profiles presented by CD spectroscopy, the perturbation caused by the D-epimer is much higher when investigated in negative membranes, as indicated by DSC, solid-state NMR of deuterated lipids, ITC, and ζ-potential assays. Our results demonstrate that D-ecPis-2s epimer exerts a higher effect on the membrane stability suggesting that somehow the D-configuration leads the peptide structure to a stronger amphipathic character when compared to L-ecPis-2s. Besides that, the hypothesis of specific aromatic interactions involving the phenylalanine residues of D-ecPis-2s leads to play an important role in the position of F1, F2, and F3 sidechains, which can be located in the hydrophobic face of the helix as well as anchoring the D-peptide into the lipid bilayer, increasing its affinity to the membrane(11).

As perspectives to this study, in order to further investigate the influence of D-Phe residue on the mode of action of ecPis-2s peptides, additional experiments will be carried out in order to obtain more structural information as well as evaluate the influence of the sequence of three phenylalanine in the peptide N-terminus. Besides that, as piscidin-2 is a histidine-enriched peptide (H4, H11, and H17), the influence of pH on the mode of action will be also investigated. Thus, the interaction of peptides and stability of anionic membranes will be also examined for both D- and L-ecPis-2s at neutral pH using biophysical and structural techniques.

Chapter 6: General conclusion

This manuscript is dedicated to recently discovered natural antimicrobial peptides from the piscidin family with a particular interest on their mechanism of action in the presence of negative membrane models. In addition, we investigated the influence of a D-amino acid residue in a motif/sequence of three phenylalanine residues and how it can modify its structure and/or lead to improvement in its biological activity.

In general, piscidin peptides are known for their broad-spectrum antimicrobial activity and are of significant interest due to their potential applications in medicine and aquaculture. Both piscidin-4 and piscidin-2 peptides are found mainly in the mast cells of fish, and they play a critical role in the innate immune response of fish by exhibiting antimicrobial, antifungal, and antiparasitic activities. As a common feature, besides exhibiting strong antimicrobial activity against a broad spectrum of microorganisms, the mode of action of piscidin-4 and piscidin-2 peptides involves membrane disruption. As shown by the calcein release measurements, all peptides can integrate into anionic vesicles and create pores [Figure 24C, Figure 34], leading to membrane rupture and in a bacterial environment causing cell lysis and death. Furthermore, piscidins peptides studied in this manuscript are characterized by their α-helical structure, as shown by CD spectroscopy [Figure 15, and Figure 39], which seems to be important for their interaction with anionic membranes.

Both peptides are similar in length, positively charged, and carry histidine residues in their composition [Table 1, and Table 4]. Given the potential pH variations in different microenvironments (e.g., surface vs. intracellular compartments), histidine's ability to change its protonation state can affect the peptide activity, and play an important role in the activity and selectivity of the piscidins studied. Nevertheless, the high degree of aromatic residues in the N-terminal portion found in both ecPiscidin-2 and ecPiscidin-4 peptides seems to be the essential structure factor to drive their mechanisms of action.

When we look at the piscidin-4 peptide, it exerts its membrane effect mainly by disrupting the vesicles, in a well-defined α-helical structure [Figure 19], parallel to the membrane surface in a carpet-like mechanism. Besides that, its behavior in aqueous or buffered media is quite interesting. Different from other peptides that present a random-coil conformation in an aqueous environment, ecPis-4s peptide acquires a defined structure with a NOE diagram that supports a helical segment from K10 to R20 [Figure 27]. Interestingly, the

N-terminal region formed by residues 1-6 (FFRHIK) is resistant to trypsin protease activity suggesting that this region is responsible for the major activity of peptide [Figure 31A, Figure 31 B]. In this way, the pre-ordered structure seems to play an essential role in protecting this peptide against complete enzymatic degradation while retaining its bacterial activity even in the presence of proteases, as observed in the kinetics of bacterial growth assays [Figure 32].

Parallel to the investigation of ecPis-4s peptide, we performed a further investigation on the influence of a D- amino acid in the activity and structural behavior of piscidin-2 epimers. Peptides containing D-residues have been described as pronounced structural preferences not followed by peptides consisting of naturally abundant L-residues. Besides that, the replacement of L- with D-residues greatly increases the stability towards proteolysis(369) as well as seems to improve the biological activities when compared to the epimeric L- form [Table 6].

Previously, our research group described the biological activity and mode of interaction of D- and L-phenylseptins epimers. Both epimers are naturally occurring peptides and the difference in antimicrobial activity was observed mainly against *S. aureus* and *X. axonopodis* bacteria strains, being increased in D-epimer by two and eight times, respectively, when compared to L-epimer(11,13). Similarly, ecPis-2s peptide presents the triple-phenylalanine *N*-terminal sequence, therefore we proposed a new D-ecPis-2s peptide derivative from piscidin-2s (L-ecPis-2s). The fundamental difference between ecPis-2s peptides is the stereochemistry at the second residue of phenylalanine (D-Phe2) which seems to play an important role on the mode of membrane interaction. Our results reveal at least, a higher activity against all bacterial strains tested and deeper insertion of D-peptide to anionic membranes when compared to the natural peptide. When compared to L-ecPis-2s peptide, the effect of D-Phe was more pronounced in dye leakage, DSC, and deuterium order parameters assays in which significant changes and higher perturbation on the lipids were observed. In some way, the aromatic interactions involving the phenylalanine residues play a significant role in the relative orientation of the F1, F2, and F3 sidechains which seems to insert them in the hydrophobic face of the helix [Figure 44]. Thus, the changes in stereochemistry might impact on the interaction behavior of ecPis-2s peptide, causing a greater anchoring of D-epimer into the lipid bilayer and increasing its activity on the membrane.

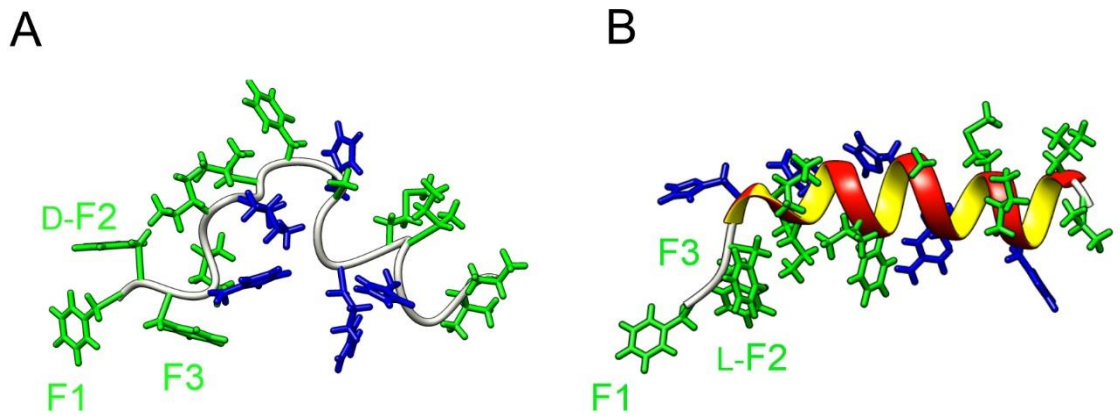

Figure 44. Three dimensional structures of ecPis-2s peptides. (A) D-ecPis-2s peptide and (B) L-ecPis-2s piscidin peptide.

Figure 44 presents again the structures of ecPis-2s peptides obtained in the presence of SDS micelles in which the three phenylalanines (F1, F2, and F3) residues are highlighted. The presence of D- amino acid, also discussed above, is an important characteristic of antimicrobial peptides which can influence on the action of peptides, enhancing the activity against bacteria strains. As observed for phenylseptin epimers peptides, the 1H chemical shifts of the D-ecPis-2s residues supported the conformational differences at the piscidin-2s peptides at the N-termini region. The previous study of our group related to phenylseptin epimers indicated that the lower chemical shift values for Hβ and aromatic hydrogens of D-Phes in comparison to those of L-Phes showed that these nuclei are involved in π interactions and therefore they are placed closer to the π-electrons of the neighboring phenylalanine aromatic rings when compared to the equivalent segment of L-Phes(370). In addition, geometrical parameters regarding the aromatic rings of F1, F2, and F3 residues were proposed based on the geometrical treatment. This behavior will be also investigated for ecPis-2s epimers peptides and can be a way to better explain the mode of action of both D- and L-ecPis-2s.

Thus, this work provides new structural features of the ecPiscidin peptides, showing a similar secondary structure profiles which are characterized by a helical segment. The D configuration of F2 seems to lead to conformational variability near the peptide N-terminus of D-ecPis-2s and to a stronger amphipathic character of the peptide structure, when compared to L-ecPis-2s which could play an important role on the interaction of the D- epimer. Therefore, specific aromatic interactions may involve the F1, F2 and F3 phenylalanine sidechains, which whether located in hydrophobic face of the helix, can anchoring the D-epimer into the lipid bilayer and increasing its affinity to the membrane. This efficient anchoring interaction of the

D-ecPis-2s N-terminus may be correlated to stronger peptide membrane interactions and to more pronounced membrane-disruptive properties, which is finally related to stronger antimicrobial activity in comparison to its L-epimer. The data presented in this work also suggests that at least initially both peptides interact with the membrane in a carpet-like mechanism as indicated by the orientational data derived from solid-state NMR, despite the difference in the interaction of the peptides with the bilayer.

Therefore, this work presents advances in the comprehension of the mechanisms of action of antimicrobial ecPiscidin-4s, and D- and L- ecPiscindin-2s peptides, which is relevant to the field. As observed to the ecPis-4s peptide, the N-terminal region of ecPis-2s peptides presents an important structure feature on the membrane interaction and biological activity. Although both epimers present similar conformational preferences as shown by CD spectroscopy [Figure 39], further structural analysis is needed to understand the role of D-phenylalanine on the increase of antimicrobial activity. In addition, structural analyses are also needed in aqueous media, since the D-epimer presents a higher aggregation degree in comparison to the L-epimer, as noted by the AUC experiments (not shown).

As this work focuses primarily on investigating the structures, membrane alignments and interactions of these peptides, we have analyzed the peptide molecules individually. However, peptide aggregation may occur and strongly influence the mechanism of action and activity, especially for the epimers peptides, as previously observed for other peptides. Further investigations of these interactions are required to fully elucidate how these peptides exhibit their antimicrobial activities. Additionally, the potential synergistic action of these compounds is another relevant aspect for future investigations, since others epimers secreted by the animal have shown higher activity. Thus, these investigations could represent an important role in the peptidase resistance being associated with the increased antimicrobial activity found for the modified peptide.

Chapter 7: Résumé de thèse

7.1 Introduction

Les peptides sont des biomolécules aux activités biologiques diverses et jouent un rôle important dans les propriétés fonctionnelles et physiologiques des organismes vivants (17,18). De même, les peptides sont formés par des résidus d'acides aminés liés de manière covalente par des liaisons amides, également appelées liaisons peptidiques (1,19).

L'activité biologique des peptides a été décrite pour la première fois par Mellander en 1950(20). Cette étude a montré que les peptides phosphorylés dérivés de la caséine augmentaient la calcification osseuse chez les enfants diagnostiqués avec le rachitisme, même en l'absence de vitamine D (20). Depuis lors, les peptides ont fait l'objet de nombreuses études qui se poursuivent jusqu'à nos jours (21).

Actuellement, il existe plusieurs plateformes ou bases de données qui classent les peptides bioactifs en fonction de leur fonction/activité comme antimicrobiens, antithrombotiques, antihypertenseurs, opioïdes, immunomodulateurs, antioxydants, cicatrisants, antidiabétiques et anti-biofilms, anticancéreux, entre autres (22–27). Ainsi, ces molécules peuvent agir principalement sur les systèmes immunitaire, digestif, gastro-intestinal, endocrinien, cardiovasculaire et nerveux, ainsi qu'avoir des propriétés préventives contre les maladies infectieuses (22,28).

Parmi les classes de peptides bioactifs, celle qui a été mise en évidence ces dernières années est celle des peptides antimicrobiens (PAM). La pertinence de l'étude des peptides antimicrobiens découle de la résistance accrue des micro-organismes aux antibiotiques conventionnels, principalement en raison de leur utilisation aveugle pour combattre les infections bactériennes (29). En conséquence, la résistance bactérienne est maintenant l'un des problèmes de santé publique les plus graves avec un impact économique mondial (30–32). Les PAM agissent en s'associant aux membranes cellulaires, principalement celles chargées négativement (18) dont l'interaction entraîne la désorganisation et/ou la perturbation de la bicouche lipidique, ce qui peut provoquer la lyse cellulaire (4,24,33). Ce mécanisme diffère du mode d'action des médicaments conventionnels, qui agissent sur des cibles spécifiques dans les cellules des agents pathogènes. Par conséquent, par rapport aux antibiotiques conventionnels,

le développement de la résistance des agents pathogènes est plus difficile lorsqu'ils sont traités avec des PAM (34). Dans ce contexte, les PAM sont apparus comme des agents antibiotiques prometteurs et une alternative dans le développement de nouveaux médicaments pour combattre les infections causées par des bactéries super-résistantes.

Bien que de nombreux peptides antimicrobiens aient été étudiés et que certains mécanismes d'action aient été proposés, leur mode d'interaction membranaire est difficile à analyser, et des études plus approfondies sont nécessaires pour répondre à certaines questions. Les connaissances acquises à partir des techniques structurales, des processus d'interaction biophysique et de la compréhension de la relation structure-activité des peptides antimicrobiens aident à la conception et au développement de molécules plus spécifiques avec un plus grand potentiel biologique, résultant en des antibiotiques plus efficaces avec une moindre toxicité.

7.2 Résistance bactérienne

Les antibiotiques ont effectivement prolongé l'espérance de vie et sont les médicaments les plus largement distribués par les industries pharmaceutiques et les plus prescrits dans les hôpitaux du monde entier (35–37). Ces médicaments sont essentiels dans les traitements de santé, en particulier dans les pays sous-développés, où les maladies causées par les infections microbiennes sont une cause fréquente de décès (38).

La résistance bactérienne, également connue sous le nom de résistance aux antibiotiques ou de résistance aux antimicrobiens (RAM), est la capacité des bactéries à résister à l'action ou aux effets des médicaments précédemment utilisés pour les traiter (30). En d'autres termes, la résistance aux antimicrobiens se produit lorsqu'un micro-organisme tel que les bactéries, les champignons et les parasites changent lorsqu'ils sont exposés à des médicaments antimicrobiens, par exemple, des antibiotiques et des médicaments antifongiques (39). En conséquence, ces médicaments deviennent inefficaces et les infections persistent dans le corps, augmentant le risque de propagation à d'autres (30). La RAM est actuellement l'un des problèmes de santé publique les plus pertinents au niveau mondial, car elle a des conséquences cliniques et économiques préoccupantes, puisque de nombreuses bactéries précédemment sensibles aux antibiotiques habituellement utilisés ne répondent plus à ces mêmes agents (31,38,40).

Bien que le développement de la résistance bactérienne aux antibiotiques soit un phénomène naturel, la surutilisation et le mésusage des antibiotiques dans les soins de santé et l'agriculture, ainsi qu'une gestion inappropriée des déchets et une transmission environnementale, ont conduit à une augmentation substantielle de la résistance aux antimicrobiens (30,35). Le processus de résistance aux antimicrobiens résulte de l'utilisation de médicaments et de la mutation génétique des bactéries (31), en plus du développement de bactéries superbactéries qui est également le résultat de l'utilisation aveugle d'antibiotiques comme en médecine, en agriculture et dans l'élevage (41); d'un mauvais contrôle des infections dans les hôpitaux et les cliniques ; d'un manque d'hygiène et d'assainissement de base (31,40), etc.

L'Organisation mondiale de la santé (OMS) a signalé que la résistance aux antimicrobiens (RAM) avait tué au moins 1,27 million de personnes dans le monde et était associée à près de 5 millions de décès en 2019 (30). Aux États-Unis, les Centers for Disease Control and Prevention (CDC) ont signalé plus de 2,8 millions de cas d'infections résistantes aux antimicrobiens chaque année, entraînant plus de 35 000 décès, comme indiqué dans le rapport 2019 sur les menaces de résistance aux antibiotiques (42). Un récent rapport du Programme des Nations Unies pour l'environnement souligne la nécessité d'accorder une attention accrue aux facteurs environnementaux favorisant le développement de bactéries résistantes aux médicaments, communément appelées "superbactéries". Le rapport prédit que d'ici 2050, les superbactéries et les formes associées de RAM pourraient entraîner jusqu'à 10 millions de décès par an, égalant le nombre annuel mondial de décès par cancer (43,44).

Il existe principalement quatre mécanismes par lesquels les bactéries résistent aux antibiotiques (50), comme le montre la Figure 1. Ce sont [1] l'inactivation du médicament médiée par une enzyme bactérienne, comme observé sur l'enzyme β-lactamase qui inactive la pénicilline G des bactéries résistantes à la pénicilline (51) ; [2] en réduisant l'absorption du médicament par une diminution de la perméabilité cellulaire, ce qui permet à certaines bactéries de modifier les composants de leur paroi cellulaire, tels que le lipide A des lipopolysaccharides ou les précurseurs du peptidoglycane, pour éviter l'interférence des antibiotiques avec la synthèse de la paroi cellulaire (52) ; [3] la modification structurelle de la cible du médicament due à une mutation génétique qui permet aux bactéries de modifier leurs sites de liaison cibles par des mutations génétiques (53,54) ; [4] l'efflux du médicament à l'extérieur de la membrane cellulaire bactérienne qui est l'expression de pompes à efflux transmembranaires. Ce processus appartient à six grandes familles et permet aux bactéries d'éjecter activement presque toutes les

classes d'antibiotiques de leur cytoplasme (55). Les plasmides, de petits éléments génétiques mobiles composés d'ADN extrachromosomique, peuvent propager des gènes de résistance entre des bactéries de la même espèce ou d'espèces différentes, le gène de résistance aux quinolones médié par plasmide en étant un exemple (50,53).

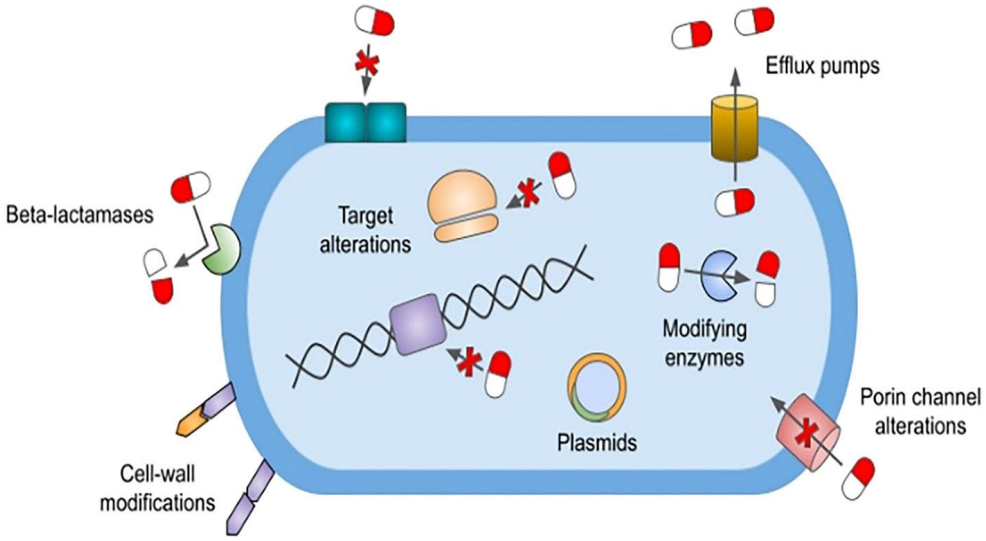

Figure 45. Mécanismes de résistance aux antimicrobiens qui représentent diverses stratégies de résistance aux antimicrobiens utilisées par les pathogènes ESKAPE (53).

Les progrès récents dans la lutte contre la résistance aux antimicrobiens englobent une gamme de stratégies, notamment des méthodologies de combinaison de médicaments, des produits basés sur des biomatériaux polymères antimicrobiens, des approches de bio-nanotechnologie et autres.

Parmi les propositions discutées ci-dessus et décrites dans la littérature, les peptides antimicrobiens (PAMs) isolés des poissons, appelés piscidines, sont une classe de biomolécules prometteuses avec une activité antimicrobienne potentielle élevée et un large spectre contre les agents pathogènes résistants (61). Les PAM sont une classe de petits peptides largement présents dans la nature et ils constituent une partie importante du système immunitaire inné de différents organismes. Contrairement aux médicaments conventionnels, qui ciblent les processus cellulaires centraux et le métabolisme de la paroi cellulaire, la principale cible des PAM est la membrane cellulaire (63,64) . Bien que ces biomolécules soient très diverses, elles possèdent plusieurs propriétés communes telles que [1] une charge nette positive, qui les aide à atteindre la surface bactérienne ; [2] une hydrophobicité élevée, et [3] une amphipathicité, caractéristiques qui, ensemble, conduisent à un coefficient de partage élevé dans la bicouche

lipidique de la membrane microbienne (65). Les études sur les PAM font partie d'un domaine de recherche encore récent qui fait face à des défis, notamment la recherche de biomolécules dans la nature, l'étude de leurs rôles dans l'immunité innée et l'identification de leurs mécanismes d'action (66,67).

7.3 Mécanisme d'action des peptides antimicrobiens

Les PAMs ont un mécanisme d'action qui diffère des antibiotiques conventionnels basés sur l'inhibition enzymatique (132). Bien que les PAM puissent perturber les cellules pathogènes de diverses manières (79), le principal mode d'action de ces molécules consiste en la perturbation et la rupture des membranes cellulaires, la fuite du contenu cytoplasmique et la lyse cellulaire qui en résulte (72,133–135). Ainsi, les PAM peuvent exercer leur activité antimicrobienne en employant des modes d'action sophistiqués, qui impliquent une interaction avec la paroi cellulaire et la membrane cellulaire, ainsi qu'en inhibant la formation de biofilms et en modulant le système immunitaire de l'hôte. L'activité des peptides antimicrobiens dépend de divers facteurs, tels que la taille, la charge, l'hydrophobicité, la structure secondaire ou le caractère amphiphile. La conformation des PAM peut également jouer un rôle important dans leur efficacité antimicrobienne. De plus, les peptides avec des structures amphipathiques peuvent interagir plus efficacement avec la membrane du pathogène.

Les effets antibactériens des PAM agissant sur la paroi cellulaire sont principalement médiés par l'interférence avec la synthèse des composants de la paroi cellulaire et la perturbation de l'intégrité de la paroi cellulaire, par exemple les PAM qui interfèrent avec la biosynthèse du peptidoglycane (PGN) (136); les PAM qui peuvent endommager l'intégrité de la paroi cellulaire en inhibant la biosynthèse de l'acide téichoïque de la paroi (WTA) ou de l'acide téichoïque de la membrane (137), exerçant ainsi un effet bactéricide sur Staphylococcus aureus résistant à la méthicilline (SARM) (137). De plus, certains PAM peuvent induire la libération d'autolysines qui dégradent les parois cellulaires bactériennes (139). Alternativement, les PAM peuvent agir sur la membrane cellulaire ou sur des cibles intracellulaires (122). Une représentation schématique du mécanisme antibactérien des PAM est présentée dans la Figure 4.

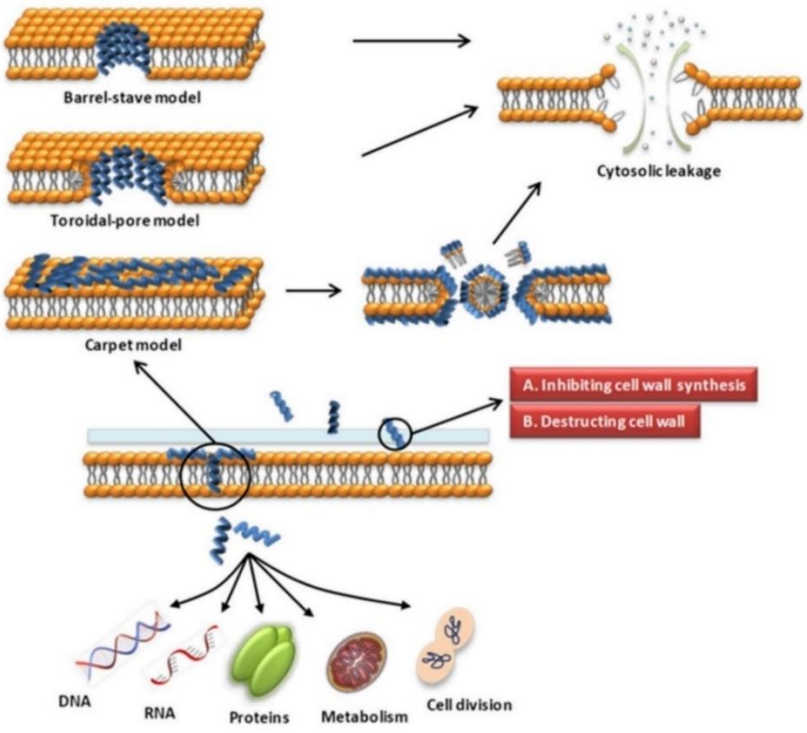

Figure 46. Différents modes d'action des peptides antimicrobiens. Les PAM peuvent avoir des effets neutralisants directs sur les bactéries, par exemple, par la perturbation de la membrane via la formation de pores ou en ciblant les structures internes des bactéries (122).

La membrane cellulaire microbienne est une cible importante de la plupart des PAM car ils agissent en perturbant l'intégrité de la membrane du pathogène (63). En outre, la différence de composition de la membrane cellulaire des mammifères est un facteur majeur dans la destruction sélective des bactéries par les PAM (79). Dans la littérature, différents modèles ont été proposés au cours des 25 dernières années qui relient l'activité des PAM sur la membrane cellulaire au résultat éventuel de la lyse osmotique (78). La majorité de ces processus commencent par différents événements se produisant au niveau de la bicouche membranaire bactérienne après l'adsorption initiale des PAM. Les mécanismes d'action des PAM connus sous le nom de modèle de tapis, modèle de tonneau et modèle de pore toroïdal sont les plus discutés dans la littérature (140). Ces modèles décrivent le mode d'interaction peptide-membrane qui conduit au processus de formation de pores basé sur un mécanisme commun qui se déroule essentiellement sur une combinaison d'effets hydrophobes et électrostatiques (141).

7.4 Peptides de piscidine

Ces dernières années, l'environnement marin a été de plus en plus exploré et est devenu l'une des sources les plus riches en peptides antimicrobiens (21,34,85). Parmi les classes de PAM trouvées dans cet environnement, les piscidines sont apparues comme l'une des familles de peptides les plus importantes (185). La piscidine est un type de PAM enrichi en histidine qui interagit avec les bicouches lipidiques en acquérant généralement des hélices α amphipathiques (101,186). Ce sont des peptides naturels communément trouvés dans différentes espèces de poissons (187), responsables des réponses immunitaires innées et présentant des activités à large spectre contre les bactéries, les champignons et même les virus (79,188). De plus, les piscidines sont trouvées dans différentes parties, notamment les mastocytes, les branchies et la peau des poissons où les peptides présentent des propriétés immunomodulatrices de cicatrisation des plaies, et où d'autres neuropeptides sont exprimés (189,190).

Bien que les PAM de piscidine en soient encore aux premiers stades de développement et n'aient pas encore atteint les phases avancées des essais cliniques, il existe quelques essais cliniques impliquant des PAM de piscidine ou leurs dérivés. L'un d'eux est le peptide antimicrobien Tilapia Piscidin 4 (TP4) qui a montré un large spectre d'activité antimicrobienne, ainsi que des propriétés anticancéreuses, immunomodulatrices et de cicatrisation des plaies (190). La nature riche en histidine des piscidines leur permet d'interagir avec les bicouches lipidiques et de présenter une perméabilisation dépendante du pH lorsque leur charge positive augmente dans des environnements acides (133). La Tilapia Piscidin 4 (TP4) est dérivée du poisson tilapia du Nil (Oreochromis niloticus) qui présente des propriétés antibactériennes, antibiofilm et de cicatrisation des plaies (193).

Le peptide antimicrobien TP4 n'est pas encore approuvé par la FDA, mais il est en essais cliniques pour le traitement de la vaginose bactérienne (VB), une infection vaginale courante causée par un déséquilibre des bactéries. La VB est répandue chez les femmes en âge de procréer et présente un taux élevé de récidive, qui peut être largement attribué à l'éradication inefficace du biofilm de VB par les antibiotiques de première ligne actuels (194). Dans une étude précédente, la piscidine 4 de tilapia (TP4) présente une activité antimicrobienne et antibiofilm à large spectre contre les bactéries associées à la VB, mais pas contre les lactobacilles bénéfiques. L'essai clinique vise à évaluer la sécurité, les effets secondaires et la dose maximale tolérable de TP4 chez les femmes atteintes de VB.

Dans cette thèse, nous nous concentrons sur le mode d'action et l'activité biologique des peptides naturels de piscidine, à savoir la Piscidine-4s (ecPis-4s), la Piscidine-2s (ecPis-2s) et une forme épimérique de l'ecPis-2s. Les peptides naturels ont d'abord été isolés d'Epinephelus coioides (mérou tacheté orange, également connu sous le nom de morue d'estuaire), un poisson communément trouvé dans les mers d'Asie (195). Ces peptides ont présenté une activité élevée contre les souches bactériennes à Gram positif (Staphylococcus aureus) et à Gram négatif (Escherichia coli, Vibrio Parahaemolyticus). Le mérou tacheté orange (E. coioides) est également la source d'autres peptides tels que l'épinécidine-1 (Epi-1) (196), qui a montré une activité efficace contre un large éventail d'infections bactériennes et virales et présente des effets immunomodulateurs (196,197).

Les peptides ecPis-4s (FFRHIKSFWKGAKAIFRGARQG-NH_2) et ecPis-2s (FFFHIIKGLFHAGRMIHGLV-NH_2) ont respectivement 22 et 20 résidus d'acides aminés et sont capables de s'organiser en structures amphipathiques (195). Comme mentionné, en plus des séquences naturelles, nous avons proposé la synthèse d'un épimère ecPis-2s en remplaçant le deuxième résidu L-Phe2 par un résidu D-Phe2, qui a été nommé D-ecPis-2s. Pour mieux comprendre le mécanisme d'action de ces peptides, cette étude a évalué le mode d'interaction membranaire des peptides ecPis-4s et L-ecPis-2s en tant que modèles potentiels d'agents thérapeutiques contre les agents pathogènes, ainsi que l'effet de l'épimérisation sur l'activité antimicrobienne et l'interaction membranaire du peptide piscidine-2.

7.5 Chapitres de recherche

7.5.1 Élucidation du mode d'interaction et de la perturbation membranaire dépendante de la concentration du peptide antimicrobien ecPis-4s

Dans ce chapitre, la structure et la topologie membranaire de l'ecPis-4s sont présentées. De plus, les caractéristiques biophysiques de l'interaction peptide-membrane ont été évaluées par spectroscopie de fluorescence, diffusion dynamique de la lumière (DLS), potentiel zêta et mesures de fuite. En outre, la thermodynamique du processus de liaison a également été étudiée par calorimétrie de titration isotherme (ITC).

La première session de résultats liée au peptide de piscidine ecPis-4s, ses propriétés et caractéristiques ont été étudiées en présence d'un environnement mimétique négatif constitué de vésicules POPC:POPG (3:1, mol:mol) ou de micelles SDS. Les essais de spectroscopie CD ont démontré que l'ecPis-4s a une structure à haute teneur en hélices en présence de vésicules POPC:POPG (3:1, mol:mol) et de micelles SDS. Des expériences de RMN en solution ont été réalisées en présence de micelles SDS-d25 chargées négativement pour déterminer la structure tridimensionnelle à haute résolution du peptide. Ces expériences confirment la conformation hélicoïdale et amphipathique sur toute la chaîne peptidique de l'ecPis-4s. La RMN à l'état solide du ^{15}N et du ^{2}H découplés des protons de bicouches lipidiques orientées macroscopiquement a été utilisée pour déterminer la topologie du peptide ecPis-4s(221,281) dans des membranes constituées de POPC:POPG (3:1, mol:mol), et dans un extrait lipidique d'E. coli. Le déplacement chimique autour de 70 ppm indique que le peptide adopte une orientation de surface avec un angle d'inclinaison proche de 90° par rapport à la surface de la bicouche. Les expériences de libération de carboxyfluorescéine (CF)(6,371) démontrent une activité lytique de ce peptide en présence de vésicules chargées négativement constituées de POPC:POPG (3:1, mol:mol). En outre, les expériences de DLS et de potentiel zêta(6) ont montré une perturbation significative de la membrane à un rapport peptide:membrane de 0,06 en présence des mêmes vésicules chargées négativement. De plus, les spectres de fluorescence du tryptophane (Trp) de l'ecPis-4s ont également été enregistrés dans des solutions tamponnées au phosphate à pH 6,0 et 8,0, respectivement, et à différentes concentrations de LUV POPC:POPG (3:1, mol:mol). Pour les deux conditions de pH, la fluorescence intrinsèque du Trp de l'ecPis-4s 4s montre une émission maximale à 350 nm en l'absence de LUV. Lorsque les vésicules POPC:POPG (3:1, mol:mol) sont titrées avec la solution d'ecPis-4s, un décalage vers le bleu est observé aux deux pH. Dans les deux cas, l'augmentation de la concentration en lipides s'accompagne d'une augmentation de l'intensité de fluorescence maximale du Trp (max) jusqu'à atteindre un plateau. Lorsque les paramètres d'ordre du deutérium du POPC-d31 ont été étudiés, la présence d'ecPis-4s a eu une influence sur la chaîne acyle zwitterionique principalement à l'intérieur du noyau de la membrane. Notamment, le désordre est plus prononcé pour le POPG-d31, ce qui suggère que ce lipide anionique s'accumule au voisinage du peptide cationique. Les expériences de titrage utilisant la fluorescence du Trp, le potentiel et les techniques ITC fournissent toutes des constantes d'affinité similaires pour l'ecPis-4s aux membranes POPC:POPG (3:1, mol:mol) qui saturent à une concentration correspondant à la neutralité de charge nominale.

En conclusion, ces résultats indiquent que la structure -hélicoïdale amphipathique du peptide ecPis-4s hautement cationique assure une haute affinité pour les membranes anioniques, entraînée par de fortes contributions électrostatiques et une insertion des chaînes latérales hydrophobes juste en dessous de l'interface membranaire. Le partitionnement résultant de l'hélice amphipathique dans l'interface membranaire à une orientation d'hélice parallèle à la surface a des effets prononcés sur la bicouche lipidique. En effet, les expériences de libération de colorant et de DLS indiquent une formation de pores et une activité lytique membranaire qui dépend de la concentration locale en peptide. Il est intéressant de noter qu'un rapport critique peptide:phospholipide d'environ 0,06 est nécessaire pour neutraliser la charge de surface de la membrane.

Dans l'ensemble, ces résultats indiquent que l'ecPis-4s suit un mode d'interaction bien défini avec la membrane anionique, où les interactions électrostatiques assurent la sélectivité pour les membranes bactériennes. Ainsi, tous ces résultats indiquent que l'ecPis-4s recouvre la surface de la membrane selon un mécanisme d'interaction suggérant une action lytique membranaire via une activité de formation de pores une fois que la concentration locale ou le peptide atteint un seuil, dans lequel le peptide ecPis-4s interagit avec une structure amphipathique bien définie avec ses chaînes latérales hydrophiles face à la solution aqueuse, et les hydrophobes face à la bicouche phospholipidique, améliorant la déstabilisation de l'ordre membranaire ainsi que son activité lytique.

7.5.2 La stabilité structurelle du peptide bioactif ecPis-4s en solution aqueuse est un déterminant de sa résistance protéolytique

Le deuxième chapitre de recherche de ce travail est également lié au peptide de piscidine ecPis-4s, cependant les études présentées ont été réalisées uniquement dans un environnement tamponné ou même en solution aqueuse. Afin d'étudier l'effet de la concentration sur les préférences conformationnelles du peptide ecPis-4s, des expériences de CD ont été réalisées à différentes gammes de concentration dans l'eau et en présence de tampon phosphate 10 mM à pH 6,0 et pH 8,0. Les spectres du peptide ecPis-4s dans une solution tamponnée à pH 8,0 (0,10, 0,20 et 0,35 mM) sont caractérisés par un maximum à ~192 nm ainsi que deux minima près de 208 nm et 222 nm qui sont indicatifs de conformations hélicoïdales ordonnées. Comme la spectroscopie CD a indiqué que l'ecPis-4s présente un certain

arrangement structurel même uniquement dans des environnements aqueux, des essais de spectroscopie RMN multidimensionnelle en solution ont été réalisés pour étudier plus en détail la structure du peptide. La structure à haute résolution a été obtenue en milieu aqueux par RMN en solution et elle présente un segment hélicoïdal défini de K10 à R20 montrant un caractère amphipathique significatif avec les quatre résidus chargés positivement (K10, K13, R17 et R20) le long de la même face de l'hélice. Des spectres de corrélation hétéronucléaire à liaisons multiples (HMBC) ont été obtenus par RMN en solution afin d'analyser plus en détail la qualité de la structure de l'ecPis-4s. Comme l'expérience HMBC donne des corrélations entre les carbones et les protons qui sont séparés par deux, trois, et parfois dans des systèmes conjugués, l'idée est d'utiliser ce spectre pour obtenir des informations sur la constante de couplage J, qui pour les couplages à trois liaisons suit la relation de Karplus, ainsi que d'obtenir les angles dièdres du squelette du peptide ecPis-4s. En outre, pour caractériser davantage le comportement du peptide ecPis-4s en fonction de sa concentration, le coefficient de diffusion a été déterminé en utilisant la RMN DOSY(328). Les expériences révèlent un coefficient de diffusion qui indique la présence exclusivement d'une structure dans la solution. De plus, une analyse de la vitesse de sédimentation (SV) du peptide ecPis-4s par ultracentrifugation analytique (AUC) a été réalisée pour évaluer l'hydrodynamique, l'auto-association, l'agrégation et la stabilité(329) du peptide ecPis-4s dans un tampon, c'est-à-dire en l'absence de membrane mimétique lipidique. La distribution du coefficient de sédimentation sw20 = (0,43 ± 0,03) S et l'estimation de MW = (2877 ± 231) Da sont compatibles avec des espèces monomériques dans la gamme de concentrations de peptide étudiée (25 - 2400 μM). De plus, la concentration critique et l'enthalpie du processus de dépliement ($\Delta H°_{unfold}$) du peptide ecPis-4s en solution tamponnée ont été évaluées en utilisant la technique de calorimétrie de titration isotherme (ITC)(284). Dans les deux milieux étudiés, le dépliement est caractérisé par des événements endothermiques avec des valeurs d'enthalpie de $\Delta H°_{unfold}$ égales à 4,4 kcal.mol-1 dans un tampon phosphate à pH 6,0, et 6,9 kcal.mol-1 à pH 8,0. De plus, le point d'inflexion observé dans les enthalpogrammes présente la concentration autour de 40 M où se produit le processus de désassemblage ou de dépliement. Des expériences de protéolyse(372) ont également été réalisées et les résultats démontrent que l'ecPis-4s est partiellement résistant à l'action de la protéinase K tandis que le peptide est rapidement dégradé en présence de trypsine. De plus, la courbe de temps de mort de la souche S. aureus révèle que le peptide ecPis-4s a atteint une performance bactéricide à 8 h, même en présence de l'enzyme protéinase K.

En conclusion, plusieurs techniques ont été utilisées pour étudier le comportement du peptide antimicrobien ecPis-4s dans une solution aqueuse et tamponnée. Les profils de structure secondaire du peptide ecPis-4s ont montré une dépendance graduelle à la concentration du peptide. La structure tridimensionnelle par RMN en solution est caractérisée par un segment hélicoïdal amphipathique de K10 à R20. Il est intéressant de noter que le N-terminus non structuré formé par quatre acides aminés aromatiques (phénylalanine, histidine) n'est pas dégradé par l'enzyme protéolytique trypsine, ce qui suggère que cette région est naturellement résistante à l'action de cette enzyme. De plus, les données de RMN DOSY et d'AUC ont indiqué un coefficient de diffusion qui est en accord avec d'autres peptides de même longueur décrits dans la littérature, et la présence d'une seule forme monomérique pour l'ecPis-4s en solution aqueuse. Le processus de dépliement des peptides ecPis-4s a été observé par ITC et la concentration d'équilibre replié/déplié déterminée pour ce peptide. De plus, l'ecPis-4s est partiellement stable et actif contre S. aureus même en présence de l'enzyme protéinase K comme le montrent les cinétiques de croissance et les essais de temps de mort. Ainsi, les résultats indiquent que la structure repliée de l'ecPis-4s en milieu aqueux joue un rôle essentiel pour protéger le peptide contre la dégradation complète des peptidases tout en conservant son activité bactérienne. Nos résultats fournissent également de nouvelles caractéristiques structurelles du peptide piscidine, et en plus de cela, les données combinées obtenues dans ce travail nous permettent de conclure que l'ecPis-4s, contrairement à la plupart des peptides AMPs, présente une structure définie ou ordonnée même avant d'atteindre la membrane cible.

7.5.3 Une étude comparative des peptides épimères D- et L-ecPis-2s : l'effet de l'acide aminé D sur les modèles mimétiques bactériens

Le troisième sujet de ce travail concerne les peptides D et L-ecPis-2s. Précédemment, notre groupe de recherche a exploré l'effet de l'épimérisation sur les activités antimicrobiennes et le mode d'interaction membranaire concernant les épimères de la phénylseptine (Phes)(11,13). La phénylseptine D et L sont des peptides naturels, l'épimérisation du deuxième résidu phénylalanine (Phe-2) a conduit à un changement conformationnel de 90° à l'extrémité N-terminale de la structure du peptide D(11), étant la raison des différences dans les activités antimicrobiennes des deux épimères(13). De même, pour la phénylseptine (Phes), ecPis-2s présente une séquence FFF dans la région N-terminale. Cependant, il n'y a pas d'occurrence

d'épimère rapportée concernant ce peptide. Par conséquent, ce présent travail rapporte des investigations sur l'interaction antimicrobienne et membranaire des épimères ecPis-2s (L- et D-ecPis-2s), qui diffèrent l'un de l'autre par le deuxième résidu phénylalanine.

Les essais biologiques ont montré que ecPis-2s et le mutant synthétique D-ecPis-2s présentent une activité antimicrobienne contre les souches bactériennes Gram-positives et Gram-négatives ; cependant, l'épimère D a montré une activité biologique plus élevée contre S. typhimurium et P. aeruginosa par rapport à l'épimère L. De plus, l'étude de la cinétique de mort bactérienne montre que l'épimère D présente également une activité plus élevée à toutes les concentrations testées, réduisant le nombre de bactéries viables. Les propriétés de formation de pores de D- et L-ecPis-2s ont été mesurées en utilisant l'approche de libération du colorant calcéine. Les données montrent que le peptide D provoque une fuite plus importante par rapport à L-ecPis-2s, aux concentrations testées [Figure 34]. Le peptide épimère D atteint également des valeurs de libération proches du maximum tandis que la valeur maximale de libération pour l'épimère L est ≤ 60% [Figure 34B].

Des essais de titrage calorimétrique ont été réalisés et ont montré des courbes de titrage isotherme typiques des réactions exothermiques avec une affinité modérée (6). Les résultats ont indiqué une constante de liaison de Kapp = 1,02 x 104 M−1 pour D-ecPis-2s en présence des LUV négatives et Kapp = 6,77 x 103 M−1, une interaction plus élevée pour les épimères D, comme le montre le tableau SM5. Lorsqu'il est calculé, le ΔGo de l'interaction peptide-membrane est également plus élevé pour D-ecPis-2s par rapport à l'épimère L. Les résultats de CD et de potentiel des peptides ecPis-2s montrent des résultats similaires. Bien que les spectres CD présentent une ellipticité molaire légèrement plus élevée pour D-ecPis-2s, les deux spectres indiquent la même préférence de structure lorsque la concentration de LUV est augmentée. À leur tour, les données de potentiel semblent présenter une interaction plus élevée pour le peptide D-ecPis-2s, montrant une augmentation plus rapide du potentiel lorsque les LUV négatives ont été titrées avec les deux peptides.

Les études DSC révèlent des changements significatifs dans la transition de phase liquide-cristalline de la membrane lors de l'interaction avec l'épimère D- par rapport à l'épimère L [Figure 35] suggérant une conséquence directe de la présence de D-Phe2. Comme observé, le Tm du DMPC:DMPG pur (3:1, mol:mol) est d'environ 23 ◦C [Figure 35] et très similaire pour toutes les compositions du système, les vésicules anioniques et les deux peptides épimères(366). Alors que D-ecPis-2s provoque un décalage d'environ 3 ◦C dans Tm (19,5 ◦C),

à 25 μM, le résultat Tm de DMPC:DMPG (3:1, mol:mol) en présence de L-ecPis-2s, à la même concentration peut être considéré comme inchangé (Tm ~ 22,7 °C). Ce résultat est principalement observé pour D-ecPis-2s indiquant une insertion élevée du peptide dans la membrane fluide DMPC:DMPG. Il est intéressant de noter que ce résultat est également étayé par des études RMN à l'état solide utilisant des phospholipides marqués. L'effet des peptides D- et L-ecPis-2s sur la stabilité de la membrane montre une différence significative dans le paramètre d'ordre du deutérium de chaque liaison C-D dans laquelle D-ecPis-2s provoque une perturbation plus élevée sur la chaîne acyle des lipides POPG-d31 [Figure 36F]. La preuve de l'insertion membranaire plus élevée de D-ecPis-2s indique également la capacité plus élevée de l'épimère à interagir avec la partie hydrophobe de la bicouche, probablement en raison du moment hydrophobe ou de la partie à l'extrémité N-terminale du peptide.

Enfin, en conséquence des interactions avec la bicouche, les épimères D- et L- semblent présenter des structures RMN tridimensionnelles similaires en solution. Cependant, les valeurs d'ellipticité molaire plus élevées, observées à partir des essais CD pour le peptide D-, indiquent une structure secondaire qui n'est pas observée par RMN en solution. D'autre part, les données RMN à l'état solide révèlent une topologie bien définie de l'épimère D dans une bicouche orientée. Ces résultats montrent ensemble que l'interaction intrinsèque du peptide avec la bicouche est différente pour les peptides avec des résidus D et L et peut également aider à expliquer la différence d'activité biologique des épimères.

En conclusion, les caractéristiques d'interaction et biophysiques des peptides épimères piscidine avec les membranes anioniques ont été rapportées dans cette étude. Bien que les deux peptides présentent la même séquence primaire, l'effet de ce remplacement semble améliorer l'activité biologique du peptide D- par rapport à l'épimère L-. Même avec des profils de conformation similaires présentés par la spectroscopie CD, la perturbation causée par l'épimère D est beaucoup plus élevée lorsqu'elle est étudiée dans des membranes négatives, comme indiqué par les essais DSC, RMN à l'état solide des lipides deutérés, ITC et potentiel. Nos résultats démontrent que l'épimère D-ecPis-2s exerce un effet plus élevé sur la stabilité de la membrane, suggérant que d'une manière ou d'une autre, la configuration D conduit la structure du peptide à un caractère amphipathique plus fort par rapport à L-ecPis-2s. En outre, l'hypothèse d'interactions aromatiques spécifiques impliquant les résidus phénylalanine de D-ecPis-2s conduit à jouer un rôle important dans la position des chaînes latérales F1, F2 et F3, qui peuvent

être situées dans la face hydrophobe de l'hélice ainsi que l'ancrage du peptide D dans la bicouche lipidique, augmentant son affinité pour la membrane (11).

7.6 Conclusion générale

Ce manuscrit est dédié aux peptides antimicrobiens naturels récemment découverts de la famille des piscidines avec un intérêt particulier pour leur mécanisme d'action en présence de modèles de membranes négatives. De plus, nous avons étudié l'influence d'un résidu d'acide aminé D dans un motif/séquence de trois résidus de phénylalanine et comment il peut modifier sa structure et/ou conduire à une amélioration de son activité biologique.

En général, les peptides de piscidine sont connus pour leur activité antimicrobienne à large spectre et présentent un intérêt significatif en raison de leurs applications potentielles en médecine et en aquaculture. Les peptides piscidine-4 et piscidine-2 sont principalement trouvés dans les mastocytes des poissons, et ils jouent un rôle essentiel dans la réponse immunitaire innée des poissons en présentant des activités antimicrobiennes, antifongiques et antiparasitaires.

Ainsi, cette thèse fournit de nouvelles caractéristiques structurelles des peptides ecPiscidine, présentant des avancées dans la compréhension des mécanismes d'action des peptides antimicrobiens ecPiscidine-4s, et D- et L-ecPiscidine-2s, ce qui est pertinent dans ce domaine. Comme observé pour le peptide ecPis-4s, la région N-terminale des peptides ecPis-2s présente une caractéristique structurelle importante sur l'interaction membranaire et l'activité biologique. Bien que les deux épimères présentent des préférences conformationnelles similaires comme le montre la spectroscopie CD [Figure 39], une analyse structurelle plus approfondie est nécessaire pour comprendre le rôle de la D-phénylalanine sur l'augmentation de l'activité antimicrobienne. De plus, des analyses structurelles sont également nécessaires en milieu aqueux, car l'épimère D présente un degré d'agrégation plus élevé par rapport à l'épimère L, comme le montrent les expériences AUC (non présentées).

Comme ce travail se concentre principalement sur l'étude des structures, des alignements membranaires et des interactions de ces peptides, nous avons analysé les molécules peptidiques individuellement. Cependant, l'agrégation des peptides peut se produire et

influencer fortement le mécanisme d'action et l'activité, en particulier pour les épimères, comme observé précédemment pour d'autres peptides. Des investigations supplémentaires de ces interactions sont nécessaires pour élucider complètement comment ces peptides exercent leurs activités antimicrobiennes. De plus, l'action synergique potentielle de ces composés est un autre aspect pertinent pour de futures investigations, car d'autres épimères sécrétés par l'animal ont montré une activité plus élevée. Ainsi, ces investigations pourraient représenter un rôle important dans la résistance aux peptidases étant associée à l'activité antimicrobienne accrue trouvée pour le peptide modifié.

Chapter 8: Appendix

Supplementary Figure 1

Characterization of the purified synthetic ecPis-4s peptide by MALDI-ToF. The molecular m/z was obtained by deconvolution of the MS-spectrum and the $[M+H]^+$ signal corresponds to the theoretical value of 2607.5 and 2611.5 m/z.

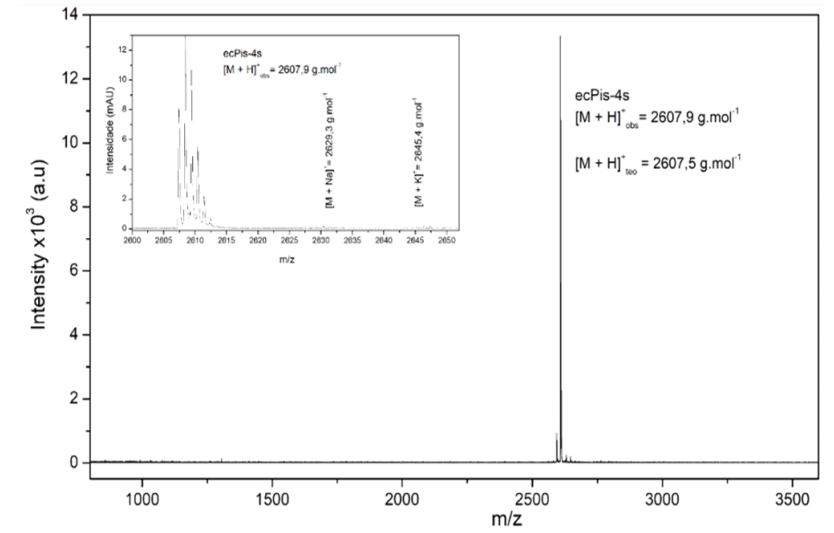

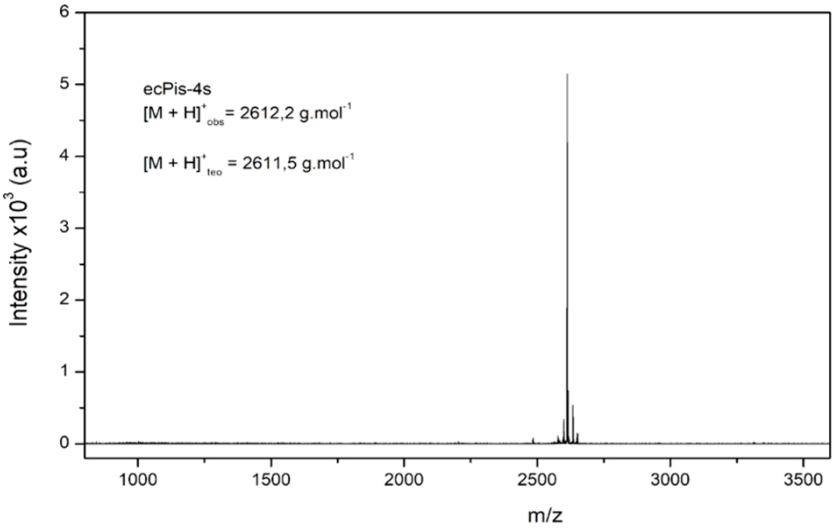

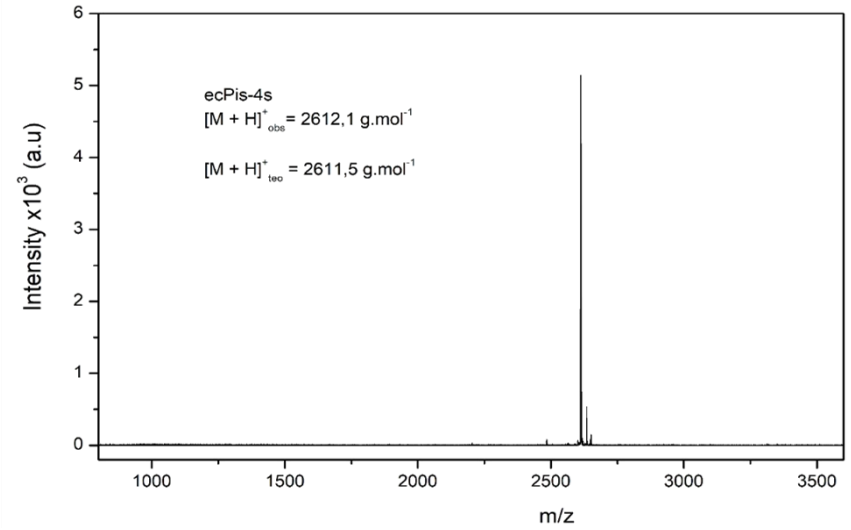

Supplementary Figure 2

CD spectra for ecPis-4s peptide in the presence of SDS micelles.

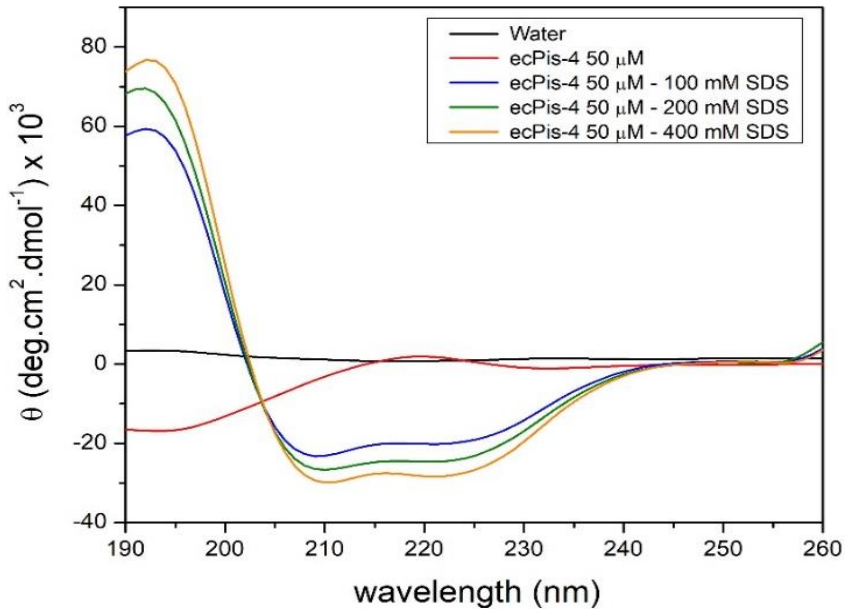

Supplementary Figure 3

Proton cross-peak regions of the TOCSY spectrum. Fingerprint (H_N-H_α correlations) of the TOCSY spectrum of 2 mM of ecPis-4s in presence of 300 mM SDS-d_{25} at 25 ºC, 500 MHz field.

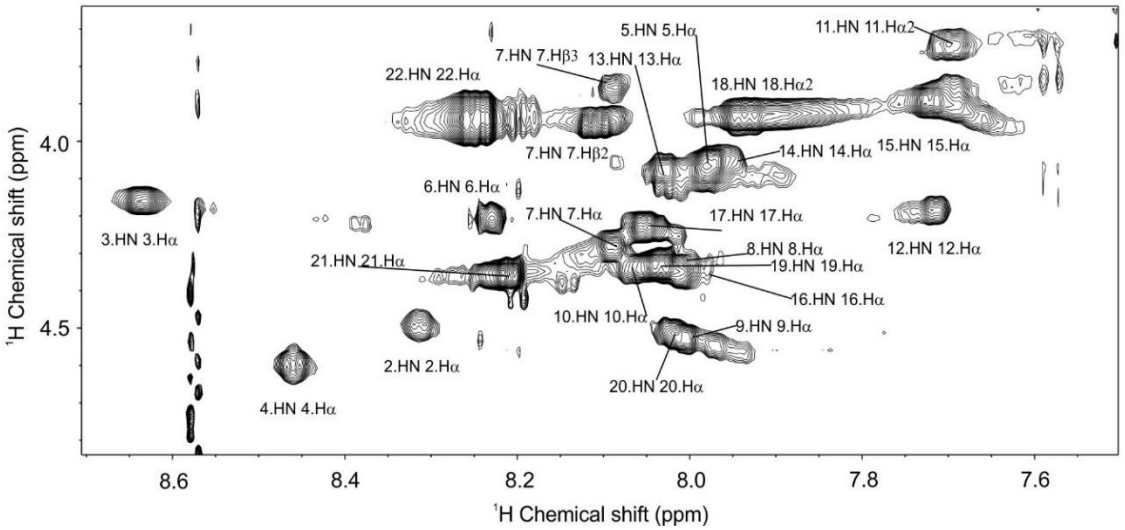

Supplementary Figure 4

NOESY connectivity diagram for ecPis-4s at 2.0 mM in 300 mM of SDS-d_{25} micelles at 25 °C.

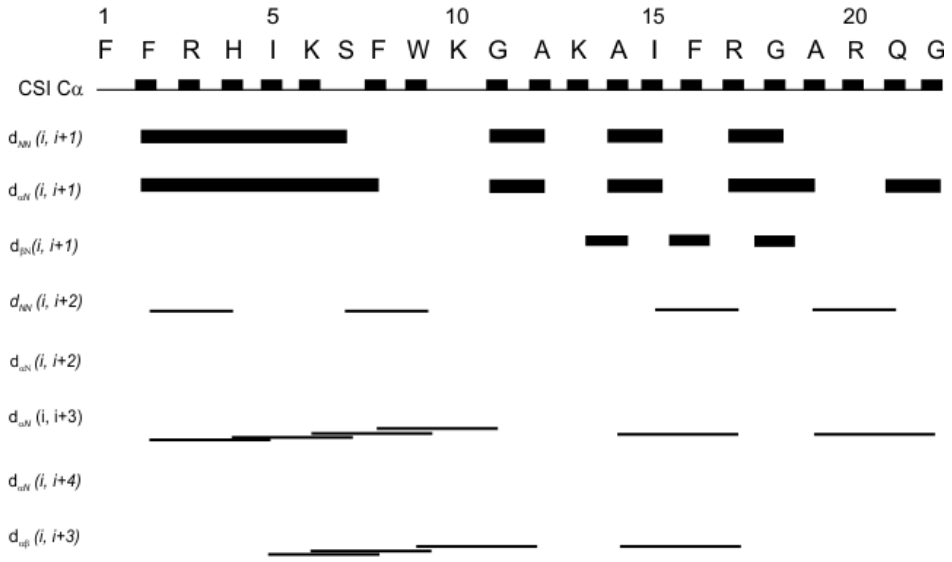

Supplementary Figure 5

Chemical-shift index (CSI) derived from the Hα (blue) and Cα (red) resonances for ecPis-4s peptide.

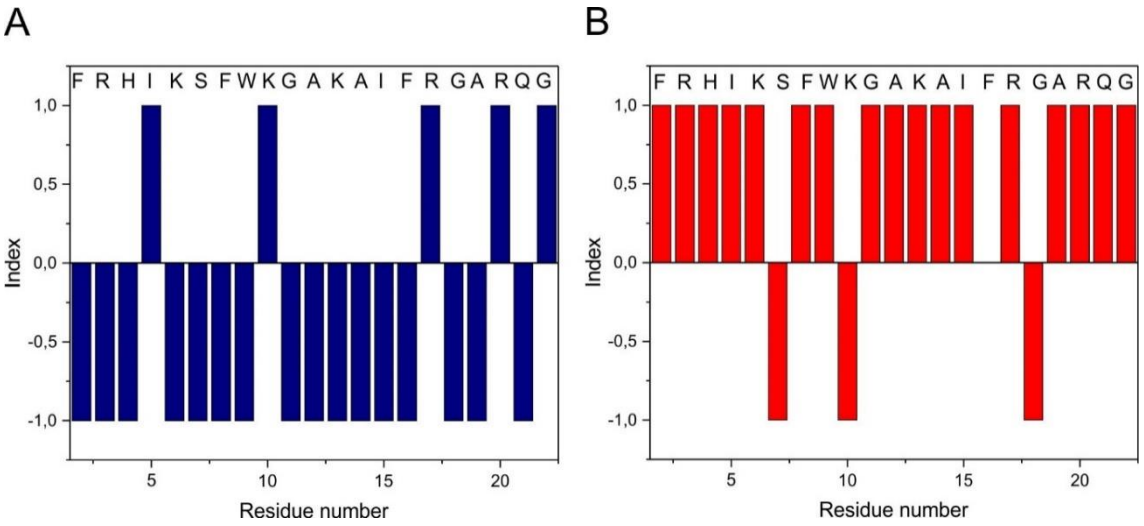

Supplementary Table 1

Summary of the structure quality analysis and statistics for ecPis-4s at 2 mM in presence of 300 mM SDS-d_{25} at 25 ºC, 500 MHz field.

Summary of structural statistics of ecPis-4s at 2.0 mM in presence of 300 mM SDS-d_{25} at 25 ºC, 500 MHz field.

ecPis-4s-NH_2	**water solution**
Total number of distance restraints	264
Number of intraresidual restraints	149
Number of sequential restraints (i, i + 1)	27
Number of medium range restraints (i, i + j), j = 2, 3, 4	58
Number of long range restraints (i, i + j), j > 4	0
Number of dihedral angle restraints	30
RMSD (Å) – all residues[a]	
Backbone	0.8 Å
Heavy atoms	1.4 Å
Ramachandran plot analysis[b]	
Residues in most favored regions	100.0 %
Residues in additional allowed regions	0.0 %
Residues in generously allowed regions	0.0 %
Residues in disallowed regions	0.0 %
Ramachandran plot analysis[c]	
Residues in most favored regions	100.0 %
Residues in additional allowed regions	0.0 %
Residues in generously allowed regions	0.0 %
Residues in disallowed regions	0.0 %

[a] RMSD values from psvs (Protein structure validation software suite – version 1.5)
[b] Ramachandran Plot Summary for all residues from Procheck
[c] Ramachandran Plot Summary for all residues from Richardson Lab's Molprobity

Supplementary Figure 6

Ramachandran plot of the ten lowest-energy solution NMR structures of ecPis-4s in presence of 300 mM SDS-d_{25} at 25 ºC, 500 MHz field.

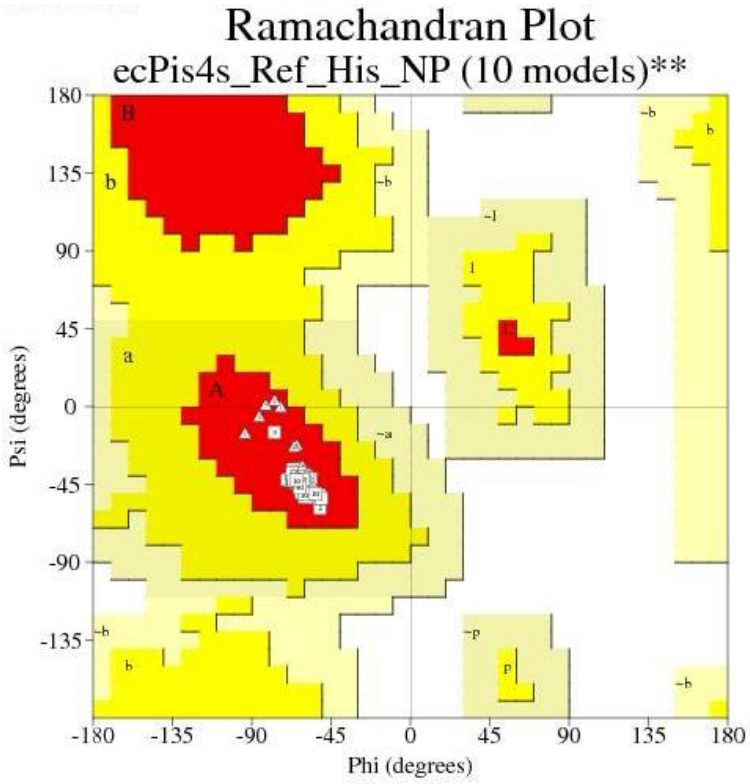

Supplementary Table 2

Measured *Kp* values by intrinsic tryptophan fluorescence emission spectra of ecPiscidin-4s peptide in the presence of POPC:POPG (3:1, mol:mol) at pH 8.0, and pH 6.0, respectively.

ecPis-4s		**Value**
pH 8	*Kp*	$(6.8 \pm 0.8) \times 10^3$ M^{-1}
	Adj. R-Square	0,9873
pH 6	*Kp*	$(2.9 \pm 0.1) \times 10^3$ M^{-1}
	Adj. R-Square	0,9706

Supplementary Figure 7

The wavelengths where maxima of the intrinsic tryptophan fluorescence emission spectra of ecPis-4s occurs are shown as a function of increasing concentrations of POPC:POPG (3:1, mol:mol) LUVs.

.

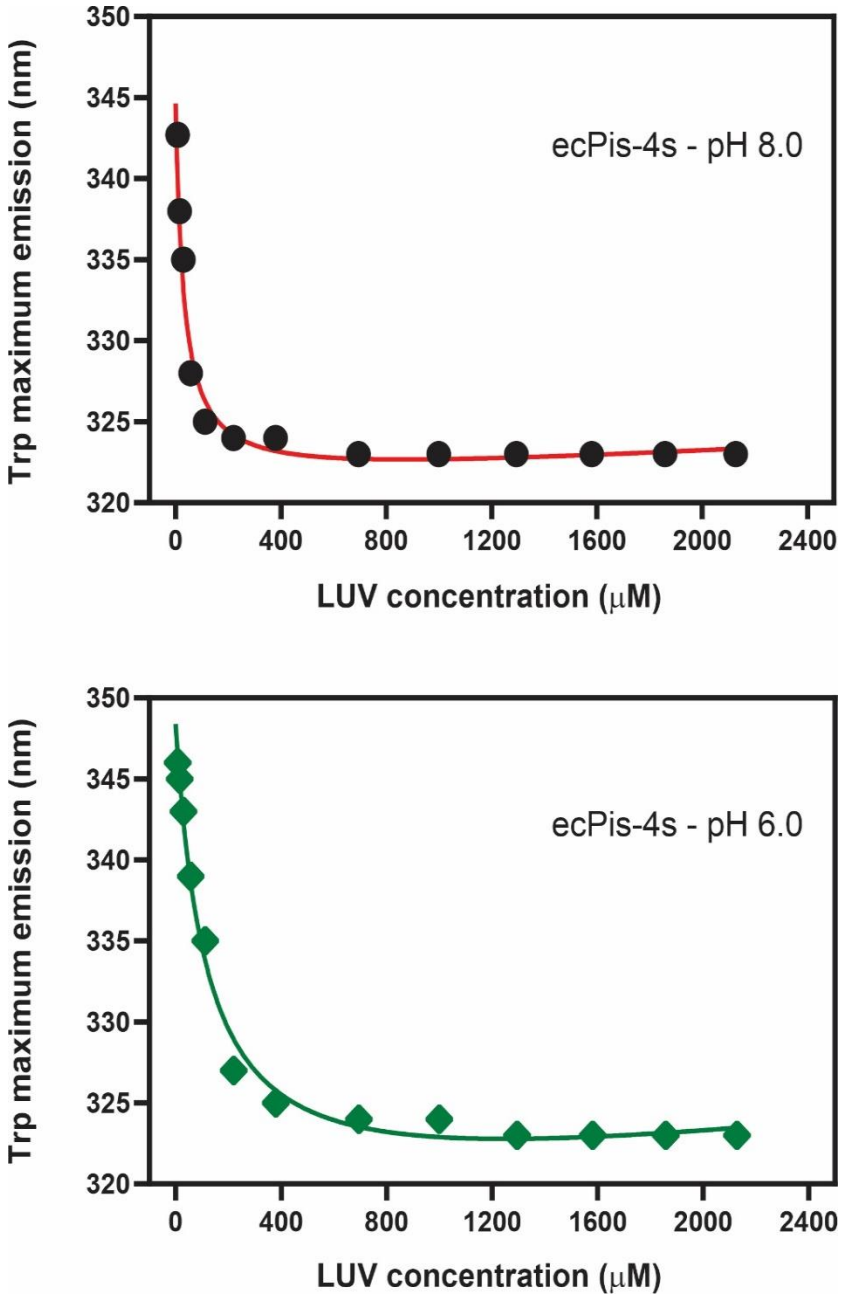

Supplementary Table 3

Thermodynamic parameters obtained after application of mathematical adjustment for ecPis-4s peptide interaction with POPC:POPG (3:1, mol:mol) LUVs.

Peptide	**n**	K_{app} **(L·mol^{-1})**	ΔG^0 **(cal·mol^{-1})**	ΔH^0 **(cal·mol^{-1})**	$-T\Delta S^0$ **(cal·mol^{-1})**	**T**
ecPis-4s	13 ± 1	4400 ± 210	-1556	-1243 ± 61	-313	25 ºC
ecPis-4s	10 ± 1	5250 ± 200	-2134	-1735 ± 78	-399	35 ºC

Supplementary Figure 8

CD for ecPis-4s (50 μM) peptide in the presence of POPC:POPG (3:1, mol:mol) at pH 6.0 and pH 8.0. Molar ellipticity as a function of the of the peptide/POPC:POPG ratio.

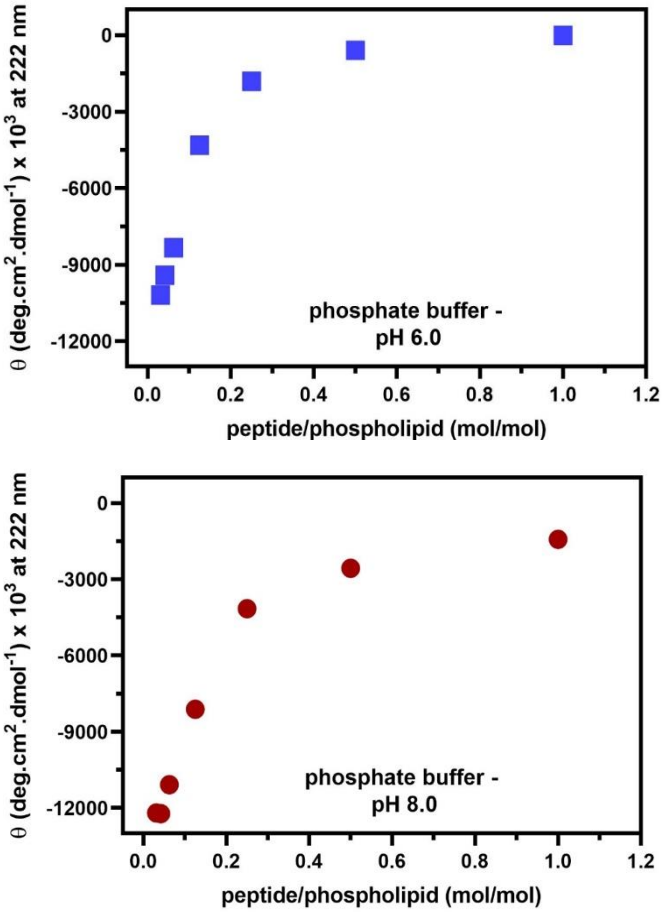

Supplementary Figure 9

Size distribution analysis by dynamic light scattering (DLS). 500 μM POPC:POPG (3:1, mol:mol) vesicles (A) and the effect of ecPis-4s addition of 0.061 (B) and 0.085 as a function of the peptide:lipid molar ratio in 10 mM pH 8.0 Tris-HCl buffer (100 mM NaCl) at 25 ºC.

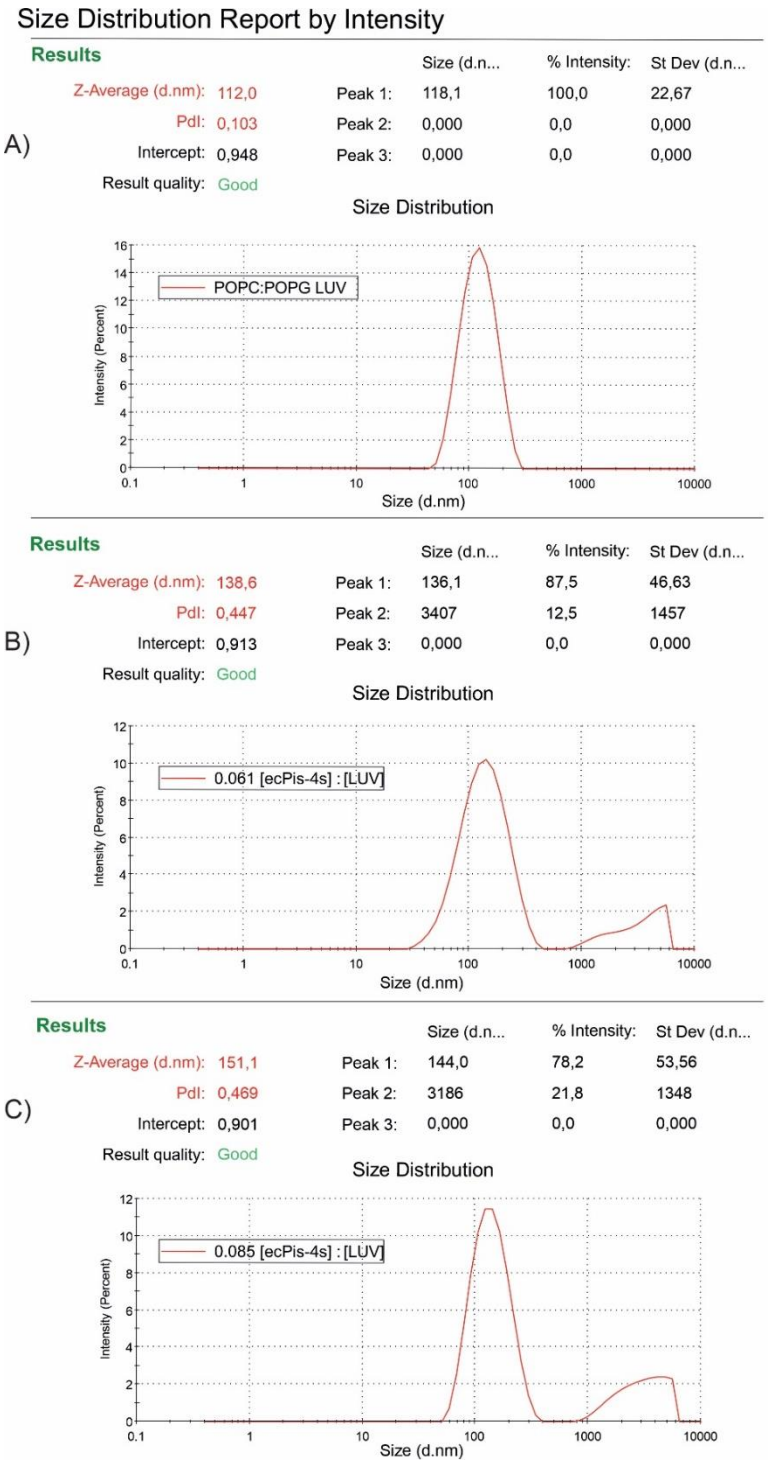

Supplementary Table 4

Summary of structural statistics of ecPis-4s at 4.0 mM in the aqueous medium at 25 °C, 600 MHz.

ecPis-4s peptide	water solution
Total number of distance restraints	496
Number of intraresidual restraints	453
Number of sequential restraints (i, i + 1)	26
Number of medium range restraints (i, i + j), j = 2, 3, 4	12
Number of long range restraints (i, i + j), j > 4	5
Number of dihedral angle restraints	0
RMSD (Å) – from K10 to R20 residues[a]	
Backbone	2.12 Å
Heavy atoms	3.95 Å
RMSD (Å) – all residues[a]	
Backbone	3.32 Å
Heavy atoms	5.18 Å
Ramachandran plot analysis[b]	2.12 Å
Residues in most favored regions	3.95 Å
Residues in additional allowed regions	17.2 %
Residues in generously allowed regions	5.6 %
Residues in disallowed regions	5.0 %
Ramachandran plot analysis[c]	
Residues in most favored regions	78.5 %
Residues in additional allowed regions	16.5 %
Residues in generously allowed regions	5 %
Residues in disallowed regions	0 %

[a] RMSD values from psvs (Protein structure validation software suite – version 1.5)
[b] Ramachandran Plot Summary for all residues from Procheck
[c] Ramachandran Plot Summary for all residues from Richardson Lab's Molprobity

Supplementary Figure 10

H^N-$H^{\alpha/\beta}$ correlations region of the TOCSY spectra of ecPis-4s (4.0 mM) in the aqueous medium at 25 °C, 600 MHz. All the spin systems are highlighted in different colors.

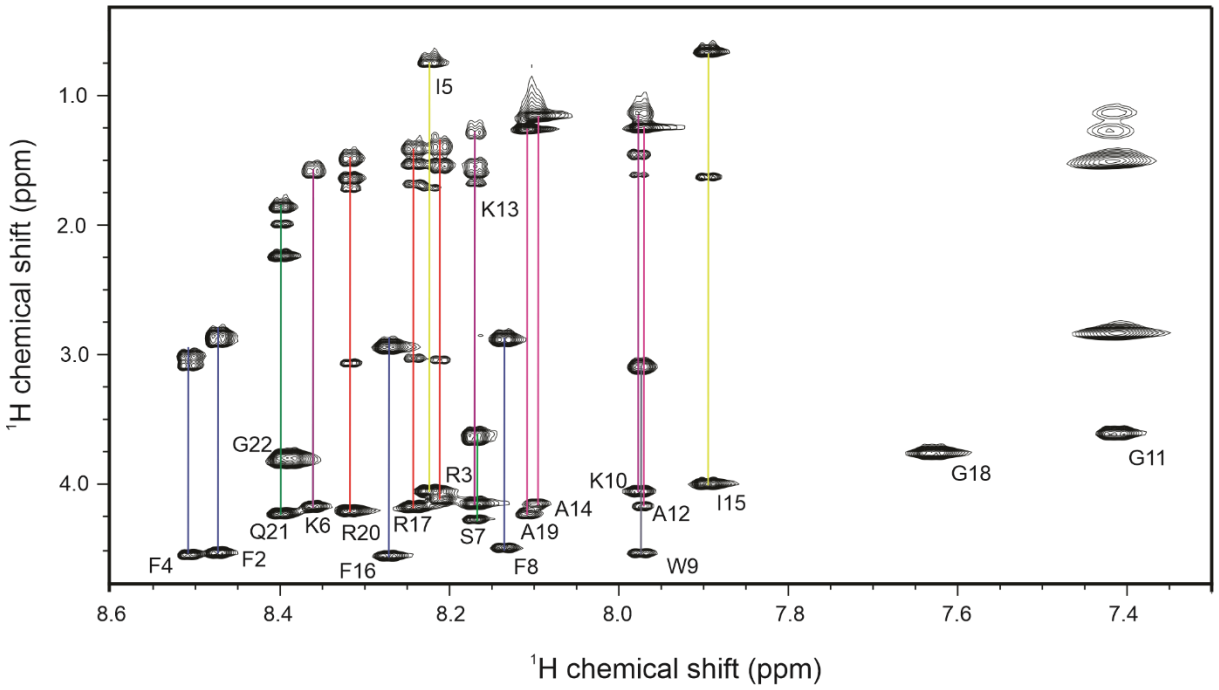

Supplementary Figure 11

NOESY connectivity diagram for ecPis-4s (4.0 mM) in aqueous solution environment, 600 MHz.

Supplementary Figure 12

CD spectra for D-ecPis-2s and L-ecPis-2s peptides in the presence of SDS micelles.

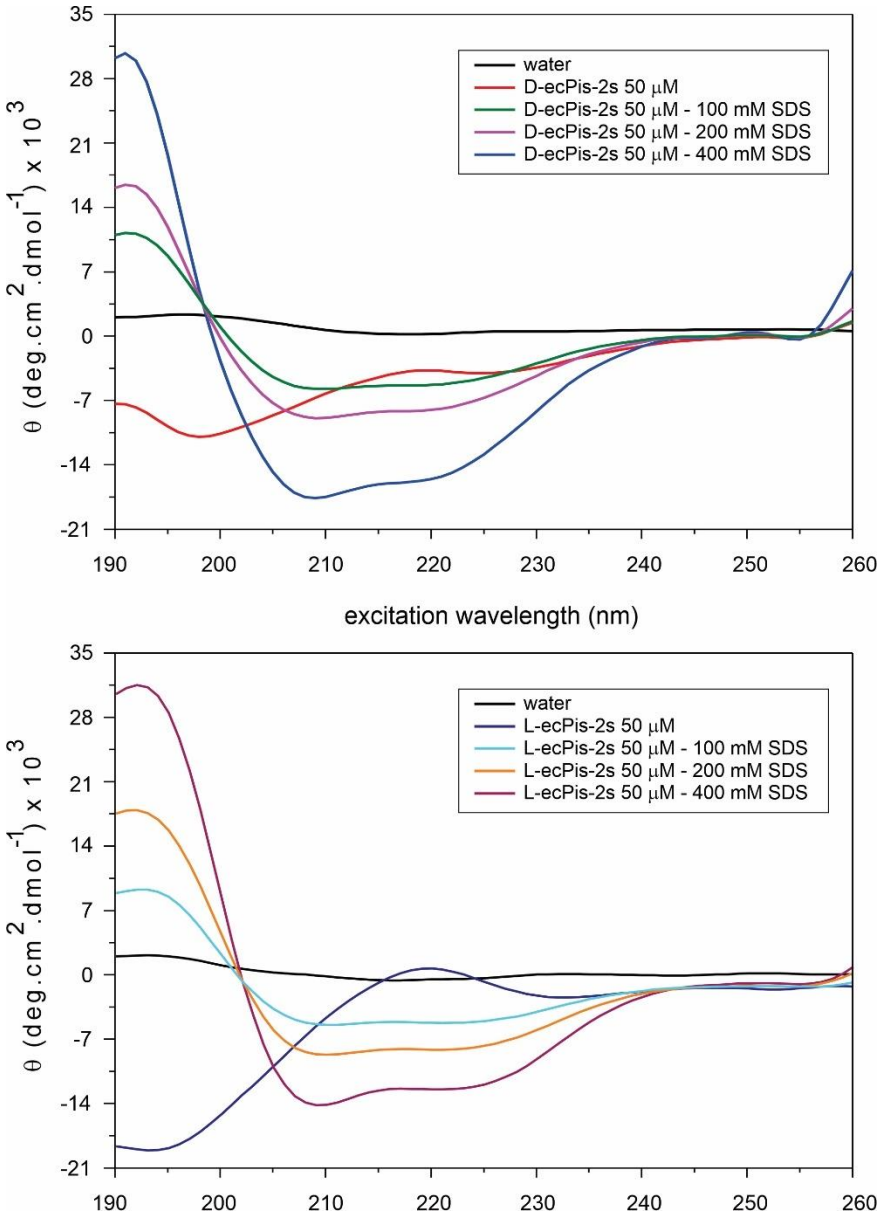

Supplementary Figure 13

NOESY connectivity diagram for D-ecPis-2s and L-ecPis-2s (2.0 mM) in SDS-d_{25} micelles, 500 MHz.

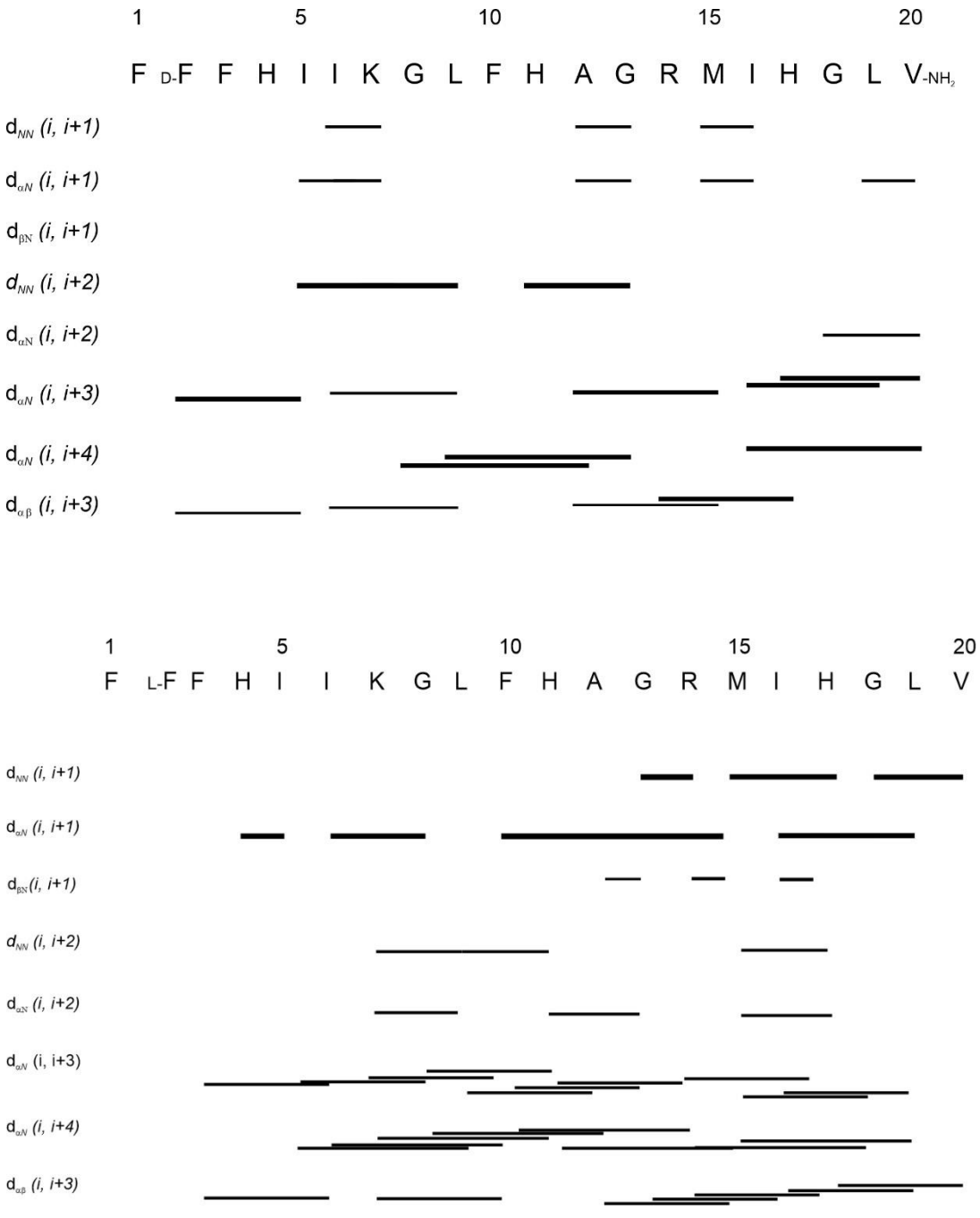

Supplementary Table 5

Summary of structural statistics of D-ecPis-2s at 2.0 mM in in SDS-d_{25} medium at 25 °C, 500 MHz.

D-ecPis-2s peptide	SDS-d_{25}
Total number of distance restraints	243
Number of intraresidual restraints	202
Number of sequential restraints (i, i + 1)	15
Number of medium range restraints (i, i + j), j = 2, 3, 4	26
Number of long-range restraints (i, i + j), j > 4	0
Number of dihedral angle restraints	0
RMSD (Å) – F1 to V20 residues[a]	4.02 Å
Backbone	2.4 Å
Heavy atoms	4.0 Å
Ramachandran plot analysis[b]	
Residues in most favored regions	42.0 %
Residues in additional allowed regions	38.7 %
Residues in generously allowed regions	18.0 %
Residues in disallowed regions	1.3 %
Ramachandran plot analysis[c]	
Residues in most favored regions	51.1 %
Residues in additional allowed regions	31.1 %
Residues in disallowed regions	17.8 %

[a] RMSD values from psvs (Protein structure validation software suite – version 1.5)
[b] Ramachandran Plot Summary for all residues from Procheck
[c] Ramachandran Plot Summary for all residues from Richardson Lab's Molprobity

Supplementary Table 6

Thermodynamic parameters obtained after application of mathematical adjustment for ecPis-2s epimer peptides in presence of POPC:POPG (3:1, mol:mol) LUVs.

Peptide	n	K_{app} (L·mol^{-1})	ΔG^0 (cal·mol^{-1})	ΔH^0 (cal·mol^{-1})	$-T\Delta S^0$ (cal·mol^{-1})	T
D-ecPis-2s	18 ± 1	10200 ± 560	-5628	-392 ± 15	-5236	35 ºC
L-ecPis-2s	11 ± 1	6770 ± 340	-5148	-528 ± 45	-4620	35 ºC

Supplementary Figure 14

Ramachandran plot of the lowest-energy solution NMR structures of D-ecPis-2s in 300 mM SDS-d_{25} micellar solution.

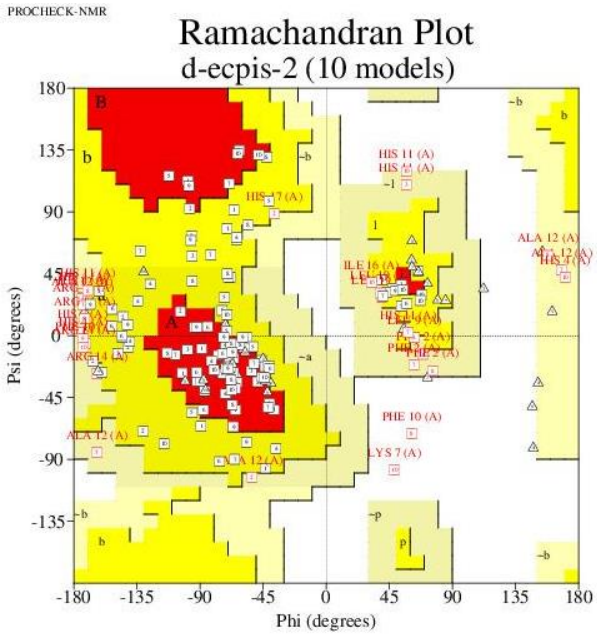

Bibliography

1. Ageitos JM, Sánchez-Pérez A, Calo-Mata P, Villa TG. Antimicrobial peptides (AMPs): Ancient compounds that represent novel weapons in the fight against bacteria. Biochem Pharmacol. 2017 Jun;133:117–38.
2. Peterson E, Kaur P. Antibiotic Resistance Mechanisms in Bacteria: Relationships Between Resistance Determinants of Antibiotic Producers, Environmental Bacteria, and Clinical Pathogens. Front Microbiol. 2018 Nov 30;9.
3. Savini F, Loffredo MR, Troiano C, Bobone S, Malanovic N, Eichmann TO, et al. Binding of an antimicrobial peptide to bacterial cells: Interaction with different species, strains and cellular components. Biochimica et Biophysica Acta (BBA) - Biomembranes. 2020 Aug;1862(8):183291.
4. Lee JK, Jeon JK, Kim SK, Byun HG. Characterization of Bioactive Peptides Obtained from Marine Invertebrates. In 2012. p. 47–72.
5. Paterson DJ, Tassieri M, Reboud J, Wilson R, Cooper JM. Lipid topology and electrostatic interactions underpin lytic activity of linear cationic antimicrobial peptides in membranes. Proceedings of the National Academy of Sciences. 2017 Oct 3;114(40).
6. Verly RM, Resende JM, Junior EFC, de Magalhães MTQ, Guimarães CFCR, Munhoz VHO, et al. Structure and membrane interactions of the homodimeric antibiotic peptide homotarsinin. Sci Rep. 2017 Jan 19;7(1):40854.
7. Mahlapuu M, Håkansson J, Ringstad L, Björn C. Antimicrobial Peptides: An Emerging Category of Therapeutic Agents. Front Cell Infect Microbiol. 2016 Dec 27;6.
8. Babii O, Afonin S, Schober T, Komarov I V., Ulrich AS. Flexibility vs rigidity of amphipathic peptide conjugates when interacting with lipid bilayers. Biochimica et Biophysica Acta (BBA) - Biomembranes. 2017 Dec;1859(12):2505–15.
9. Shai Y. Mechanism of the binding, insertion and destabilization of phospholipid bilayer membranes by α-helical antimicrobial and cell non-selective membrane-lytic peptides. Biochimica et Biophysica Acta (BBA) - Biomembranes. 1999 Dec;1462(1–2):55–70.
10. Matsuzaki K. Molecular Action Mechanisms and Membrane Recognition of Membrane-Acting Antimicrobial Peptides. YAKUGAKU ZASSHI. 1997;117(5):253–64.
11. Munhoz VHO, Ferreira CS, Nunes LO, Santos TL, Aisenbrey C, Adão R, et al. Epimers l- and d-Phenylseptin: How the relative stereochemistry affects the peptide-membrane

interactions. Biochimica et Biophysica Acta (BBA) - Biomembranes. 2021 Nov;1863(11):183708.

12. Hong SY, Oh JE, Lee KH. Effect of D-amino acid substitution on the stability, the secondary structure, and the activity of membrane-active peptide. Biochem Pharmacol. 1999 Dec 1;58(11):1775–80.
13. de Magalhães MTQ, Barbosa EA, Prates M V., Verly RM, Munhoz VHO, de Araújo IE, et al. Conformational and Functional Effects Induced by D- and L-Amino Acid Epimerization on a Single Gene Encoded Peptide from the Skin Secretion of Hypsiboas punctatus. PLoS One. 2013 Apr 2;8(4):e59255.
14. Mignogna G, Simmaco M, Kreil G, Barra D. Antibacterial and haemolytic peptides containing D-alloisoleucine from the skin of Bombina variegata. EMBO J. 1993 Dec;12(12):4829–32.
15. Montecucchi PC, Henschen A. Amino acid composition and sequence analysis of sauvagine, a new active peptide from the skin of Phyllomedusa sauvagei. Int J Pept Protein Res. 1981 Aug;18(2):113–20.
16. Erspamer V, Melchiorri P, Falconieri-Erspamer G, Negri L, Corsi R, Severini C, et al. Deltorphins: a family of naturally occurring peptides with high affinity and selectivity for delta opioid binding sites. Proc Natl Acad Sci U S A. 1989 Jul;86(13):5188–92.
17. Peighambardoust SH, Karami Z, Pateiro M, Lorenzo JM. A Review on Health-Promoting, Biological, and Functional Aspects of Bioactive Peptides in Food Applications. Biomolecules. 2021 Apr 23;11(5):631.
18. Akbarian M, Khani A, Eghbalpour S, Uversky VN. Bioactive Peptides: Synthesis, Sources, Applications, and Proposed Mechanisms of Action. Int J Mol Sci. 2022 Jan 27;23(3):1445.
19. Zhu M, Liu P, Niu ZW. A perspective on general direction and challenges facing antimicrobial peptides. Chinese Chemical Letters. 2017 Apr;28(4):703–8.
20. Mellander O. The physiological importance of the casein phosphopeptide calcium salts. II. Peroral calcium dosage of infants. Acta Soc Med Ups. 1950 Dec;55(5–6):247–55.
21. Sánchez A, Vázquez A. Bioactive peptides: A review. Food Quality and Safety [Internet]. 2017 Mar 1;1(1):29–46. Available from: https://doi.org/10.1093/fqsafe/fyx006
22. Chung PY, Khanum R. Antimicrobial peptides as potential anti-biofilm agents against multidrug-resistant bacteria. J Microbiol Immunol Infect. 2017 Aug;50(4):405–10.

23. Sun X, Li Y, Liu T, Li Z, Zhang X, Chen X. Peptide-based imaging agents for cancer detection. Adv Drug Deliv Rev. 2017 Feb;110–111:38–51.
24. Daliri E, Oh D, Lee B. Bioactive Peptides. Foods. 2017 Apr 26;6(5):32.
25. Mansour SC, Pena OM, Hancock REW. Host defense peptides: front-line immunomodulators. Trends Immunol. 2014 Sep;35(9):443–50.
26. Memarpoor-Yazdi M, Asoodeh A, Chamani J. A novel antioxidant and antimicrobial peptide from hen egg white lysozyme hydrolysates. J Funct Foods [Internet]. 2012;4(1):278–86. Available from: https://www.sciencedirect.com/science/article/pii/S1756464611001101
27. Perez Espitia PJ, de Fátima Ferreira Soares N, dos Reis Coimbra JS, de Andrade NJ, Souza Cruz R, Alves Medeiros EA. Bioactive Peptides: Synthesis, Properties, and Applications in the Packaging and Preservation of Food. Compr Rev Food Sci Food Saf. 2012 Mar 29;11(2):187–204.
28. Albenzio M, Santillo A, Caroprese M, Della Malva A, Marino R. Bioactive Peptides in Animal Food Products. Foods. 2017 May 9;6(5):35.
29. Silveira GP, Nome F, Gesser JC, Sá MM, Terenzi H. Estratégias utilizadas no combate a resistência bacteriana. Quim Nova. 2006 Jul;29(4):844–55.
30. WHO. https://www.who.int/news-room/fact-sheets/detail/antibiotic-resistance . 2023. Antibiotic Resistance.
31. Loureiro RJ, Roque F, Teixeira Rodrigues A, Herdeiro MT, Ramalheira E. Use of antibiotics and bacterial resistances: brief notes on its evolution. Revista Portuguesa de Saúde Pública. 2016 Jan;34(1):77–84.
32. Nelson RE, Hatfield KM, Wolford H, Samore MH, Scott RD, Reddy SC, et al. National Estimates of Healthcare Costs Associated With Multidrug-Resistant Bacterial Infections Among Hospitalized Patients in the United States. Clinical Infectious Diseases. 2021 Jan 29;72(Supplement_1):S17–26.
33. Bechinger B. The SMART model: Soft Membranes Adapt and Respond, also Transiently, in the presence of antimicrobial peptides. Journal of Peptide Science. 2015 May 18;21(5):346–55.
34. Semreen MH, El-Gamal MI, Abdin S, Alkhazraji H, Kamal L, Hammad S, et al. Recent updates of marine antimicrobial peptides. Saudi Pharmaceutical Journal. 2018 Mar;26(3):396–409.

35. Nepal G, Bhatta S. Self-medication with Antibiotics in WHO Southeast Asian Region: A Systematic Review. Cureus. 2018 Apr 5;
36. Morgan DJ, Okeke IN, Laxminarayan R, Perencevich EN, Weisenberg S. Non-prescription antimicrobial use worldwide: a systematic review. Lancet Infect Dis. 2011 Sep;11(9):692–701.
37. Col NF, O'Connor RW. Estimating Worldwide Current Antibiotic Usage: Report of Task Force 1. Clinical Infectious Diseases. 1987 May 1;9:S232–43.
38. WHO. The Evolving Threat of Antimicrobial Resistance: Options for Action. 2012.
39. Pan American Health Organization. https://www.paho.org/en/topics/antimicrobial-resistance#:~:text=Antimicrobial%20resistance%20happens%20when%20microorganisms,%2C%20antimalarials%2C%20and%20anthelmintics. 2021. Antimicrobial Resistance.
40. Tang KWK, Millar BC, Moore JE. Antimicrobial Resistance (AMR). Br J Biomed Sci. 2023 Jun 28;80.
41. Mehadi M, Hassan Chowdhury MM, Kubra K, Islam M, Rahman M, Mehedy M. Indiscriminate Uses of Antibiotics as a Threat to Public Health Demand Implementation of Effective Drug Practices and Enhancement of Public Awareness in Bangladesh. European Journal of Scientific Research. 2015 Jul 1;133:187–95.
42. CDC. Antibiotic resistance threats in the United States, 2019. Atlanta, Georgia. Department of Health and Human Services; 2019 Nov.
43. Salam MdA, Al-Amin MdY, Salam MT, Pawar JS, Akhter N, Rabaan AA, et al. Antimicrobial Resistance: A Growing Serious Threat for Global Public Health. Healthcare. 2023 Jul 5;11(13):1946.
44. Wall S. Prevention of antibiotic resistance – an epidemiological scoping review to identify research categories and knowledge gaps. Glob Health Action. 2019 Dec 13;12(sup1):1756191.
45. Murray CJL, Ikuta KS, Sharara F, Swetschinski L, Robles Aguilar G, Gray A, et al. Global burden of bacterial antimicrobial resistance in 2019: a systematic analysis. The Lancet. 2022 Feb;399(10325):629–55.
46. Lee MY, Park SC, Jung M, Shin MK, Kang HL, Baik SC, et al. Cell-selectivity of tryptophan and tyrosine in amphiphilic α-helical antimicrobial peptides against drug-resistant bacteria. Biochem Biophys Res Commun. 2018 Oct;505(2):478–84.

47. Badshah SL, Ullah A. New developments in non-quinolone-based antibiotics for the inhibiton of bacterial gyrase and topoisomerase IV. Eur J Med Chem. 2018 May;152:393–400.
48. Hemeg H. Nanomaterials for alternative antibacterial therapy. Int J Nanomedicine. 2017 Nov;Volume 12:8211–25.
49. Yousefi M, Dadashpour M, Hejazi M, Hasanzadeh M, Behnam B, de la Guardia M, et al. Anti-bacterial activity of graphene oxide as a new weapon nanomaterial to combat multidrug-resistance bacteria. Materials Science and Engineering: C. 2017 May;74:568–81.
50. Parmanik A, Das S, Kar B, Bose A, Dwivedi GR, Pandey MM. Current Treatment Strategies Against Multidrug-Resistant Bacteria: A Review. Curr Microbiol. 2022 Dec 3;79(12):388.
51. Gaglio R, Couto N, Marques C, de Fatima Silva Lopes M, Moschetti G, Pomba C, et al. Evaluation of antimicrobial resistance and virulence of enterococci from equipment surfaces, raw materials, and traditional cheeses. Int J Food Microbiol. 2016 Nov;236:107–14.
52. Davin-Regli A, Bolla JM, James C, Lavigne JP, Chevalier J, Garnotel E, et al. Membrane Permeability and Regulation of Drug Influx and Efflux in Enterobacterial Pathogens. Curr Drug Targets. 2008 Sep 1;9(9):750–9.
53. Karukappadath RM, Sirbu D, Zaky A. Drug-resistant bacteria in the critically ill: patterns and mechanisms of resistance and potential remedies. Frontiers in Antibiotics. 2023 Jun 30;2.
54. Rice LB, Carias LL, Rudin S, Hutton R, Marshall S, Hassan M, et al. Role of Class A Penicillin-Binding Proteins in the Expression of β-Lactam Resistance in *Enterococcus faecium*. J Bacteriol. 2009 Jun;191(11):3649–56.
55. Pang Z, Raudonis R, Glick BR, Lin TJ, Cheng Z. Antibiotic resistance in Pseudomonas aeruginosa: mechanisms and alternative therapeutic strategies. Biotechnol Adv. 2019 Jan;37(1):177–92.
56. Dharmaratne MPJ, Manoraj A, Thevanesam V, Ekanayake A, Kumar NS, Liyanapathirana V, et al. Terminalia bellirica fruit extracts: in-vitro antibacterial activity against selected multidrug-resistant bacteria, radical scavenging activity and cytotoxicity study on BHK-21 cells. BMC Complement Altern Med. 2018 Dec 7;18(1):325.

57. Rajput A, Bhamare KT, Mukhopadhyay A, Rastogi A, Sakshi, Kumar M. Efficacy of Anti-Biofilm Agents in Targeting ESKAPE Pathogens with a Focus on Antibiotic Drug Resistance. In 2020. p. 177–99.
58. Yu W, Zhang J, Tong J, Zhang L, Zhan Y, Huang Y, et al. In Vitro Antimicrobial Activity of Fosfomycin, Vancomycin and Daptomycin Alone, and in Combination, Against Linezolid-Resistant Enterococcus faecalis. Infect Dis Ther. 2020 Dec 22;9(4):927–34.
59. Gabrielyan L, Hakobyan L, Hovhannisyan A, Trchounian A. Effects of iron oxide (Fe_3O_4) nanoparticles on *Escherichia coli* antibiotic-resistant strains. J Appl Microbiol. 2019 Apr 8;126(4):1108–16.
60. Zykov IN, Frimodt-Møller N, Småbrekke L, Sundsfjord A, Samuelsen Ø. Efficacy of mecillinam against clinical multidrug-resistant Escherichia coli in a murine urinary tract infection model. Int J Antimicrob Agents. 2020 Feb;55(2):105851.
61. Kim SY, Zhang F, Gong W, Chen K, Xia K, Liu F, et al. Copper regulates the interactions of antimicrobial piscidin peptides from fish mast cells with formyl peptide receptors and heparin. J Biol Chem. 2018 Oct 5;293(40):15381–96.
62. Huan Y, Kong Q, Mou H, Yi H. Antimicrobial Peptides: Classification, Design, Application and Research Progress in Multiple Fields. Front Microbiol. 2020 Oct 16;11.
63. Kumar P, Kizhakkedathu J, Straus S. Antimicrobial Peptides: Diversity, Mechanism of Action and Strategies to Improve the Activity and Biocompatibility In Vivo. Biomolecules. 2018 Jan 19;8(1):4.
64. Conlon JM, Mechkarska M, Lukic ML, Flatt PR. Potential therapeutic applications of multifunctional host-defense peptides from frog skin as anti-cancer, anti-viral, immunomodulatory, and anti-diabetic agents. Peptides (NY). 2014 Jul;57:67–77.
65. Yeaman MR, Yount NY. Mechanisms of Antimicrobial Peptide Action and Resistance. Pharmacol Rev. 2003 Mar 1;55(1):27–55.
66. Biswaro LS, da Costa Sousa MG, Rezende TMB, Dias SC, Franco OL. Antimicrobial Peptides and Nanotechnology, Recent Advances and Challenges. Front Microbiol. 2018 May 8;9.
67. Gomes B, Augusto MT, Felício MR, Hollmann A, Franco OL, Gonçalves S, et al. Designing improved active peptides for therapeutic approaches against infectious diseases. Biotechnol Adv. 2018 Mar;36(2):415–29.

68. Torres MDT, Sothiselvam S, Lu TK, de la Fuente-Nunez C. Peptide Design Principles for Antimicrobial Applications. J Mol Biol. 2019 Aug;431(18):3547–67.
69. Patocka J, Nepovimova E, Klimova B, Wu Q, Kuca K. Antimicrobial Peptides: Amphibian Host Defense Peptides. Curr Med Chem. 2019;26(32):5924–46.
70. Lai Y, Villaruz AE, Li M, Cha DJ, Sturdevant DE, Otto M. The human anionic antimicrobial peptide dermcidin induces proteolytic defence mechanisms in staphylococci. Mol Microbiol. 2007 Jan 29;63(2):497–506.
71. Pane K, Durante L, Crescenzi O, Cafaro V, Pizzo E, Varcamonti M, et al. Antimicrobial potency of cationic antimicrobial peptides can be predicted from their amino acid composition: Application to the detection of "cryptic" antimicrobial peptides. J Theor Biol. 2017 Apr;419:254–65.
72. Hale JD, Hancock RE. Alternative mechanisms of action of cationic antimicrobial peptides on bacteria. Expert Rev Anti Infect Ther. 2007 Dec 10;5(6):951–9.
73. Ramazi S, Mohammadi N, Allahverdi A, Khalili E, Abdolmaleki P. A review on antimicrobial peptides databases and the computational tools. Database. 2022 Mar 19;2022.
74. Wang G, Li X, Wang Z. APD3: the antimicrobial peptide database as a tool for research and education. Nucleic Acids Res. 2016 Jan 4;44(D1):D1087–93.
75. Prates MV; JCB. Peptídeos Antimicrobianos - Biotecnologia. In: Biotecnologia Ciência e Desenvolvimento. 2000. p. 30–6.
76. Wu Q, Patočka J, Kuča K. Insect Antimicrobial Peptides, a Mini Review. Toxins (Basel). 2018 Nov 8;10(11).
77. Wu R, Patocka J, Nepovimova E, Oleksak P, Valis M, Wu W, et al. Marine Invertebrate Peptides: Antimicrobial Peptides. Front Microbiol. 2021 Dec 16;12.
78. Rima M, Rima M, Fajloun Z, Sabatier JM, Bechinger B, Naas T. Antimicrobial Peptides: A Potent Alternative to Antibiotics. Antibiotics. 2021 Sep 10;10(9):1095.
79. Zhang QY, Yan ZB, Meng YM, Hong XY, Shao G, Ma JJ, et al. Antimicrobial peptides: mechanism of action, activity and clinical potential. Mil Med Res. 2021 Sep 9;8(1):48.
80. Pasupuleti M, Schmidtchen A, Malmsten M. Antimicrobial peptides: key components of the innate immune system. Crit Rev Biotechnol. 2012 Jun 11;32(2):143–71.
81. Groisman EA. How bacteria resist killing by host-defense peptides. Trends Microbiol. 1994 Nov;2(11):444–9.

82. Yazici A, Ortucu S, Taskin M, Marinelli L. Natural-based Antibiofilm and Antimicrobial Peptides from Microorganisms. Curr Top Med Chem. 2018;18(24):2102–7.
83. Moyer TB, Heil LR, Kirkpatrick CL, Goldfarb D, Lefever WA, Parsley NC, et al. PepSAVI-MS Reveals a Proline-rich Antimicrobial Peptide in Amaranthus tricolor. J Nat Prod. 2019 Oct 25;82(10):2744–53.
84. Lee JH, Seo M, Lee HJ, Baek M, Kim IW, Kim SY, et al. Anti-Inflammatory Activity of Antimicrobial Peptide Allomyrinasin Derived from the Dynastid Beetle, Allomyrina dichotoma. J Microbiol Biotechnol. 2019 May 28;29(5):687–95.
85. Ryan JT, Ross RP, Bolton D, Fitzgerald GF, Stanton C. Bioactive Peptides from Muscle Sources: Meat and Fish. Nutrients. 2011 Aug 31;3(9):765–91.
86. Li B, Lyu P, Xie S, Qin H, Pu W, Xu H, et al. LFB: A Novel Antimicrobial Brevinin-Like Peptide from the Skin Secretion of the Fujian Large Headed Frog, Limnonectes fujianensi. Biomolecules. 2019 Jun 21;9(6).
87. van Hoek ML, Prickett MD, Settlage RE, Kang L, Michalak P, Vliet KA, et al. The Komodo dragon (Varanus komodoensis) genome and identification of innate immunity genes and clusters. BMC Genomics. 2019 Aug 30;20(1):684.
88. Wang X, Sun Y, Wang F, You L, Cao Y, Tang R, et al. A novel endogenous antimicrobial peptide CAMP $_{211\text{-}225}$ derived from casein in human milk. Food Funct. 2020;11(3):2291–8.
89. Mattick ATR, Hirsch A. Further observations on an inhibitory substance (nisin) from lactic streptococci. Lancet. 1947 Jul 5;2(6462):5–8.
90. Essig A, Hofmann D, Münch D, Gayathri S, Künzler M, Kallio PT, et al. Copsin, a novel peptide-based fungal antibiotic interfering with the peptidoglycan synthesis. J Biol Chem. 2014 Dec 12;289(50):34953–64.
91. Srivastava S, Dashora K, Ameta KL, Singh NP, El-Enshasy HA, Pagano MC, et al. Cysteine-rich antimicrobial peptides from plants: The future of antimicrobial therapy. Phytother Res. 2021 Jan;35(1):256–77.
92. Höng K, Austerlitz T, Bohlmann T, Bohlmann H. The thionin family of antimicrobial peptides. PLoS One. 2021;16(7):e0254549.
93. Li J, Hu S, Jian W, Xie C, Yang X. Plant antimicrobial peptides: structures, functions, and applications. Bot Stud. 2021 Apr 29;62(1):5.
94. Taveira GB, Mello ÉO, Souza SB, Monteiro RM, Ramos AC, Carvalho AO, et al. Programmed cell death in yeast by thionin-like peptide from Capsicum annuum fruits

involving activation of caspases and extracellular H+ flux. Biosci Rep. 2018 Apr 27;38(2).

95. Tang SS, Prodhan ZH, Biswas SK, Le CF, Sekaran SD. Antimicrobial peptides from different plant sources: Isolation, characterisation, and purification. Phytochemistry. 2018 Oct;154:94–105.
96. Gourbal B, Pinaud S, Beckers GJM, Van Der Meer JWM, Conrath U, Netea MG. Innate immune memory: An evolutionary perspective. Immunol Rev. 2018 May;283(1):21–40.
97. Loch G, Zinke I, Mori T, Carrera P, Schroer J, Takeyama H, et al. Antimicrobial peptides extend lifespan in Drosophila. PLoS One. 2017;12(5):e0176689.
98. Yang D, Biragyn A, Kwak LW, Oppenheim JJ. Mammalian defensins in immunity: more than just microbicidal. Trends Immunol. 2002 Jun;23(6):291–6.
99. Avila EE. Functions of Antimicrobial Peptides in Vertebrates. Curr Protein Pept Sci. 2017;18(11):1098–119.
100. Muncaster S, Kraakman K, Gibbons O, Mensink K, Forlenza M, Jacobson G, et al. Antimicrobial peptides within the Yellowtail Kingfish (Seriola lalandi). Dev Comp Immunol. 2018 Mar;80:67–80.
101. Mihailescu M, Sorci M, Seckute J, Silin VI, Hammer J, Perrin BS, et al. Structure and Function in Antimicrobial Piscidins: Histidine Position, Directionality of Membrane Insertion, and pH-Dependent Permeabilization. J Am Chem Soc. 2019 Jun 26;141(25):9837–53.
102. Pan CY, Chen JC, Chen TL, Wu JL, Hui CF, Chen JY. Piscidin is Highly Active against Carbapenem-Resistant Acinetobacter baumannii and NDM-1-Producing Klebsiella pneumonia in a Systemic Septicaemia Infection Mouse Model. Mar Drugs. 2015 Apr 14;13(4):2287–305.
103. van Harten RM, van Woudenbergh E, van Dijk A, Haagsman HP. Cathelicidins: Immunomodulatory Antimicrobials. Vaccines (Basel). 2018 Sep 14;6(3).
104. Chen C, Wang A, Zhang F, Zhang M, Yang H, Li J, et al. The protective effect of fish-derived cathelicidins on bacterial infections in zebrafish, Danio rerio. Fish Shellfish Immunol. 2019 Sep;92:519–27.
105. Wei L, Yang J, He X, Mo G, Hong J, Yan X, et al. Structure and function of a potent lipopolysaccharide-binding antimicrobial and anti-inflammatory peptide. J Med Chem. 2013 May 9;56(9):3546–56.

106. Rajasekaran G, Kumar SD, Yang S, Shin SY. The design of a cell-selective fowlicidin-1-derived peptide with both antimicrobial and anti-inflammatory activities. Eur J Med Chem. 2019 Nov 15;182:111623.
107. Young-Speirs M, Drouin D, Cavalcante PA, Barkema HW, Cobo ER. Host defense cathelicidins in cattle: types, production, bioactive functions and potential therapeutic and diagnostic applications. Int J Antimicrob Agents. 2018 Jun;51(6):813–21.
108. Huynh E, Penney J, Caswell J, Li J. Protective Effects of Protegrin in Dextran Sodium Sulfate-Induced Murine Colitis. Front Pharmacol. 2019;10:156.
109. Pérez-Peinado C, Dias SA, Domingues MM, Benfield AH, Freire JM, Rádis-Baptista G, et al. Mechanisms of bacterial membrane permeabilization by crotalicidin (Ctn) and its fragment Ctn(15-34), antimicrobial peptides from rattlesnake venom. J Biol Chem. 2018 Feb 2;293(5):1536–49.
110. Fruitwala S, El-Naccache DW, Chang TL. Multifaceted immune functions of human defensins and underlying mechanisms. Semin Cell Dev Biol. 2019 Apr;88:163–72.
111. Gurao A, Kashyap SK, Singh R. β-defensins: An innate defense for bovine mastitis. Vet World. 2017 Aug;10(8):990–8.
112. Wang R, Ma D, Lin L, Zhou C, Han Z, Shao Y, et al. Identification and characterization of an avian β-defensin orthologue, avian β-defensin 9, from quails. Appl Microbiol Biotechnol. 2010 Jul 16;87(4):1395–405.
113. Mookherjee N, Anderson MA, Haagsman HP, Davidson DJ. Antimicrobial host defence peptides: functions and clinical potential. Nat Rev Drug Discov. 2020 May 27;19(5):311–32.
114. Mant CT, Jiang Z, Gera L, Davis T, Nelson KL, Bevers S, et al. De Novo Designed Amphipathic α-Helical Antimicrobial Peptides Incorporating Dab and Dap Residues on the Polar Face To Treat the Gram-Negative Pathogen, *Acinetobacter baumannii*. J Med Chem. 2019 Apr 11;62(7):3354–66.
115. Jiang S, Deslouches B, Chen C, Di ME, Di YP. Antibacterial Properties and Efficacy of a Novel SPLUNC1-Derived Antimicrobial Peptide, α4-Short, in a Murine Model of Respiratory Infection. mBio. 2019 Apr 9;10(2).
116. Mishra B, Reiling S, Zarena D, Wang G. Host defense antimicrobial peptides as antibiotics: design and application strategies. Curr Opin Chem Biol. 2017 Jun;38:87–96.

117. Chow LNY, Choi KYG, Piyadasa H, Bossert M, Uzonna J, Klonisch T, et al. Human cathelicidin LL-37-derived peptide IG-19 confers protection in a murine model of collagen-induced arthritis. Mol Immunol. 2014 Feb;57(2):86–92.
118. Piyadasa H, Hemshekhar M, Altieri A, Basu S, van der Does AM, Halayko AJ, et al. Immunomodulatory innate defence regulator (IDR) peptide alleviates airway inflammation and hyper-responsiveness. Thorax. 2018 Oct;73(10):908–17.
119. Li D, Wang W, Shi H shan, Fu Y jie, Chen X, Chen X cheng, et al. Gene therapy with beta-defensin 2 induces antitumor immunity and enhances local antitumor effects. Hum Gene Ther. 2014 Jan;25(1):63–72.
120. Li J, Koh JJ, Liu S, Lakshminarayanan R, Verma CS, Beuerman RW. Membrane Active Antimicrobial Peptides: Translating Mechanistic Insights to Design. Front Neurosci. 2017 Feb 14;11.
121. Talapko J, Meštrović T, Juzbašić M, Tomas M, Erić S, Horvat Aleksijević L, et al. Antimicrobial Peptides—Mechanisms of Action, Antimicrobial Effects and Clinical Applications. Antibiotics. 2022 Oct 16;11(10):1417.
122. Li X, Zuo S, Wang B, Zhang K, Wang Y. Antimicrobial Mechanisms and Clinical Application Prospects of Antimicrobial Peptides. Molecules. 2022 Apr 21;27(9):2675.
123. Reusch W. www2.chemistry.msu.edu/faculty/reusch/virttxtjml/protein2.htm . 2013. Peptides & Proteins.
124. Rozek A, Friedrich CL, Hancock RE. Structure of the bovine antimicrobial peptide indolicidin bound to dodecylphosphocholine and sodium dodecyl sulfate micelles. Biochemistry. 2000 Dec 26;39(51):15765–74.
125. Schibli DJ, Nguyen LT, Kernaghan SD, Rekdal Ø, Vogel HJ. Structure-Function Analysis of Tritrpticin Analogs: Potential Relationships between Antimicrobial Activities, Model Membrane Interactions, and Their Micelle-Bound NMR Structures. Biophys J. 2006 Dec;91(12):4413–26.
126. Schibli DJ, Hwang PM, Vogel HJ. Structure of the Antimicrobial Peptide Tritrpticin Bound to Micelles: A Distinct Membrane-Bound Peptide Fold ‡. Biochemistry. 1999 Dec 1;38(51):16749–55.
127. Sitaram N, Subbalakshmi C, Nagaraj R. Indolicidin, a 13-residue basic antimicrobial peptide rich in tryptophan and proline, interacts with Ca(2+)-calmodulin. Biochem Biophys Res Commun. 2003 Oct 3;309(4):879–84.

128. Mondal S, Adler-Abramovich L, Lampel A, Bram Y, Lipstman S, Gazit E. Formation of functional super-helical assemblies by constrained single heptad repeat. Nat Commun. 2015 Oct 15;6(1):8615.
129. Woolfson DN. The Design of Coiled-Coil Structures and Assemblies. In: Advances in Protein Chemistry. 2005. p. 79–112.
130. Hollmann A, Martinez M, Maturana P, Semorile LC, Maffia PC. Antimicrobial Peptides: Interaction With Model and Biological Membranes and Synergism With Chemical Antibiotics. Front Chem. 2018 Jun 5;6.
131. Bechinger B, Gorr SU. Antimicrobial Peptides: Mechanisms of Action and Resistance. J Dent Res. 2017 Mar 25;96(3):254–60.
132. Lohner K, Prenner EJ. Differential scanning calorimetry and X-ray diffraction studies of the specificity of the interaction of antimicrobial peptides with membrane-mimetic systems. Biochimica et Biophysica Acta (BBA) - Biomembranes. 1999 Dec;1462(1–2):141–56.
133. Lee TH, N. Hall K, Aguilar MI. Antimicrobial Peptide Structure and Mechanism of Action: A Focus on the Role of Membrane Structure. Curr Top Med Chem. 2015 Sep 16;16(1):25–39.
134. Babakhani A, Gorfe AA, Kim JE, McCammon JA. Thermodynamics of Peptide Insertion and Aggregation in a Lipid Bilayer. J Phys Chem B. 2008 Aug 1;112(34):10528–34.
135. Zasloff M. Magainins, a class of antimicrobial peptides from Xenopus skin: isolation, characterization of two active forms, and partial cDNA sequence of a precursor. Proceedings of the National Academy of Sciences. 1987 Aug;84(15):5449–53.
136. Le CF, Fang CM, Sekaran SD. Intracellular Targeting Mechanisms by Antimicrobial Peptides. Antimicrob Agents Chemother. 2017 Apr;61(4).
137. Hussein M, Karas JA, Schneider-Futschik EK, Chen F, Swarbrick J, Paulin OKA, et al. The Killing Mechanism of Teixobactin against Methicillin-Resistant Staphylococcus aureus: an Untargeted Metabolomics Study. mSystems. 2020 Jun 30;5(3).
138. Shukla R, Medeiros-Silva J, Parmar A, Vermeulen BJA, Das S, Paioni AL, et al. Mode of action of teixobactins in cellular membranes. Nat Commun. 2020 Jun 5;11(1):2848.
139. Bierbaum G, Sahl HG. Autolytic system of Staphylococcus simulans 22: influence of cationic peptides on activity of N-acetylmuramoyl-L-alanine amidase. J Bacteriol. 1987 Dec;169(12):5452–8.

140. Andersson DI, Hughes D, Kubicek-Sutherland JZ. Mechanisms and consequences of bacterial resistance to antimicrobial peptides. Drug Resistance Updates. 2016 May;26:43–57.
141. Nguyen LT, Haney EF, Vogel HJ. The expanding scope of antimicrobial peptide structures and their modes of action. Trends Biotechnol. 2011 Sep;29(9):464–72.
142. Lohner K. New strategies for novel antibiotics: peptides targeting bacterial cell membranes. Gen Physiol Biophys. 2009;28(2):105–16.
143. Dijksteel GS, Ulrich MMW, Middelkoop E, Boekema BKHL. Review: Lessons Learned From Clinical Trials Using Antimicrobial Peptides (AMPs). Front Microbiol. 2021 Feb 22;12.
144. Mihajlovic M, Lazaridis T. Antimicrobial peptides bind more strongly to membrane pores. Biochimica et Biophysica Acta (BBA) - Biomembranes. 2010 Aug;1798(8):1494–502.
145. Haney EF, Nathoo S, Vogel HJ, Prenner EJ. Induction of non-lamellar lipid phases by antimicrobial peptides: a potential link to mode of action. Chem Phys Lipids. 2010 Jan;163(1):82–93.
146. Mattila JP, Sabatini K, Kinnunen PKJ. Oxidized phospholipids as potential molecular targets for antimicrobial peptides. Biochimica et Biophysica Acta (BBA) - Biomembranes. 2008 Oct;1778(10):2041–50.
147. Marquette A, Bechinger B. Biophysical Investigations Elucidating the Mechanisms of Action of Antimicrobial Peptides and Their Synergism. Biomolecules. 2018 Apr 18;8(2):18.
148. Aisenbrey C, Bechinger B. Molecular Packing of Amphipathic Peptides on the Surface of Lipid Membranes. Langmuir. 2014 Sep 2;30(34):10374–83.
149. Vácha R, Frenkel D. Simulations Suggest Possible Novel Membrane Pore Structure. Langmuir. 2014 Feb 11;30(5):1304–10.
150. Bechinger B. Insights into the mechanisms of action of host defence peptides from biophysical and structural investigations. Journal of Peptide Science. 2011 May 28;17(5):306–14.
151. Leber R, Pachler M, Kabelka I, Svoboda I, Enkoller D, Vácha R, et al. Synergism of Antimicrobial Frog Peptides Couples to Membrane Intrinsic Curvature Strain. Biophys J. 2018 Apr;114(8):1945–54.

152. Sinha S, Zheng L, Mu Y, Ng WJ, Bhattacharjya S. Structure and Interactions of A Host Defense Antimicrobial Peptide Thanatin in Lipopolysaccharide Micelles Reveal Mechanism of Bacterial Cell Agglutination. Sci Rep. 2017 Dec 19;7(1):17795.
153. Robert É, Lefèvre T, Fillion M, Martial B, Dionne J, Auger M. Mimicking and Understanding the Agglutination Effect of the Antimicrobial Peptide Thanatin Using Model Phospholipid Vesicles. Biochemistry. 2015 Jun 30;54(25):3932–41.
154. Severina E, Severin A, Tomasz A. Antibacterial efficacy of nisin against multidrug-resistant Gram- positive pathogens. Journal of Antimicrobial Chemotherapy. 1998 Mar 1;41(3):341–7.
155. Stevens KA, Sheldon BW, Klapes NA, Klaenhammer TR. Nisin treatment for inactivation of Salmonella species and other gram-negative bacteria. Appl Environ Microbiol. 1991 Dec;57(12):3613–5.
156. Prince A, Sandhu P, Ror P, Dash E, Sharma S, Arakha M, et al. Lipid-II Independent Antimicrobial Mechanism of Nisin Depends On Its Crowding And Degree Of Oligomerization. Sci Rep. 2016 Nov 29;6(1):37908.
157. Petrof EO, Dhaliwal R, Manzanares W, Johnstone J, Cook D, Heyland DK. Probiotics in the critically ill. Crit Care Med. 2012 Dec;40(12):3290–302.
158. Blay G Le, Lacroix C, Zihler A, Fliss I. In vitro inhibition activity of nisin A, nisin Z, pediocin PA-1 and antibiotics against common intestinal bacteria. Lett Appl Microbiol. 2007 Sep;45(3):252–7.
159. Shin JM, Ateia I, Paulus JR, Liu H, Fenno JC, Rickard AH, et al. Antimicrobial nisin acts against saliva derived multi-species biofilms without cytotoxicity to human oral cells. Front Microbiol. 2015 Jun 18;6.
160. Mitra D, Yadav A, Prithyani S, John L, Rodrigues S, Shah R. The antiplaque efficacy of lantibiotic Nisin extract mouthrinse. J Indian Soc Periodontol. 2019;23(1):31.
161. Meikle TG, Conn CE, Separovic F, Drummond CJ. Exploring the structural relationship between encapsulated antimicrobial peptides and the bilayer membrane mimetic lipidic cubic phase: studies with gramicidin A′. RSC Adv. 2016;6(73):68685–94.
162. Van Epps HL. René Dubos: unearthing antibiotics. J Exp Med. 2006 Feb 20;203(2):259–259.
163. David JM, Rajasekaran AK. Gramicidin A: A New Mission for an Old Antibiotic. J Kidney Cancer VHL. 2015 Jan 18;2(1):15–24.

164. Zavascki AP, Goldani LZ, Li J, Nation RL. Polymyxin B for the treatment of multidrug-resistant pathogens: a critical review. Journal of Antimicrobial Chemotherapy. 2007 Oct 3;60(6):1206–15.
165. Morrison DC, Jacobs DM. Binding of polymyxin B to the lipid A portion of bacterial lipopolysaccharides. Immunochemistry. 1976 Oct;13(10):813–8.
166. Schroeder G, Brandenburg K, Seydel U. Polymyxin B induces transient permeability fluctuations in asymmetric planar lipopolysaccharide/phospholipid bilayers. Biochemistry. 1992 Jan 28;31(3):631–8.
167. Li J, Nation RL, Milne RW, Turnidge JD, Coulthard K. Evaluation of colistin as an agent against multi-resistant Gram-negative bacteria. Int J Antimicrob Agents. 2005 Jan;25(1):11–25.
168. Falagas ME, Kasiakou SK, Tsiodras S, Michalopoulos A. The Use of Intravenous and Aerosolized Polymyxins for the Treatment of Infections in Critically Ill Patients: A Review of the Recent Literature. Clin Med Res. 2006 Jun 1;4(2):138–46.
169. Warschawski DE, Arnold AA, Beaugrand M, Gravel A, Chartrand É, Marcotte I. Choosing membrane mimetics for NMR structural studies of transmembrane proteins. Biochimica et Biophysica Acta (BBA) - Biomembranes. 2011 Aug;1808(8):1957–74.
170. Mäler L. Solution NMR studies of cell-penetrating peptides in model membrane systems. Adv Drug Deliv Rev. 2013 Jul;65(8):1002–11.
171. Hine R. Membrane. In: Facts on File Dictionary of Biology. 3rd ed. New York; 1991. p. 198.
172. Alves AC, Ribeiro D, Nunes C, Reis S. Biophysics in cancer: The relevance of drug-membrane interaction studies. Biochimica et Biophysica Acta (BBA) - Biomembranes. 2016 Sep;1858(9):2231–44.
173. Lucio M, Lima JLFC, Reis S. Drug-Membrane Interactions: Significance for Medicinal Chemistry. Curr Med Chem. 2010 Jun 1;17(17):1795–809.
174. Cross TA, Sharma M, Yi M, Zhou HX. Influence of solubilizing environments on membrane protein structures. Trends Biochem Sci. 2011 Feb;36(2):117–25.
175. Arora A, Abildgaard F, Bushweller JH, Tamm LK. Structure of outer membrane protein A transmembrane domain by NMR spectroscopy. Nat Struct Biol. 2001 Apr 1;8(4):334–8.

176. Papavoine CHM, Konings RNH, Hilbers CW, van de Ven FJM. Location of M13 Coat Protein in Sodium Dodecyl Sulfate Micelles As Determined by NMR. Biochemistry. 1994 Nov 8;33(44):12990–7.
177. Jarvet J, Zdunek J, Damberg P, Gräslund A. Three-Dimensional Structure and Position of Porcine Motilin in Sodium Dodecyl Sulfate Micelles Determined by ^{1}H NMR. Biochemistry. 1997 Jul 1;36(26):8153–63.
178. van Swaay D, deMello A. Microfluidic methods for forming liposomes. Lab Chip [Internet]. 2013;13(5):752. Available from: https://xlink.rsc.org/?DOI=c2lc41121k
179. Deleu M, Crowet JM, Nasir MN, Lins L. Complementary biophysical tools to investigate lipid specificity in the interaction between bioactive molecules and the plasma membrane: A review. Biochimica et Biophysica Acta (BBA) - Biomembranes. 2014 Dec;1838(12):3171–90.
180. Karmakar S, Maity P, Halder A. Charge-Driven Interaction of Antimicrobial Peptide NK-2 with Phospholipid Membranes. ACS Omega. 2017 Dec 31;2(12):8859–67.
181. Walrant A, Correia I, Jiao CY, Lequin O, Bent EH, Goasdoué N, et al. Different membrane behaviour and cellular uptake of three basic arginine-rich peptides. Biochimica et Biophysica Acta (BBA) - Biomembranes. 2011 Jan;1808(1):382–93.
182. Mäler L, Gräslund A. Artificial Membrane Models for the Study of Macromolecular Delivery. In 2009. p. 129–39.
183. Aisenbrey C, Bertani P, Bechinger B. Solid-State NMR Investigations of Membrane-Associated Antimicrobial Peptides. In: Methods in Molecular Biology . 2010. p. 209–33.
184. Knobloch J, Suhendro DK, Zieleniecki JL, Shapter JG, Köper I. Membrane–drug interactions studied using model membrane systems. Saudi J Biol Sci. 2015 Nov;22(6):714–8.
185. Bae JS, Jung JM, An CM, Kim JW, Hwang SD, Kwon MG, et al. Piscidin: Antimicrobial peptide of rock bream, Oplegnathus fasciatus. Fish Shellfish Immunol. 2016 Apr;51:136–42.
186. Noga EJ, Silphaduang U, Park NG, Seo JK, Stephenson J, Kozlowicz S. Piscidin 4, a novel member of the piscidin family of antimicrobial peptides. Comp Biochem Physiol B Biochem Mol Biol. 2009 Apr;152(4):299–305.

187. Mehrnejad F, Zarei M. Molecular Dynamics Simulation Study of the Interaction of Piscidin 1 with DPPC Bilayers: Structure-Activity Relationship. J Biomol Struct Dyn. 2010 Feb;27(4):551–9.
188. Salger SA, Cassady KR, Reading BJ, Noga EJ. A Diverse Family of Host-Defense Peptides (Piscidins) Exhibit Specialized Anti-Bacterial and Anti-Protozoal Activities in Fishes. PLoS One. 2016 Aug 23;11(8):e0159423.
189. Zaccone G, Capillo G, Fernandes JMO, Kiron V, Lauriano ER, Alesci A, et al. Expression of the Antimicrobial Peptide Piscidin 1 and Neuropeptides in Fish Gill and Skin: A Potential Participation in Neuro-Immune Interaction. Mar Drugs. 2022 Feb 17;20(2):145.
190. Su BC, Liu YC, Ting CH, Lyu PC, Chen JY. Antimicrobial Peptide TP4 Targets Mitochondrial Adenine Nucleotide Translocator 2. Mar Drugs. 2020 Aug 9;18(8).
191. Hazam PK, Cheng CC, Hsieh CY, Lin WC, Hsu PH, Chen TL, et al. Development of Bactericidal Peptides against Multidrug-Resistant Acinetobacter baumannii with Enhanced Stability and Low Toxicity. Int J Mol Sci. 2022 Feb 16;23(4):2191.
192. Pan CY, Tsai TY, Su BC, Hui CF, Chen JY. Study of the Antimicrobial Activity of Tilapia Piscidin 3 (TP3) and TP4 and Their Effects on Immune Functions in Hybrid Tilapia (Oreochromis spp.). PLoS One. 2017 Jan 13;12(1):e0169678.
193. Huang HN, Chan YL, Wu CJ, Chen JY. Tilapia Piscidin 4 (TP4) Stimulates Cell Proliferation and Wound Closure in MRSA-Infected Wounds in Mice. Mar Drugs. 2015 May 6;13(5):2813–33.
194. Lin WC, Chen YR, Chuang CM, Chen JY. A Cationic Amphipathic Tilapia Piscidin 4 Peptide-Based Antimicrobial Formulation Promotes Eradication of Bacterial Vaginosis-Associated Bacterial Biofilms. Front Microbiol. 2022 Mar 23;13.
195. Zhuang Z rui, Yang X dong, Huang X zi, Gu H xian, Wei H yin, He Y jun, et al. Three new piscidins from orange-spotted grouper (Epinephelus coioides): Phylogeny, expression and functional characterization. Fish Shellfish Immunol. 2017 Jul;66:240–53.
196. Yin ZX, He W, Chen WJ, Yan JH, Yang JN, Chan SM, et al. Cloning, expression and antimicrobial activity of an antimicrobial peptide, epinecidin-1, from the orange-spotted grouper, Epinephelus coioides. Aquaculture. 2006 Mar 31;253(1–4):204–11.
197. Pan CY, Chen JY, Cheng YSE, Chen CY, Ni IH, Sheen JF, et al. Gene Expression and Localization of the Epinecidin-1 Antimicrobial Peptide in the Grouper (*Epinephelus*

coioides), and Its Role in Protecting Fish Against Pathogenic Infection. DNA Cell Biol. 2007 Jun;26(6):403–13.

198. Bonduelle C. Secondary structures of synthetic polypeptide polymers. Polym Chem. 2018;9(13):1517–29.
199. Johnson WC. Secondary Structure of Proteins Through Circular Dichroism Spectroscopy. Annu Rev Biophys Biophys Chem. 1988 Jun;17(1):145–66.
200. Krittanai C, Johnson WC. Correcting the Circular Dichroism Spectra of Peptides for Contributions of Absorbing Side Chains. Anal Biochem. 1997 Nov;253(1):57–64.
201. Baldauf C, Rossi M. Going clean: structure and dynamics of peptides in the gas phase and paths to solvation. Journal of Physics: Condensed Matter. 2015 Dec 16;27(49):493002.
202. Wei Y, Thyparambil AA, Latour RA. Protein helical structure determination using CD spectroscopy for solutions with strong background absorbance from 190 to 230nm. Biochimica et Biophysica Acta (BBA) - Proteins and Proteomics. 2014 Dec;1844(12):2331–7.
203. Gusmão KAG, dos Santos DM, Santos VM, Cortés ME, Reis PVM, Santos VL, et al. Ocellatin peptides from the skin secretion of the South American frog Leptodactylus labyrinthicus (Leptodactylidae): characterization, antimicrobial activities and membrane interactions. Journal of Venomous Animals and Toxins including Tropical Diseases. 2017 Dec 19;23(1):4.
204. Williamson MP. Peptide Structure Determination by NMR. In: Spectroscopic Methods and Analyses. New Jersey: Humana Press; 1993. p. 69–86.
205. Wimmer R, Uggerhøj LE. Determination of Structure and Micellar Interactions of Small Antimicrobial Peptides by Solution-State NMR. In 2017. p. 73–88.
206. Raghothama S. NMR of peptides. J Indian Inst Sci. 2010 Jan 1;90.
207. Kawano K, Yoneya T, Miyata T, Yoshikawa K, Tokunaga F, Terada Y, et al. Antimicrobial peptide, tachyplesin I, isolated from hemocytes of the horseshoe crab (Tachypleus tridentatus). NMR determination of the beta-sheet structure. J Biol Chem. 1990 Sep 15;265(26):15365–7.
208. Wüthrich K. NMR with Proteins and Nucleic Acids. Europhysics News. 1986 Jul 13;17(1):11–3.
209. Haney EF, Vogel HJ. Chapter 1 NMR of Antimicrobial Peptides. In 2009. p. 1–51.

210. Markley JL, Bax A, Arata Y, Hilbers CW, Kaptein R, Sykes BD, et al. Recommendations for the presentation of NMR structures of proteins and nucleic acids. Eur J Biochem. 1998 Aug 15;256(1):1–15.
211. Wodtke R, Ruiz-Gómez G, Kuchar M, Pisabarro MT, Novotná P, Urbanová M, et al. Cyclopeptides containing the DEKS motif as conformationally restricted collagen telopeptide analogues: synthesis and conformational analysis. Org Biomol Chem. 2015;13(6):1878–96.
212. Wishart DS, Sykes BD. Chemical shifts as a tool for structure determination. In 1994. p. 363–92.
213. Shen Y, Delaglio F, Cornilescu G, Bax A. TALOS+: a hybrid method for predicting protein backbone torsion angles from NMR chemical shifts. J Biomol NMR. 2009 Aug 23;44(4):213–23.
214. Brünger AT, Adams PD, Rice LM. New applications of simulated annealing in X-ray crystallography and solution NMR. Structure. 1997 Mar;5(3):325–36.
215. Munhoz VHO. Análise estrutural e topológica de peptídeos bioativos em meios biomiméticos de membranas. [Belo Horizonte]: UFMG; 2012.
216. Brünger AT, Krukowski A, Erickson JW. Slow-cooling protocols for crystallographic refinement by simulated annealing. Acta Crystallogr A. 1990 Jul 1;46(7):585–93.
217. Sargsyan K, Grauffel C, Lim C. How Molecular Size Impacts RMSD Applications in Molecular Dynamics Simulations. J Chem Theory Comput. 2017 Apr 11;13(4):1518–24.
218. Haney EF, Hunter HN, Matsuzaki K, Vogel HJ. Solution NMR studies of amphibian antimicrobial peptides: Linking structure to function? Biochimica et Biophysica Acta (BBA) - Biomembranes. 2009 Aug;1788(8):1639–55.
219. Bechinger B. The structure, dynamics and orientation of antimicrobial peptides in membranes by multidimensional solid-state NMR spectroscopy. Biochimica et Biophysica Acta (BBA) - Biomembranes. 1999 Dec;1462(1–2):157–83.
220. Aisenbrey C, Marquette A, Bechinger B. The Mechanisms of Action of Cationic Antimicrobial Peptides Refined by Novel Concepts from Biophysical Investigations. In 2019. p. 33–64.
221. Bechinger B, Sizun C. Alignment and structural analysis of membrane polypeptides by ^{15}N and ^{31}P solid-state NMR spectroscopy. Concepts in Magnetic Resonance Part A. 2003 Jul 18;18A(2):130–45.

222. Aisenbrey C, Bechinger B. Tilt and Rotational Pitch Angle of Membrane-Inserted Polypeptides from Combined 15N and 2H Solid-State NMR Spectroscopy. Biochemistry. 2004 Aug 1;43(32):10502–12.
223. Bechinger B, Seelig J. Conformational changes of the phosphatidylcholine headgroup due to membrane dehydration. A 2H-NMR study. Chem Phys Lipids. 1991 May;58(1–2):1–5.
224. Bechinger B, Resende JM, Aisenbrey C. The structural and topological analysis of membrane-associated polypeptides by oriented solid-state NMR spectroscopy: Established concepts and novel developments. Biophys Chem. 2011 Jan;153(2–3):115–25.
225. Salnikov ES, Anantharamaiah GM, Bechinger B. Supramolecular Organization of Apolipoprotein-A-I-Derived Peptides within Disc-like Arrangements. Biophys J. 2018 Aug;115(3):467–77.
226. Seelig J. Deuterium magnetic resonance: theory and application to lipid membranes. Q Rev Biophys. 1977 Aug 17;10(3):353–418.
227. Seelig J. Thermodynamics of lipid–peptide interactions. Biochimica et Biophysica Acta (BBA) - Biomembranes. 2004 Nov;1666(1–2):40–50.
228. Baranauskiene L, Kuo TC, Chen WY, Matulis D. Isothermal titration calorimetry for characterization of recombinant proteins. Curr Opin Biotechnol. 2019 Feb;55:9–15.
229. Chaires JB. Calorimetry and Thermodynamics in Drug Design. Annu Rev Biophys. 2008 Jun;37(1):135–51.
230. Frasca V. Biophysical characterization of antibodies with isothermal titration calorimetry. J Appl Bioanal. 2016 Jul 13;2(3):90–102.
231. Dumas P, Ennifar E, Da Veiga C, Bec G, Palau W, Di Primo C, et al. Extending ITC to Kinetics with kinITC. In 2016. p. 157–80.
232. Stetefeld J, McKenna SA, Patel TR. Dynamic light scattering: a practical guide and applications in biomedical sciences. Biophys Rev. 2016 Dec 6;8(4):409–27.
233. Kaszuba M, McKnight D, Connah MT, McNeil-Watson FK, Nobbmann U. Measuring sub nanometre sizes using dynamic light scattering. Journal of Nanoparticle Research. 2008 May 26;10(5):823–9.
234. Bhattacharjee S. DLS and zeta potential – What they are and what they are not? Journal of Controlled Release. 2016 Aug;235:337–51.

235. Mendoza-Espinosa P, Moreno A, Castillo R, Mas-Oliva J. Lipid dependant disorder-to-order conformational transitions in apolipoprotein CI derived peptides. Biochem Biophys Res Commun. 2008 Jan;365(1):8–15.
236. Freire JM, Domingues MM, Matos J, Melo MN, Veiga AS, Santos NC, et al. Using zeta-potential measurements to quantify peptide partition to lipid membranes. European Biophysics Journal. 2011 Apr 13;40(4):481–7.
237. Santos NC, Prieto M, Castanho MARB. Quantifying molecular partition into model systems of biomembranes: an emphasis on optical spectroscopic methods. Biochimica et Biophysica Acta (BBA) - Biomembranes. 2003 Jun;1612(2):123–35.
238. Roversi D, Troiano C, Salnikov E, Giordano L, Riccitelli F, De Zotti M, et al. Effects of antimicrobial peptides on membrane dynamics: A comparison of fluorescence and NMR experiments. Biophys Chem. 2023 Sep;300:107060.
239. Mokhtar DM, Zaccone G, Alesci A, Kuciel M, Hussein MT, Sayed RKA. Main Components of Fish Immunity: An Overview of the Fish Immune System. Fishes. 2023 Feb 5;8(2):93.
240. Mulero I, Noga EJ, Meseguer J, García-Ayala A, Mulero V. The antimicrobial peptides piscidins are stored in the granules of professional phagocytic granulocytes of fish and are delivered to the bacteria-containing phagosome upon phagocytosis. Dev Comp Immunol. 2008;32(12):1531–8.
241. Silphaduang U, Colorni A, Noga E. Evidence for widespread distribution of piscidin antimicrobial peptides in teleost fish. Dis Aquat Organ. 2006 Oct 27;72:241–52.
242. Lauth X, Shike H, Burns JC, Westerman ME, Ostland VE, Carlberg JM, et al. Discovery and Characterization of Two Isoforms of Moronecidin, a Novel Antimicrobial Peptide from Hybrid Striped Bass. Journal of Biological Chemistry. 2002 Feb;277(7):5030–9.
243. Feng CY, Johnson SC, Hori TS, Rise M, Hall JR, Gamperl AK, et al. Identification and analysis of differentially expressed genes in immune tissues of Atlantic cod stimulated with formalin-killed, atypical *Aeromonas salmonicida*. Physiol Genomics. 2009 May;37(3):149–63.
244. Salnikov ES, Glattard E, Lointier M, Raya J, Juhl DW, Saad A, et al. New Concepts for the Mechanisms of Action of Antimicrobial Peptides from Solid-state NMR Investigations. In: NMR Spectroscopy for Probing Functional Dynamics at Biological Interfaces. The Royal Society of Chemistry; 2022. p. 583–613.

245. Aisenbrey C, Michalek M, Salnikov ES, Bechinger B. Solid-state NMR approaches to study protein structure and protein-lipid interactions. Methods Mol Biol. 2013;974:357–87.
246. Bax A. TWO-DIMENSIONAL NMR AND PROTEIN STRUCTURE. Annu Rev Biochem. 1989 Jun;58(1):223–56.
247. Chan WC, White PD. Fmoc solid phase peptide synthesis : a practical approach / edited by Weng C. Chan and Peter D. White. Oxford: Oxford University Press; 2000. (Practical approach series ; 222).
248. Santos NC, Prieto M, Castanho MARB. Interaction of the Major Epitope Region of HIV Protein gp41 with Membrane Model Systems. A Fluorescence Spectroscopy Study. Biochemistry. 1998 Jun 1;37(24):8674–82.
249. Marsh D. Handbook of Lipid Bilayers. CRC Press; 2013.
250. Coutinho A, Prieto M. Self-association of the polyene antibiotic nystatin in dipalmitoylphosphatidylcholine vesicles: a time-resolved fluorescence study. Biophys J. 1995 Dec;69(6):2541–57.
251. Willker W, Leibfritz D, Kerssebaum R, Bermel W. Gradient selection in inverse heteronuclear correlation spectroscopy. Magnetic Resonance in Chemistry. 1993 Mar 14;31(3):287–92.
252. Schanda P, Kupče Ē, Brutscher B. SOFAST-HMQC Experiments for Recording Two-dimensional Deteronuclear Correlation Spectra of Proteins within a Few Seconds. J Biomol NMR. 2005 Dec;33(4):199–211.
253. Johnson BA, Blevins RA. NMR View: A computer program for the visualization and analysis of NMR data. J Biomol NMR. 1994 Sep;4(5):603–14.
254. Hyberts SG, Goldberg MS, Havel TF, Wagner G. The solution structure of eglin c based on measurements of many NOEs and coupling constants and its comparison with X-ray structures. Protein Science. 1992 Jun 31;1(6):736–51.
255. Delaglio F, Grzesiek S, Vuister GeertenW, Zhu G, Pfeifer J, Bax A. NMRPipe: A multidimensional spectral processing system based on UNIX pipes. J Biomol NMR. 1995 Nov;6(3).
256. Nabuurs SB, Spronk CAEM, Vriend G, Vuister GW. Concepts and tools for NMR restraint analysis and validation. Concepts in Magnetic Resonance Part A. 2004 Jul 30;22A(2):90–105.

257. Rice LM, BrüNger AT. Torsion angle dynamics: Reduced variable conformational sampling enhances crystallographic structure refinement. Proteins: Structure, Function, and Bioinformatics. 1994 Aug 3;19(4):277–90.
258. Stein EG, Rice LM, Brünger AT. Torsion-Angle Molecular Dynamics as a New Efficient Tool for NMR Structure Calculation. Journal of Magnetic Resonance. 1997 Jan;124(1):154–64.
259. Schwieters C, Kuszewski J, Mariusclore G. Using Xplor–NIH for NMR molecular structure determination. Prog Nucl Magn Reson Spectrosc. 2006 Mar 31;48(1):47–62.
260. Koradi R, Billeter M, Wüthrich K. MOLMOL: A program for display and analysis of macromolecular structures. J Mol Graph. 1996 Feb;14(1):51–5.
261. Pettersen EF, Goddard TD, Huang CC, Couch GS, Greenblatt DM, Meng EC, et al. UCSF Chimera—A visualization system for exploratory research and analysis. J Comput Chem. 2004 Oct;25(13):1605–12.
262. Bhattacharya A, Tejero R, Montelione GT. Evaluating protein structures determined by structural genomics consortia. Proteins: Structure, Function, and Bioinformatics. 2007 Mar 13;66(4):778–95.
263. Kemayo Koumkoua P, Aisenbrey C, Salnikov E, Rifi O, Bechinger B. On the design of supramolecular assemblies made of peptides and lipid bilayers. Journal of Peptide Science. 2014 Jul 7;20(7):526–36.
264. Rance M, Byrd RA. Obtaining high-fidelity powder spectra in anisotropic media: Phase-cycled Hahn echo spectroscopy. Journal of Magnetic Resonance (1969). 1983 Apr;52(2):221–40.
265. Davis JH, Jeffrey KR, Bloom M, Valic MI, Higgs TP. Quadrupolar echo deuteron magnetic resonance spectroscopy in ordered hydrocarbon chains. Chem Phys Lett. 1976 Sep;42(2):390–4.
266. Bechinger B, Opella SJ. Flat-coil probe for NMR spectroscopy of oriented membrane samples. Journal of Magnetic Resonance (1969). 1991 Dec;95(3):585–8.
267. Hediger S, Meier BH, Kurur ND, Bodenhausen G, Ernst RR. NMR cross polarization by adiabatic passage through the Hartmann—Hahn condition (APHH). Chem Phys Lett. 1994 Jun;223(4):283–8.
268. Bertani P, Raya J, Bechinger B. 15N chemical shift referencing in solid state NMR. Solid State Nucl Magn Reson. 2014 Jul;61–62:15–8.

269. Resende JM, Verly RM, Aisenbrey C, Cesar A, Bertani P, Piló-Veloso D, et al. Membrane Interactions of Phylloseptin-1, -2, and -3 Peptides by Oriented Solid-State NMR Spectroscopy. Biophys J. 2014 Aug;107(4):901–11.
270. Bloom M, Davis JH, Mackay AL. Direct determination of the oriented sample nmr spectrum from the powder spectrum for systems with local axial symmetry. Chem Phys Lett. 1981 May;80(1):198–202.
271. Batchelder LS, Niu CH, Torchia DA. Methyl reorientation in polycrystalline amino acids and peptides: a deuteron NMR spin-lattice relaxation study. J Am Chem Soc. 1983 Apr 1;105(8):2228–31.
272. Bukovics E. R. Storm, Wahrscheinlichkeitsrechnung, mathematische Statistik und statistische Qualitätskontrolle. 284 S. m. 66 Bildern, 53 Tab. u. 17 Tafeln. Leipzig 1965. Fachbuchverlag. Preis geb. MDN 17,50. ZAMM - Journal of Applied Mathematics and Mechanics / Zeitschrift für Angewandte Mathematik und Mechanik. 1966 Jan 22;46(6):405–405.
273. Reis PVM, Lima VM, Souza KR, Cardoso GA, Melo-Braga MN, Santos DM, et al. Synthetic Peptides Derived From Lycosa Erythrognatha Venom: Interaction With Phospholipid Membranes and Activity Against Resistant Bacteria. Front Mol Biosci. 2021 Jun 8;8.
274. Alvarez C, Casallanovo F, Shida CS, Nogueira L V., Martinez D, Tejuca M, et al. Binding of sea anemone pore-forming toxins sticholysins I and II to interfaces—Modulation of conformation and activity, and lipid–protein interaction. Chem Phys Lipids. 2003 Jan;122(1–2):97–105.
275. Greenfield NJ. Using circular dichroism spectra to estimate protein secondary structure. Nat Protoc. 2006 Dec 25;1(6):2876–90.
276. Lakowicz JR. Principles of Fluorescence Spectroscopy. 3rd ed. Lakowicz JR, editor. Boston, MA: Springer US; 2006.
277. Mello LR, Hamley IW, Castelletto V, Garcia BBM, Lourenço TC, Vassiliades S V., et al. Self-assembly and intracellular delivery of DNA by a truncated fragment derived from the *Trojan* peptide *Penetratin*. Soft Matter. 2020;16(20):4746–55.
278. Dickson JS, Koohmaraie M. Cell surface charge characteristics and their relationship to bacterial attachment to meat surfaces. Appl Environ Microbiol. 1989 Apr;55(4):832–6.

279. Tremblay ML, Banks AW, Rainey JK. The predictive accuracy of secondary chemical shifts is more affected by protein secondary structure than solvent environment. J Biomol NMR. 2010 Apr 6;46(4):257–70.
280. Santos TL, Moraes A, Nakaie CR, Almeida FCL, Schreier S, Valente AP. Structural and Dynamic Insights of the Interaction between Tritrpticin and Micelles: An NMR Study. Biophys J. 2016 Dec;111(12):2676–88.
281. Bechinger B, Salnikov ES. The membrane interactions of antimicrobial peptides revealed by solid-state NMR spectroscopy. Chem Phys Lipids. 2012 Apr;165(3):282–301.
282. Scherer PG, Seelig J. Electric charge effects on phospholipid headgroups. Phosphatidylcholine in mixtures with cationic and anionic amphiphiles. Biochemistry. 1989 Sep 19;28(19):7720–8.
283. Harmouche N, Bechinger B. Lipid-Mediated Interactions between the Antimicrobial Peptides Magainin 2 and PGLa in Bilayers. Biophys J. 2018 Sep;115(6):1033–44.
284. Tiné MR, Alderighi M, Duce C, Ghezzi L, Solaro R. Effect of temperature on self-assembly of an ionic tetrapeptide. J Therm Anal Calorim. 2011 Jan 8;103(1):75–80.
285. Domingues MM, Santiago PS, Castanho MARB, Santos NC. What can light scattering spectroscopy do for membrane-active peptide studies? Journal of Peptide Science. 2008 Apr 14;14(4):394–400.
286. Nunes LO, Munhoz VHO, Sousa AA, de Souza KR, Santos TL, Bemquerer MP, et al. High-resolution structural profile of hylaseptin-4: Aggregation, membrane topology and pH dependence of overall membrane binding process. Biochimica et Biophysica Acta (BBA) - Biomembranes. 2021 May;1863(5):183581.
287. Aranda-Espinoza H, Berman A, Dan N, Pincus P, Safran S. Interaction between inclusions embedded in membranes. Biophys J. 1996 Aug;71(2):648–56.
288. Mason AJ, Gasnier C, Kichler A, Prévost G, Aunis D, Metz-Boutigue MH, et al. Enhanced Membrane Disruption and Antibiotic Action against Pathogenic Bacteria by Designed Histidine-Rich Peptides at Acidic pH. Antimicrob Agents Chemother. 2006 Oct;50(10):3305–11.
289. Georgescu J, Munhoz VHO, Bechinger B. NMR Structures of the Histidine-Rich Peptide LAH4 in Micellar Environments: Membrane Insertion, pH-Dependent Mode of Antimicrobial Action, and DNA Transfection. Biophys J. 2010 Oct;99(8):2507–15.

290. Wolf J, Aisenbrey C, Harmouche N, Raya J, Bertani P, Voievoda N, et al. pH-Dependent Membrane Interactions of the Histidine-Rich Cell-Penetrating Peptide LAH4-L1. Biophys J. 2017 Sep;113(6):1290–300.
291. Oregioni A, Stieglitz B, Kelly G, Rittinger K, Frenkiel T. Determination of the pKa of the N-terminal amino group of ubiquitin by NMR. Sci Rep. 2017 Mar 2;7(1):43748.
292. Seelig J. Titration calorimetry of lipid–peptide interactions. Biochimica et Biophysica Acta (BBA) - Reviews on Biomembranes. 1997 Mar;1331(1):103–16.
293. Beschiaschvili G, Seelig J. Melittin binding to mixed phosphatidylglycerol/phosphatidylcholine membranes. Biochemistry. 1990 Jan 9;29(1):52–8.
294. Blondelle SE, Houghten RA. Hemolytic and antimicrobial activities of the twenty-four individual omission analogs of melittin. Biochemistry. 1991 May 1;30(19):4671–8.
295. Subbalakshmi C, Krishnakumari V, Sitaram N, Nagaraj R. Interaction of indolicidin, a 13-residue peptide rich in tryptophan and proline and its analogues with model membranes. J Biosci. 1998 Mar 1;23(1):9–13.
296. Mor A, Nicolas P. The NH2-terminal alpha-helical domain 1-18 of dermaseptin is responsible for antimicrobial activity. Journal of Biological Chemistry. 1994 Jan;269(3):1934–9.
297. Dathe M, Nikolenko H, Meyer J, Beyermann M, Bienert M. Optimization of the antimicrobial activity of magainin peptides by modification of charge. FEBS Lett. 2001 Jul 20;501(2–3):146–50.
298. Wenk MR, Seelig J. Magainin 2 Amide Interaction with Lipid Membranes: Calorimetric Detection of Peptide Binding and Pore Formation. Biochemistry. 1998 Mar 1;37(11):3909–16.
299. Melo MN, Ferre R, Castanho MARB. Antimicrobial peptides: linking partition, activity and high membrane-bound concentrations. Nat Rev Microbiol. 2009 Mar;7(3):245–50.
300. Della Pelle G, Perà G, Belardinelli MC, Gerdol M, Felli M, Crognale S, et al. Trematocine, a Novel Antimicrobial Peptide from the Antarctic Fish Trematomus bernacchii: Identification and Biological Activity. Antibiotics. 2020 Feb 6;9(2):66.
301. Czaplewski L, Bax R, Clokie M, Dawson M, Fairhead H, Fischetti VA, et al. Alternatives to antibiotics—a pipeline portfolio review. Lancet Infect Dis. 2016 Feb;16(2):239–51.

302. El Shazely B, Yu G, Johnston PR, Rolff J. Resistance Evolution Against Antimicrobial Peptides in Staphylococcus aureus Alters Pharmacodynamics Beyond the MIC. Front Microbiol. 2020 Feb 14;11.
303. Nan YH, Bang JK, Jacob B, Park IS, Shin SY. Prokaryotic selectivity and LPS-neutralizing activity of short antimicrobial peptides designed from the human antimicrobial peptide LL-37. Peptides (NY). 2012 Jun;35(2):239–47.
304. Zai Y, Xi X, Ye Z, Ma C, Zhou M, Chen X, et al. Aggregation and Its Influence on the Bioactivities of a Novel Antimicrobial Peptide, Temporin-PF, and Its Analogues. Int J Mol Sci. 2021 Apr 26;22(9):4509.
305. Raimondo D, Andreotti G, Saint N, Amodeo P, Renzone G, Sanseverino M, et al. A folding-dependent mechanism of antimicrobial peptide resistance to degradation unveiled by solution structure of distinctin. Proceedings of the National Academy of Sciences. 2005 May 3;102(18):6309–14.
306. Petkov P, Lilkova E, Ilieva N, Litov L. Self-Association of Antimicrobial Peptides: A Molecular Dynamics Simulation Study on Bombinin. Int J Mol Sci. 2019 Nov 1;20(21):5450.
307. Remington JM, Liao C, Sharafi M, Ste.Marie EJ, Ferrell JB, Hondal RJ, et al. Aggregation State of Synergistic Antimicrobial Peptides. J Phys Chem Lett. 2020 Nov 5;11(21):9501–6.
308. Hara T, Kodama H, Kondo M, Wakamatsu K, Takeda A, Tachi T, et al. Effects of peptide dimerization on pore formation: Antiparallel disulfide-dimerized magainin 2 analogue. Biopolymers. 2001 Apr 5;58(4):437–46.
309. Rink R, Arkema-Meter A, Baudoin I, Post E, Kuipers A, Nelemans SA, et al. To protect peptide pharmaceuticals against peptidases. J Pharmacol Toxicol Methods. 2010 Mar;61(2):210–8.
310. Grune T, Jung T, Merker K, Davies KJA. Decreased proteolysis caused by protein aggregates, inclusion bodies, plaques, lipofuscin, ceroid, and 'aggresomes' during oxidative stress, aging, and disease. Int J Biochem Cell Biol. 2004 Dec;36(12):2519–30.
311. Luchini ND, Broderick GA, Combs DK. Characterization of the proteolytic activity of commercial proteases and strained ruminal fluid. J Anim Sci. 1996;74(3):685.
312. Fu Z, Akula S, Thorpe M, Hellman L. Marked difference in efficiency of the digestive enzymes pepsin, trypsin, chymotrypsin, and pancreatic elastase to cleave tightly folded proteins. Biol Chem. 2021 Jun 25;402(7):861–7.

313. Hadwan MH, Al-Obaidy SSM, Al-Kawaz HS, Almashhedy LA, Kadhum MA, Khudhair DA, et al. An optimized protocol to assess trypsin activity in biological samples. Monatshefte für Chemie - Chemical Monthly. 2023 Feb 4;154(2):267–77.
314. Dau T, Bartolomucci G, Rappsilber J. Proteomics Using Protease Alternatives to Trypsin Benefits from Sequential Digestion with Trypsin. Anal Chem. 2020 Jul 21;92(14):9523–7.
315. Cronier S, Gros N, Tattum MH, Jackson GS, Clarke AR, Collinge J, et al. Detection and characterization of proteinase K-sensitive disease-related prion protein with thermolysin. Biochemical Journal. 2008 Dec 1;416(2):297–305.
316. KRAUS E, FEMFERT U. Proteinase K from the Mold *Tritirachium album* Limber. Specificity and Mode of Action. Hoppe Seylers Z Physiol Chem. 1976 Jan;357(2):937–48.
317. Hwang TL, Shaka AJ. Water Suppression That Works. Excitation Sculpting Using Arbitrary Wave-Forms and Pulsed-Field Gradients. J Magn Reson A. 1995 Feb;112(2):275–9.
318. Balbo A, Zhao H, Brown PH, Schuck P. Assembly, Loading, and Alignment of an Analytical Ultracentrifuge Sample Cell. Journal of Visualized Experiments. 2009 Nov 5;(33).
319. Schuck P, MacPhee CE, Howlett GJ. Determination of Sedimentation Coefficients for Small Peptides. Biophys J. 1998 Jan;74(1):466–74.
320. Schuck P. Size-Distribution Analysis of Macromolecules by Sedimentation Velocity Ultracentrifugation and Lamm Equation Modeling. Biophys J. 2000 Mar;78(3):1606–19.
321. Lebowitz J, Lewis MS, Schuck P. Modern analytical ultracentrifugation in protein science: A tutorial review. Protein Science. 2002 Sep;11(9):2067–79.
322. Zhao H, Brautigam CA, Ghirlando R, Schuck P. Overview of Current Methods in Sedimentation Velocity and Sedimentation Equilibrium Analytical Ultracentrifugation. Curr Protoc Protein Sci. 2013 Feb 15;71(1).
323. Brautigam CA. Calculations and Publication-Quality Illustrations for Analytical Ultracentrifugation Data. In 2015. p. 109–33.
324. Klijn JE, Kevelam J, Engberts JBFN. Aggregation Behavior of Mono-endcapped Hydrophobically Modified Poly(sodium acrylate)s in Aqueous Solution. J Colloid Interface Sci. 2000 Jun;226(1):76–82.

325. Ling LL, Schneider T, Peoples AJ, Spoering AL, Engels I, Conlon BP, et al. Erratum: A new antibiotic kills pathogens without detectable resistance. Nature. 2015 Apr 25;520(7547):388–388.
326. Romeiro RS. Métodos em bacteriologia de plantas. In: 1st ed. 2001.
327. Kelly SM, Jess TJ, Price NC. How to study proteins by circular dichroism. Biochimica et Biophysica Acta (BBA) - Proteins and Proteomics. 2005 Aug;1751(2):119–39.
328. Vasile F, Rossi D, Collina S, Potenza D. Diffusion-Ordered Spectroscopy and Saturation Transfer Difference NMR Spectroscopy Studies of Selective Interactions between ELAV Protein Fragments and an mRNA Target. European J Org Chem. 2014 Oct 17;2014(29):6399–404.
329. Cole JL, Lary JW, P. Moody T, Laue TM. Analytical Ultracentrifugation: Sedimentation Velocity and Sedimentation Equilibrium. In 2008. p. 143–79.
330. Dam J, Schuck P. Calculating Sedimentation Coefficient Distributions by Direct Modeling of Sedimentation Velocity Concentration Profiles. In 2004. p. 185–212.
331. Dalla Serra M, Cirioni O, Vitale RM, Renzone G, Coraiola M, Giacometti A, et al. Structural Features of Distinctin Affecting Peptide Biological and Biochemical Properties. Biochemistry. 2008 Jul 1;47(30):7888–99.
332. Loll PJ, Miller R, Weeks CM, Axelsen PH. A ligand-mediated dimerization mode for vancomycin. Chem Biol. 1998 May;5(5):293–8.
333. Hornef MW, Pütsep K, Karlsson J, Refai E, Andersson M. Increased diversity of intestinal antimicrobial peptides by covalent dimer formation. Nat Immunol. 2004 Aug 4;5(8):836–43.
334. Batista CVF, Scaloni A, Rigden DJ, Silva LR, Rodrigues Romero A, Dukor R, et al. A novel heterodimeric antimicrobial peptide from the tree-frog *Phyllomedusa distincta*. FEBS Lett. 2001 Apr 6;494(1–2):85–9.
335. Lee IH, Lee YS, Kim CH, Kim CR, Hong T, Menzel L, et al. Dicynthaurin: an antimicrobial peptide from hemocytes of the solitary tunicate, Halocynthia aurantium. Biochimica et Biophysica Acta (BBA) - General Subjects. 2001 Aug;1527(3):141–8.
336. Jang WS, Kim KN, Lee YS, Nam MH, Lee IH. Halocidin: a new antimicrobial peptide from hemocytes of the solitary tunicate, *Halocynthia aurantium*. FEBS Lett. 2002 Jun 19;521(1–3):81–6.

337. Yomogida S, Nagaoka I, Yamashita T. Purification of the 11- and 5-kDa Antibacterial Polypeptides from Guinea Pig Neutrophils. Arch Biochem Biophys. 1996 Apr;328(2):219–26.
338. Scocchi M, Zelezetsky I, Benincasa M, Gennaro R, Mazzoli A, Tossi A. Structural aspects and biological properties of the cathelicidin PMAP-36. FEBS J. 2005 Sep 15;272(17):4398–406.
339. Mortazavi SH, Bozorgmehr MR, Heravi MM. Structure of the Cyclic, Cationic Antimicrobial Peptide (KKWWKF) in Octanol Solution: <i>in silico</i> Approach. Indonesian Journal of Chemistry. 2020 May 22;20(6):1283.
340. Clark TD, Bartolotti L, Hicks RP. The application of DOSY NMR and molecular dynamics simulations to explore the mechanism(s) of micelle binding of antimicrobial peptides containing unnatural amino acids. Biopolymers. 2013 Aug 25;99(8):548–61.
341. Balbo A, Schuck P. Analytical Ultracentrifugation in the Study of Protein Self-association and Heterogeneous Protein-Protein Interactions. In: Protein-Protein Interactions: A Molecular Cloning Manual [Internet]. 2005. p. 253–77. Available from: https://api.semanticscholar.org/CorpusID:30783714
342. Kandiyal PS, Kim JY, Fortunati DL, Mok KH. Size Determination of Protein Oligomers/Aggregates Using Diffusion NMR Spectroscopy. In 2019. p. 173–83.
343. Henriksen JR, Andresen TL. Thermodynamic Profiling of Peptide Membrane Interactions by Isothermal Titration Calorimetry: A Search for Pores and Micelles. Biophys J. 2011 Jul;101(1):100–9.
344. Fazly Bazzaz BS, Seyedi S, Hoseini Goki N, Khameneh B. Human Antimicrobial Peptides: Spectrum, Mode of Action and Resistance Mechanisms. Int J Pept Res Ther. 2021 Mar 30;27(1):801–16.
345. Moretta A, Scieuzo C, Petrone AM, Salvia R, Manniello MD, Franco A, et al. Antimicrobial Peptides: A New Hope in Biomedical and Pharmaceutical Fields. Front Cell Infect Microbiol. 2021 Jun 14;11.
346. Manniello MD, Moretta A, Salvia R, Scieuzo C, Lucchetti D, Vogel H, et al. Insect antimicrobial peptides: potential weapons to counteract the antibiotic resistance. Cellular and Molecular Life Sciences. 2021 May 17;78(9):4259–82.
347. Puan SL, Erriah P, Baharudin MMA adil, Yahaya NM, Kamil WNIWA, Ali MSM, et al. Antimicrobial peptides from Bacillus spp. and strategies to enhance their yield. Appl Microbiol Biotechnol. 2023 Sep 14;107(18):5569–93.

348. Shi G, Kang X, Dong F, Liu Y, Zhu N, Hu Y, et al. DRAMP 3.0: an enhanced comprehensive data repository of antimicrobial peptides. Nucleic Acids Res. 2022 Jan 7;50(D1):D488–96.
349. Joshi S, Bisht GS, Rawat DS, Kumar A, Kumar R, Maiti S, et al. Interaction studies of novel cell selective antimicrobial peptides with model membranes and E. coli ATCC 11775. Biochimica et Biophysica Acta (BBA) - Biomembranes. 2010 Oct;1798(10):1864–75.
350. Lipkin R, Lazaridis T. Computational studies of peptide-induced membrane pore formation. Philosophical Transactions of the Royal Society B: Biological Sciences. 2017 Aug 5;372(1726):20160219.
351. Krauson AJ, He J, Wimley WC. Gain-of-Function Analogues of the Pore-Forming Peptide Melittin Selected by Orthogonal High-Throughput Screening. J Am Chem Soc. 2012 Aug 1;134(30):12732–41.
352. Salvador P, Tsai IH (Midas), Dannenberg JJ. J-coupling constants for a trialanine peptide as a function of dihedral angles calculated by density functional theory over the full Ramachandran space. Physical Chemistry Chemical Physics. 2011;13(39):17484.
353. Karplus M. Contact Electron-Spin Coupling of Nuclear Magnetic Moments. J Chem Phys. 1959 Jan 1;30(1):11–5.
354. Andersen NH, Chen C, Marschner TM, Krystek SR, Bassolino DA. Conformational isomerism of endothelin in acidic aqueous media: a quantitative NOESY analysis. Biochemistry. 1992 Feb 11;31(5):1280–95.
355. Pielak GJ, Li C, Miklos AC, Schlesinger AP, Slade KM, Wang GF, et al. Protein Nuclear Magnetic Resonance under Physiological Conditions. Biochemistry. 2009 Jan 20;48(2):226–34.
356. Kawale AA, Burmann BM. Characterization of backbone dynamics using solution NMR spectroscopy to discern the functional plasticity of structurally analogous proteins. STAR Protoc. 2021 Dec;2(4):100919.
357. Kapil S, Sharma V. d-Amino acids in antimicrobial peptides: a potential approach to treat and combat antimicrobial resistance. Can J Microbiol. 2021 Feb;67(2):119–37.
358. Abdulbagi M, Wang L, Siddig O, Di B, Li B. D-Amino Acids and D-Amino Acid-Containing Peptides: Potential Disease Biomarkers and Therapeutic Targets? Biomolecules. 2021 Nov 18;11(11):1716.

359. Lu X, Zhu X, Guo H, Que H, Wang D, Liang D, et al. Investigation on the thermal degradation behavior of enzymatic hydrolysis lignin with or without steam explosion treatment characterized by TG-FTIR and Py-GC/MS. Biomass Convers Biorefin. 2022 Dec 5;12(12):5825–34.
360. Sim JY, Kim S, Lee J, Lim H, Kim HH, Park ZY, et al. A significantly enhanced antibacterial spectrum of D-enantiomeric lipopeptide bactenecin. Biochem Biophys Res Commun. 2019 Jun;514(2):497–502.
361. Navon-Venezia S, Feder R, Gaidukov L, Carmeli Y, Mor A. Antibacterial Properties of Dermaseptin S4 Derivatives with In Vivo Activity. Antimicrob Agents Chemother. 2002 Mar;46(3):689–94.
362. Shang D, Li X, Sun Y, Wang C, Sun L, Wei S, et al. Design of Potent, Non-Toxic Antimicrobial Agents Based upon the Structure of the Frog Skin Peptide, Temporin-1CEb from Chinese Brown Frog, *Rana chensinensis*. Chem Biol Drug Des. 2012 May 16;79(5):653–62.
363. Chen J, Falla TJ, Liu H, Hurst MA, Fujii CA, Mosca DA, et al. Development of protegrins for the treatment and prevention of oral mucositis: Structure-activity relationships of synthetic protegrin analogues. Biopolymers. 2000;55(1):88–98.
364. Nunes LO. Investigações estruturais e biofísicas da interação peptídeo-membrana: um estudo dos casos hilaseptina P4 e ecPiscidina-2s. UFVJM; 2021.
365. Naghili H, Tajik H, Mardani K, Razavi Rouhani SM, Ehsani A, Zare P. Validation of drop plate technique for bacterial enumeration by parametric and nonparametric tests. Vet Res Forum. 2013;4(3):179–83.
366. Bayerl TM, Köchy T, Brückner S. On the modulation of a high-enthalpy pretransition in binary mixtures of DMPC and DMPG by polar headgroup interaction. Biophys J. 1990 Mar;57(3):675–80.
367. Pandit G, Sarkar T, S. R. V, Debnath S, Satpati P, Chatterjee S. Delineating the Mechanism of Action of a Protease Resistant and Salt Tolerant Synthetic Antimicrobial Peptide against *Pseudomonas aeruginosa*. ACS Omega. 2022 May 10;7(18):15951–68.
368. Bellotto O, Semeraro S, Bandiera A, Tramer F, Pavan N, Marchesan S. Polymer Conjugates of Antimicrobial Peptides (AMPs) with d-Amino Acids (d-aa): State of the Art and Future Opportunities. Pharmaceutics. 2022 Feb 19;14(2):446.
369. Feng Z, Xu B. Inspiration from the mirror: D-amino acid containing peptides in biomedical approaches. Biomol Concepts. 2016 Jun 1;7(3):179–87.

370. Yao J, Dyson HJ, Wright PE. Three-dimensional structure of a type VI turn in a linear peptide in water solution Evidence for stacking of aromatic rings as a major stabilizing factor. J Mol Biol. 1994 Nov;243(4):754–66.
371. Verly RM, Rodrigues MA, Daghastanli KRP, Denadai AML, Cuccovia IM, Bloch C, et al. Effect of cholesterol on the interaction of the amphibian antimicrobial peptide DD K with liposomes. Peptides (NY). 2008 Jan;29(1):15–24.
372. Fontana A, De Laureto PP, De Filippis V, Scaramella E, Zambonin M. Probing the partly folded states of proteins by limited proteolysis. Fold Des. 1997 Apr 1;2(2):R17–26.

Kelton RODRIGUES DE SOUZA

Biophysical and structural studies of bioactive peptides derived from the piscidin family in anionic membrane models

Résumé

Les peptides antimicrobiens sont prometteurs pour la conception de nouveaux médicaments antibactériens en raison de leur faible tendance au développement de résistance et de leur capacité à éliminer les bactéries multirésistantes. Nos investigations visent à étudier les mécanismes d'action des nouveaux peptides des ecPis-4s et ecPis-2s. De plus, nous avons proposé d'étudier la forme épimérique de l'ecPis-2s, puisqu'il a été rapporté qu'un peptide antimicrobien naturel contenant des résidus D- avait de larges activités antimicrobiennes. Les résultats obtenus indiquent que les ecPis-4s adoptent une conformation hélicoïdale amphipathique bien définie, orientée parallèlement à la surface de la bicouche phospholipidique, avec une forte affinité pour les membranes anioniques et une activité lytique dépendante de la concentration. En ce qui concerne les peptides épimères, nos résultats montrent que l'épimère D-ecPis-2s exerce un effet plus remarquable sur la stabilité de la membrane. La configuration des acides aminés D- semble donner à la structure peptidique un caractère amphipathique plus important comparé au peptide naturel L-ecPis-2s.

Mots clés : Peptide antimicrobien ; Membrane lipidique ; Interaction peptide-membrane ; RMN du liquide ; RMN du solide ; Calorimétrie de titrage isotherme.

Abstract

Antimicrobial peptides hold promise for the design of new antibacterial drugs due to their low tendency for resistance development and their ability to eliminate multidrug-resistant bacteria. Our investigations aim to study the mechanisms of action of the new ecPis-4s and ecPis-2s peptides. Furthermore, we proposed to study the epimeric form of ecPis-2s, since natural antimicrobial peptides containing D- residues have been reported to have broad antimicrobial activities. The results obtained indicate that ecPis-4s adopt a well-defined amphipathic helical conformation, oriented parallel to the surface of the phospholipid bilayer, with a strong affinity for anionic membranes and a concentration-dependent lytic activity. Regarding epimeric peptides, our results show that the epimeric D-ecPis-2s exerts a more remarkable effect on membrane stability. The D- amino acid configuration appears to give the peptide structure a greater amphipathic character compared to the natural L-ecPis-2s peptide.

Keywords: Antimicrobial peptide ; Lipid membrane ; Peptide-membrane interaction ; Liquid NMR ; solid-state NMR ; Isothermal titration calorimetry.